

A Wire Indent Profiling System for the Assessment of Bond and Splitting Propensity of Prestressing Wires Used in Pretensioned Concrete Railroad Ties

KSU-21-11**April 2021****Dr. B. Terry Beck, Mechanical & Nuclear Engineering, KSU****Aaron A. Robertson, M.S., Mechanical & Nuclear Engineering, KSU****Dr. Robert J. Peterman, Civil Engineering, KSU****Dr. Kyle A. Riding, Civil and Coastal Engineering, UF**

Abstract

The focus of this research was the creation of an automatic non-contact laser-based indent profiling system for the purpose of rapidly assessing geometrical characteristics of indented wires used in the manufacture of pretensioned concrete railroad ties. The process of measuring indent geometrical characteristics by traditional means is a time-consuming process which severely limits the frequency of testing and prevents statistically relevant sample sizes. In parallel with concrete prism transfer length and splitting propensity testing conducted in conjunction with this project, this system was used to identify which indent characteristics were directly related to both bond and splitting propensity in pretensioned concrete ties. This report details the automation of this indent profiling system and the results obtained for many different indented wires that were currently or historically used to manufacture pretensioned concrete railroad ties.

Corresponding Author: Dr. B. Terry Beck (tbeck@ksu.edu)



U.S. Department of Transportation
Federal Railroad Administration

The contents of this report reflect the views of the authors, who are responsible for the facts and accuracy of the information presented herein. This document is disseminated in the interest of information exchange. The report is funded, partially or entirely, by a grant from the U.S. Department of Transportation's University Transportation Centers Program. However, the U.S. Government assumes no liability for the contents or use thereof.



METRIC/ENGLISH CONVERSION FACTORS

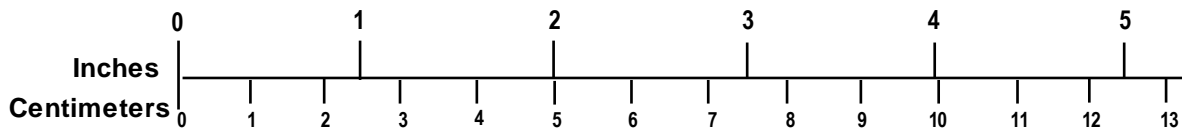
ENGLISH TO METRIC

LENGTH (APPROXIMATE)	
1 inch (in)	= 2.5 centimeters (cm)
1 foot (ft)	= 30 centimeters (cm)
1 yard (yd)	= 0.9 meter (m)
1 mile (mi)	= 1.6 kilometers (km)
AREA (APPROXIMATE)	
1 square inch (sq in, in ²)	= 6.5 square centimeters (cm ²)
1 square foot (sq ft, ft ²)	= 0.09 square meter (m ²)
1 square yard (sq yd, yd ²)	= 0.8 square meter (m ²)
1 square mile (sq mi, mi ²)	= 2.6 square kilometers (km ²)
1 acre = 0.4 hectare (he)	= 4,000 square meters (m ²)
MASS - WEIGHT (APPROXIMATE)	
1 ounce (oz)	= 28 grams (gm)
1 pound (lb)	= 0.45 kilogram (kg)
1 short ton = 2,000 pounds (lb)	= 0.9 tonne (t)
VOLUME (APPROXIMATE)	
1 teaspoon (tsp)	= 5 milliliters (ml)
1 tablespoon (tbsp)	= 15 milliliters (ml)
1 fluid ounce (fl oz)	= 30 milliliters (ml)
1 cup (c)	= 0.24 liter (l)
1 pint (pt)	= 0.47 liter (l)
1 quart (qt)	= 0.96 liter (l)
1 gallon (gal)	= 3.8 liters (l)
1 cubic foot (cu ft, ft ³)	= 0.03 cubic meter (m ³)
1 cubic yard (cu yd, yd ³)	= 0.76 cubic meter (m ³)
TEMPERATURE (EXACT)	
$[(x-32)(5/9)]^{\circ}\text{F} = y^{\circ}\text{C}$	

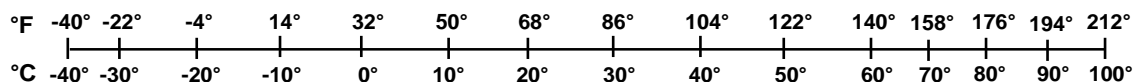
METRIC TO ENGLISH

LENGTH (APPROXIMATE)	
1 millimeter (mm)	= 0.04 inch (in)
1 centimeter (cm)	= 0.4 inch (in)
1 meter (m)	= 3.3 feet (ft)
1 meter (m)	= 1.1 yards (yd)
1 kilometer (km)	= 0.6 mile (mi)
AREA (APPROXIMATE)	
1 square centimeter (cm ²)	= 0.16 square inch (sq in, in ²)
1 square meter (m ²)	= 1.2 square yards (sq yd, yd ²)
1 square kilometer (km ²)	= 0.4 square mile (sq mi, mi ²)
10,000 square meters (m ²)	= 1 hectare (ha) = 2.5 acres
MASS - WEIGHT (APPROXIMATE)	
1 gram (gm)	= 0.036 ounce (oz)
1 kilogram (kg)	= 2.2 pounds (lb)
1 tonne (t)	= 1,000 kilograms (kg)
	= 1.1 short tons
VOLUME (APPROXIMATE)	
1 milliliter (ml)	= 0.03 fluid ounce (fl oz)
1 liter (l)	= 2.1 pints (pt)
1 liter (l)	= 1.06 quarts (qt)
1 liter (l)	= 0.26 gallon (gal)
1 cubic meter (m ³)	= 36 cubic feet (cu ft, ft ³)
1 cubic meter (m ³)	= 1.3 cubic yards (cu yd, yd ³)
TEMPERATURE (EXACT)	
$[(9/5)y + 32]^{\circ}\text{C} = x^{\circ}\text{F}$	

QUICK INCH - CENTIMETER LENGTH CONVERSION



QUICK FAHRENHEIT - CELSIUS TEMPERATURE CONVERSION



For more exact and or other conversion factors, see NIST Miscellaneous Publication 286, Units of Weights and Measures. Price \$2.50 SD Catalog No. C13 10286

Updated 6/17/98

Acknowledgements

The authors gratefully acknowledge the Federal Railroad Administration (FRA) for providing the funding that made this research possible. The cooperation and resources provided by Nucor-LMP is also gratefully acknowledged. A special thanks to John Bloomfield at the Advanced Manufacturing Institute (AMI) for his excellent implementation of our concepts of the automated wire indent profiling system into practical functioning systems with excellent performance.

Contents

Acknowledgements	ii
Illustrations	v
Tables	viii
Executive Summary	9
1. Introduction	10
1.1 Background	10
1.2 Objectives	13
1.3 Organization of the Report	14
2. Methods of Indent Geometry Measurement	16
2.1 ASTM A881	16
2.2 ISO 16120	17
2.3 Early Wire Scanning Measurement Technology	18
2.4 Insufficiencies with Current Methods	19
3. Development of the Indent Profiling System	21
3.1 Initial Specifications	21
3.2 Component Selection	23
3.3 System Layout Overview	23
4. Scanning Process	26
4.1 Interface Layout	26
4.2 Traverse Control, Rotation Control, and Carriage Homing	30
4.3 Filter Settings and Data Visualization	31
4.4 Scan File Format	34
5. System Calibration	36
5.1 The Necessity of System Calibration	36
5.2 Correcting for Sensor Skew	37
5.3 Off-Bore Rotation (Wire Bow)	38
5.4 Measurement Uncertainty and Repeatability	39
5.5 Machined Indents	43
6. Process for Extracting Indent Geometry	46
6.1 Scan Splicing	46
6.2 Indent Row Detection	48
6.3 Determining Indent Location and Orientation	51
6.4 Indent Isolation	52
6.5 Trapezoid Fit of Least Squares	53
6.6 Obtaining Primary Geometric Features	55
6.7 File Report Format	57
6.8 Post-Processing, Statistics Generation, Histograms	59

7.	Overview of Collected Data.....	60
7.1	Cover Testing Wires	61
7.2	Crosstie Wires (Extracted).....	71
7.3	Machined Indent Wires.....	76
8.	Repetition Demonstration	83
8.1	Observations of Indent Repetition	83
8.2	Differing Indents for Individual Rows.....	85
9.	Correlations.....	87
9.1	Correlation of 2D Parameters to 3D Parameters.....	87
9.2	Empirical Concrete Prism Data	92
9.3	Transfer Length Correlations	95
9.4	Crack Length Correlations (Splitting Propensity)	99
10.	Go/No-Go Criteria	104
10.1	Evaluation by ASTM A881/ ISO 16120.....	104
10.2	Comparison to Correlations	106
11.	Conclusions.....	108
12.	References.....	120
	Appendix A. Wire Report Summary	124
	Appendix B. LabVIEW VI Layout.....	240
	Abbreviations and Acronyms	243

Illustrations

Figure 1.1: ASTM A881 Geometrical Feature Requirements	11
Figure 1.2: Schematic of Indented Wire Measurement (Point Laser)	12
Figure 1.3: Manufacture of Prestressing Wire Indents	13
Figure 2.1: ISO 16120 Geometrical Feature Requirements.....	17
Figure 2.2: Early Indent Profiling Technology	18
Figure 2.3: Early Scan of WF Wire Type	19
Figure 2.4: Indent Profiling System Scan	20
Figure 3.1: Schematic of Proposed Indent Profiling System.....	21
Figure 3.2: Key 3D Wire Indent Geometrical Features	22
Figure 3.3: Layout of Indent Profiling System	24
Figure 3.4: Close-up of Scanning Head and Bushing Guide	25
Figure 4.1: Wire Type WF.....	26
Figure 4.2: Wire Scanner Interface	27
Figure 4.3: Wire Scan Reporter Interface	28
Figure 4.4: Wire Scan Reporter Interface (Indent Viewer)	30
Figure 4.5: Movement Control Default Settings.....	31
Figure 4.6: Profile Averaging	32
Figure 4.7: Boxcar Averaging on Simulated Data.....	33
Figure 4.8: Scan Refinement of Wire Type WF	33
Figure 4.9: Schematic of Indented Wire Measurement (Sheet Laser).....	34
Figure 4.10: Scanning Grid Spacing	35
Figure 4.11: Scan File Format	35
Figure 5.1: Calibration Cylinder Scan	37
Figure 5.2: The Effect of Wire Bow on Off-Bore Rotations	38
Figure 5.3: Trued Calibration Cylinder Height-Map.....	40
Figure 5.4: Trued Calibration Cylinder Histogram.....	40
Figure 5.5: System Repeatability	41
Figure 5.6: Laser Speckle Interference	42
Figure 5.7: Automated LSI System on Concrete Ties in Plant.....	42
Figure 5.8: Sample Scan of Machined Indent (30°)	43
Figure 5.9: Basis for Feature Extraction (Trapezoid Slice)	44

Figure 5.10: Trapezoidal Slice for a Machined Indent (30°)	44
Figure 5.11: Measured Sidewall Angle Relationship	45
Figure 6.1: Outcome of Scan Splicing.....	46
Figure 6.2: Increased Measurement Uncertainty at Edges of Line-Scan.....	47
Figure 6.3: Method for Joining Overlapping Scan Segments.....	48
Figure 6.4: Indent Rows From Average Trilobal Profile (Wire Type “WF”)	49
Figure 6.5: Indent Rows From Profile Linearity (Wire Type “WF”).....	50
Figure 6.6: Indent Row Detection.....	50
Figure 6.7: Determining Pitch and Orientation Angle.....	51
Figure 6.8: Wire Scan Reporter Indent Partitioning	52
Figure 6.9: Wire Scan Reporter Indent Isolation	52
Figure 6.10: Applicability of Trapezoidal Curve Fit	53
Figure 6.11: Trapezoid Fit of Least Squares.....	54
Figure 6.12: Trapezoid Fit of Indent Slant Profile (Wire WM).....	55
Figure 6.13: 2D Wire Indent Geometrical Features.....	56
Figure 6.14: 3D Wire Indent Geometrical Features.....	57
Figure 6.15: Indent Profiling System Initial Report (Global Block)	58
Figure 6.16: Indent Profiling System Initial Report (Indent Block).....	59
Figure 6.17: Data Report Flowchart	59
Figure 7.1: Digital Microscope Images of Cover Testing Wires.....	62
Figure 7.2: Scan Segment of Wire Type WF.....	63
Figure 7.3: Variation of Sidewall Angles on the Right Side (Wire WP).....	65
Figure 7.4: Variation of Sidewall Angles on the Right Side (Wire WF).....	66
Figure 7.5: Variation of Sidewall Angles Between Sides (Wire WF).....	67
Figure 7.6: Measured Variations of Indent Volume	67
Figure 7.7: Measured Variations of Indent Average Depth.....	68
Figure 7.8: Measured Variations of Average Indent Sidewall Angle (Left Side)	69
Figure 7.9: Measured Variations of Average Indent Sidewall Angle (Right Side).....	69
Figure 7.10: Measured Variations of Indent Sidewall Area (Left Side).....	70
Figure 7.11: Measured Variations of Indent Sidewall Area (Right Side).....	70
Figure 7.12: Concrete Crosstie Scans	72
Figure 7.13: Digital Microscope Images of Extracted Crosstie Wires	73
Figure 7.14: Severely Malformed Indents (Crosstie Wire L-1).....	75

Figure 7.15: Similarities Between Wire WM and Wire M-1.....	76
Figure 7.16: Endmill Geometry Used to Create Machined Indents.....	77
Figure 7.17: Picture of Wires With Machined Indents	77
Figure 7.18: Digital Microscope Images of Machined Wires.....	78
Figure 7.19: Shadowgraph Imaging of Machined Indent	79
Figure 8.1: Isolation of Indent Roller Defects	83
Figure 8.2: Defects Near Beginning of Scan	84
Figure 8.3: Digital Microscope Image of Deformed Indent (Wire WF).....	84
Figure 8.4: Defects Near End of Scan	85
Figure 8.5: Comparison of Adjacent Indent Defects	85
Figure 9.1: Centerline Depth (2D) vs. Average Depth (3D).....	89
Figure 9.2: Centerline Sidewall Length (2D) vs. Sidewall Area (3D).....	89
Figure 9.3: Centerline Sidewall Angle (2D) vs. Average Sidewall Angle (3D).....	90
Figure 9.4: Centerline Profile Area (2D) vs. Indent Volume (3D).....	90
Figure 9.5: Multiple 2D Parameters Used to Evaluate Indent Volume	91
Figure 9.6: Multiple 2D Parameters Used to Evaluate Sidewall Area	92
Figure 9.7: Concrete Prism Schematics	93
Figure 9.8: Transfer Length	94
Figure 9.9: Concrete Prism Crack Map	94
Figure 9.10: Transfer Length vs. 3D Indent Parameters (Constant Release Strength).....	96
Figure 9.11: Transfer Length vs. 3D Indent Parameters (Variable Release Strength)	97
Figure 9.12: Transfer Length vs. 2D Indent Parameters (Variable Release Strength)	98
Figure 9.13: Cracked Prism	99
Figure 9.14: Crack Length Correlation (Tucson Aggregate).....	100
Figure 9.15: Crack Length Correlation (Granite Aggregate).....	101
Figure 9.16: Crack Length Correlation (Pea Gravel Aggregate).....	102
Figure 9.17: Crack Length Correlations (All Aggregates)	103
Figure 10.1: Measured Variations of Indent Pitch.....	104
Figure 10.2: Measured Variations of Indent Centerline Depth.....	105
Figure 10.3: Measured Variations of Indent Length (Centerline)	106

Tables

Table 1: ASTM A881 Wire Indent Dimensions	11
Table 2: ISO 16120 Wire Indent Dimensions (Indent Type T4)	18
Table 3: Wires Included in Study	60
Table 4: Cover Testing Wire Indentation Data (Means)	64
Table 5: Cover Testing Wire Indentation Data (Standard Deviations).....	64
Table 6: Concrete Crosstie Types	71
Table 7: Concrete Crosstie Extracted Wire Types.....	73
Table 8: Crosstie Wire Indentation Data	75
Table 9: Machined Wire Identification	79
Table 10: Machined Wire Indentation Data.....	80
Table 11: Verification of Sidewall Angle Extraction Algorithm.....	81
Table 12: Potential Correlations of 2D and 3D Parameters.....	88

Executive Summary

The Indent Profiling System is a non-contact laser-based device capable of measuring the indentation geometry of steel wires used in the manufacture of concrete railroad ties. It was designed to address the shortcomings of the current manual methods used to assess the quality of indented wires. The manual methods provide insufficient sample sizes due to the time-consuming nature of the measurements, furthermore, the collected information is challenging to extract in a repeatable manner using manual procedures. The indent profiling system remedies these issues by analyzing all of the unique indents formed by the indent rollers during the manufacturing process and extracting the geometric features in a repeatable, accurate manner.

During phase I of this project the key objective was to design and implement an automated indent profiling system to produce unbiased, statistically-relevant sample sizes. After motion control and data acquisition of the system was implemented, calibration techniques and data manipulation steps were developed to enhance the quality of the data being received. Then, the system would be applied to measure specimens of known geometry to verify the correct and reliable operation of the system and quantify expected measurement uncertainties.

Phase II of the project involved the application of the Indent Profiling System to measure the indent characteristics of a multitude of indented wires. A sampling of these wires would be from those used in modern industry, a subset would be wires that were extracted from historical crossties that had been in track for upwards of multiple decades, and another set of wires were created with known “machined indents” for use with system checkout. In conjunction with the transfer length and splitting propensity testing of concrete prisms for this project, the Indent Profiling System results were then used to extensively investigate which geometrical parameters of indented wires contribute most significantly, or detrimentally, to prestressed member performance criteria.

During the project, the Indent Profiling System proved its ability to accurately extract indentation geometry of the wires subjected to test. The calibration procedures and wire cast correction algorithms ensured that wire scans were generated with micron levels of precision. From these calibrated scans, the system could extract dozens of geometric parameters, analyzing hundreds of unique indents at a time. This allowed for manufacturing variations to be analyzed from indent to indent and on a row-by-row basis. Furthermore, the results from the Indent Profiling System were correlated with empirical performance characteristics of prisms constructed using the same wires. Strong correlations were developed that related indentation features with wire-concrete performance criteria such as transfer length and splitting propensity. The Indent Profiling System represents a departure from current manual measurement methodologies, collecting quantities of data that can adequately characterize the manufacturing process and has been used to further the understanding of how indentation geometry directly contributes to desirable performance characteristics.

1. Introduction

The main focus of the research effort reported here is on the creation of an automatic non-contact laser based indent profiling system for the purpose of rapidly assessing geometrical characteristics of indented wires used in the manufacture of prestressed concrete. The process of measuring geometrical indent characteristics by traditional means is a time consuming process which severely limits the frequency of testing and prevents statistically relevant sample sizes.

In parallel with the concrete prism transfer length and splitting propensity testing conducted in conjunction with this project, this system was used to identify which indent characteristics were directly related to important performance criteria in prestressed concrete ties. The effects of dozens of different wires and indent geometries were evaluated using this system. During the testing phase, these same wires were used to evaluate more than one hundred prestressed concrete prisms. The ability to obtain detailed indent geometry characteristics quickly was essential in order to provide enough data to establish statistically-relevant correlations with concrete prism results. This report details the automation of this indent profiling system and its application to measure geometric characteristics of indented steel wires and how these characteristics correspond to critical performance criteria in prestressed members.

1.1 Background

Prestressed concrete railroad ties have become increasingly popular in the United States, and are an essential component for high speed railway lines. In order for these prestressed concrete ties to function adequately over their expected service life, the ties must be designed to withstand the extremely large impact loads applied near the member ends. In order to optimize the design of the ties, the prestressing force must be fully introduced into the railroad tie at a location well before the rail load is applied. The length required to transfer the prestress force into the concrete member is referred to as the “Transfer Length” [1],[2],[3].

Extensive research has been conducted by the project team during the past 6 years to establish the concrete strength and prestressing steel properties that must be provided to ensure that transfer lengths will be shorter than the distance from the end of the tie to the rail seat location [4]-[33]. In the FRA-funded research project titled “Quantifying the Effect of Prestressing Steel and Concrete Variables on the Transfer Length in Pretensioned Concrete Crossties,” the researchers were able to successfully identify the key wire indent geometry features that correlate with transfer length for a given concrete strength, specifically the indent volume and the indent sidewall area. This has included not only a systematic investigation of the influence of the detailed geometrical characteristics of the prestressing steel wires [6],[11]-[13],[16]-[17][19][24][26], but also the study of other variables such as release strength and concrete mix. Furthermore, of critical importance to this research has been the development of a rapid non-contact optical method of assessing transfer length [5][7][10][14][15][20],[23][27][34][35]. The goal of this work has been the practical development of a robust, accurate system that can be used to measure transfer length as a quality control parameter.

Furthermore, the previous research found that certain indent characteristics were common in concrete railroad ties where splitting along the prestressing tendon has occurred [36]. The characteristics common to ties that have experienced splitting include a larger indent depth along with a shallow indent sidewall angle.

While the findings in the previous research program are very helpful to understanding concrete tie behavior, there still does not exist the means to eliminate the risk of prestressing wires with undesirable indent characteristics from being utilized in the manufacture of ties. This is primarily due the fact that there has not been a viable means to automatically inspect the indented-wire indent properties without a significant time delay between sampling and measurement results.

With advancements in laser-based measurement tools, there now exists the technical ability to be able to inspect the key wire indent parameters that influence tie performance in a matter of minutes. Hence, there is an unprecedented opportunity to be able to directly implement the existing research findings to prevent wires with harmful indent characteristics from being installed in concrete railroad ties. Automated measurement of the indent characteristics would be most beneficial at the steel wire drawing facility, so that wire indent quality can be monitored in an ongoing basis and necessary process adjustments made so that wires with poor indent characteristics are never shipped to concrete tie producer plants.

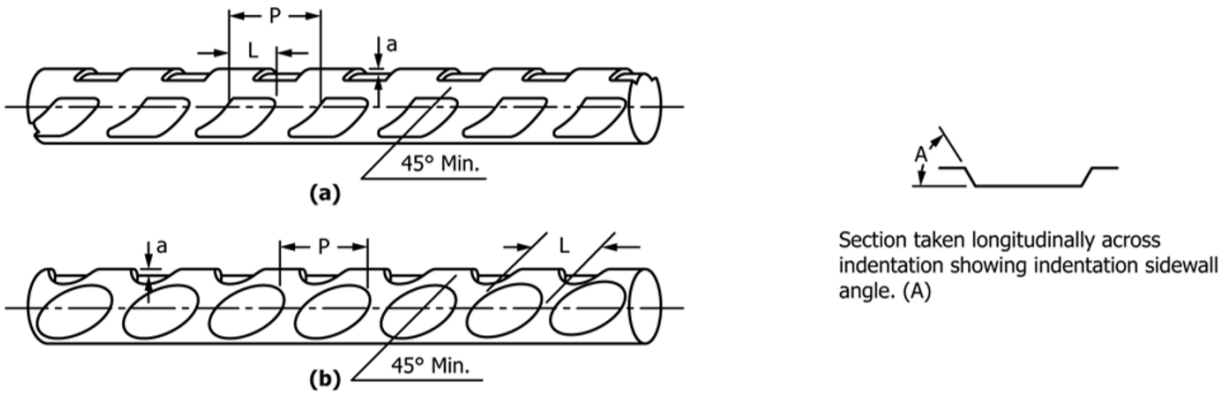


Figure 1.1: ASTM A881 Geometrical Feature Requirements

The current standard for prestressing steel reinforcement wire design is ASTM A881-2016. This document specifies the requirements for the material, mechanical properties, indentation geometry, packaging and other general requirements of the reinforcement wire. This includes the indent geometry requirements for the indent edge wall angle (A), indent depth (a), indent length (L), and pitch/period (P). The dimensions are illustrated in the Figure 1.1.

It is also stated that the indent will be orientated at an angle of at least 45° . Table 1 shown below indicates acceptable values for two wire types within the standard. The 5.32mm (.2094in) diameter wire was within the scope of the previous research.

Table 1: ASTM A881 Wire Indent Dimensions

Nominal Wire Diameter, in. [mm]	Depth, a , in. [mm]	Nominal Length, L ,		Nominal Pitch, P ,	
		in. [mm]	[mm]	in. [mm]	[mm]
0.198 [5.03]	$0.005 + 0.001, -0.002$ [0.13 + 0.02, -0.05]	0.138 ± 0.02	[3.5 ± 0.5]	0.217 ± 0.02	[5.5 ± 0.5]
0.2094 [5.32]	0.0045 ± 0.0014 [0.115 ± 0.035]	0.138 ± 0.02	[3.5 ± 0.5]	0.215 ± 0.011	[5.46 ± 0.29]

The standard does not provide a detailed requirement as to how the indents shall be measured. This is left to be decided amongst the purchaser and supplier. The current standard does not state which geometrical features of the wire contribute the greatest to the wires performance. The

current methods of using depth micrometers and probes do not analyze the full non-uniform surface profile of the indents. As such, geometrical features such as the indent edge wall angle are not constant and can vary significantly throughout the indent feature. Furthermore, extraction of these features is very time-consuming.

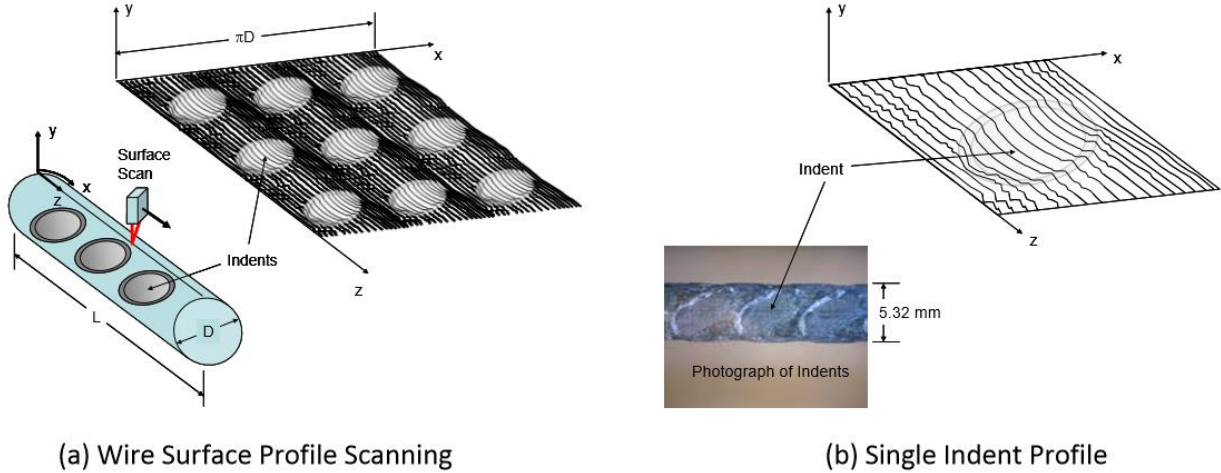


Figure 1.2: Schematic of Indented Wire Measurement (Point Laser)

Such features as indent pattern shape, depth of indent, lateral dimensions of indent, and tilt of indent, have been shown to directly affect bond. Having detailed indent surface profile data has enabled researchers to test out different transfer length and pullout correlation scenarios with a variety of potentially important indent parameters (beyond the gross indent parameters measured under ASTM A-881 standards), and establish which has the most influence as well as the relative extent of the influence on bond quality. This was accomplished by using readily available laser-based surface metrology equipment to obtain surface scans of samples of the different wires and indent patterns, containing one or more indents. The previous system developed a detailed digitized surface profile mapping of the wire indent features, such as is depicted in Figure 1.2. To the degree possible, the mapping was extended over multiple indents such as is shown in Figure 1.2(a), and it was also possible to focus on a single indent at a time for isolation of key geometrical features as suggested in Figure 1.2(b).

Since it is clear that all indents will not be identical, multiple indents are required to provide a valid statistical sampling of the geometrical characteristics. Furthermore, it is clear that the indent rollers in Figure 1.3(a) have a “repeat” associated with the number of teeth around their circumference as seen in Figure 1.3(b). The earlier system was not capable of addressing this “repeat cycle” because of the large amount of time required. Furthermore, the scanning laser sensor system utilized only a point-wise measurement of the wire surface position, as suggested in Figure 1.2(a).

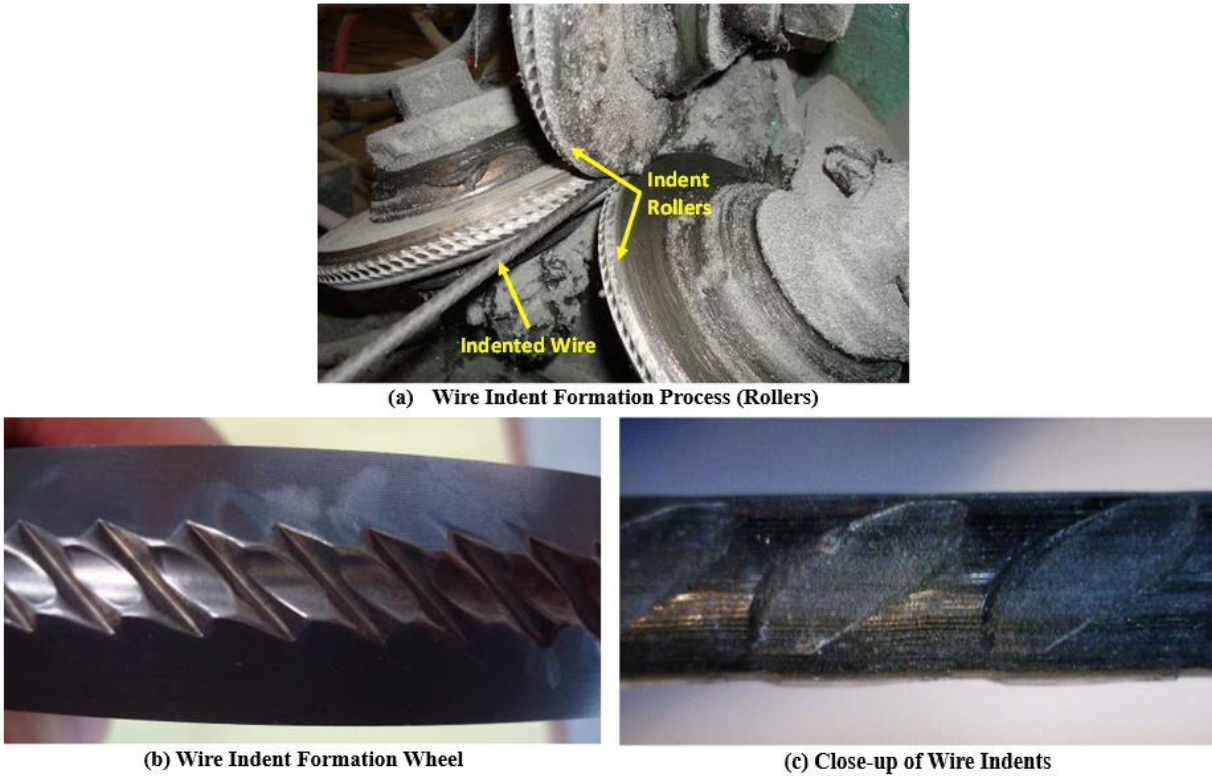


Figure 1.3: Manufacture of Prestressing Wire Indents

1.2 Objectives

With respect to the development of the non-contact indent profiling system, the research can be divided into two primary phases. During phase I of this project the key objective was to design and implement an automated indent profiling system to produce unbiased, statistically-relevant sample sizes. After motion control and data acquisition of the system was implemented, calibration techniques and data manipulation steps were to be developed to enhance the quality of the data being received. Then, the system would be applied to measure specimens of known geometry to verify the correct and reliable operation of the system and quantify expected measurement uncertainties. The main aspects of this phase are summarized below.

- (1) Selection of components to meet desired measurement accuracies, specimen sizes, and system automation. Multiple non-contact measurement systems were investigated for integration into the system.
- (2) Assembly and automation of the LabVIEW based Indent Profiling System capable of rotating a wire specimen and axially traversing to capture a full repetition of indent geometry. This was accomplished by the Advanced Manufacturing Institute (AMI) at Kansas State University.
- (3) Development and testing of the data acquisition software and calibration steps to mitigate sensor skew. Furthermore, software based elimination of off-bore rotations would be

introduced to enhance data acquisition quality. Mesh manipulations steps would then be used to refine the resulting scans prior to data processing.

- (4) Implementation of algorithms to join scan segments, isolate individual indents, and extract useful geometrical parameters. Separate processing software would be developed so that the processing can be done independently of the data acquisition process.
- (5) Analysis of the scanning system results. A checkout of the system would be done with specimens of known geometry to verify the accurate operation of the system and to get a grasp on the resolution that the indent profiling system is capable of.

Phase II of the project involved the application of the Indent Profiling System to measure the indent characteristics of a multitude of indented wires. A sampling of these wires would be from those used in modern industry, a subset would be wires that were extracted from historical crossties that had been in track for upwards of multiple decades, and another set of wires were created with known “machined indents” for use with system checkout. In conjunction with the transfer length and splitting propensity testing of concrete prisms for this project, the Indent Profiling System results would then be used to extensively investigate which geometrical parameters of indented wires contribute most significantly, or detrimentally, to prestressed member performance criteria. The main aspects of this second phase are show below.

- (1) Data acquisition of a multitude of indented wires. Focusing on the “chevron” style indent used predominately in industry; multiple modern, historical, and custom fabricated wires were assessed by the system. Extensive statistics pertaining to geometrical parameters would be collected for later use in correlations.
- (2) Deliver ASTM A881 and ISO 16120 reports of wires scanned by the system to comply with current measurement standards used by industry. Once the geometrical parameters are known that influence important performance criteria, motivation will be discovered that highlights the deficiencies of current indented wire measurement standards.
- (3) Testing of the statistical significance of the collected data, row by row indent variations of the prestressing steel wires, and indent pattern repetition detection of the profiling system. These results are then compared with data extracted by current indent measurement standards which collect much smaller quantities of data.
- (4) Correlate captured indent geometrical features against empirical data such as transfer length and total crack length of prestressed concrete specimens tested in conjunction with this research project and prior projects to determine which indent features contribute most significantly to performance.

1.3 Organization of the Report

Chapter 2 presents the current methods for measuring indent geometry and the inherent difficulties and shortcomings associated with them. This provides the motivation for the development of the optically based indent profiling system used in conjunction with the extensive transfer length and splitting propensity measurements conducted in this research project.

Chapter 3 highlights the development of the indent profiling system. Comparisons are made with the earlier version of the wire scanning technology and the significant advantages of the line scan laser are discussed.

Chapter 4 introduces the interface layout of the indent profiling system. The basics of operation are provided, including movement control of the wire specimen being scanned, and data processing settings along with data visualization is presented.

Chapter 5 emphasizes the need for sensor calibration and software elimination of off-bore rotations. Initial checkout scans are then compared to “master” specimens of known dimensions to verify the accuracy of the calibrations.

Chapter 6 provides the scan manipulation steps and algorithms that are used to extract useful indent features. The processing procedure is generalized enough to allow for any arbitrary indent geometry to be processed in the future.

Chapter 7 overviews the data collected via the indent profiling system for a variety of wire types. The high level overview of the data is provided, the important features are highlighted, the statistical validity is discussed, and comparisons are made with specimens of known indent geometry.

Chapter 8 shows the use of the collected indent geometrical parameters in correlations to determine which features contribute the most to prestressed member performance. Specifically, the indent data is compared with the extensive transfer length and splitting propensity measurements conducted in this project and previous projects to better understand which indent parameters contribute to desirable crosstie performance.

Chapter 9 presents the capability of the indent profiling system to detect the repetition of the indent rollers used to manufacture the indented wires. This represents the ability of the system to measure the entire pattern of the indented wires during the manufacturing process and showcases the statistically relevant sample sizes that the system is capable of.

Chapter 10 discusses the use of Go/No-Go criteria for determining if a wire should be subject to rejection. The use of the developed correlations or mutual agreement between the producer and the consumer can be used to assess the validity of the produced wire.

Chapter 11 presents the conclusions, the high level takeaways, and the recommendations from the data that the indent profiling system has provided. The need is highlighted for more in-depth indent geometry measurement standards that focus on the features that relate most strongly to performance criteria.

2. Methods of Indent Geometry Measurement

2.1 ASTM A881

The measurement standard most commonly used in industry in the United States for indented, low-relaxation steel reinforcement wire design for use in prestressed concrete is ASTM A881-2016. This standard documents the requirements for the material, mechanical properties, packaging, other general characteristics, and most importantly, the requirements for the indentation geometry of the wire. The material properties to be measured by ASTM A881 include tensile strength, load at one percent elongation, elongation after fracture, and a bend test. However, the material properties specified by the standard are largely irrelevant to the scope of this report.

The required geometrical parameters specified by this standard are directly applicable to two specific indentation types, chevron and elliptical. It further specifies general criteria that the indented wires must meet: the indentations shall be in three rows that are equally spaced about the circumference of the wire, with one row of indents inclined oppositely in direction to the other two. A dictation on the quality of the indents is also made, pitch and shape should be consistent with no more than 10% being malformed across a two foot segment of wire, judged visually. Criteria for what counts as a deformity is mutually agreed upon between the producer and consumer.

Furthermore, it includes the indent geometry requirements for the indentation sidewall angle (A), indent depth (a), indent length (L), indent pitch/period (P), and orientation angle. The dimensions are illustrated in Figure 1.1. The allowable depth (a), nominal length (L), and nominal pitch (P) are allowed to fall in a range depending on the nominal diameter of the wire, the particular values are specified in Table 1. Indentation sidewall angle is measured along the center of an indent. The maximum and minimum allowable values, along with the measurement procedure to obtain the parameter, is once again left to a mutual agreement between the producer and consumer. Indent depth is found by taking the average of six or more random indentations measured at the deepest depth. Additionally, the requirement is made for the orientation angle to be no less than 45° , but no provisions are made to state the method of measurement used to determine such a parameter.

This measurement standard suffers from a variety of shortcomings. First, it does not provide detailed requirements as to how the indentations shall be measured or even how many are to be measured. These decisions are left to be made amongst the producer and consumer. Second, the standard does not state the resolution of the measurement devices used; a depth micrometer with a resolution of 0.001" (25.4 μ m) would be a poor choice for a shallow indent with a 60-80 micron depth. Third, where are the critical measurement points to be located, and how are parameters such as orientation angle measured in a reliable way? Is orientation angle determined visually? Which reference point is used to determine maximum depth since the height along the edge of the indent varies from location to location? What constitutes as a deformed indent? When is a deformity severe enough to be detrimental to the performance characteristics of the wire?

The current methods of using depth micrometers and probes do not fully analyze the complete non-uniform surface profile of the indents. Additionally, geometrical features such as indent sidewall angle are not constant and are varying throughout the indent feature. Furthermore, the extraction of these features is time consuming. Finally, perhaps most importantly, the current

standard does not state which geometrical features of the wire contribute most significantly to the wires performance. Such features as indent volume, indent sidewall angle, pattern shape, indent depth, and indent width have been shown to directly affect transfer length and splitting propensity, but many of these parameters are not included in ASTM A881.

2.2 ISO 16120

Another measurement standard which is commonly used to assess prestressing steels is ISO 16120. It covers the general requirements for prestressing steel wire, strands, and rods. Similarly to ASTM A-881, this standard provides criteria that the steel must satisfy along with the measurement of indent geometry that is within the scope of this report. The indentation characteristics which are subject to measurement are as follows: indent length (L), indent depth (a_{\max}), indent spacing (c), indent distance (e), average diameter, and ovality. The geometrical characteristics apply to the “chevron” indent patterns that are summarized in Figure 2.1.

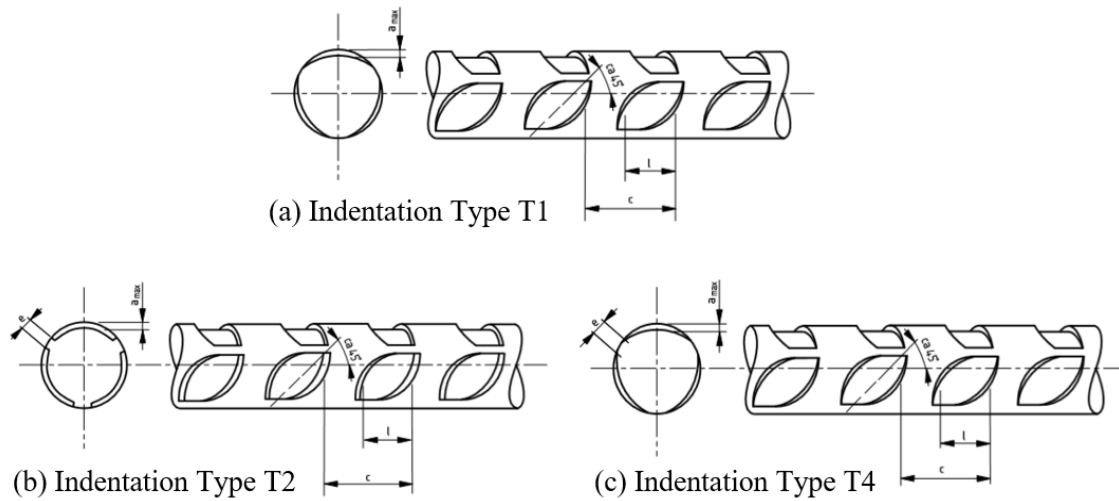


Figure 2.1: ISO 16120 Geometrical Feature Requirements

ISO 16120 is similar to ASTM A881 in many regards. One line of indentations shall be at a contrary angle to the others, additionally, the nominal depth, length, and spacing must fall in a range of allowable values based on wire diameter. The example dimensions for the common chevron indentation of type T4 are illustrated in Table 2. Nominal diameter (d) is measured by traditional means, in which a wire of a given length and mass yields the average diameter since the density of steel is a known quantity. Ovality is evaluated by computing the difference between the maximum and minimum diameters in any section of the wire. Further guidance for the measurement of indent length, depth, spacing, and distance are not provided by the standard in any capacity.

Table 2: ISO 16120 Wire Indent Dimensions (Indent Type T4)

Dimensions in mm						
Nominal wire diameter d	Indentation depth a_{\max}			Length l	Spacing c	Sum of indentation distances $\sum e$
	Range of nominal values		Tolerance on chosen nominal depth			
	from	to				
≤ 5	0,06	0,13	$\pm 0,03$	$3,5 \pm 0,5$	$5,5 \pm 0,5$	$\sum e \leq 0,2\pi \cdot d$
> 5 to 8	0,09	0,16	$\pm 0,04$	$5,0 \pm 0,5$	$8,0 \pm 0,5$	
> 8 to 11	0,10	0,20	$\pm 0,05$	$5,0 \pm 0,5$	$8,0 \pm 0,5$	

Unfortunately, ISO 16120 suffers the same shortcomings of the previously discussed standard. Little guidance is given in the measurement process to ensure reliability and accuracy of the geometrical features. Determination of critical measurement points is not provided and there is no discussion about the number of observations necessary to determine if a wire is consistent during the manufacturing process from indent to indent. Furthermore, it does not identify which geometrical parameters are significantly related to performance criteria and does not necessarily prevent wires with poor indent characteristics from being shipped to concrete tie producer plants.

2.3 Early Wire Scanning Measurement Technology

To measure indent geometry features in greater detail, a non-contact method based on displacement laser technology was developed at Kanas State University prior to the current FRA research effort [37]. The operation of the system and the scanning process it used is illustrated in Figure 1.2 which shows a point laser traversing along the length of an indented wire to capture line scans of the complex surface features. A depiction of an early version of the wire scanning measurement technology is contained in Figure 2.2.

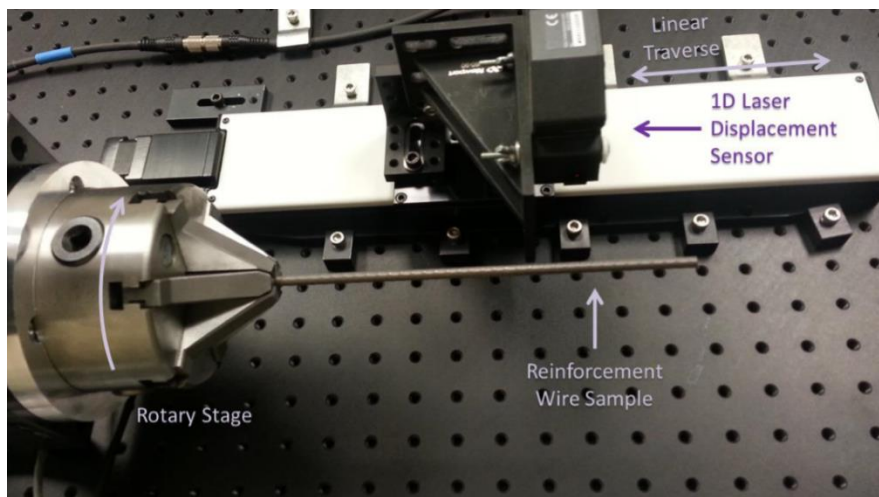


Figure 2.2: Early Indent Profiling Technology

Steps were taken to minimize mechanical misalignment of the system, an important process when measurements on the order of microns are being conducted. Additionally, great care

needed to be applied to correctly remove the cast of the wire “bow” and minimize off-bore rotations due to the large unsupported length of the wire. The system was comprised of a rotary stage and a linear stage to provide automation control. While the system had very high precision due to the use of a blue point laser, it did not come without disadvantages since traversing the length of the wire was a tedious process. The primary disadvantage of a point laser is implied in the name of the device; it can only measure a single point at a time. It took upwards of 10 hours to scan and process a segment of wire of only one inch in length, this constitutes 9 full indents that are included in single scan reliably for a 5.32mm wire. A significant improvement in measurement technology would be necessary to reduce scan times and make the system practical to implement in a production environment.



Figure 2.3: Early Scan of WF Wire Type

An example of the high resolution that the early wire profiling system was capable of is highlighted in Figure 2.3. The uncertainty of the displacement laser measurement was a fraction of a micron leading to noise free scans. From the high resolution scans, algorithms were developed to extract useful geometrical features such as indent depth, pitch, length, sidewall angle, width, volume, sidewall area, orientation, and more. Once the indent features were extracted, sets of parameters were successfully correlated with transfer length measurements on concrete prisms comprised of the same wires that were subjected to scanning. It was found that certain indent features such as indent volume and indent sidewall area had a significant influence on performance criteria, namely transfer length. This early wire scanning system was the precursor to the one that is the primary focus of this report and is the original device that provided the impetus to reevaluate current wire measurement standards to more accurately reflect the parameters that are directly related to indented wire performance.

2.4 Insufficiencies with Current Methods

In summary, the following insufficiencies with current measurement standards pertaining to indented steel wires are as follows. First, common measurement standards such as ASTM A881 and ISO 16120 do not identify which geometrical parameters contribute most significantly to the performance of the wire. Second, the measurement procedures for obtaining the required indent features for the standard do not provide repeatable, reliable results between different operators. Often the measurement process is determined by mutual agreement between the producer and the consumer and is not a standard measurement that can be compared with other manufacturing processes or products. Third, determining indent geometry for the current measurement standards is a laborious endeavor; it is time consuming and does not integrate easily into a production environment. Often, wire samples are sent out to measurement labs only when

process changes have been made to check for compliance with the measurement standards. This is hardly ideal since the manufacturing process of indented steels wires varies on an hourly basis as the indent roller teeth wear down, rather than on a sparse interval as the testing schedule implies. Finally, sample sizes are not statistically relevant due to the time it takes to collect the data and the inherent uncertainties with the current measurement processes. The low sample sizes fail to capture the intricacies of the manufacturing process since no two indents are identical and significant variance can be seen across neighboring indent rows.

The early wire scanning technology took great strides to address the insufficiencies with the current measurement standards and attempted to more accurately understand the relationship between geometrical indent features and favorable performance criteria. The system could collect high resolution data and extract a variety of indent features above and beyond those dictated by current measurement standards. Some key indent features were found that corresponded with desirable wire performance. Additionally, it could extract features in a reliable, predictable manner across a wide variety of tested wires. However, the system was too slow to be a device that would be applicable to a production environment and mostly found use as a research tool. The system could not collect statistically relevant sample sizes that accurately characterize the manufacturing process of the wires due to the considerable time it took to operate.

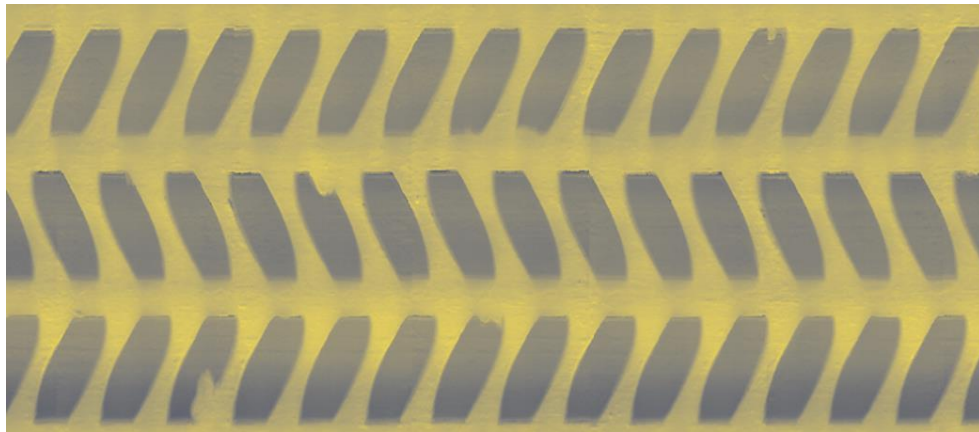


Figure 2.4: Indent Profiling System Scan

A device is needed that has the desirable capabilities of the early wire scanning system and addresses the majority of its faults. Such a device is described in great detail in the remainder of this report. The indent profiling system that was the direct result of this research effort is significantly faster and collects statistically relevant sample sizes. A scan from the indent profiling system can be viewed in Figure 2.4 in which a 26 inch length of wire was scanned comprised of over 330 indents, coincidentally, it is the same wire from Figure 2.3. This device will prove to be a valuable research tool and provide the necessary data to evaluate which indent features are important to measure and how those same features correspond to wire performance.

3. Development of the Indent Profiling System

The desire to create a more capable wire scanning system led Kansas State University researchers to partner with Nucor-LMP (an indented prestressing wire manufacturer) and the Advanced Manufacturing Institute (a company that specializes in prototype development) in order to create a non-contact wire indent profiling system to provide an unbiased evaluation of the indent characteristics that are critical to the performance of concrete railroad ties. Physical measurements of the wire indentations will be obtained by using a 2-dimensional line laser that is focused on a wire as it rotates about its longitudinal axis. Then, the key indent parameters that have been previously shown strongly correlated with transfer length and splitting potential [37] will be automatically determined from the resulting scan.

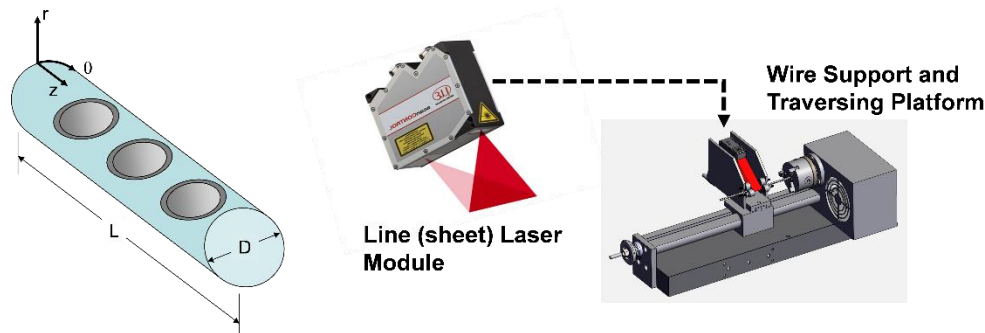


Figure 3.1: Schematic of Proposed Indent Profiling System

A simplified schematic representation of the proposed system is illustrated in Figure 3.1. Rotation of the wire underneath the sheet laser results in the effective “unwrapping” of the indent profile. This section reviews the development of the Indent Profiling System.

3.1 Initial Specifications

The ability for wire manufacturers to ideally implement the wire indent research findings will require more statistical data to be collected about indent variations along the wire length, so that proper tolerances for the key indent parameters can be established. Thus, a system is needed that can assess the multitudes of wire sizes and indent features that are common in industry. Therefore, it is desirable that the system is able to measure wires with nominal diameters ranging from 4mm to 12mm, these constitute a significant portion of wires that are produced. Additionally, the system should be able to measure wires of varying depth; shallow indents are on the order 50 μ m and the deepest indents that can be made in practice are nearly 300 μ m. Characterization of the entire indent pattern formed by the indent rollers is a primary goal of this research in order to collect statistically relevant sample sizes and obtain a better grasp on the manufacturing intricacies of the indented wires. Indent rollers are typically 8 inches in diameter, therefore, the system should be capable of measuring 25 inch (640mm) lengths of wire at a minimum. Finally, quick scan acquisition leads to the requirement of a line based scanner; 20 μ m spacing between points and resolutions at or below 2 μ m are likely obtainable. The desired initial system specifications are specified in the list below.

- (a) Range of Indent Depth (50-300 μm)
- (b) Resolution of Local Depth (2 μm)
- (c) Range of Wire Diameters (4.5-12 mm)
- (d) Optical Line Sensor (2 μm resolution, 1280 points over 25mm width)
- (e) Wire Surface Roughness (10-15 μm)
- (f) Length of Carriage Travel (30 inches)

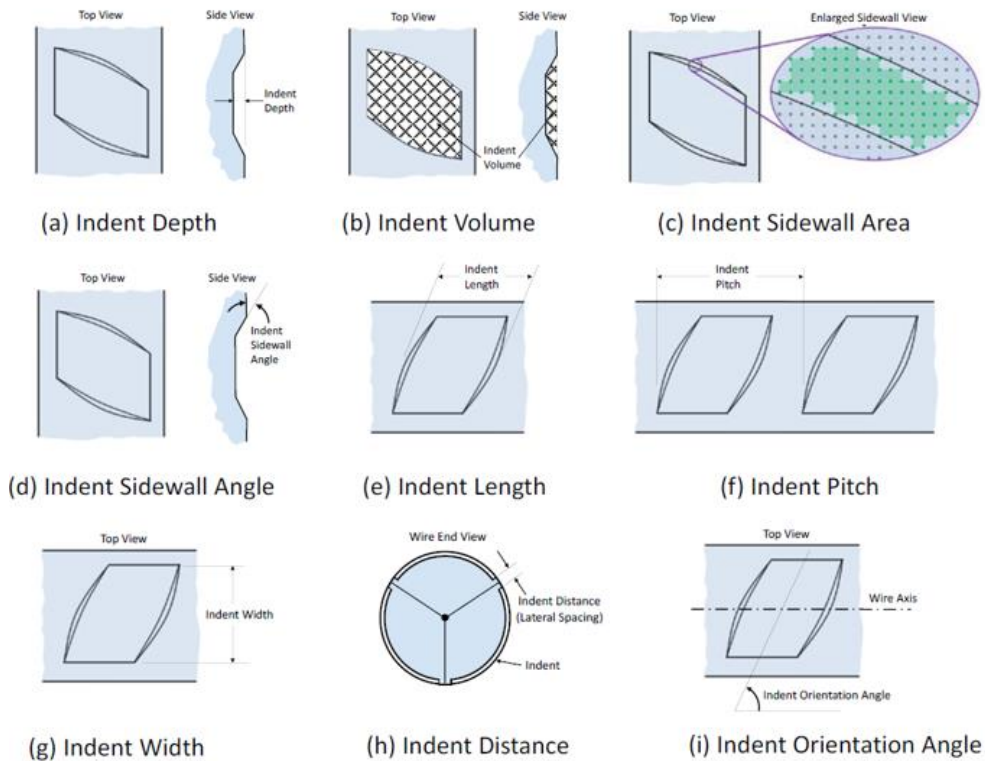


Figure 3.2: Key 3D Wire Indent Geometrical Features

The primary 3D indent features to be measured by the indent profiling system are given below and are illustrated in Figure 3.2. Note that the specific geometrical features required to be measured by ASTM A881 and ISO 16120 are identified in this list. Additionally, the list of measured features includes parameters that have been identified from previous research to influence transfer length and splitting propensity and may be critical quality control parameters. The indent parameters to be captured along with targeted minimum uncertainties are listed below.

(a) Indent Depth	[3 μm]	(ASTM A881, ISO 16120)
(b) Indent Volume	[0.020mm ³]	
(c) Indent Sidewall Angle	[2 degrees]	(ASTM A881)
(d) Indent Sidewall Area	[0.005mm ²]	(ASTM A881)

(e) Indent Length	[20 μ m]	(ASTM A881, ISO 16120)
(f) Indent Pitch	[20 μ m]	(ASTM A881, ISO 16120)
(g) Indent Width	[20 μ m]	
(h) Indent Distance	[20 μ m]	(ISO 16120)
(i) Indent Orientation Angle	[2 degrees]	(ASTM A881)

3.2 Component Selection

One of the primary requirements of the newly developed indent profiling system is to obtain statistically relevant sample sizes, as such, significant lengths of wire would have to be scanned in short order to be of use in a production environment. This required a departure from the displacement point laser that was used in the precursor to this system in favor of a line-scan based laser module. Line scan lasers offer a considerable increase in data acquisition rates in comparison to point lasers; increases in scan rates are on the order of multiple magnitudes. This is due to the fact that line lasers cast a sheet of light that is then received on an imaging array, thus allowing hundreds or thousands of data points to be collected in a single measurement. A blue line-scan laser (405nm) was selected for this high accuracy application. It is well known that laser uncertainty is related to the spot size of the laser, the point of greatest focus, and spot size is a function of laser wavelength. Higher frequency lasers have shorter wavelengths and are therefore capable of higher accuracies.

A commercially available laser line scan module was selected with a line width of 16mm, allowing it to view multiple indent profiles in a single measurement. The module can collect 800 points of data across the 16mm reference distance, with an average profile data interval of 20 μ m displacement between measurement points. Furthermore, it is possible to achieve repeatabilities on the order of a couple microns with the module when it is measuring a sufficiently diffuse surface. The previous wire indent measurement system utilized a pointwise laser and had a spatial resolution of a few tenths of a micron, the current light sheet system has a spatial resolution on the order of a few microns. However, the measurement process is greatly enhanced by the compromise between high spatial resolution and measurement speed. Additionally, prior research indicated that the extreme resolutions of the previous system was unnecessary as far as the measurement of indented wire geometry was concerned [37].

Stepper motors and a small lathe chassis were selected to provide the automation of the system. Motion control of the rotation of the wire and the translation of the lathe carriage allowed for wires of 30 inches in length to be completely scanned by the selected laser module. Due to the high spatial resolution that the laser line scan module provided, angular resolution of the wire rotation needed to be of similar or greater accuracy. For this purpose, an optical encoder with a maximum angular resolution of 7200 positions (line scans) per 360-degree revolution was selected. The high angular resolution that the optical encoder can provide allows for the “super sampling” of data to help eliminate noise due to localized reflections from the metal wire surface.

3.3 System Layout Overview

Once hardware selection was finalized, the construction of the Indent Profiling System took place at the Advanced Manufacturing Institute. The prototype design illustrated in Figure 3.1

was not far off from the final system design. A picture overviewing the layout of the constructed indent profiling system can be seen in Figure 3.3. The base component of the system is a small lathe chassis with a distance between centers of 30 inches and a swing of 4 inches. Two stepper motors provide automation control of the system. One motor is connected via pulley to the head of the lathe and provides rotation control of the wire rotation with an angular resolution of 0.05 degrees. The second stepper motor is attached to the lead screw of the lathe and controls the translation of the lathe carriage to sub-micron precision.

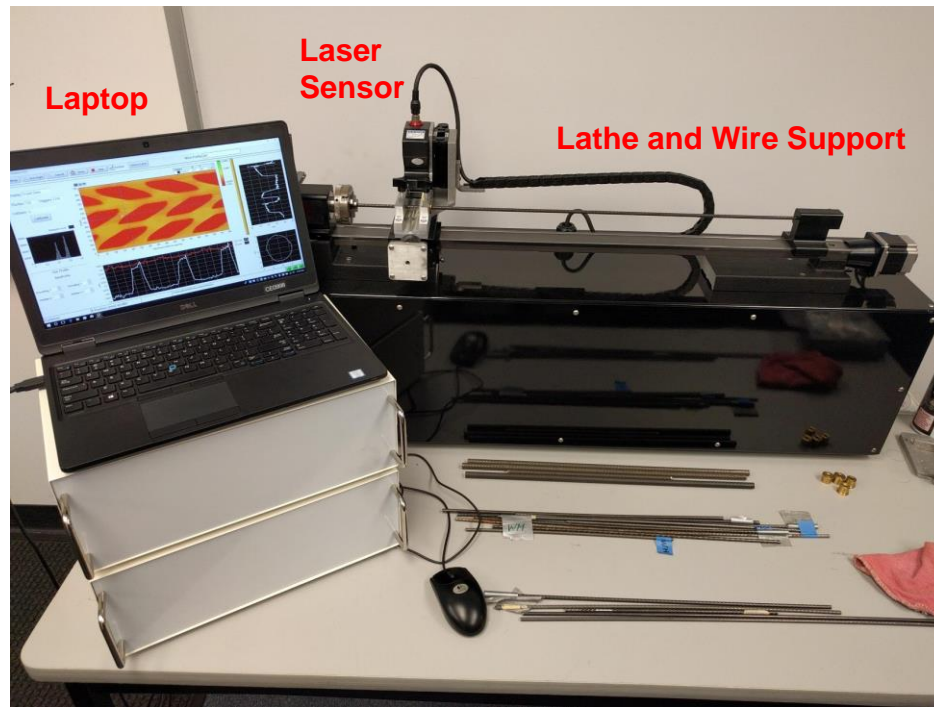


Figure 3.3: Layout of Indent Profiling System

An aluminum frame is mounted on the lathe carriage; to this frame the laser line-scan module is mounted with the laser sheet of the plane intersecting the bore axis of the lathe coincidentally. A precision linear translation stage separates the line scanner from the aluminum frame, the laser module is adjusted in elevation via a micrometer stage to align the sheet laser with the bore axis of the lathe. The aluminum frame houses brass bushings to help guide the indented wire along the bore axis of the lathe. It should be noted that the indented wire is spooled after manufacture, and all wires exhibit some bending. A close-up view of the scanning head, micrometer stage, and bushing guide for the alignment of the wire is shown in Figure 3.4. The bushings shown in Figure 3.4 helps to guide the wire, keeping it more aligned as the scanning operation traverses the entire length of the wire segment under test. Below the lathe and scanning assembly is a black metal box, to which the lathe is mounted. This box houses all of the laser controllers, motor controllers, power converters, and industrial computer equipment to operate the scanning system. A laptop or desktop is used to interface with the indent profiling system. This concludes the overview of the indent profiling system layout.

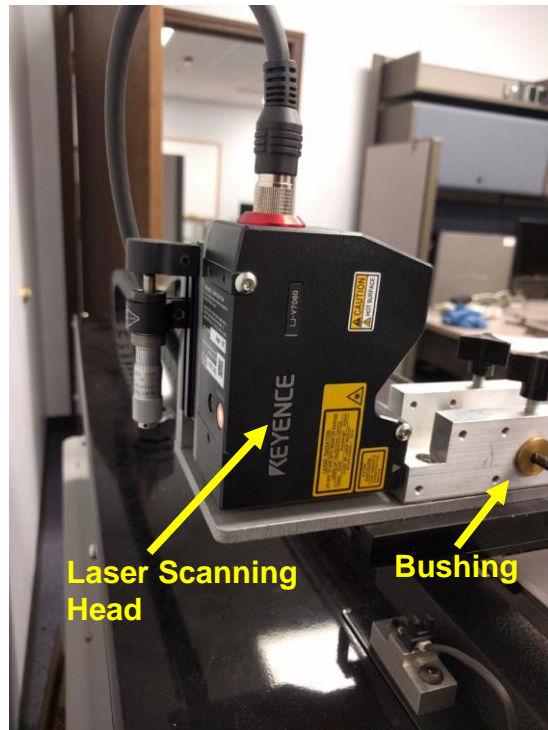


Figure 3.4: Close-up of Scanning Head and Bushing Guide

4. Scanning Process

This section summarizes the use of the software and its interface to scan a segment of indented wire and process the resulting geometrical features. The indent profiler can be generalized into two primary system components, the hardware and the software. The hardware is used in the data acquisition stage, and the software is used to capture, store, manipulate the scan files, and process the data. The operator interfaces with the scanning hardware and processes the data through the use of two separate programs, the first of which is a program used to acquire the detailed wire indent geometry via the line-scan module and lathe assembly and is aptly named “Wire Scanner”. This program is used to upload scanner settings to the laser head, name files, calibrate the scanning system, and capture scan segments for later processing. It is important to note that this program requires the computer to be physically tethered to the scanning hardware during the data streaming process and cannot be used as a standalone application.

The processing of the captured indent geometry provided by the indent profiling system is accomplished with a standalone application called “Wire Scan Reporter”. This program utilizes saved indent scans, and thus, can be used independently of the indent profiling system hardware. This program provides the facilities to align the generated scans if required, isolate individual indents, omit particular indents from inclusion in the final reports in the event of damage, extract useful indent geometrical features, and generate comprehensive reports of the processing results. This section is not intended to be a comprehensive user guide of the system, but rather, provides insight into how the indented wire geometry is scanned, how the data is stored, and how it is processed via the aforementioned programs. The wire featured in the interface examples in the following scanning process sections can be seen in Figure 4.1, the digital microscope image is of wire type WF.

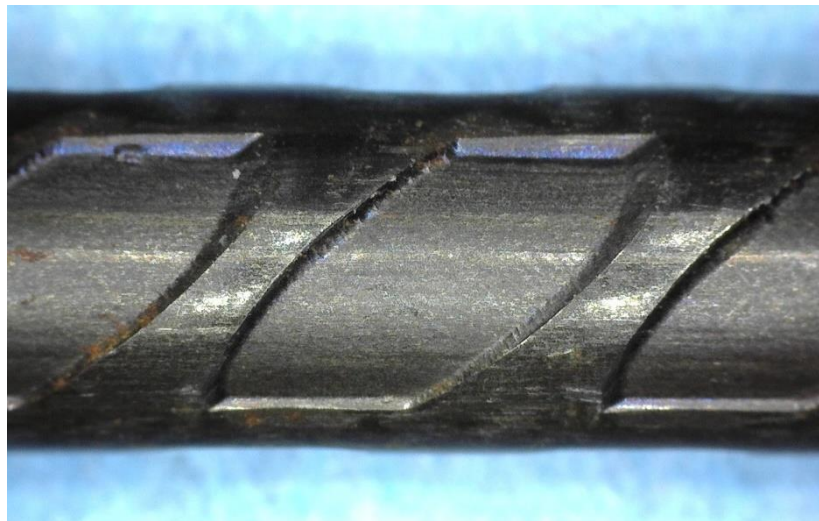


Figure 4.1: Wire Type WF

4.1 Interface Layout

As stated previously, the primary objective of the wire scanning program is to interface with the scanning hardware, receive the data stream, and visualize the data. It can also be used to calibrate the alignment of the indent profiling system, control the movement of the scanning system via automation or direct user command, change scanner settings, apply data filters to

refine the data, and visualize the data as it is being received. The interface layout of the wire scanner program is provided in Figure 4.2, this is the main screen that the user interacts with during the data capture stage.

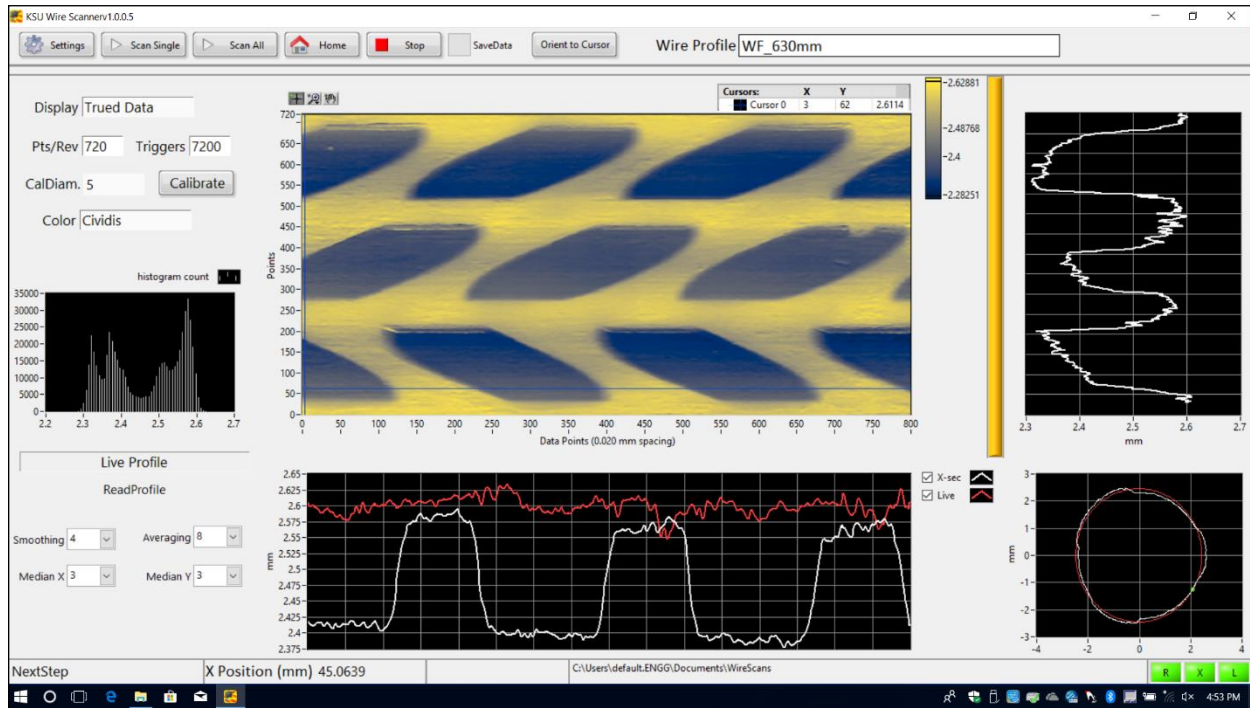


Figure 4.2: Wire Scanner Interface

The top bar of the wire scanner interface, read from left to right, contains the basic system settings, scan command buttons, homing and system stop control buttons, selection of data saving, orient to cursor command, and the wire profile naming box. The system settings allow the user to change the target velocity and acceleration of the rotation and linear movement control. Additionally, it can be used to set the desired scan width and total scan length of the specimen. Maximum scan width is limited to 16mm due to the design limits imposed by the line laser, and is nominally left at 15mm to omit scan noise at the edge of the laser sheet. Maximum scan length can be set to 640mm, or 760mm if the tailstock of the lathe assembly is removed. The Scan Single command will capture a single scan segment at the current carriage location, whereas Scan All will capture all of the scan segments to satisfy the scan length and scan width specified in the system settings (a scan width of 15mm and total scan length of 60mm will generate 4 scans). The Save Data checkmark box controls whether or not the data will be saved to the disk, and is typically disengaged when the system and the indented wire are being aligned. The Home button will cause the carriage to return to the point closest to the lathe chuck and will align the rotation of the lathe head to zero degrees, the Stop button aborts any commanded movement. The Orient to Cursor button is used after a Scan Single command is given and a captured scan is received; the user can then put a crosshair on the scan window that will be the newly desired origin of the scan, this is traditionally placed on the center of a rib between the indent rows. Finally, the Wire Profile naming box allows the user to specify the name of the scan, typically, this is the specimen identifier and the length of the scan.

In the center of the screen the most recently captured scan is displayed, also called the “heat-map” frequently throughout this report; it is worthy to note that this is a misnomer and it should be called a “height-map” instead. The height scale of the scan can be adjusted via the bar directly to the right of the scan display. The crosshair dictates which of the data profiles will be displayed in the black boxes both to the bottom and to the right of the scan capture “heat-map” window. In white, the bottom box shows the selected data profile along the longitudinal length of the wire, and the right box shows the measured circumferential profile that wraps around the wire. The red line in the bottom box shows the current signal from the laser head which can be at an arbitrary location with respect to the crosshair origin. The bottom right box displays the profile shape of the scan at the crosshair location, analogous to if the wire were to be sliced like a loaf of bread, this shape is typically trilobal for indented wires due to how the wire is squeezed by the indent rollers during manufacture.

On the left side of the interface is a histogram showing the binned height profile of the captured scan. After calibration corrections and wire bow removal have automatically been applied, this should form a bimodal distribution for an ideally manufactured wire, but typical manufacturing variations from indent row to indent row prevent this from being realizable. Figure 4.2 clearly shows that this is indeed the case with wire type WF; however, this will be the subject of detailed discussion in Section 7. The left side of the interface allows the operator to display the type of data (raw or trued), the number of desired line-scans per revolution (pts/rev), and the number of encoder pulses to trigger. Additionally, the user can select the height map coloring scheme. Detailed discussion of the calibration method will be elucidated in following section, Section 5. Furthermore, the filter settings, seen in the bottom left hand corner of Figure 4.2, will be elaborated on in the subsection directly following this one, Section 4.3.

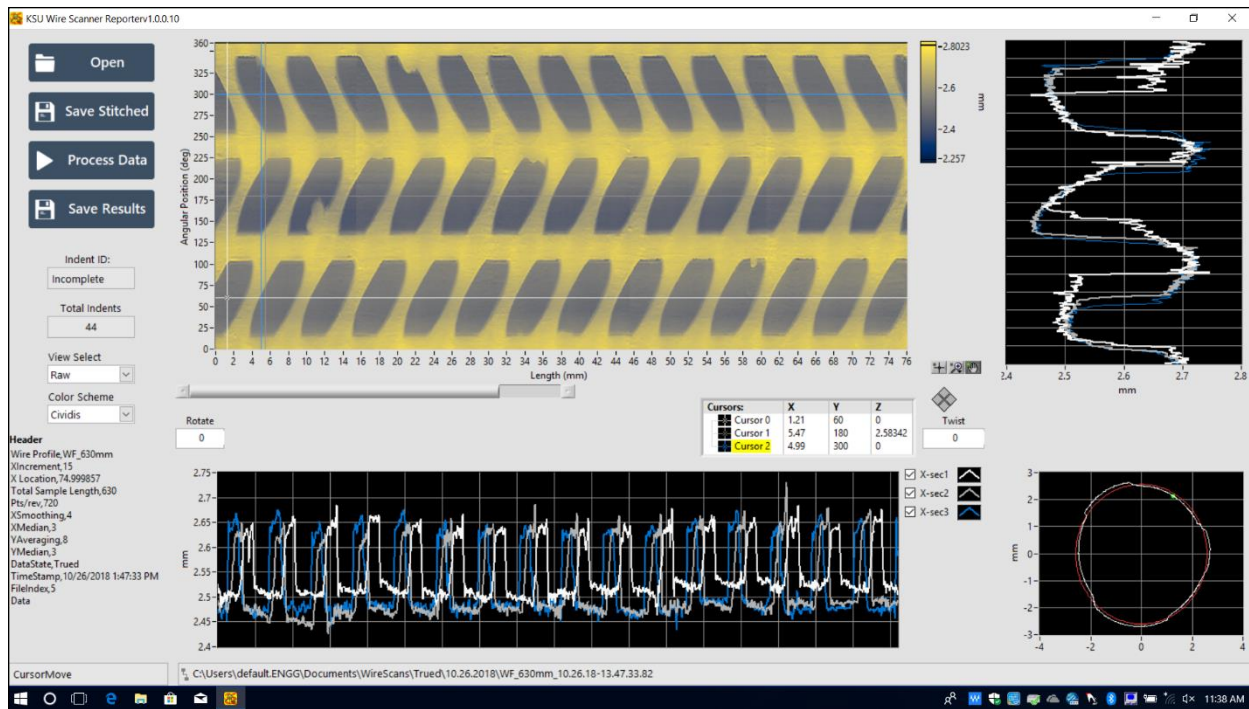


Figure 4.3: Wire Scan Reporter Interface

As stated at the beginning of the section, the processing application can be used independently of the indent profiling system hardware since it relies on loaded scans rather than a live data stream. The objective of this program is to load the captured scan segments, allow the operator to align the scan if necessary, and, most importantly, extract the indent geometrical features. The wire scan reporter program is similar in appearance to the previous program, the interface of the wire scan reporter program is provided in Figure 4.3 and Figure 4.4, wire type WF is the example specimen once again.

The heatmap display port, the data profile windows, and the wire profile window are similar in appearance to the previous program with the following exceptions. First, the heatmap viewport shows the combined scan segments that were loaded from the selected files and provides a scrollbar to view the wire along the length of the cumulative scan. Second, tree data crosshairs are provided so that the data profiles of all three indent rows can be visually compared; note how no red line is available to show the current laser line-scan reading since this application does not need to be connected to the indent profiling system to operate. Third, two boxes are provided for the operator to adjust the alignment of the scan if necessary (rotation and twist), some wires are produced with a 30° twist per 2 foot length, and thus, must be straightened out with software for the processing algorithms to successfully extract the indent feature geometry.

The left side of the interface contains the following information and commands, explained from top to bottom, and are summarized as follows. The Open button allows the operator to select which contiguous scan segments are to be loaded. Once loaded, the continuous, spliced scan is displayed in the heatmap viewport in the center of the screen. The Save Stitched button will save the continuous, spliced scan to file; this allows a single scan file to be loaded later instead of selecting a multitude of individual scans. Saving the entire continuous scan affords the luxury of being able to easily visualize the entire scan in secondary programs for data visualization. The Process Data button will extract the indent geometric features using the algorithms highlighted in Section 6: Process for Extracting Indent Geometry, the results are then placed in a report file. The Save Report button saves the generated report file to disk in the location where the scan files were loaded from. The Indent ID box shows which indent is currently selected by “cursor 0”, stating the indent row and indent number of the selected indent. The Total Indents box details the number of complete indents that were found via the indent isolation algorithm. View Select will show the currently loaded continuous scan on the main viewport if “Raw” is selected, the detected indent boundaries are shown when “Partitioned” is selected, and only the valid, complete indents if “Fitted” is selected which is only accessible after the data has been successfully processed. The color scheme of the height-map can once again be chosen. The Header information on the bottom left side of the interface will be the information that will be stamped at the beginning of the results file.

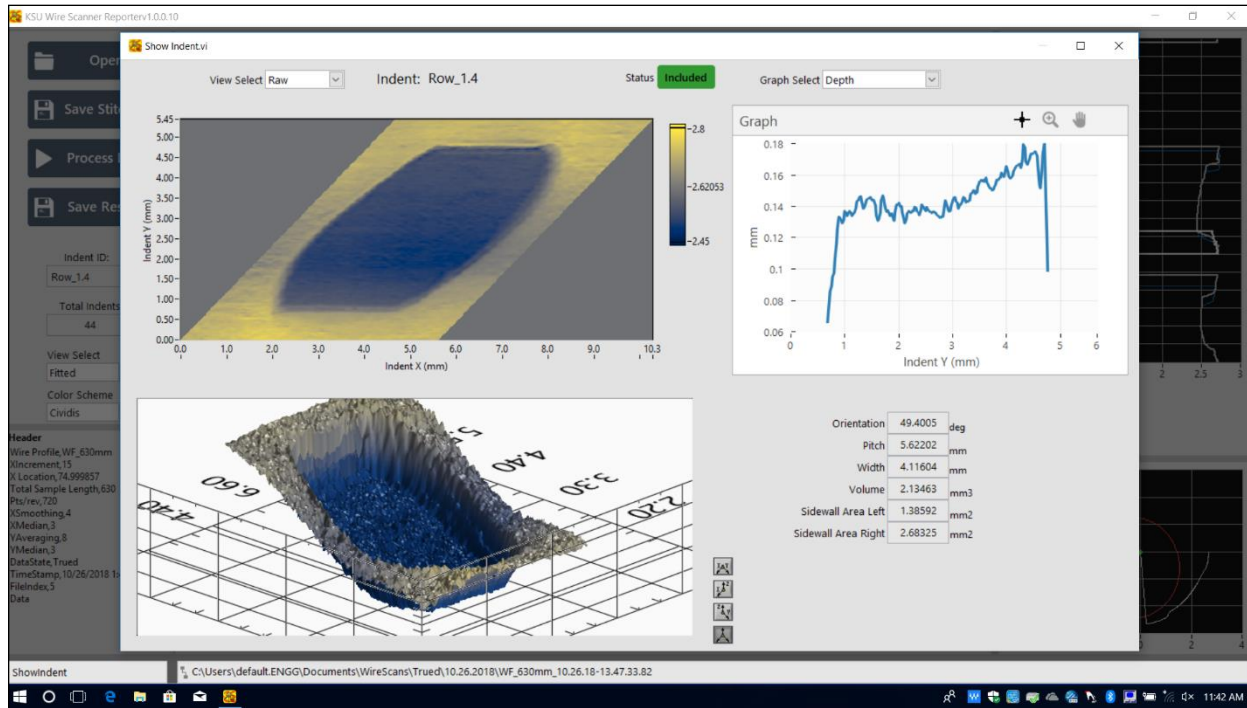


Figure 4.4: Wire Scan Reporter Interface (Indent Viewer)

The wire scan reporter has an additional useful feature, the ability to look at a specific indent; this functionality is highlighted in Figure 4.4. The selected indent is shown in heatmap form in the top left corner, and a three-dimensional render of the scan is shown in the bottom left corner, typically with a highly exaggerated axis in the height direction. The heatmap and three-dimensional rendering can be switched between the raw data view and the fitted data view. The raw data view displays the indent from the scan data directly, whereas the fitted data view omits the raw data and shows the trapezoid profiles of best fit that match the indent geometry. The fitting of trapezoidal profiles, once again, will be subjected to further discussion in Section 6. Furthermore, the right-hand side of the interface in this view shows geometrical indent features that were extracted for the particular selected indent in tabulated form, geometrical values that vary as a function of location along the indent can be selected in the plot located in the top right corner of the interface. Finally, the status tab allows the operator to choose whether the selected indent should be included or excluded from the report file. As a default, this option is set to include the indent in the report, however, in the rare circumstance that a scanning issue is preventing the feature extraction algorithms from obtaining realistic values the operator can simply choose to omit the data. The programs summarized in this section are easy to use and an operator can learn how to successfully utilize the system in less than half an hour. For the sake of posterity and completeness, the LabVIEW virtual interfaces that run the indent profiling system and the programs summarized in this section can be viewed in Appendix B. It is by no means comprehensive due to the complexity of the program but should serve as an example as to how the LabVIEW program operates.

4.2 Traverse Control, Rotation Control, and Carriage Homing

Movement control, traverse and rotation, can be commanded automatically by the program, or manually by the user. In either case, non-contact optical limit switches prevent the carriage from

impacting any hard stops on the lathe structure and the operator can utilize the Stop command which aborts any commanded movement. The operator can manually command rotation of the lathe head, and thus, wire specimen, by using [rcrtl + ↑] and [rcrtl + ↓], and linear motion by using [rcrtl + ←] and [rcrtl + →].

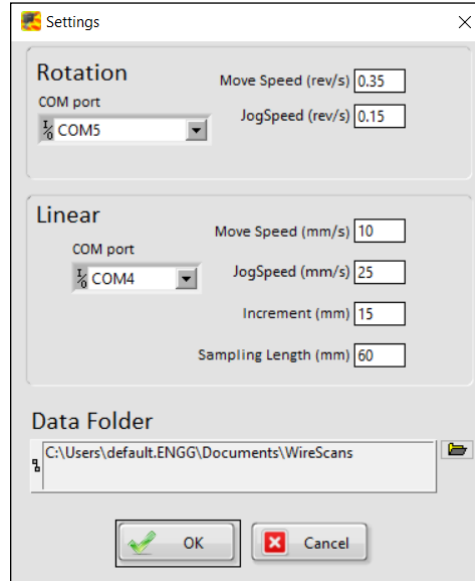


Figure 4.5: Movement Control Default Settings

Movement speeds are dictated by the system settings tab in the “Wire Scan” program; move speed is the velocity that is commanded by manual control, jog speed is the velocity used by automation control. A depiction of the default motion control settings is seen in Figure 4.5. By default, the rotation move speed is 0.35mm/s and the rotation jog speed is 0.15mm/s. The default linear motion control has a move speed of 10mm/s, and a jog speed of 25mm/s. Under the default settings it takes about 25 seconds to manually traverse the length of the bed. Furthermore, manual rotation control is slow so that the operator can more easily set the angular position of the wire being scanned. In automatic mode, it takes approximately 3 seconds to take a single scan and approximately 2 seconds for the carriage to translate into position to proceed with the next measurement. Thus, it takes around 5 minutes to scan a 2 foot length of wire. After the wire specimen has been scanned the Home command can be used which returns the carriage to the location closest to the lathe chuck.

4.3 Filter Settings and Data Visualization

The final group of settings that are accessible in the “Wire Scan” program pertain to scan data line refinement. These settings can be seen in the bottom left corner of the wire scan program interface in Figure 4.2. Non-contact laser based systems, despite the tremendous accuracies that the hardware is capable of, do not produce perfect data particularly when working with data on the scale of microns. A more detailed discussion of the measurement accuracy due to the optical uncertainty of this particular system can be viewed in Section 5.4. Two of the settings, averaging and smoothing, contribute most significantly to refining the quality of the laser line scan data being received by the indent profiling system.

The first of these settings, averaging, is made possible due to the high resolution rotary encoder that was selected to measure the angular position of the specimen being subjected to scanning. The rotary encoder is capable of providing 7200ppr (pulses per revolution). For a wire of 5.32mm nominal diameter, this corresponds to the ability to measure angular position with a circumferential resolution of $2.3\mu\text{m}$ on the surface of the wire. Since the line-laser module has an axial resolution of $20\mu\text{m}$ between points this indicates that the rotary encoder has a resolution that is nearly an order of magnitude of improvement over the laser sensor. Since, for mesh refinement reasons, it is desirable to have axial and circumferential resolutions that are similar in value, the excess resolution that the rotatory encoder provides allows for the effective “super sampling” of data. The averaging setting allows the indent profiling system to capitalize on this method, by capturing excess data about the measurement point the adjacent profiles can be averaged together to help filter out noise. This profile averaging process can be visualized in Figure 4.6, which could easily be confused with a modern art piece; the colored lines indicate individual line-scans while the black line is the average of all adjacent colored profiles. By default, this setting uses 8 profiles to perform averaging on; in this case, the 4 profiles on either side of the reference profile, the center profile, are all averaged together, thus reducing measurement uncertainty.

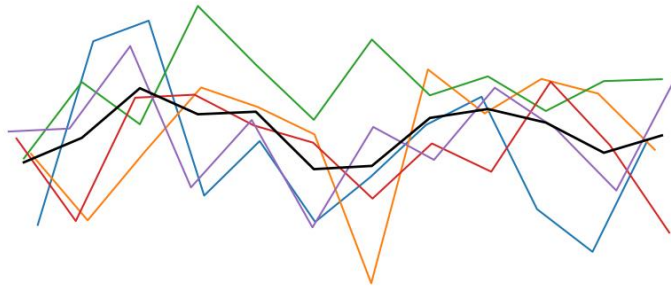


Figure 4.6: Profile Averaging

The second setting used for data line refinement is boxcar averaging. This simple method involves the refinement of a single profile by averaging a point with its neighboring points within a certain proximity. If the measurement uncertainty is sufficiently random, this proves to be an exceptionally effective method in reducing the apparent scatter of the data and contributes significantly to mesh refinement and data visualization. The method of boxcar averaging is illustrated in Figure 4.7, in which, a typical indent centerline profile is simulated with an average depth of $100\mu\text{m}$, and an indent sidewall angle of 20° ; these numbers are typical of indented wires that are 5.32mm in diameter (the angle is exaggerated in the plot due to the axes having highly different aspect ratios). A measurement uncertainty of $8.3\mu\text{m}$ is applied to the ideal profile and boxcar averaging is carried out on the simulated data; the reason for the $8.3\mu\text{m}$ measurement uncertainty will be made clear in Section 5.4. From the plot, it is apparent that 5-point boxcar averaging, in which a single point is averaged with the 2 points on either side, provides a significant improvement in scan quality. Boxcar smoothing, coupled with the profile averaging listed above can produce line-scans with significantly less measurement noise.

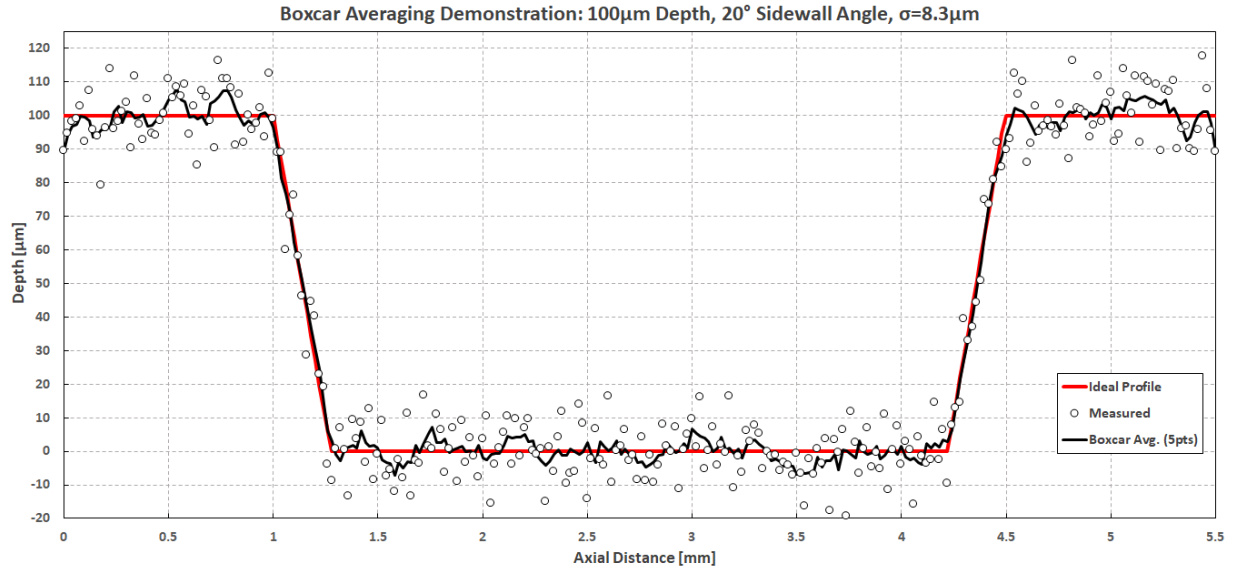


Figure 4.7: Boxcar Averaging on Simulated Data

Further processing steps are applied to the line scans prior to being subjected to the averaging and smoothing refinements. Points that are generated that fall outside of the 4-12mm wire diameter scanning range are rejected and patched with the data of neighboring points. These errant points are often the result of corner reflections on the wire surface that cause the scanner to record unrealistic data. Any errant points that fall within the valid wire diameter scanning range are subjected to statistical filters, since the uncertainty of the system is known, the system can remove points that are statistically unlikely to exist by comparing the errant value to neighboring points. After the errant points have removed and the averaging and smoothing steps have been applied, the scan mesh is left in a high quality state. Figure 4.8 illustrates the scan refinement process on a scanned wire; once again, the height axis is exaggerated to help portray the effect.

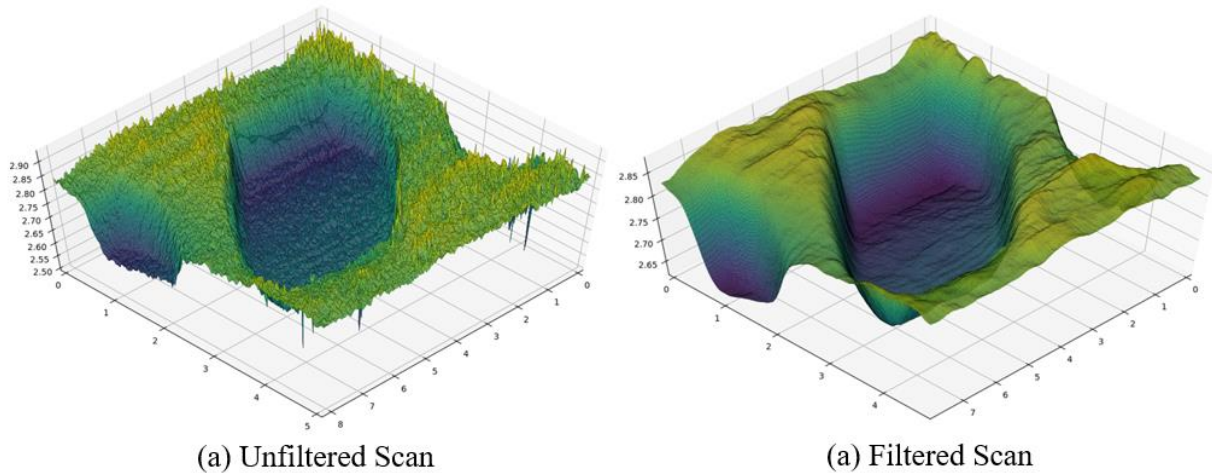


Figure 4.8: Scan Refinement of Wire Type WF

4.4 Scan File Format

The final discussion of this section will encompass the layout of scan file format now that the scanning and filtering processes have been explained. During the scanning process the wire is rotated along its longitudinal axis, as it does so, the light sheet of the laser module captures height profiles of the indented wire geometry at specific encoder pulses. As the wire is rotated the scanning process essentially “unwraps” the height profile of the indented wire and converts it into a two dimensional array that contains the height information at a given location, this is called the height-map or heat-map. This height-map is made from the composite of the high-resolution slices and is illustrated in the upper right corner of Figure 4.9.

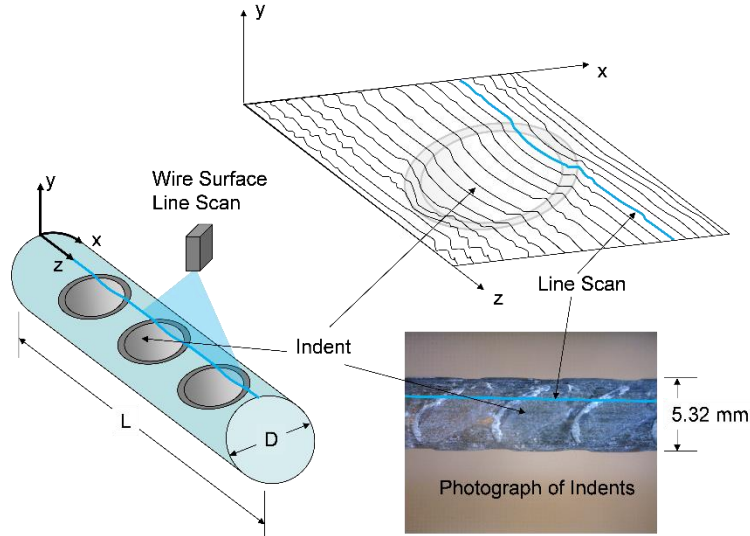


Figure 4.9: Schematic of Indented Wire Measurement (Sheet Laser)

The axial spacing of the data points is held constant by the sheet laser module, maintaining an axial spatial resolution of $20\mu\text{m}$ between points. It is desirable to maintain a uniform grid spacing for mesh manipulation, therefore, the circumferential resolution must also approximately be $20\mu\text{m}$. A depiction of the scanning grid based on spatial resolutions is summarized in Figure 4.10. The circumferential spacing is dictated by EQN 4.1, which shows that the circumferential resolution is a function of the wire diameter and n , the number of encoder triggers per revolution. For a 5.32mm diameter wire, and 720 encoder pulses per revolution a circumferential resolution of $23\mu\text{m}$ is obtained, sufficiently close to the goal of $20\mu\text{m}$. From the aforementioned relation, it is obvious that wires of larger diameter will need a higher number of encoder pulses for data acquisition since the circumference of the wire is physically larger if uniform grid spacing is to be honored.

$$\Delta d_{\theta} = \pi \times \frac{d_{\text{wire}}}{n} \quad (4.1)$$

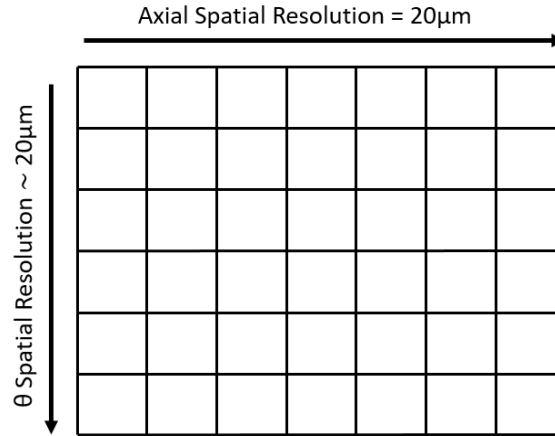


Figure 4.10: Scanning Grid Spacing

The scan format is composed of the header information that is listed in the Wire Scan program and the two dimensional height-map of the scanned segment. The layout of the scan file is shown in Figure 4.11. Each row of the two dimensional data array represents a single line scan with 800 unique height values, corresponding to the scan line width of 16mm with a spatial resolution of 20μm and is the result of a single encoder pulse. A 5.32mm wire will need 720 profile captures to maintain a roughly equal grid spacing, thus the WF wire represented in Figure 4.11 will have a scan file with 720 data rows as it is a 5.32mm wire specimen.

Wire Profile	WF_630mm				
XIncrement	15				
X Location	0				
Total Sample Length	630				
Pts/rev	720				
XSmoothing	4				
XMedian	3				
YAveraging	8				
YMedian	3				
DataState	Trued				
TimeStamp	10/26/2018 13:47				
FileIndex	0				
Data					
2.7008	2.7033	2.7046	2.7057	2.7059	2.706
2.7007	2.7055	2.7048	2.7052	2.7049	2.7046
2.702	2.7009	2.6996	2.6979	2.6963	2.6957
2.6965	2.6969	2.6935	2.6919	2.6913	2.6922
2.703	2.7042	2.7016	2.6997	2.6984	2.6979
2.6912	2.6902	2.6883	2.6883	2.6903	2.694
2.6814	2.6789	2.6788	2.6794	2.6823	2.6869
2.6674	2.6661	2.6662	2.668	2.6718	2.676
2.6673	2.6672	2.6676	2.6682	2.6696	2.6712
2.668	2.6679	2.6666	2.6669	2.6687	2.6719
2.6711	2.6777	2.672	2.6681	2.6639	2.6608
2.6887	2.6884	2.6784	2.6718	2.6665	2.663
Scanner Index: j = 0,1,...,799 (800pts)					

Encoder Index = 0,1,...,Pts/rev

Figure 4.11: Scan File Format

5. System Calibration

Non-contact laser based systems are capable of incredible accuracies, particularly once effective data filtering techniques are implemented. However, no mechanical system or measurement specimen is perfect and thus pose significant problems to measurement accuracy. Misalignments that are considered tiny have large ramifications when measurements are being conducted on the scale of microns. The natural cast “bow” of the wire along with sensor skew and how to mitigate them is the primary focus of this section. The reduction of sensor skew via the use of a correction map generated by a calibration cylinder will be the first topic of discussion, followed by the development of an effective process to correct for non-concentric specimen chucking and the bow that is inherent in indented steel wires. Later stages of this section will discuss measurement uncertainty and repeatability of the system after the scans have been corrected for sensor misalignment and wire bow, and finally, the measurement of indents that were machined with known indentation characteristics will be analyzed to verify the accuracy of the system.

5.1 The Necessity of System Calibration

Laser line-scan modules, or any laser based displacement measurement system for that matter, measures a displacement based on the reference point of the system. This reference point is often called the laser spot, also known as the point of greatest focus; coincidentally, it is also the location of which measurement uncertainty is minimized since the uncertainty is directly proportional to the spot size. For the indent profiling system, it is desirable to locate this reference point, or line in the case of the sheet laser, on the surface of the wire with the laser sheet coincident with the bore axis of the lathe assembly that applies the rotation to the wire being scanned. If this is accomplished, then the true height-map of the wire being scanned will be ascertained, neglecting wire bow. However, perfect alignment of a mechanical system is not realizable and generates error where misalignment exists. To put the importance of correcting for system misalignment into perspective, if the laser head is misaligned by 0.1° in the yaw rotation for a scan width of 16mm, an error of $28\mu\text{m}$ is induced across the scan length, keep in mind that most wire indents are $100\mu\text{m}$ deep. Alignment of the mechanical system can only go so far, even with the inclusion of precision linear translation stages and micrometers to assist with the alignment of the system. However, a majority of the alignment error can be mitigated by scanning a specimen with known physical dimensions and applying a correction map to the captured data to account for the misalignment of the system. This calibration procedure is summarized in the following section.

Wire cast “bow” is another problem that requires correction via wire guides and software steps. Indented steel wire has a natural cast and is stored in wire spools; the natural cast of the wires can be a few inches over a 2 foot segment of wire. This poses significant problems when it comes to accurate measurement of the wire surface as the centroid of the wire profile is no longer in alignment with the rotational axis of the scanning system. As the wire is constrained by the alignment bushings on the carriage frame it forms a parabolic curve. Once scanned, this observation can be used to correct for the wire bow, thus straightening the wire and forming an ideal scan; this procedure will be the primary focus of Section 5.3. When system misalignment and wire bow have been properly accounted for, the indent profiling system is capable of measuring profiles with micron levels of precision.

5.2 Correcting for Sensor Skew

5.2.1 Sensor Misalignment Leads to Distorted Data

For the sake of illustration, imagine the wire is suspended horizontally. Now envision being in the cockpit of a plane flying straight towards the wire with the wings parallel to the wire length. The plane represents the line-scan laser scanning the surface of the wire, casting a sheet of light that measures the surface. The visualization concerning the plane is convenient way of describing the orientation of the scanner in the discussion to follow: pitch involves aiming the scanner sheet up or down, yaw rotates the sheet left and right, and roll rotates the laser sheet as if the plane was spinning about the axis from nose to tail.

If the sheet laser is perfectly aligned with the wire (pitch, yaw, roll equal 0°) and the reference point is in the perfect position, then the ideal scan of the wire is obtained and the measured height-map perfectly matches the surface of the scanned wire. If the scanner is perfectly aligned, but too close to the surface then the object will appear too large since the scanner is measuring a larger displacement with respect to the reference point; conversely, being too far away makes the object too small. If the yaw error is introduced, then the resulting scan appears as a truncated cone. If pitch error is introduced, the size of the cylinder appears incorrect, slightly larger than the ideal case. If roll error is introduced, then the scan forms a hyperboloid. Any of these errors are cumulative and significantly affect the resulting scan profile. However, once it is understood that the alignment errors involved are small, the distortion caused by the misalignment of the sensor is predominately second order in nature. By scanning a specimen of known geometry, it is possible to apply a correction map to the captured data, placing the data points where they truly belong as if system misalignment did not exist in the first place.

5.2.2 Calibration Cylinder

For the calibration process, specimens with well-known geometrical properties are required; precision ground cylinders are ideal specimens to use for this purpose, since the nominal diameter is constant about the length of the specimen. A scan of such precision ground cylinder is seen in Figure 5.1.

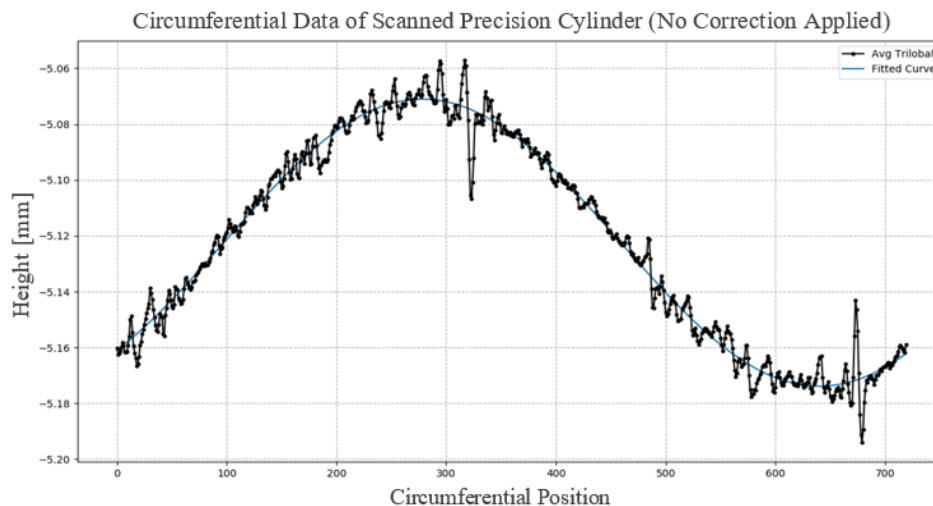


Figure 5.1: Calibration Cylinder Scan

Figure 5.1 represents the uncalibrated data obtained when a precision ground cylinder is scanned, the particular data shown in the figure is the height profile measurements along the circumference of the cylinder at a given point. Through this data, a line of best fit is obtained via a Fourier transform, the phase of which, is locked to 360° . The runout measured, which is the amplitude of the fit, is the culmination of the non-concentric chucking of the precision ground cylinder in the lathe chuck, off axis rotations caused slight angular misalignment of the specimen in the chuck, and finally, of primary interest, the distortion caused by the misalignment of the system. By applying similar Fourier analysis on every scanned circumferential section, it is possible to isolate the error caused by specimen alignment and runout since the precision ground cylinder is approximately a perfect cylinder with a constant diameter. The remaining error is the byproduct of system sensor misalignment alone, neglecting thermal disturbances. This, as expected, generates a displacement correction map for a specimen of given size, in which, the alignment errors are approximately second order. When a new scan is made, the calibration map is added to it, thus accounting for the misalignment error of the system and placing the measured data in the correct location. An example of the calibration results can be seen in Figure 5.3 in which the calibration cylinder has been corrected for system misalignment; the calibrated scanned diameter is within 1 micron of the nominal diameter specified by the precision ground cylinder.

5.3 Off-Bore Rotation (Wire Bow)

Indented wires, as stated previously, have an amount of cast “wire bow” for a given length of wire. The manufacturing process leaves a natural bow in the wire that is often not removed, some wires exhibit cast of multiple inches across a 2 foot length. The indent profiling system uses bushings on the carriage to center the wire for the line-scanner, support the length of the wire, and minimize wire bow; the bushings have an internal diameter that closely matches the maximum diameter of the particular wire specimen being scanned. The cast of the wire is constrained by the two bushings, alleviating the severity of the inherent bow, but not completely eliminating it. This represents a problem, the off-axis rotation of wire cross-sections due to the bow causes an unavoidable distortion in the scan. In this situation, the longitudinal axis of the wire is not in line with the bore-axis of the lathe.

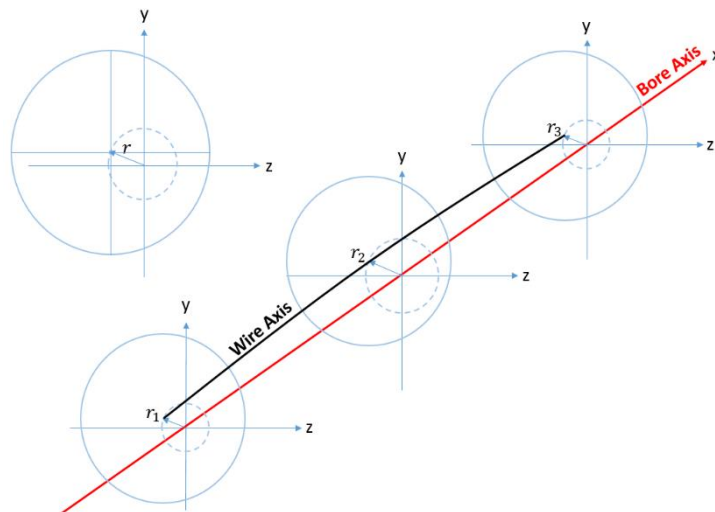


Figure 5.2: The Effect of Wire Bow on Off-Bore Rotations

Wire cast “bow” can be corrected through the use of certain processing steps. As the wire is constrained by the alignment bushings on the carriage frame it forms a parabolic curve; technically, this curve is circular in nature, but the small arc segment constrained by the bushings is considered parabolic. An illustration of the effect of wire-bow on off-bore rotations is given in Figure 5.2. Once it is understood that the wire bow centroid follows a parabolic arc, the procedure listed below can be used to manipulate the scan and correct the indented wire to a straight cylinder, free of bow distortions.

- (a) Identify bow direction and indent row locations using Fourier transforms.
- (b) For each slice of the wire profile, compute the axis offset, r , using the non-indented rows.
- (c) Fit the axis offsets to a parabolic equation, $r = f(z)$.
- (d) Using the parabolic equation and bow direction, remap the distorted data to an ideal cylinder with no bow.

This method is effective at eliminating the bow inherent to the indented steel wires being scanned. After it is properly executed, little to no trace of the bow exists. After the calibration map has been applied and the wire bow has been removed the wire scan is in an ideal state and is ready for processing by the algorithms described in Section 6.

5.4 Measurement Uncertainty and Repeatability

Once sensor misalignment has been dealt with via the aforementioned calibration steps and off-bore rotations caused by nonconcentric specimen chucking or inherent wire bow has been eliminated through software correction, an ideal, trued scanned surface is obtained. The trued scan is largely error free from the distortions caused by sensor misalignment or cast of the specimen; accuracy to the true specimen dimensions is on the order of microns. By scanning a specimen of well-known geometrical properties, such as the precision ground cylinder used in the prior section, and applying the necessary corrections, it is possible to obtain an assessment of the uncertainty and repeatability of the optical system, in this case, a laser-line module. A scan was taken of such precision ground cylinder with a nominal diameter of 5.04mm, with a tolerance of ± 0.001 mm, and a maximum RMS surface roughness of $0.25\mu\text{m}$. The resulting height-map of the precision ground cylinder after calibrations and off-axis rotations have been applied can be viewed in Figure 5.3. Note how the measured diameter is only $1\mu\text{m}$ off from the nominal diameter of the calibration cylinder, this indicates that an ideal scan has been achieved; to put it in perspective, the width of a thick human hair is on the order of $100\mu\text{m}$.

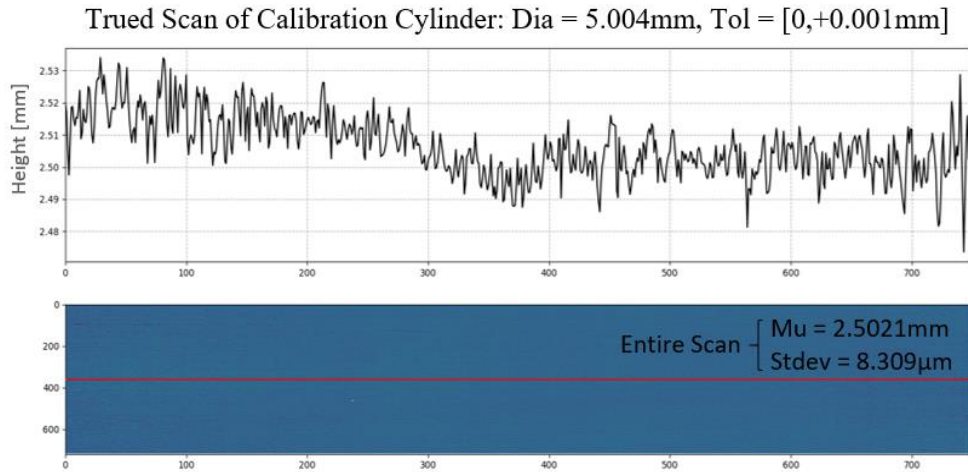


Figure 5.3: Trued Calibration Cylinder Height-Map

A histogram of the binned heights of the trued calibration cylinder height-map is provided in Figure 5.4. From the histogram, it is clear that the scatter of the measurements from the optical system follows a Gaussian distribution as expected. However, the uncertainty is computed to be $8.3\mu\text{m}$, well above the theoretical uncertainty ($<2\mu\text{m}$) of a blue laser with spot width of $45\mu\text{m}$. As an aside, the laser module can never hope to measure the surface roughness of the calibration cylinder in the first place since the RMS roughness is smaller than the resolution that the laser module is capable of, and thus, is not the direct limiting factor in the measurement uncertainty.

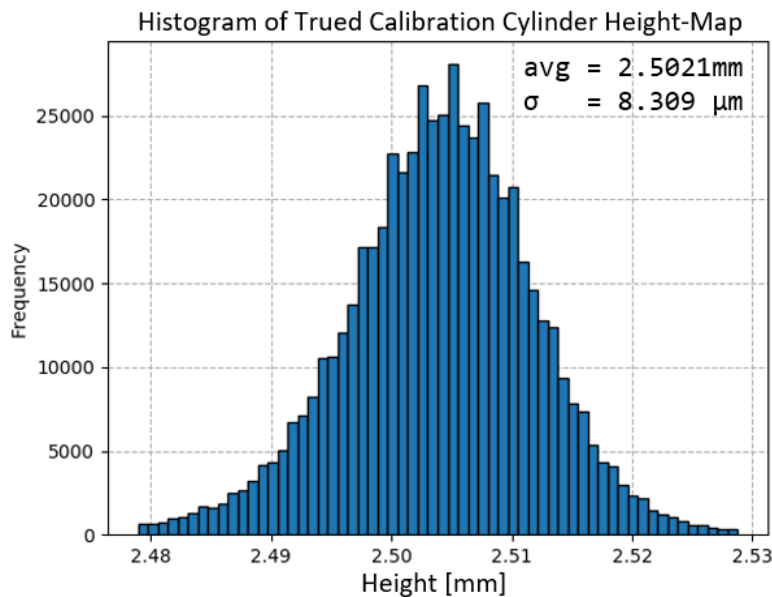


Figure 5.4: Trued Calibration Cylinder Histogram

By looking at adjacent laser scan profiles it becomes apparent where the source of the higher than expected measurement uncertainty comes from. Figure 5.5 shows five adjacent data lines from the measured of a indented wire rib, from this figure it is obvious that the low frequency and high frequency noise show significant similarities across adjacent profiles separated just microns apart from one another and still being partially illuminated from the same laser light sheet. The same figure shows high system repeatability when the same location is scanned, on

the order of less than two microns. The similarity of the low and high frequency content across adjacent profiles is indicative of broadband noise, and thus, implies that laser speckle interference (LSI) is the culprit of the higher than expected measurement uncertainty.

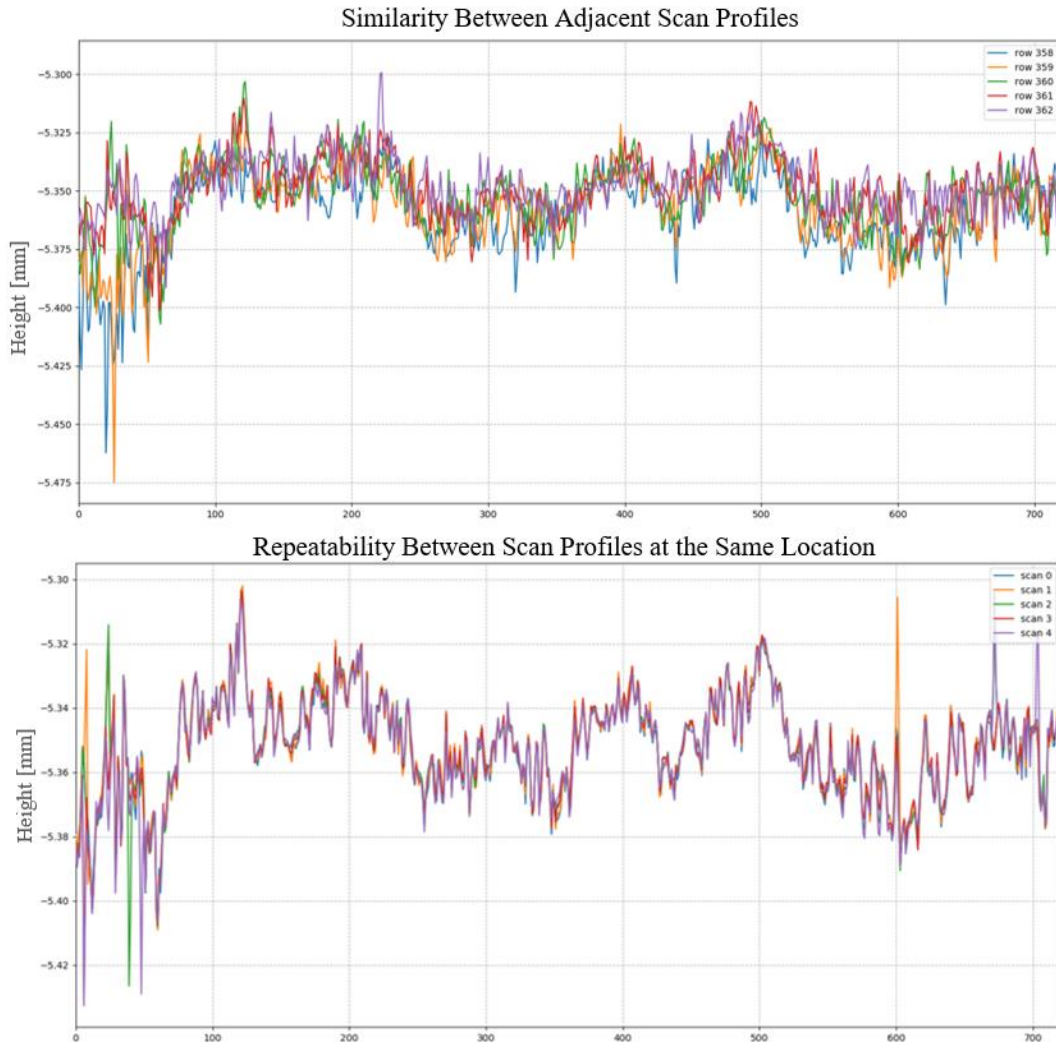


Figure 5.5: System Repeatability

Laser speckle interference is inherently broadband and is a mostly unavoidable phenomenon when a coherent light source illuminates a surface. This effect is illustrated in Figure 5.6, in which a coherent light source impinges upon a surface of given roughness and reflectivity, scattering light off and generating constructive and destructive interference at a given distance away from the illuminated surface, such as where an imaging array is located.

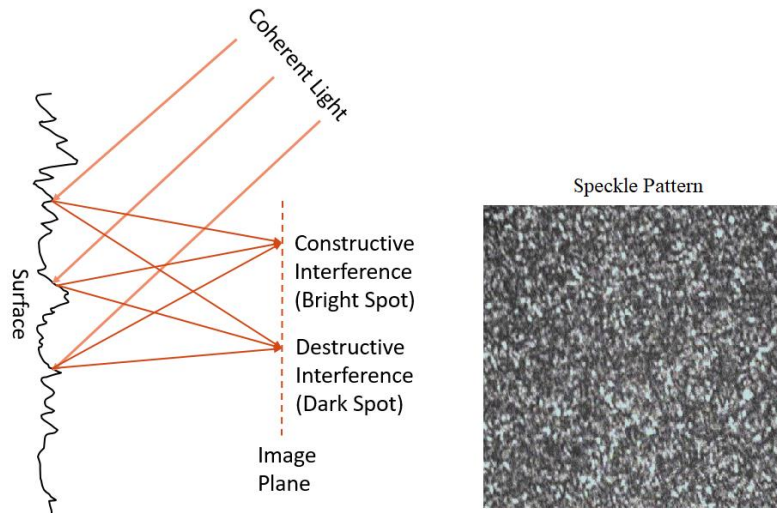


Figure 5.6: Laser Speckle Interference

This effect is generally undesirable from a measurement accuracy standpoint as it represents noise that cannot be filtered out because it is broadband. However, sometimes this effect can be used positively as a method to conduct measurements, Figure 5.7 highlights such a system. The laser speckle interferometer was made for a prior FRA project to measure strain profiles of prestressed concrete railroad ties. It used laser speckle pattern images to correlate displacements using a known gauge length between the imaging systems, and thus, could use the effect of laser speckle to accurately determine displacements. However, in the application of the indent profiling system such an effect is undesirable as it degrades the quality of the measured displaced laser profile with broadband noise that cannot be filtered out, leaving the laser line scanner with a measurement uncertainty of $8.3\mu\text{m}$.



Figure 5.7: Automated LSI System on Concrete Ties in Plant

This measurement uncertainty is significantly reduced by the filtering and averaging techniques applied in Section 4. The system is accurate enough to receive reliable measurements on most indented wire geometry in practice since indent depths of 5.32mm wire are typically on the order of $100\mu\text{m}$, an order of magnitude above the measurement uncertainty of the system. Additionally, the system is not taking single measurements in the basin of the indent and a single

measurement on the crest of the indent, it is taking hundreds of measurements. The blue line laser was selected due to the high amount of data that it could acquire over the given area of interest, and has a level of measurement uncertainty that is amenable to the measurement of most indent geometries in practice. The amount of data collected, coupled with the reasonable uncertainty of the measurements and the processing algorithms highlighted in Section 6, lead to reliable extraction of indent geometrical features.

5.5 Machined Indents

In this section the system was used to measure the characteristics of machined indents, which represent indent shapes of known geometry. This is done in order to verify the correction steps in the aforementioned sections and test out the algorithms that will be explained in great detail in the following section, Section 6. These indents were made by machining grooves with an end mill in the sides of wire similar to the wire used in the manufacturer of typical prestressed indented wire. A photograph of a resulting sample row of these indents is shown in Figure 5.8, which represents a groove made with an end mill having a 30° chamfer angle, with an equivalent machined indent orientation of 45° . The blue line shown in the Figure represents the scan path of the laser line scan at a single rotation angle position corresponding to the center of the indent row. It should be noted that these machined indents, unlike actual indents which are formed by deforming (indenting) the wire surface, are created by removing a small amount of material from the associated wire via an end mill. These fabricated indents provide an ideal test case for the checkout of indent feature extraction algorithms since they represent features of known geometry.

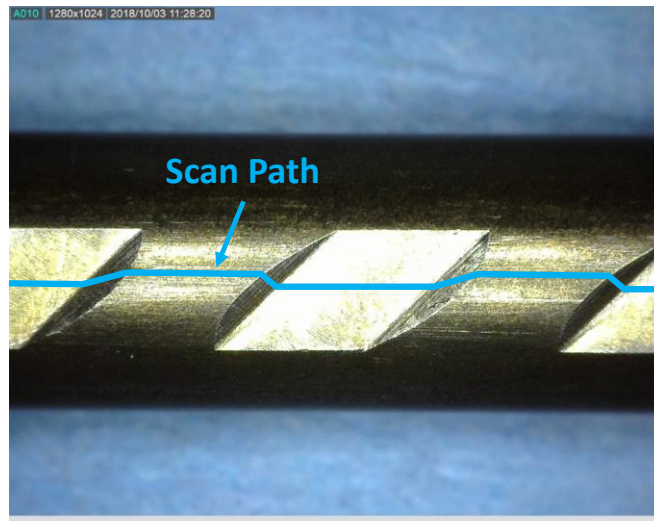


Figure 5.8: Sample Scan of Machined Indent (30°)

The basic concept behind the feature extraction algorithms in the current profiling system is to reduce the indent shape to a series of slices that can be approximately represented by a curve fit, typically a trapezoidal shape for a chevron style of indent, as suggested in Figure 5.9. This trapezoidal shape is well-suited for the basic Chevron indent profile, the indent most common in industry; however, the trapezoidal shape would not apply to a dot shaped indent.

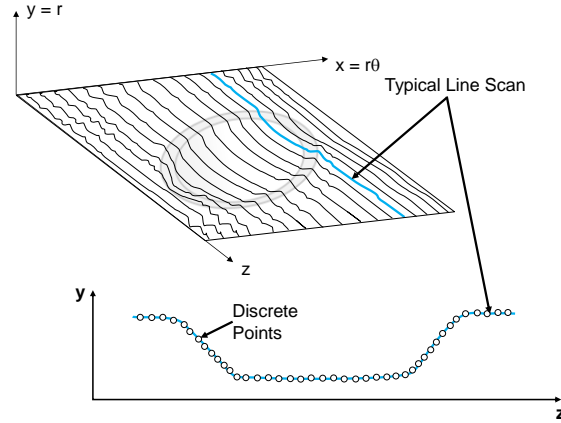


Figure 5.9: Basis for Feature Extraction (Trapezoid Slice)

This type of trapezoidal fit is shown applied to a longitudinal slice through the center of the machined indent shown in Figure 5.8, along with some characteristic measurements of the sidewall angles, is shown in Figure 5.10. While the machined indents represent the ideal indent geometry, having straight sidewalls, basins, and crests, the fit of a trapezoid to the indent profiles of manufactured indented wires is a fantastically close approximation to real wire geometry.

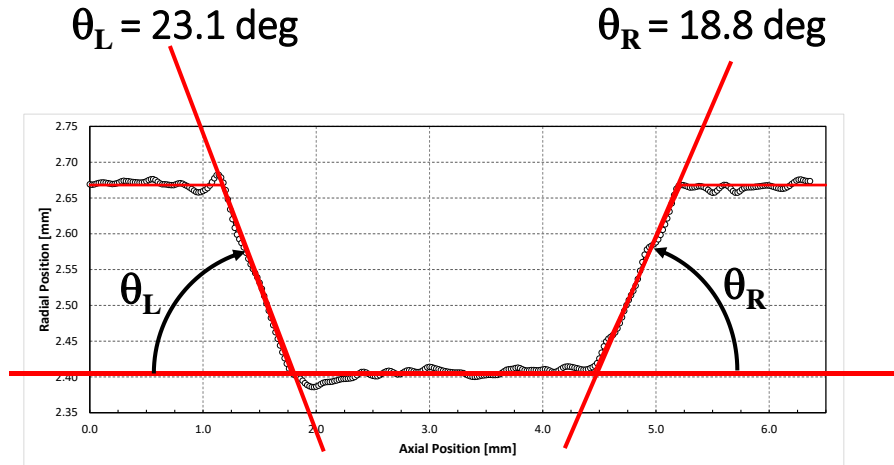


Figure 5.10: Trapezoidal Slice for a Machined Indent (30°)

Note that the measured sidewall angles do not correspond to the 30° end mill chamfer angle. The reason for this can be explained by considering the diagram shown in Figure 5.11, which compares the end mill chamfer angle, θ , to the actual measured indent sidewall angle, ϕ . The simple algebraic relationship shown in the Figure follows directly from the relationship between the blue line scan and the red end mill chamfer line. For a 30 deg chamfer angle and a 45° orientation angle, the resulting theoretically measured sidewall angle for the machined indent is

$$\tan \phi = \frac{1}{\sqrt{2}} \tan \theta = \frac{1}{\sqrt{2}} \tan(30 \text{ deg}) = 22.2 \text{ deg}$$

which compares well to the values measured on the left and right sides of the machined indent, as shown in Figure 5.11. It is important to note that this relationship is valid for indent centerline geometry.

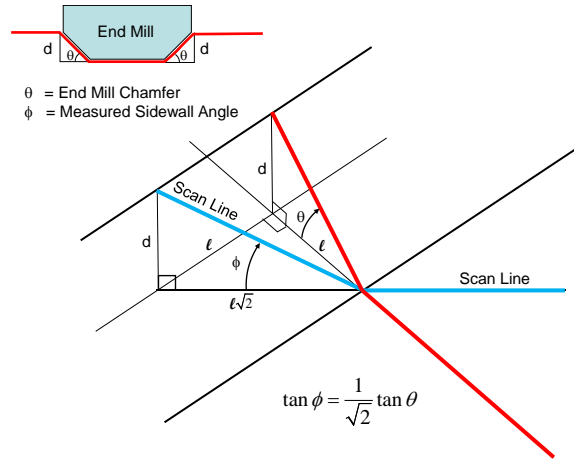


Figure 5.11: Measured Sidewall Angle Relationship

Furthermore, the data summarized in Figure 5.10 indicates an indent depth, measured along the centerline, of $270\mu\text{m}$ (0.0106in). Comparison with a mechanical dial indicator with a resolution of 0.001in yielded a measured indent centerline depth of 0.010in of the same indent, a reasonable agreement considering the resolution limitation of the dial indicator.

This measurement example highlights the effectiveness of the aforementioned correction steps, demonstrates how closely a trapezoidal shape approximates indents of known geometry (and later, formed geometry), and generates confidence in the reliability of the system at extracting accurate indent features. A multitude of machined wires from a prior FRA project, representing 12 specimens of varying sidewall angles and depths, were measured by the indent profiling system and will be the subject of further discussion in Section **Error! Reference source not found.** Furthermore, multiple modern wires that have recently seen use in industry, as well as indented wires extracted from concrete cross-ties that have been in service spanning the course years to multiple decades, will be subjected to processing as well. The discussion of the results generated by the indent profiling system will come after an explanation of the feature extraction algorithms is given in the section that immediately follows.

6. Process for Extracting Indent Geometry

The primary objective of the indent profiling system, above all else, is to accurately extract the geometrical features of the wires that have been scanned. Prior sections have been dedicated to the acquisition of scan data, the refinement of the captured data, and development of calibration techniques used to generate data that is ideal for processing. The following section will focus on the development of algorithms that will be used for the extraction of indent geometry.

The algorithms highlighted below will be well suited for analyzing chevron type indentations, by far the most common type of indentation seen in industry, seeing extensive use in smaller diameter wires. Other indentation types include wires with dotted or spiral shaped features; however, these indentation types are not as prevalent. The indent feature extraction process is generalized enough to work for any discrete indentation type that is formed into individual rows. The general process that indent feature extraction utilizes is described in the following steps. First, the individual, trued scans are spliced together to form one contiguous scan that will be subjected to feature recognition. Second, the locations of individual indents are determined by row position, indentation pitch, and the orientation of the indents; individual indents are then isolated for feature extraction. Third, each indent is processed by algorithms appropriate for the indentation style to obtain the important features of the indentation; the algorithms used to extract the indent features of chevron type indents are implemented differently than those used for dotted indentations. Finally, after all isolated indents have been subjected to processing, a report is generated summarizing the results. The final report includes: results summarized in ASTM A881 and ISO 16120 format, an example height-map of the scanned indented wire, and detailed statistics and histograms showing variations on a row-by-row basis, in addition to the primary results file. A detailed discussion of the results obtained using the algorithms below will be the subject of Section 7, and the wire report summaries of wires relevant to the scope of this report are detailed in Appendix B.

6.1 Scan Splicing

Up until the point of feature extraction scans are contained as individual segments. However, for the purpose of indent isolation and feature extraction the scans must be joined into one continuous entity as illustrated in Figure 6.1.

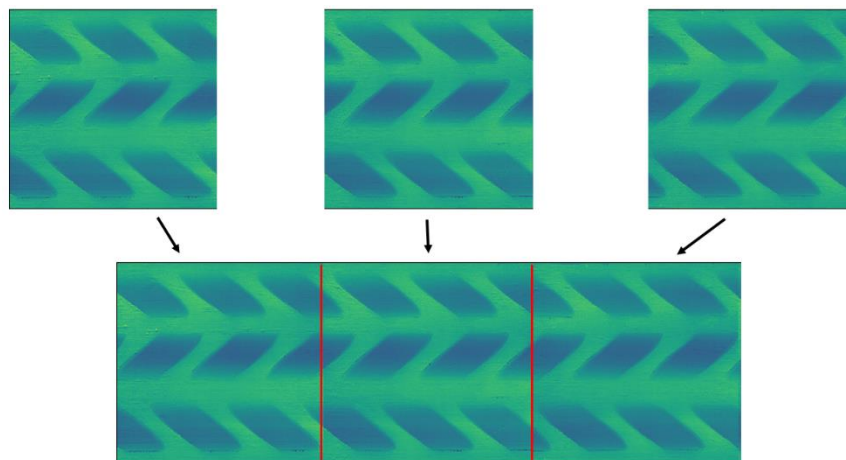


Figure 6.1: Outcome of Scan Splicing

In order to obtain statistically relevant sample sizes, it is desired to capture the entire pattern formed by the indent rollers on the steel wire, as those indents represent statistically unique samples. As such, scans with a total length of 25 inches (630mm) are common in order to capture one full repetition of the wire pattern, corresponding to indent rollers of 8 inches in diameter commonly seen in industry. The line-scan module utilized by the indent profiling system captures the indent surface features across a 16mm length. However, it should be noted that line-scan lasers see increased measurement uncertainties at the extremities of the scanning width. This is an unavoidable byproduct of mathematics related to the processing of the edges of the imaged profile, however, the discussion of sensor binning and detailed Fourier analysis used to process the image profiles are outside of the scope of this report. A visualization of the increased measurement uncertainty at the fringes of the full scan can be viewed in Figure 6.2 which highlights the undesirable effect on a scan that has not been subjected to the calibration procedure.

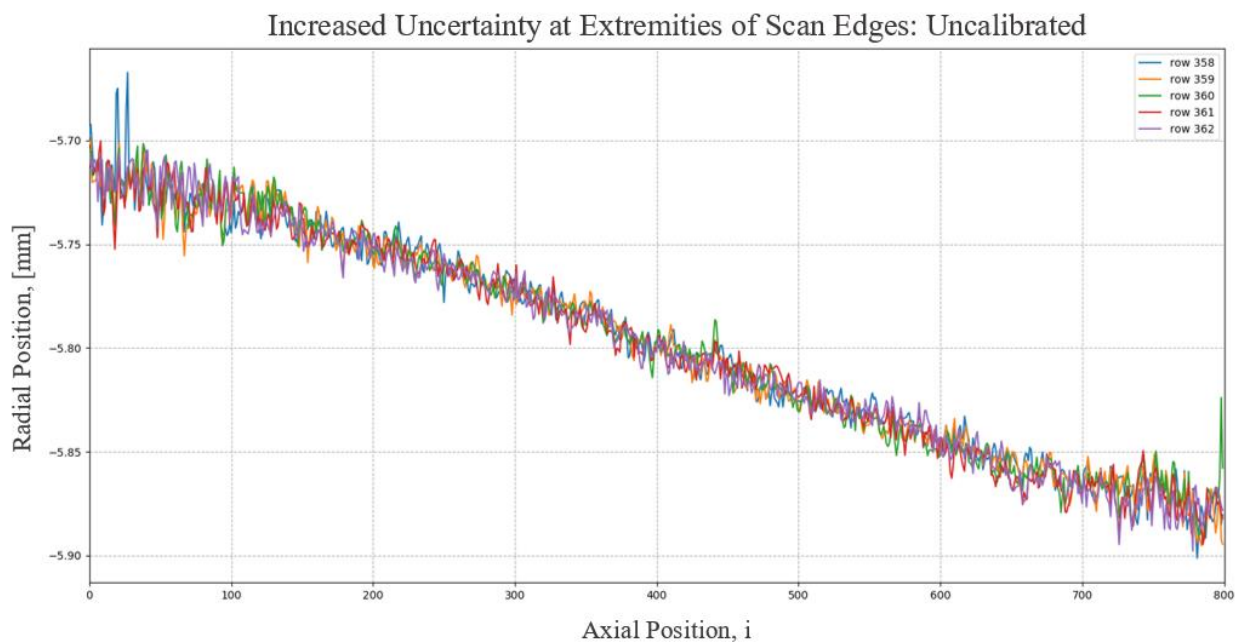


Figure 6.2: Increased Measurement Uncertainty at Edges of Line-Scan

From the standpoint of statistics collection it is favorable to have measurement uncertainties that are consistent throughout the range of the data. Section 5.4 contained a detailed discussion of the measurement uncertainty of the system once calibration procedures were applied; a measurement uncertainty of 8.3 microns was determined for 90% of the scan in the center of the profile. Instead of inheriting the increased measurement uncertainty at the edges of the scans it is more reasonable to omit the edges of the scan. By settling with a scan width of 15mm instead of the initial 16mm, it is possible to ignore the effects of increased uncertainty at the edges of the scan. For a 630mm scan length, with a 15mm scan width, this corresponds to 42 scans of the wire specimen to be captured.

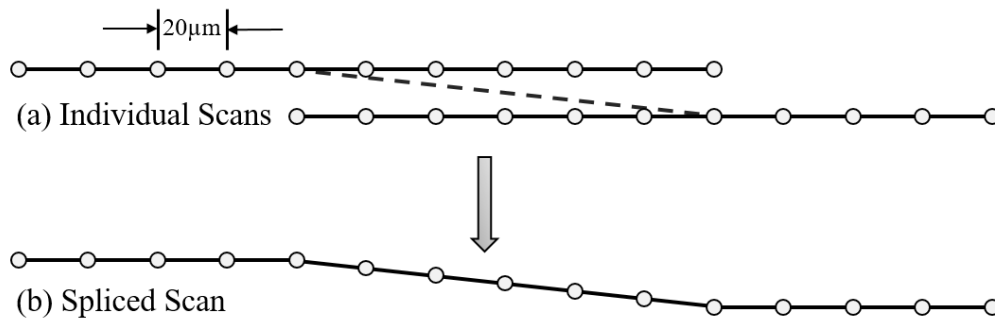


Figure 6.3: Method for Joining Overlapping Scan Segments

Due to the accuracy of the scanning procedure after calibrations and data correction steps have been applied, it is possible to simply align the scan profiles from end to end, illustrated as such in Figure 6.1. However, it is also possible to overlap the edges of the scans as seen in Figure 6.3(a), interpolate between the two overlapped sections, and obtain a smoothly spliced section as illustrated in Figure 6.3(b). From a feature extraction perspective, this interpolation step affects nothing, however, it does make the contiguous scan more attractive from a data visualization standpoint as it does not leave a step of a couple of microns at the transition created between the scan segments. Once a contiguous scan has been formed from its component scans, it is then possible to proceed with data visualization and feature recognition and extraction as highlighted in the subsections below.

6.2 Indent Row Detection

With the creation of a contiguous scan the procedure of feature recognition can begin. However, prior to isolating individual indents for analysis, it is necessary to determine the location of the indent rows that the indentations form. From the manufacturing process, the indent rollers form discrete indents, with a particular spacing (pitch), into rows separated at equal intervals about the circumference of the wire. Once the positions of the indent rows have been detected with respect to the scan, later processing steps will be used to locate the individual indents that compose the row.

6.2.1 Averaged Trilobal Shape and Fourier Analysis

The majority of indented wires used in industry are manufactured with three indented rows, equally spaced about the circumference of the wire, with one of the rows having an orientation contrary to the other two. In practice, the indent rows are not equally spaced about the circumference of the wire due to imperfections in the manufacturing process, but the following method still stands. The observation of a finite number of equally spaced rows trivializes the detection of the indent row positions. Each longitudinal profile of the continuous scan can be averaged, yielding the average trilobal shape of the wire as a function of angular position. A trilobal shape is a mix between a circle and a triangle; as the indent rollers press the indents into the wire, the steel is deformed, and thus, forms a shape that is roughly trilobal in nature. The cross-sectional view of a wire shown in the bottom right corner of Figure 4.2 clearly illustrates the trilobal shape of a scanned indented wire.

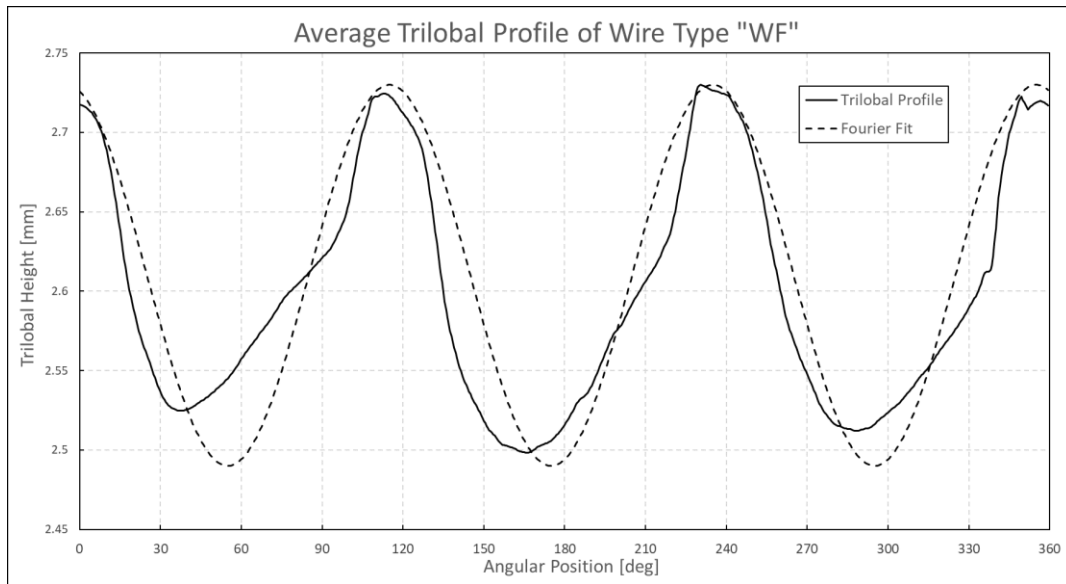


Figure 6.4: Indent Rows From Average Trilobal Profile (Wire Type “WF”)

From the trilobal profile, it can be seen that there are three distinct peaks and troughs that represent where the indent rows are with respect to the scan, an example of which, can be visualized in Figure 6.4. From Figure 6.4, it is clear that the indent ribs, the areas that are largely unaffected by the deformation process caused by the indent rollers, occur at positional increments of 115° , 235° , and 355° with respect to the scan origin. Note how those values are separated by increments of 120° , implying three equally spaced rows. By applying a Fourier transform of fixed phase on the averaged trilobal profile data, it is possible to extract the points that separate the indent rows. The separation points are represented by the peaks of the fitted sinusoidal function illustrated in Figure 6.4. The method of using Fourier transforms to analyze the indent row locations based on the average trilobal profile of the scan yields accurate results and is applicable to any wire composed of an arbitrary number of equally spaced indents rows.

6.2.2 Alternative Method: Determining Linearity

An alternative procedure can be used to automatically determine the locations of indent rows. This method can be applied to a wire with an arbitrary number of indented rows with equal spacing, or more interestingly, unequal spacing. Instead of using Fourier transforms to analyze the averaged trilobal shape of the wire being scanned, this method assesses the linearity of the longitudinal profiles that the scan is composed of. Since the contiguous scan is comprised of individual scans that have had calibration and wire-bow corrections applied, the ribs between the indented rows are mostly free from the deformations caused by the indent rollers. As such, the longitudinal profiles along the ribs of the wire are significantly linear. By assessing the linearity of the longitudinal profiles as a function of angular position, it is possible to ascertain the regions that describe the indented rows. This can be seen in Figure 6.5 which shows a depiction of the linearity of the longitudinal profiles of wire type “WF”.

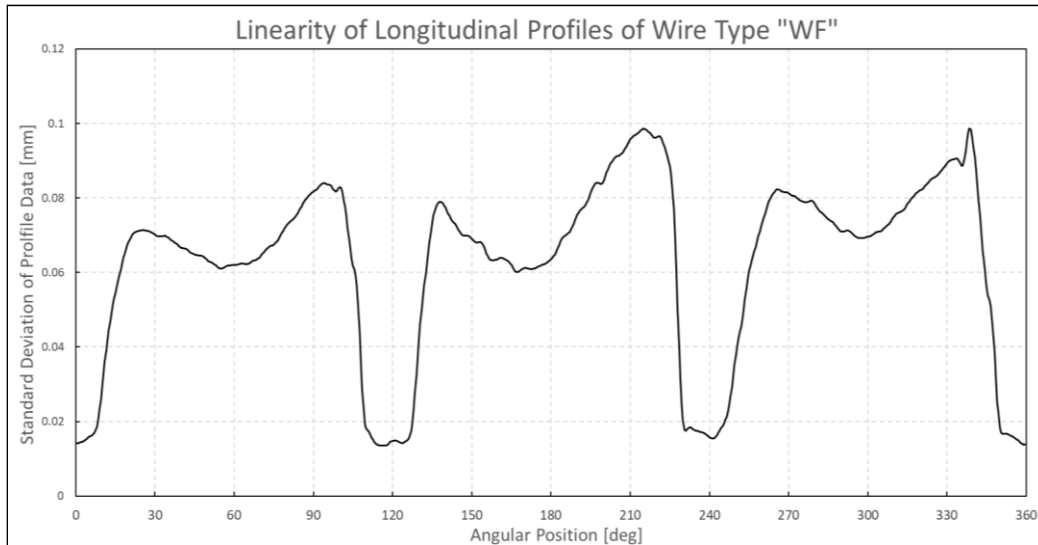


Figure 6.5: Indent Rows From Profile Linearity (Wire Type “WF”)

Due to how the scans are aligned, linearity is analogous to the assessment of the standard deviations of the longitudinal profiles. From Figure 6.5 it is clear that the points of highest linearity occur where the standard deviations of the profiles are lowest, thus, it can be determined from this particular example that the indent row transition points are located at 120°, 240°, and 360°. Figure 6.6 is a composite illustration of the previous figure with height-map of wire type “WF”; it clearly shows how profile linearity corresponds with indent row transitions. This methodology is a reliable way of extracting the points at which the transition between indent rows occur. Furthermore, it works for any arbitrary number of indent rows, or indent rows with unequal circumferential spacing. When paired with robust basin detection algorithms, the linearity of the data as a function of angular position can be analyzed, and indent row transition points can be determined with high precision.

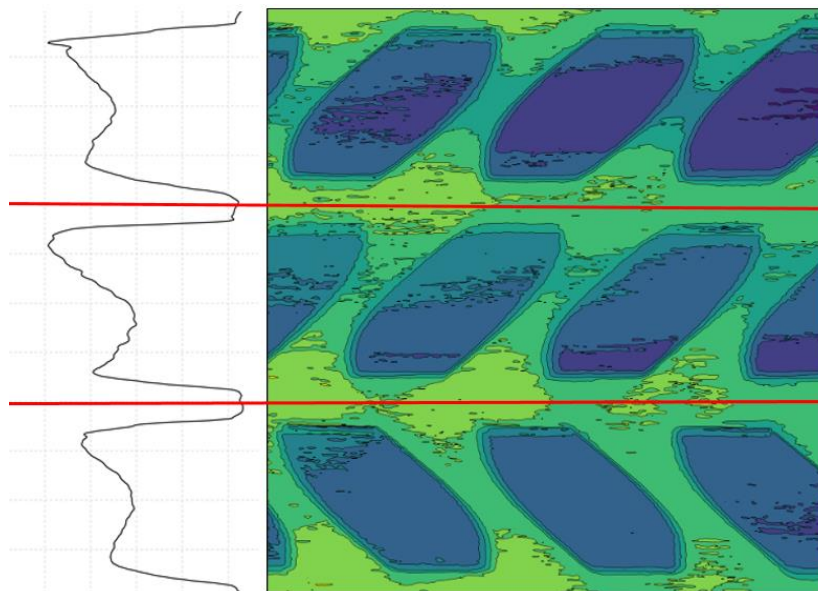


Figure 6.6: Indent Row Detection

6.3 Determining Indent Location and Orientation

Once the indent row locations have been identified by the algorithms detailed in the section above, the detection of individual indents can proceed. To successfully isolate indents, the topic of subsection 6.4, a determination of pitch and orientation for the indents contained by each row is required. Indent pitch is determined using the following process. First, the centerline of each indent row is selected, located directly in between the indent row transition points. Along the centerline profile are the depressions caused by the indents. Upon the centerline profile, Fourier analysis is once again preformed, obtaining the pitch between the indents in the associated row. This can be visualized in Figure 6.7(a) which illustrates the pitch between neighboring indents, determined from the Fourier analysis.

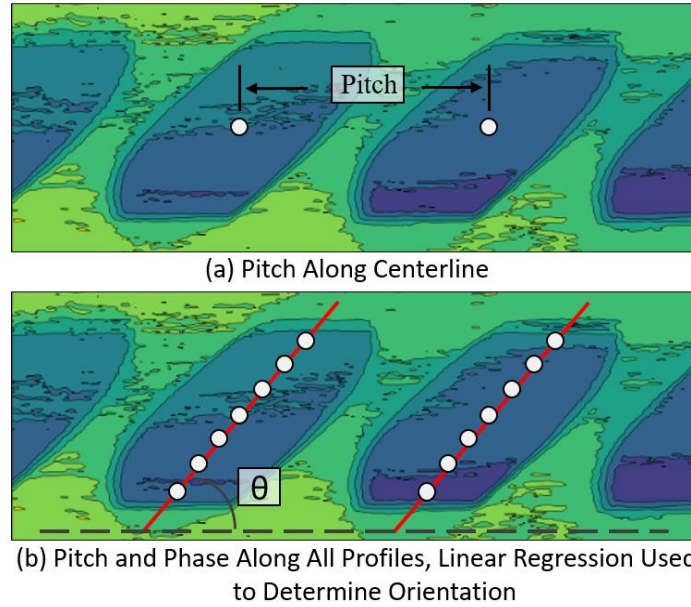


Figure 6.7: Determining Pitch and Orientation Angle

Next, the extraction of indent orientation is necessary. Holding the previously calculated pitch constant, Fourier analysis is carried out on the rows adjacent to the centerline profile to obtain the phase offset of the adjacent profiles with respect to the centerline profile. This processing is carried out on all profiles contained by the width of the indent; the profiles that are contained by the indent width are determined by the linearity of the profiles, or the magnitude ratio of the Fourier analysis. The obtained pitch and phase offset points are illustrated in Figure 6.7(b) as white dots representing the location of the trough of the Fourier transforms on the longitudinal profiles. Through these points, a line of best fit is calculated, seen as a red line in Figure 6.7(b), thus determining orientation of the given row. This methodology is then applied to every indent row, calculating indent pitch and orientation to a high degree of accuracy. Because of how orientation of computed, each indent row is given one orientation angle associated with all of the indents contained by the row.

6.4 Indent Isolation

The one hurdle remaining prior to geometrical feature extraction, is the isolation of individual indents from the rest of the scan. In this process, the indent row locations, along with indent pitch and orientation are used to determine the bounds of the individual indents. Figure 6.8 provides a depiction of the detected boundaries of the indents based on indentation orientation, indent pitch, and indent row width for wire type WF; this is applied on all three rows of wire.

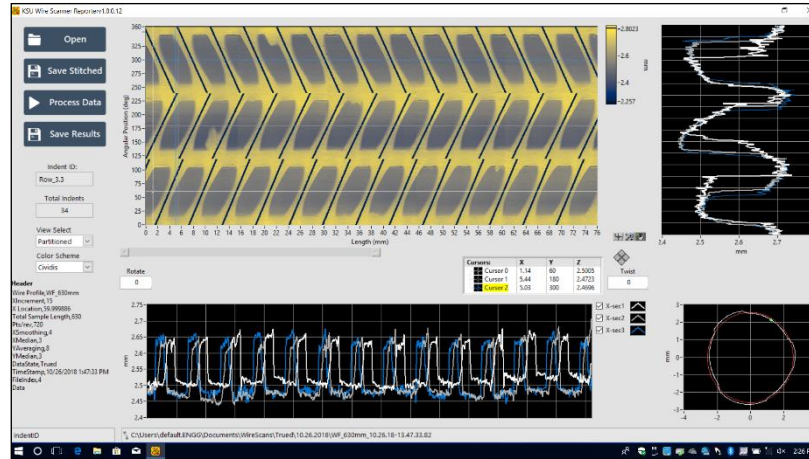


Figure 6.8: Wire Scan Reporter Indent Partitioning

The calculated boundaries of the individual indents are then compared with the limits of the contiguous scan. If an indent is not completely contained within the bounds of the scan, it is classified as a “partial” indent, and thus, is omitted since complete data does not exist for it. The picture contained in Figure 6.9 shows the “complete” indents that fall within the confines of the acquired data. Once the indents have been successfully isolated, they can be subjected to the feature extraction process summarized in the following subsections.

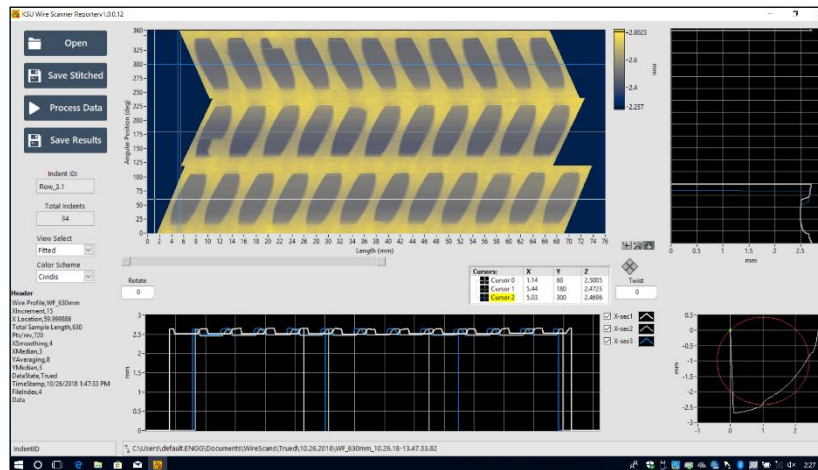


Figure 6.9: Wire Scan Reporter Indent Isolation

6.5 Trapezoid Fit of Least Squares

The majority of the processing procedures up until this point, from data collection to indent isolation, have been generalized enough to work for any arbitrary indentation style. However, there is a departure in the universal aspect of the processing, as individual indent styles must be processed in fundamentally different ways depending on the features that they possess. As stated previously, one cannot use the same set of feature extraction algorithms used for a chevron type indentation on a different wire that utilizes a dotted pattern. A majority of small diameter indented wires used in industry rely on chevron style indents to increase the bond characteristics between the wire and concrete. Thus, the processing algorithms highlighted in this section and the remaining subsections will be focused on the feature extraction of chevron style indents. Furthermore, the results summarized in Section 7 will exclusively detail the chevron style indents that were included within the scope of this research project. It should be emphasized that the generalization of the steps leading up to this point would allow the further development of feature extraction algorithms for indentations of different geometry, namely, dotted or spiral patterns.

The data contained by the isolated indents is well behaved, being thoroughly conditioned by the filtering and corrections highlighted in the previous sections. The primary task remaining is to determine a suitable curve fitting algorithm to identify the critical indent features contained by the data profiles, turning otherwise random data into usable results. Chevron style indents are known for having predictable profile characteristics, featuring flat indent crests and basins, along with straight transitions between these points. Scans were taken of various 5.32mm chevron wires by utilizing the indent profiling system. The centerline profiles of a sampling of these wires is illustrated in Figure 6.10(a). Note the striking similarity between the longitudinal profiles. While the magnitude of the relative depths and sidewall angles differ, all of these profiles can be described under one category, trapezoidal.

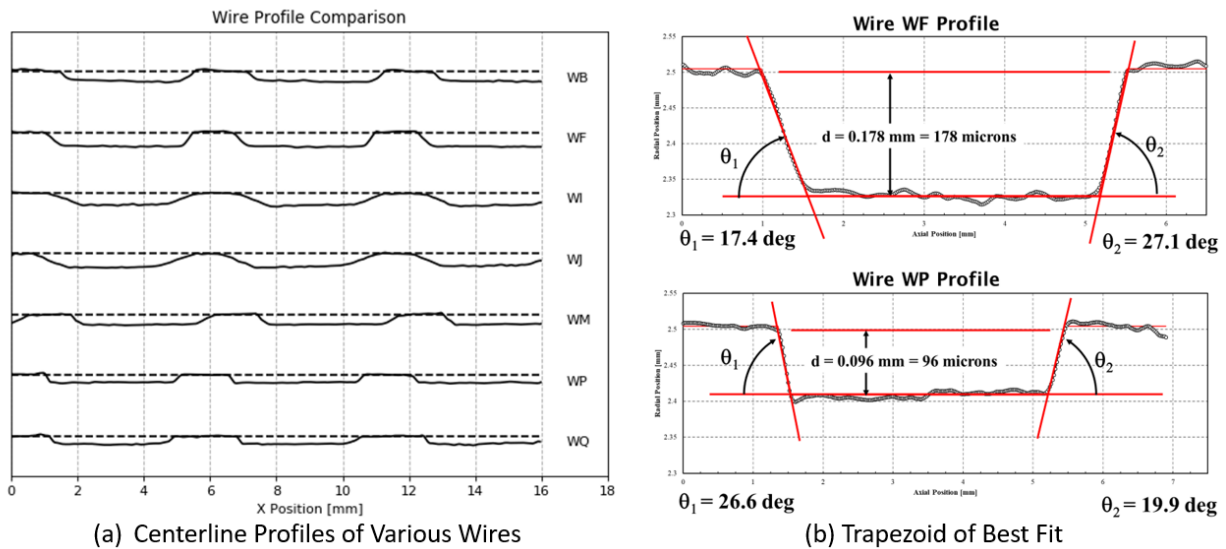


Figure 6.10: Applicability of Trapezoidal Curve Fit

Initial manual processing attempts of the longitudinal profiles is depicted in Figure 6.10(b), clearly showing the applicability of the trapezoidal curve fit to the data profiles. This was repeated across multiple chevron indents and the same success was universally observed. Therefore, in order to extract useful geometrical features from the profiles a trapezoidal curve fitting algorithm was developed.

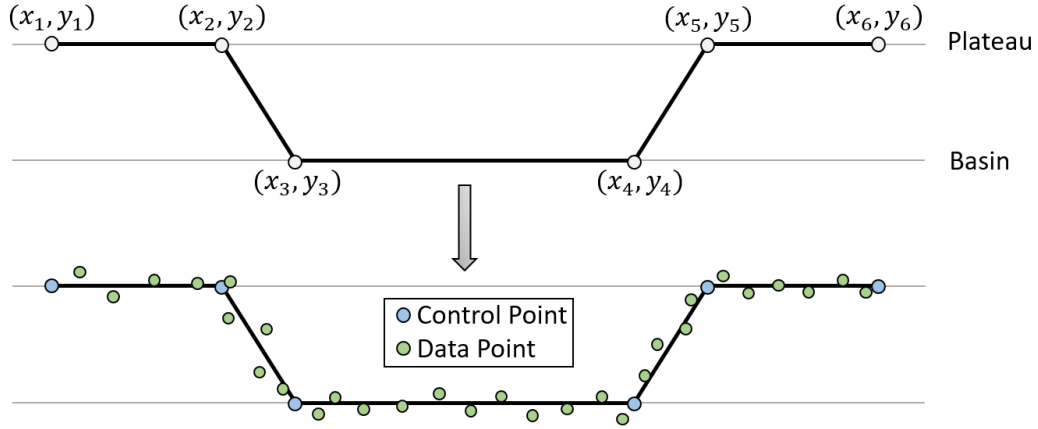


Figure 6.11: Trapezoid Fit of Least Squares

The algorithm is summarized graphically in Figure 6.11, in which, a trapezoid fit of least squares is used to apply a line of best fit to the selected data. The purpose of a least squares algorithm is to minimize the difference between the fitted lines, or lines in the case of a trapezoid fit, and the data visualized as green dots in the figure above. When the minimization of the error between the target profile and the data is achieved, the control points represent the idealized profile fitting the data.

For the case of the trapezoid fit applied to chevron style indents, only two possibilities for the measured heights exists: the top of the indent, and the bottom of the indent. This means that for the aforementioned curve fit, the following must hold true,

$$y_{top} = y_1 = y_2 = y_5 = y_6$$

with the additional requirement,

$$y_{bottom} = y_3 = y_4$$

Further restrictions are applied to limit the curve fitting algorithms, limiting the cases of mathematical degeneracy that prevent realistic solutions,

$$y_{top} > y_{bottom}$$

In addition to,

$$x_1 < x_2 < x_3 < x_4 < x_5 < x_6$$

6.6 Obtaining Primary Geometric Features

The general guideline for the extraction of the geometrical features of an isolated indent are as follows. A trapezoidal fit of least squares is applied on every eligible longitudinal profile of the indent; an eligible profile is defined as falling within the “width” of the detected indent. From these idealized two dimensional profiles the following critical geometry for a chevron type indent is obtained for the particular profile: depth, indent length, basin length, sidewall angles, sidewall lengths, and profile area. The two dimensional results for each profile are then recorded. It is possible to have a centerline depth, an average depth (across all observed profiles), and a maximum/minimum depth (also observed across all profiles). This can also be applied to any other two dimensional parameter obtained from analysis.

Three dimensional indent features are constructed from the 2 dimensional profile results. The integration of profile areas across the width of the indent yields volume, the integration of indent lengths across the width gives planform area, and the integration of sidewall lengths across the indent width obtains sidewall area, and so on and so forth. The integration interval is small, on the order of $20\mu\text{m}$, thus the results obtained via integration are accurate. A more detailed explanation of the extracted variables and how these variables relate to the captured profiles are the subject of the subsections to follow.

6.6.1 Analyzing Width

An assessment of indent width is necessary prior to obtaining other geometrical features. Indent width, in addition to being a reportable geometrical parameter, is used to determine regions of the isolated indent that are eligible for feature extraction. The slant profile of the indent, visualized as the red lines in Figure 6.7(b), are also trapezoidal in nature. By applying a trapezoid fit on the isolated indent slant profile, it is possible to acquire the width of the indent. Figure 6.12 highlights the applicability of using trapezoid fits on the slant profile; the line of best fit overlaps the measured data, indicating excellent agreement. However, it would significantly degrade the quality of the data extraction process if extremely shallow profiles were allowed to be included within the width of the indent, thus, the width of the indent is defined as where the average profiles exceed a depth of $20\mu\text{m}$.

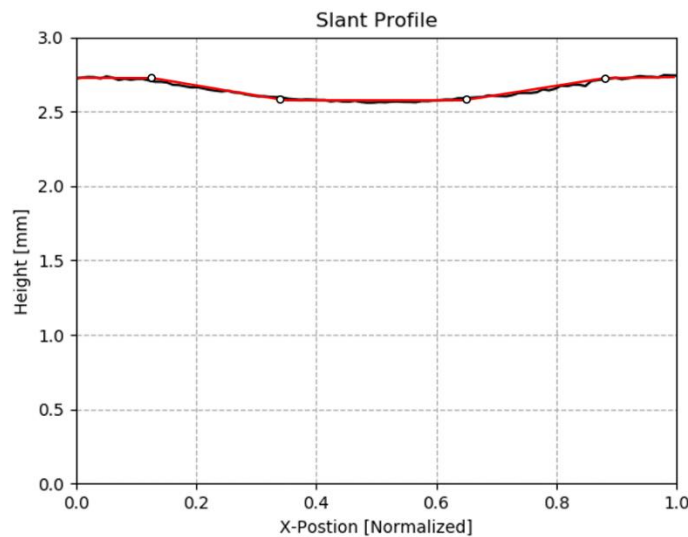


Figure 6.12: Trapezoid Fit of Indent Slant Profile (Wire WM)

6.6.2 2-D Geometry

The two dimensional geometry is summarized by the features extracted directly through the use of the trapezoidal fit of least squares. These two dimensional features are illustrated below in Figure 6.13, which overviews the primary 2D characteristics; the only 2D feature omitted from the illustration is basin length, which is length of the bottom horizontal line of the curve fit. The observation of pitch in the two dimensional context is redundant since it has already been ascertained in a previous section and was used to determine the bounds of the indent isolation. An important observation is made that two geometrical features obtained from the curve fit have values that are dependent on the side of the indent in which they are measured. Sidewall angle and sidewall length are such values. Sidewall angle for example, will have a separate value related to the left and right side of the profile. All of these two dimensional values are obtained from every longitudinal profile that is contained by the width of the indent, and thus, all of these 2D values vary as a function of location along the width of the indent. All of these values are recorded in the results file generated by the indent profiling system and are integral to the calculation of the three dimensional geometry in the section that immediately follows.

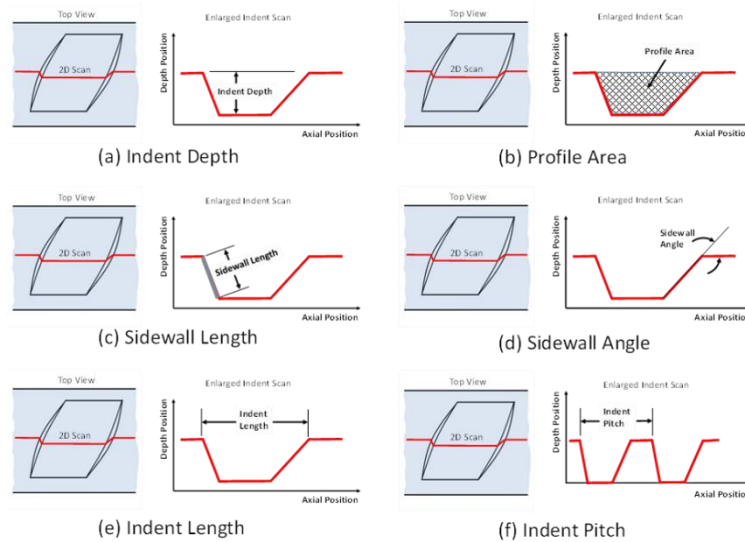


Figure 6.13: 2D Wire Indent Geometrical Features

6.6.3 3-D Geometry

The three dimensional geometry extracted by the indent profiling system relies on the integration of two dimensional parameters, or observations that rely on the conglomeration of sets of two dimensional data (such as average depth). To put it simply, the three dimensional geometry is data that cannot be computed from two dimensional data acquired for a single profile alone. The key 3D profiles to be measured by the indent profiling system are illustrated in Figure 6.14, this is the same illustration from Section 3 but is reproduced here for convenience. A brief description is given in the following paragraph for how each 3D parameter highlighted by the figure below is calculated. Note that every 3D parameter is computed as a scalar value and does not vary as a function of indent width, in contrary to the 2D parameters.

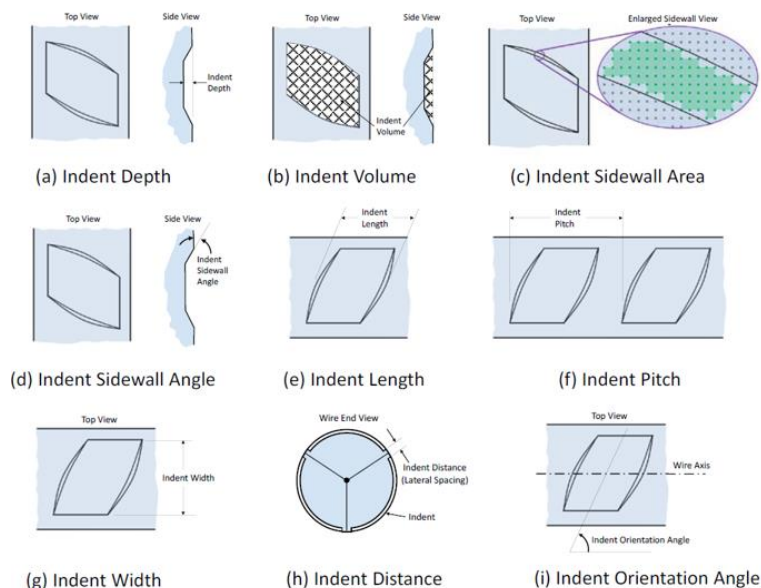


Figure 6.14: 3D Wire Indent Geometrical Features

Indent depth is computed as the average depth of all of the accumulated two dimensional profiles. Indent volume is the integration of all profile areas across the width of the indent. Likewise, sidewall area is the integration of the 2D sidewall lengths across the width of the indent; two sidewall areas exist, left and right. Indent sidewall angle (3D) is the average sidewall angle of the two dimensional parameters: two sidewall angles exist, left and right. Indent length (3D) is the average indent length of the two dimensional parameters. Pitch is classified as a 3D parameter since it is computed based on all of the indents contained by a single indent row, rather than a single isolated indent. Pitch has the same value that is obtained by the algorithms in Section 6.3; each row has a separate pitch value. Indent width for each isolated indent is obtained using the method elucidated in Section 6.6.1 prior to 2D feature extraction. Indent distance is the average rib spacing determined by the profile linearity procedure listed in Section 6.2.2. Finally, indent orientation angle is computed per row in Section 6.3. One additional three dimensional indent feature not illustrated in Figure 6.14 is planform area, which involves the integration of all indent lengths across the width of the indent.

The geometric features listed in this section and the prior section play a crucial role in quality control. A selection of chevron type wires from modern industry, historical concrete crossties, and fabricated specimens were processed by the indent profiling system; the results of which will be the main source of discussion in Section 7. Furthermore, the three dimensional data has been shown to correlate favorably with certain performance criteria, particularly transfer length and splitting propensity. The significance of the two-dimensional and three dimensional data on wire-concrete performance characteristics will be the primary subject of Section 9.

6.7 File Report Format

The discussion of this brief section will encompass the layout of processing results file format now that the data acquisition and feature extraction processes have been explained. The processing results file details the 2D and 3D geometrical features extracted from the scanned wire; additionally, it records the curve fit data of all longitudinal profiles that were processed for

each individual indent. The file can be divided into two main components: the global data block and the indent data blocks associated with the individual isolated indents.

A depiction of the global data block can be visualized in Figure 6.15. Similarly to the wire scan report, a short header is provided prior to the data, in which, the basic characteristics of the scan subjected to processing are recorded. Below the header, a high level overview of the processing results is given, most notably, the nominal diameter of the scanned wire, the number of isolated indents that were subjected to processing, and the IDs of any isolated indents that were manually omitted from the report by the operator. Next, variables that are unique per indent row are tabulated. These variables include the orientation angle of the indents in the row, the average width of the indents per row, and the physical spacing between the indent rows that the rib occupies (the region in which no indentations occur along the length of the wire). Below that, an array is listed: the global data block. The global data block contains any variable that represents a single value for an isolated indent. Each indent is specified by the row that it occupies and its position within the row, providing a unique identifier for the isolated indent. The following scalar 3D values are recorded per indent: volume, pitch, width, sidewall area (left and right), average depth, and average sidewall angle (left and right). Further post-processing of the results file by a separate program generates a more exhaustive list of 2D and 3D parameters, 38 overall, far too many to conveniently name in this short section.

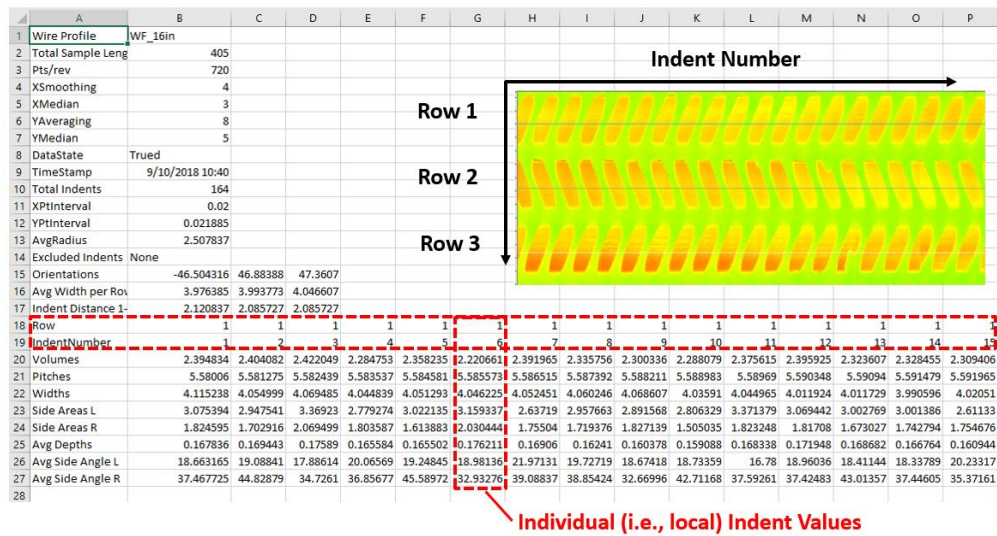


Figure 6.15: Indent Profiling System Initial Report (Global Block)

The second component of the processing report file contains the indent data blocks associated with the individual isolated indents. Figure 6.16 provides an overview of the layout of a typical indent data block, which contains the information for a single indent. Each indent data block contains a header, the top of which highlights the ID of the isolated indent, along with information related to the coordinate system of the indent. Scalar, unique values for the indent directly follow, such as orientation, volume, pitch, width, and sidewall areas of the indent. These values are also seen in the global data block. Finally, an array can be seen that summarizes the results of each trapezoid fit applied to each line-scan that falls within the width of the indent. From this information, everything can be calculated through the use of a results file post-processor, centerline depth, maximum sidewall angle, average indent length, etc. An indent

[illegible]

6.8 Post-Processing, Statistics Generation, Histograms

```
graph LR; TS([Trued Scan]) --> R[Results]; R --> PPR[Post-Processed Results]; PPR --> S[Statistics]; TS --> HMR[Height-Map Renders]; R --> Rpt[Reports: ASTM A881 ISO 16120]; PPR --> H[Histograms]
```

From the calibrated scans, images of the height-maps and three-dimensional views of the wires can be rendered to show the physical surface features. By utilizing the initial processing results file, reports can be created for common measurement standards, namely ASTM A881 and ISO 16120 as discussed in Section 2. Further post-processing of the initial report yields additional 2D and 3D parameters that prove to be useful in characterizing the manufacturing process of the indented wires, or are related to wire-concrete performance criteria. By analyzing the post-processed results, detailed statistics can be ascertained, along with histograms that visualize variations in the measured features. A potentially limitless ability exists to envision and process the captured data, but these represent the results that are of immediate interest to the scope of this research.

7. Overview of Collected Data

With respect to the development of the non-contact indent profiling system, the research was divided into two primary phases. During phase I of this project the key objective was to design and implement an automated indent profiling system to produce unbiased, statistically-relevant sample sizes. After motion control and data acquisition of the system was implemented, calibration techniques and data manipulation steps were developed to enhance the quality of the data being received, and algorithms were implemented for feature extraction. Then, the system would be applied to measure specimens of known geometry to verify the correct and reliable operation of the system and quantify expected measurement uncertainties as described in the prior sections.

Phase II of the project involved the application of the Indent Profiling System to measure the indent characteristics of a multitude of indented wires; the discussion of the geometric feature data extracted by the indent profiling system will be the primary subject of this section. A sampling of these wires will be from those used in modern industry, a subset will be wires that were extracted from historical crossties that had been in track for upwards of multiple decades, and another set of wires were created with known “machined indents” for use with system checkout. In conjunction with the transfer length and splitting propensity testing of concrete prisms for this project, the indent profiling system results will then be used to extensively investigate which geometrical parameters of indented wires contribute most significantly, or detrimentally, to prestressed member performance criteria. The correlation of the indent profiling system results with performance criteria will be extensively discussed in Section 8.

Table 3: Wires Included in Study

Processed Wires		
Cover Testing	Crosstie Wires	Machined Wires
WB	E-1	15
WD	F-1	15-.16-T1
WF	H-1	30-.16-T1
WG	J-1	45-.16-T2
WH	K-1	60-.16-T1
WI	L-1	75-.16-T1
WJ	M-1	90-.16-T3
WM		X1
WP		X2
WQ		X3
		X4
		X5

The first set of wires, those commonly used in modern industry, represent a wide variety of indent depths and indentation shapes, additionally, the wires feature considerable differences in sidewall angles used in practice. These selected wires share a common “chevron” pattern and

are nominally 5.32mm in diameter. The geometrical results obtained from these modern wires were used to analyze the variations of the individual parameters on a row-by-row basis and across the entire specimen. Furthermore, concrete prestressed prisms were created using the same wires; the geometrical features could then be correlated against measured performance criteria of the test prisms, thus determining which geometrical characteristics have the most significant influence on wire-concrete performance. Wires extracted from pre-existing concrete railroad ties in service represent the second set of wires. These wires form the basis for wire geometry that tends to work well in practice, as many of the crossties that the wires were extracted from performed favorably over the course of decades. Some of the concrete ties were subjected to an estimated 4 billion gross axle tons of loading during the service life of the tie, indicating favorable wire-concrete performance. The third group of wires, those with fabricated “machined” indents, were used for system calibration and verification of feature extraction algorithms. A list of the wires included in the study is provided in Table 3; the first wire group corresponds to “Cover Testing” wires. A detailed discussion of the indentation features of all three wire groups subjected to processing by the indent profiling system will occur in the following subsections.

7.1 Cover Testing Wires

A large subset of the wires subjected to testing included wires that are frequently used in modern industry. These wires represent a wide variety of indent depths and indentation shapes, additionally, the wires feature considerable differences in sidewall angles used in practice. A majority of these wires were amassed through prior FRA research projects in addition to wires provided by Nucor-LMP, a commercial partner in the current FRA research project outlined by this report. The wires contained by this group, representing ten unique chevron type wires, will be used to satisfy a critical component of the second phase of this project. First, the geometric features of these 10 unique wires will be extracted by the indent profiling system. Second, the captured indented wire geometry will then be used in conjunction with empirical data obtained from prestressed concrete prisms created using the same ten wires. The concrete prisms were constructed with the purpose of measuring the effect of reduced concrete cover on wire-concrete performance criteria, thus, the wires in this group are named the “cover testing” wires. From this combined information, indentation geometry can be correlated with wire-concrete performance criteria such as transfer length and splitting propensity to quantitatively determine which indent features contribute most significantly, or detrimentally, to desirable performance characteristics. The subject of correlations will be the source of extensive discussion in section 9.

Furthermore, large quantities and lengths of wires exist for this group. Thus, statistically relevant sample sizes can be obtained, allowing the indent profiling system to analyze the manufacturing intricacies of the wires on a row-by-row basis as hundreds of indents can be sampled per wire specimen. No manufacturing process is perfect; the information extracted by the indent profiling system will be used to highlight the significant manufacturing variations seen in individual wires. The indent profiling system will be used on the wires in this group to capture a full revolution of the indent rollers, representing the capture of all statistically unique indents formed by the manufacturing process. Further discussion of the wire pattern repetition that this system is capable of detecting makes use of the data captured for this group of wires and will be overviewed in section 8.

7.1.1 Cover Testing Wire Specimens

Ten unique chevron type indented wires from modern industry were included in this area of the project. These wires were subjected to scanning by the indent profiling system. The extracted geometry would then be used to investigate the statistical significance of the captured data, investigate the manufacturing differences of indent geometry on a row-by-row basis, and provide the information necessary to assist with the correlation of wire features with wire-concrete performance criteria. The ten cover testing wire specimens were cut to 36 inch lengths; the specimens were stored in sealed PVC tubes prior to use, and thus, were free from any signs of corrosion that would impair wire scanning. Digital microscope images of the ten cover test wires are provided in Figure 7.1, this composite image covering all of the cover testing wires demonstrates the diversity of geometric features that the group possesses. The wire naming conventions were adopted from prior FRA research projects; the nondescript naming identifiers protect the identities of the wire manufacturers of each specimen.

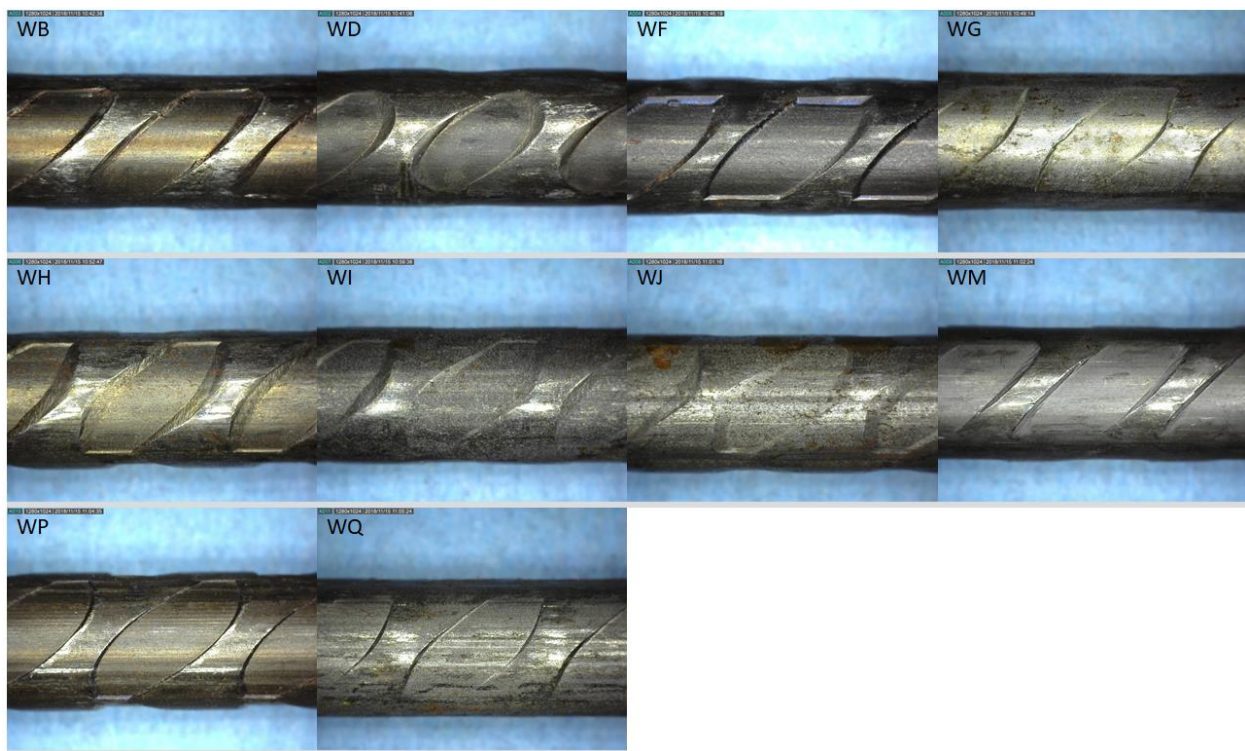


Figure 7.1: Digital Microscope Images of Cover Testing Wires

From the figure above, it is clear that all of the wires conform to a general chevron pattern; WD may appear to be elliptical in nature, but closer observation reveals that the top and bottom of the indent, from the perspective of the image, form horizontal lines. Some notable observations of the digital microscope images of the cover testing wires are as follows. Wire types WF and WH appear to be the deepest indentations of the lot, this assessment arises from the fact that the indentations are deep enough to justify having a sidewall angle at the top and bottom of the indent rather than just the right and left side. This observation, coupled with the generous planform area, would indicate that these indents will have the largest volumes in comparison to the rest. Furthermore, the shallowest indents appear to be WG and WQ, both are unlikely to have an average depth that exceeds 60-70 μm , or volumes that are larger than 1 mm^3 .

Additionally, it appears that WH, WI and WJ have similar sidewall angles of around 10° and most likely contain the shallowest sidewall angles out of the entire cover testing wire group. Furthering this observation, wires WH and WJ should have the largest sidewall areas once indentation depth has been considered along with the shallow sidewall angles. All indentations appear to have an orientation angle that comfortably exceeds 45° by visual inspection. The steepest sidewall angles observable by the microscope images are wires WF, WM, and WP; all of these indents feature crisp sidewall angles that are 20° or larger. Finally, wire WF appears to have the highest manufacturing quality out of any of the wires in the group, exhibiting minor imperfections caused by the occasional damaged indent roller tooth, cleanly made indents, and created from a wire with no inherent cast. A contour plot of a scan segment of wire type WF clearly demonstrates the crispness of the indentation pattern, illustrated in Figure 7.2.

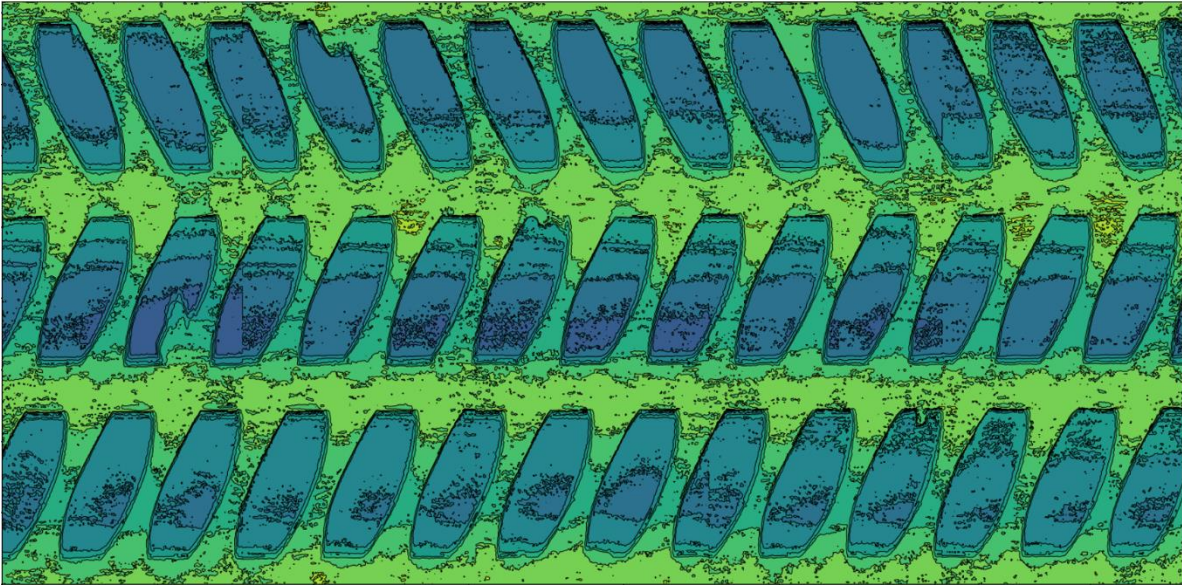


Figure 7.2: Scan Segment of Wire Type WF

7.1.2 General Data

The ten chevron type indented wires used for cover testing were subjected to processing by the indent profiling system. Each specimen in the group was successfully scanned; 25 inches (630mm) of each wire was scanned, capturing enough data to characterize a complete repetition of the indent rollers. By capturing the indentation pattern caused by one full revolution of the indent rollers, all statistically unique indents formed by the manufacturing process can be evaluated, leading to statistically significant sample sizes. On average, over 300 unique indents were scanned per cover testing wire specimen, representing over 100 indents per row. This allows for the visualization of manufacturing variations over the span of the entire wire, or on a row-by-row basis. The data captured by the indent profiling system on the ten cover testing wire specimens is summarized in Table 4, in which the mean values of all scanned indents are tabulated. Table 5 follows shortly thereafter, which summarizes the standard deviations of the same data set.

Table 4: Cover Testing Wire Indentation Data (Means)

Indent Data (Cover Testing Wires)										
	ID	Nominal Dia [mm]	Orientat-ion [deg]	Total Indents	Volume [mm ³]	S.W. Area [mm ²]	Avg Depth [mm]	S.W. Angle [deg]	Avg Length [mm]	Pitch [mm]
Mean	WB	5.153	47.7	302	1.696	2.922	0.119	20.24	4.060	5.580
	WD	5.257	57.8	337	1.600	2.744	0.141	18.62	3.512	5.548
	WF	5.195	48.4	333	2.446	2.452	0.163	24.33	4.014	5.604
	WG	5.324	56.1	332	0.760	2.317	0.066	16.07	3.885	5.644
	WH	5.107	51.0	332	2.154	3.961	0.164	9.83	3.676	5.599
	WI	5.208	50.1	335	1.102	2.850	0.094	9.69	3.436	5.593
	WJ	5.211	50.8	333	1.428	3.638	0.123	9.75	3.411	5.609
	WM	5.175	47.3	334	1.252	2.062	0.101	18.98	4.085	5.564
	WP	5.283	50.3	315	1.745	1.803	0.117	33.96	3.444	5.581
	WQ	5.288	55.8	332	0.776	2.149	0.067	17.75	3.878	5.645
S.W. Area: The average sidewall area of the left and right side of the indents.										
S.W. Angle: The average sidewall angle of the left and right side of the indents.										

Table 5: Cover Testing Wire Indentation Data (Standard Deviations)

Indent Data (Cover Testing Wires)										
	ID	Nominal Dia [mm]	Orientat-ion [deg]	Total Indents	Volume [mm ³]	S.W. Area [mm ²]	Avg Depth [mm]	S.W. Angle [deg]	Avg Length [mm]	Pitch [mm]
Standard Deviation	WB			302	0.219	0.679	0.009	9.15	0.149	0.015
	WD			337	0.109	0.568	0.010	5.12	0.158	0.013
	WF			333	0.145	0.829	0.011	11.91	0.098	0.020
	WG			332	0.059	0.573	0.006	6.32	0.113	0.003
	WH			332	0.193	0.468	0.015	2.14	0.068	0.004
	WI			335	0.104	0.420	0.006	2.94	0.093	0.010
	WJ			333	0.080	0.767	0.008	2.36	0.087	0.004
	WM			334	0.100	0.562	0.005	8.48	0.049	0.006
	WP			315	0.132	0.413	0.012	17.53	0.101	0.005
	WQ			332	0.069	0.469	0.006	7.59	0.100	0.003
S.W. Area: The average sidewall area of the left and right side of the indents.										
S.W. Angle: The average sidewall angle of the left and right side of the indents.										

It should be noted that the parameters contained by the tables listed above come directly from the requirements of the two main indented wire measurement standards, as well as parameters that were found to correlate favorably with wire-concrete performance criteria. Many more geometric parameters are computed by the indent profiling system, but the tabulated information represents a sampling of the most important ones.

From the tabulated information above, the following observations can be made. The majority of the wires would be classified as 5.32mm wires under ASTM A881 due to the listed nominal wire diameter. As predicted by the inspection of the digital microscope images, all wire types comfortably exceed an orientation angle of 45°. Furthermore, the smallest indents by volume are WG and WQ, not passing 1mm³, while the largest indents are WF and WH; the tabulated data matches the previous observations of the digital microscope images. It was predicted that the

indents with the shallowest sidewall angles would be wires WH, WI, and WJ, being less than 10°; this is supported by the data tables. Unsurprisingly, the indentations of wire types WF, WM, and WP encompassed some of the steepest sidewall angles of the group, being joined by WB and WD in exceeding sidewall angles of 18°. Furthermore, a majority of these wire types would pass the measurement requirements set out by ASTM A881 highlighted in section 2.1.

The most important takeaway from the tables listed above, is the inherently high standard deviations of some of the parameters, namely sidewall angle and sidewall area. It will be discussed in the subsection that immediately follows that the standard deviations of parameters for each individual row can be significantly lower than the standard deviations of the entire sample, implying that each row is statistically different from its companions. It is often insufficient to trust mean values that represent the entire sample when significant manufacturing variations exist on a row-by-row basis. The manufacturing variations of the measured cover testing wires scanned by the indent profiling system is highlighted in the following subsection.

7.1.3 Statistical Variation

The ability of the indent profiling system to collect statistically relevant sample sizes, in which, all unique indents formed by one complete repetition of the indent rollers are captured, allow for the analysis of geometric parameters on a row-by-row basis. No manufacturing process is perfect, and thus, it is expected that variations exist between neighboring rows, and within the individual rows themselves. These variations can be the byproduct of multitude of things: unequal indent roller pressure, damaged roller teeth of individual rollers, improper geometry of the roller teeth, and this list goes on. This subsection highlights the importance of using statistically relevant sample sizes to analyze the intricacies of the manufacturing process of the resulting indentation geometry and the ability of the indent profiling system to provide the necessary data.

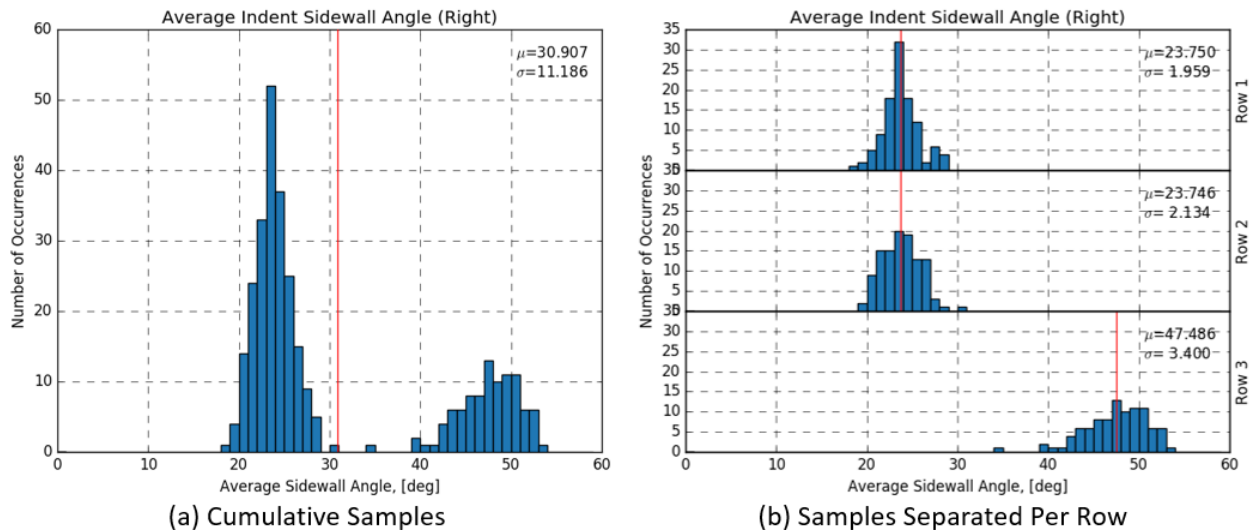


Figure 7.3: Variation of Sidewall Angles on the Right Side (Wire WP)

The previous subsection noted the presence of unusually high standard deviations of some of the parameters listed in Table 5. The deviations of the sidewall angles and sidewall areas of wire types WF and WP represented a large percentage of the mean measured values in Table 4. For example, the standard deviations of the average indent sidewall angles (right side) of all

observed samples for wire type WP is 11.19° , whereas the standard deviations of the same parameter per row do not exceed 3.40° . Note that these values do not correspond directly to the data tabulated in Table 4 and Table 5 since those tables specifically list the average sidewall angles of the combined left and right sides. Since the standard deviations of parameters for each individual row can be significantly lower than the standard deviations of the entire sample, it implies that each row is statistically different from its companions. This is clearly emphasized in Figure 7.3, in which, histograms of the average sidewall angle of the right side of the indent are provided for the cumulative samples, and on a row-by-row basis. Figure 7.3(a) represents a bimodal distribution, with the peak on the left side rising significantly above the peak on the right. This implies that the two rows on the right side of the indent contain shallower sidewall angles than the third row. This is confirmed by Figure 7.3(b), which indeed shows that one indent row has sidewall angles that are twice as steep as the other two rows on the right side.

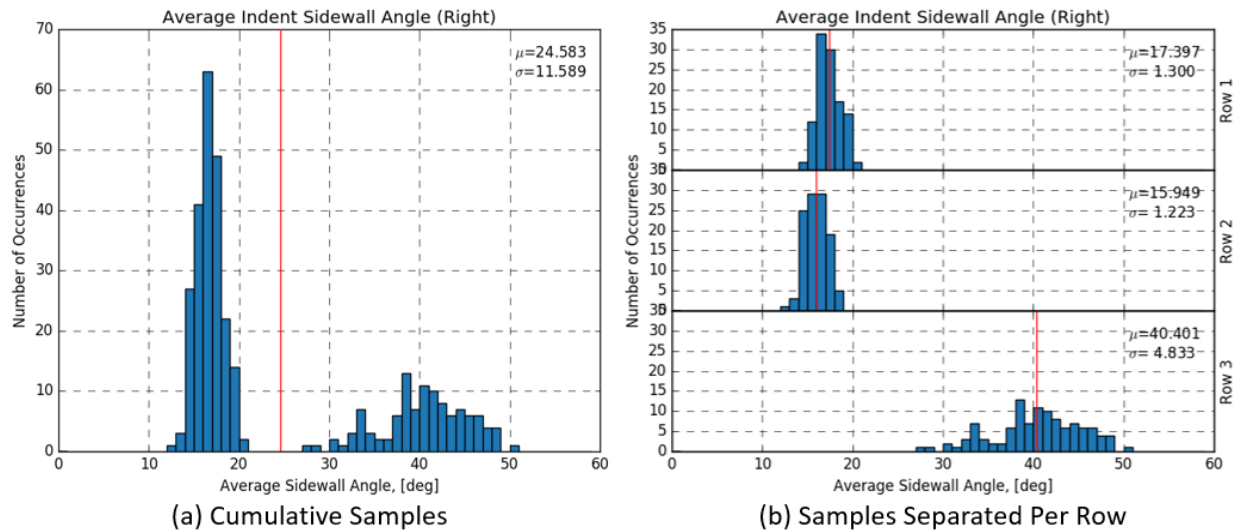


Figure 7.4: Variation of Sidewall Angles on the Right Side (Wire WF)

From the data contained by Table 5, it is obvious that wire type WF suffers from the same problems that WP has in regards to inconsistent sidewall angles on a row-by-row basis. Figure 7.4, which shows data pertaining to wire type WF, shares the same story and observation that Figure 7.3 does. It is worthy to note that the statistical distribution of the row containing the steeper sidewall angles is so far away from its shallower counterparts that the independent statistical distributions do not overlap at any point.

Furthermore, the severity in the differences of the parameters on a row-by-row basis are not isolated to a single side of the indent. In the case of average sidewall angles, the disparity between rows can persist on both the right and left side of the indentations. This is illustrated by the histograms provided in Figure 7.5, which display the variations of sidewall angles per side and per row. Note how the two rows with steeper sidewall angles on the left side of the indent switch to being shallow on the right side of the indent; the third row, shows the opposite trend. It is unlikely that the large variations in sidewall angles are desirable, or even intended, from a manufacturing standpoint; however, up until this point it has not been possible to capture statistically significant sample sizes of sidewall angle per row, and thus, the manufacturer is likely unaware that this disparity even exists.

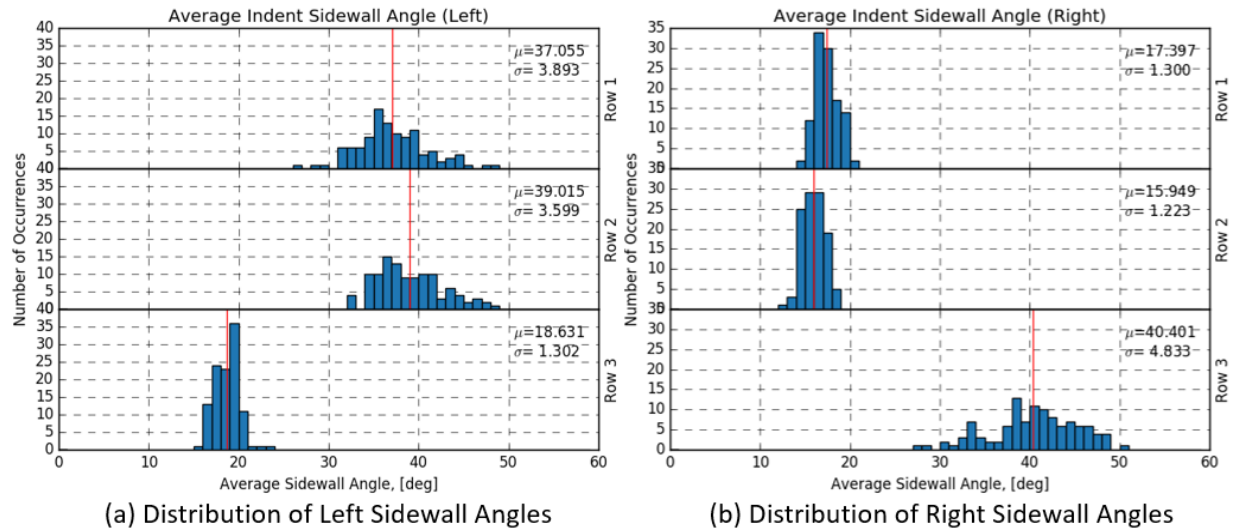


Figure 7.5: Variation of Sidewall Angles Between Sides (Wire WF)

For each cover testing wire, a length of 25 inches (630mm) was scanned and subjected to processing, thus, over 300 total intents per specimen were analyzed, representing over 100 indentations per row. Enough data is captured per scan to be statistically relevant, this can be seen by the histograms shown in the aforementioned figures in this section that clearly show the statistical distributions of the indent parameters on a cumulative and row-by-row basis. Thus, it is useful to bound the collected data with confidence intervals that can accurately describe the range that a majority of the captured data encompasses. A confidence interval of 95% was applied to some of the critical geometric parameters listed in Table 4 per indentation row to help visualize the measured variations of the collected data. Confidence intervals of 95% are favored by statisticians to provide bounds on where 95% of the measured values are expected to be found.

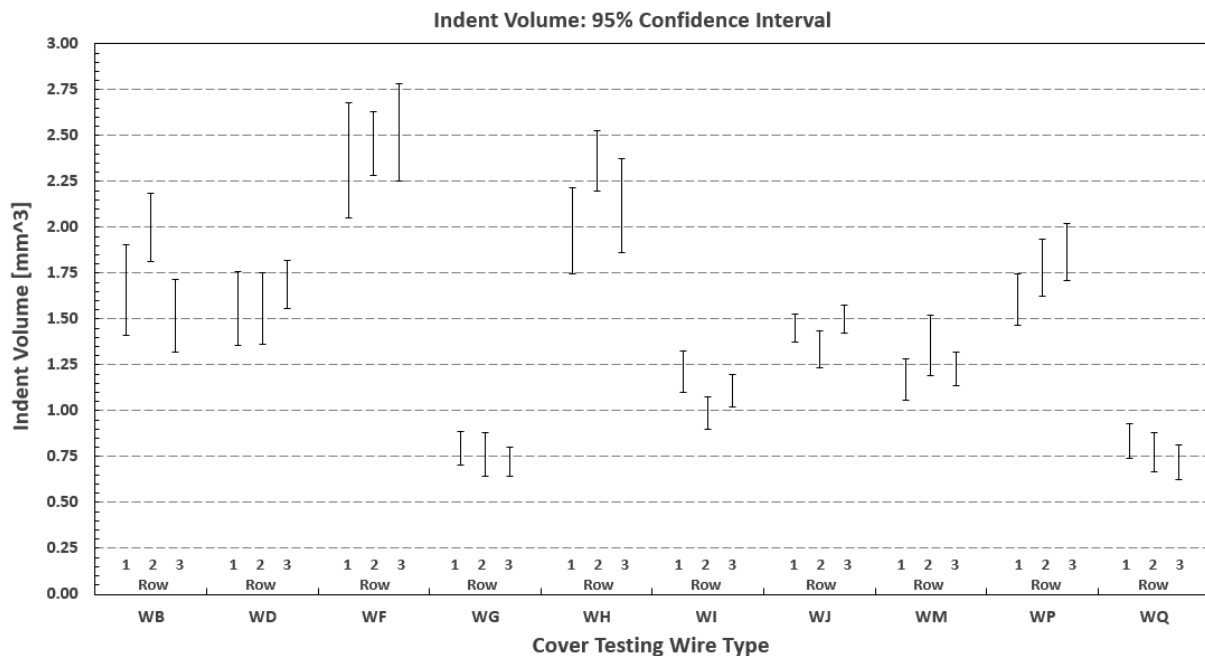


Figure 7.6: Measured Variations of Indent Volume

The plot provided above in Figure 7.6 details the measured variations of indentation volume per row and per wire type. Once again, the error bars show where 95% of the data is expected to reside within the particular data pool. For example, 95% of the indent samples for row 1 on wire type WB are expected to fall in the range of 1.41mm^3 to 1.91mm^3 . Specimens in which the confidence bars significantly overlap one another across all three indent rows, implies that every row shares similar manufacturing variations. Wire specimens WG and WQ are prime examples of this, visualized in Figure 7.6, and consequently have exceptionally low standard deviations for indent volumes, measured across all indents, summarized in Table 5. In contrast, wire types WB and WH have widely different measured indent volumes per row; some of the data per row hardly overlaps the data of neighboring rows, implying large manufacturing variations exist.

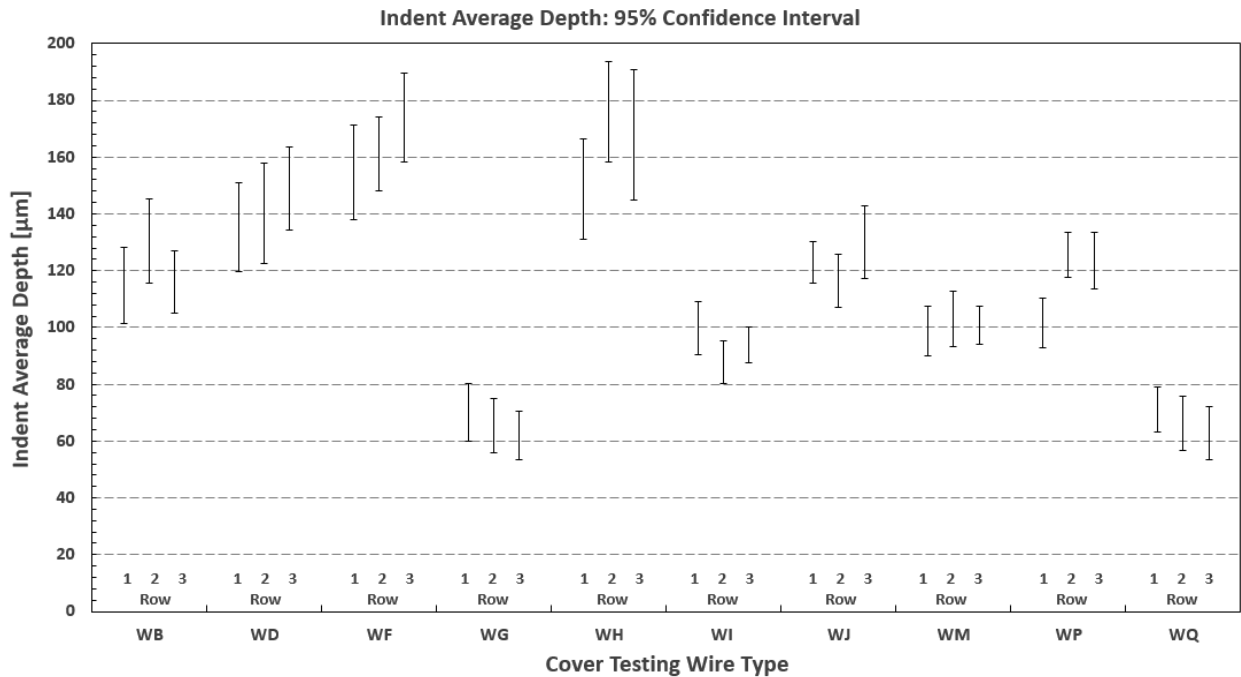


Figure 7.7: Measured Variations of Indent Average Depth

Figure 7.7 depicts the variations of average measured indentation depths and shows similar trends to the aforementioned volume plot. Wire types WD, WG, WM, and WQ have confidence intervals that closely match across rows, resulting in standard deviations that constitute a low percentage of the mean values tabulated in the prior subsection. Furthermore, wires WH and WP have rows with significantly different manufacturing characteristics when it comes to average indentation depth. Figure 7.7 also visually indicates that WH possesses the deepest indentations, whereas WG and WQ are the shallowest. It is worthy to note that Figure 7.6 and Figure 7.7 share significant similarities in the overall shape of the plot. This is due to the fact that indentation volume and indentation depth are highly correlated with one another and will be discussed more thoroughly in section 9.

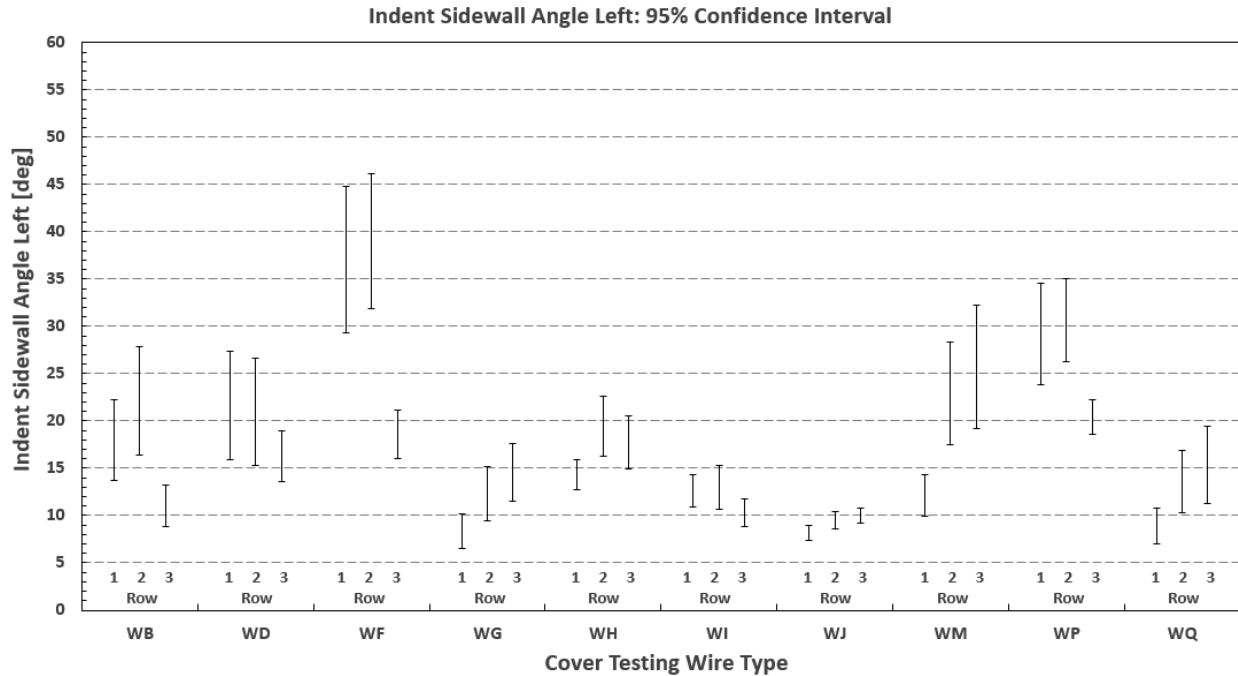


Figure 7.8: Measured Variations of Average Indent Sidewall Angle (Left Side)

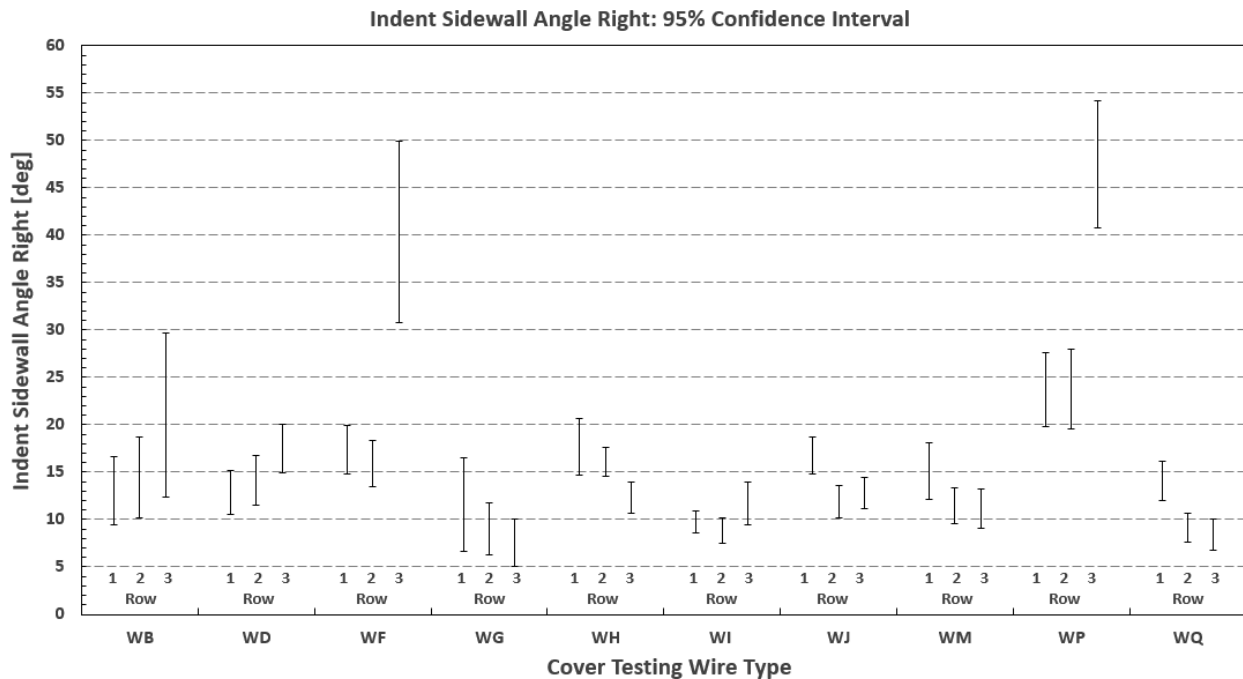


Figure 7.9: Measured Variations of Average Indent Sidewall Angle (Right Side)

Figure 7.8 and Figure 7.9 portray the measured variations of the average indent sidewall angles of the left and right side of the indentations respectively, per row. These plots are in clear agreement with the manufacturing variations highlighted in histograms contained by Figure 7.3, Figure 7.4, and Figure 7.5. Wire types WF and WP have vastly different indentation angles per

row as indicated by the confidence interval plots. Both of these plots imply that indentation sidewall angle is exceptionally challenging to manufacture consistently in comparison to other parameters. Sidewall angle is highly sensitive to slight variations in indentation depth and the span over which the sidewall occurs.

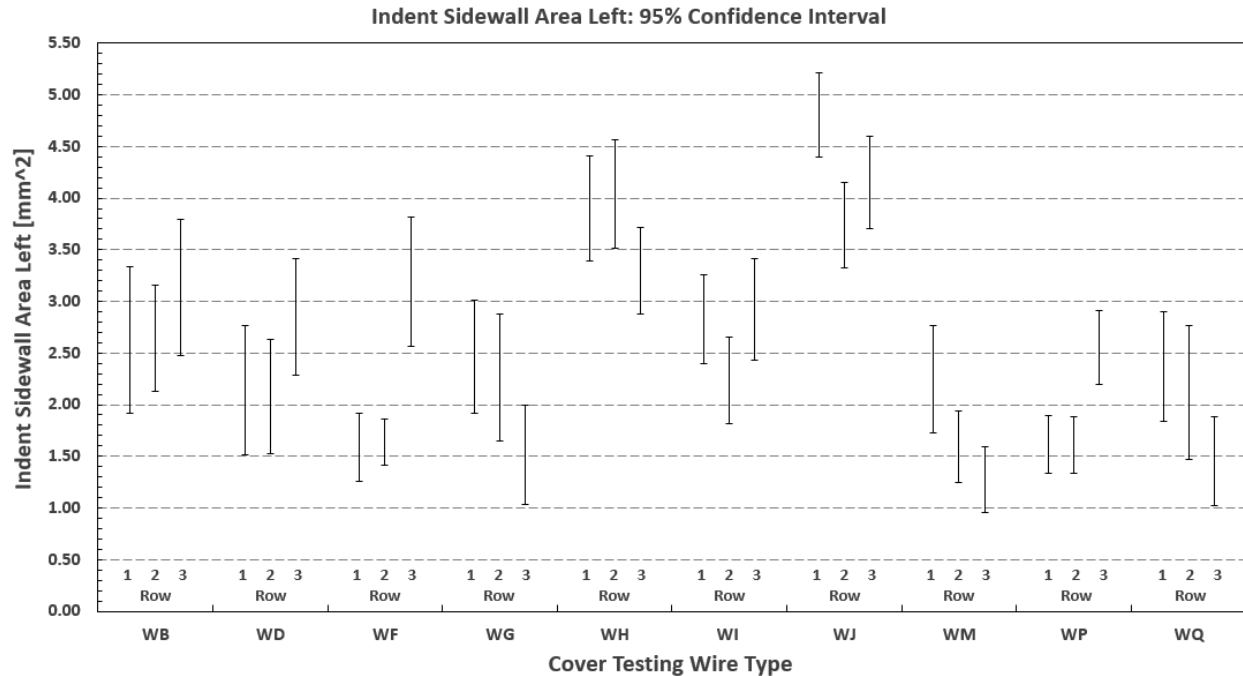


Figure 7.10: Measured Variations of Indent Sidewall Area (Left Side)

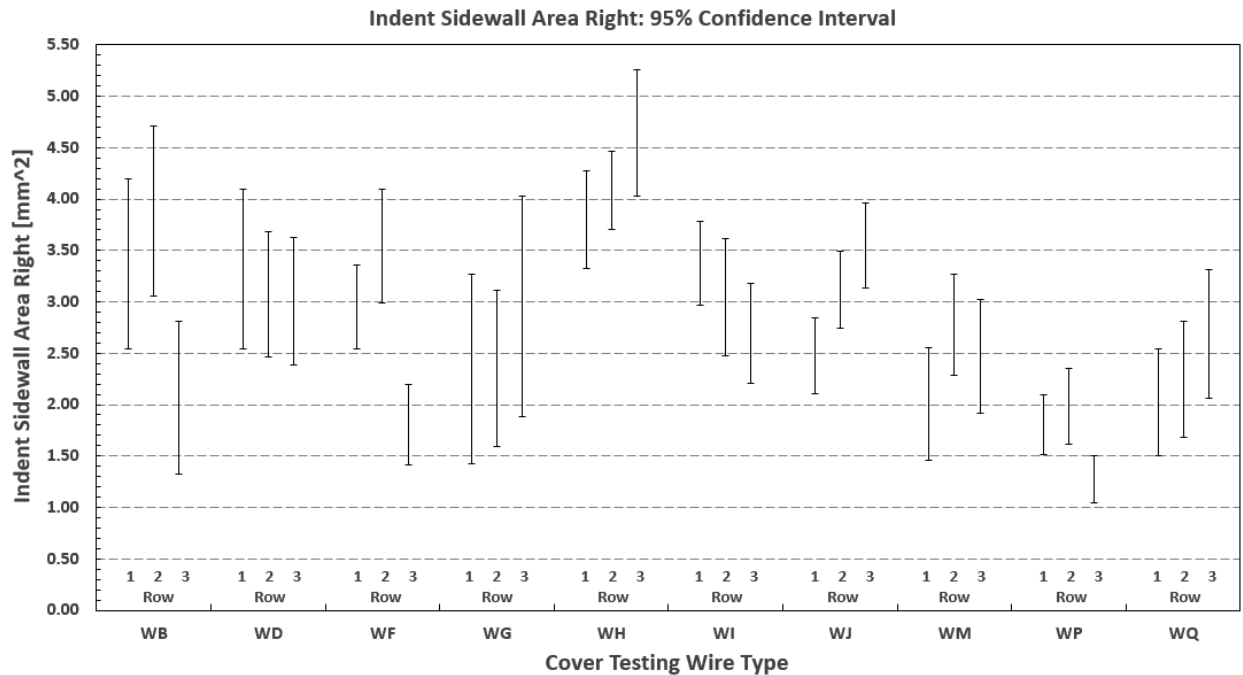


Figure 7.11: Measured Variations of Indent Sidewall Area (Right Side)

Figure 7.10 and Figure 7.11 show the measured variations of the indent sidewall area per row. The most notable takeaway from this set of plots is that sidewall area is challenging to maintain consistently as well; this is evident from the fact that many of the confidence intervals across rows of the same wire type do not overlap. Furthermore, the standard errors of the computed confidence intervals are a large percentage of the measured mean values. This indicates that not only are the rows significantly different, but measured values of sidewall area in individual rows can vary drastically. This is due to the fact that sidewall area is a fundamentally three-dimensional parameter that is heavily influenced by many other variables, namely, indent width, average indent depth, and the sidewall angle of the particular side in which the sidewall area is being measured. Any variations of those statistics corresponds to a change in sidewall area, and thus, the manufacturing uncertainty of sidewall area is higher since it is a product of its base parameters.

The indent profiling system has demonstrated the ability to capture statistically relevant sample sizes of many critical indentation characteristics. By scanning the wire pattern that is the result of one complete revolution of the indent rollers, all statistically unique indentations from the manufacturing process are accurately represented. This allows the indent profiling system to analyze the manufacturing intricacies of the wires on a row-by-row basis as hundreds of indents can be sampled per wire specimen. No manufacturing process is perfect and the information extracted by the indent profiling system has been successfully used to highlight the significant manufacturing variations seen in individual wires.

7.2 Crosstie Wires (Extracted)

A subset of the wires selected for analysis by the indent profiling system were extracted from preexisting concrete railroad ties that saw many years of service. The concrete railroad ties were subjected to extensive measurements for other categories of the overall FRA research project. Other areas of the project collected detailed three-dimensional crosstie geometry data through the use of a separate laser scanning system and great effort was taken to determine the residual prestress force that remained in the concrete railroad ties after years of service.

Table 6: Concrete Crosstie Types

ID	Quantity	Manufacturer	Alternate ID	Wire #	Length
A	6	Itisa	136 RE	4	8'3"
B	6	Unknown	N/A	7	8'6"
C	6	FLORIDA EAST COAST	N/A	6	9'0"
D	6	SAN-VEL	Sante Fe	8	8'6"
E	6	CXT GRAND ISLAND	CXT497S	18	8'6"
F	6	CONFORCE COSTAIN	CN 60A	26	8'3"
G	6	KOPPERS	CSX	8	8'6"
H	6	ROCLA	N/A	24	8'6"
J	6	ROCLA	N/A	24	8'3"
K	6	COSTAIN GENSTAR	CP RAIL	24	8'6"
L	6	CXT	BN100	28	8'3"
M	6	ROCLA	BN100	28	8'3"

Twelve unique crosstie types were included in that component of the research project, detailed in Table 6 and Figure 7.12. After preliminary testing was completed, a subset of the ties were cut along the cross-section pertaining to the rail seat, the section upon which the steel rail sits, in order to verify the geometry of the section. As a result of this saw-cut operation, the last 22 inches of the crossties were cut off, allowing for extraction of the wires and strands from the

crossties. These crosstie wires provide a unique historical basis in which the modern wires can be compared to.

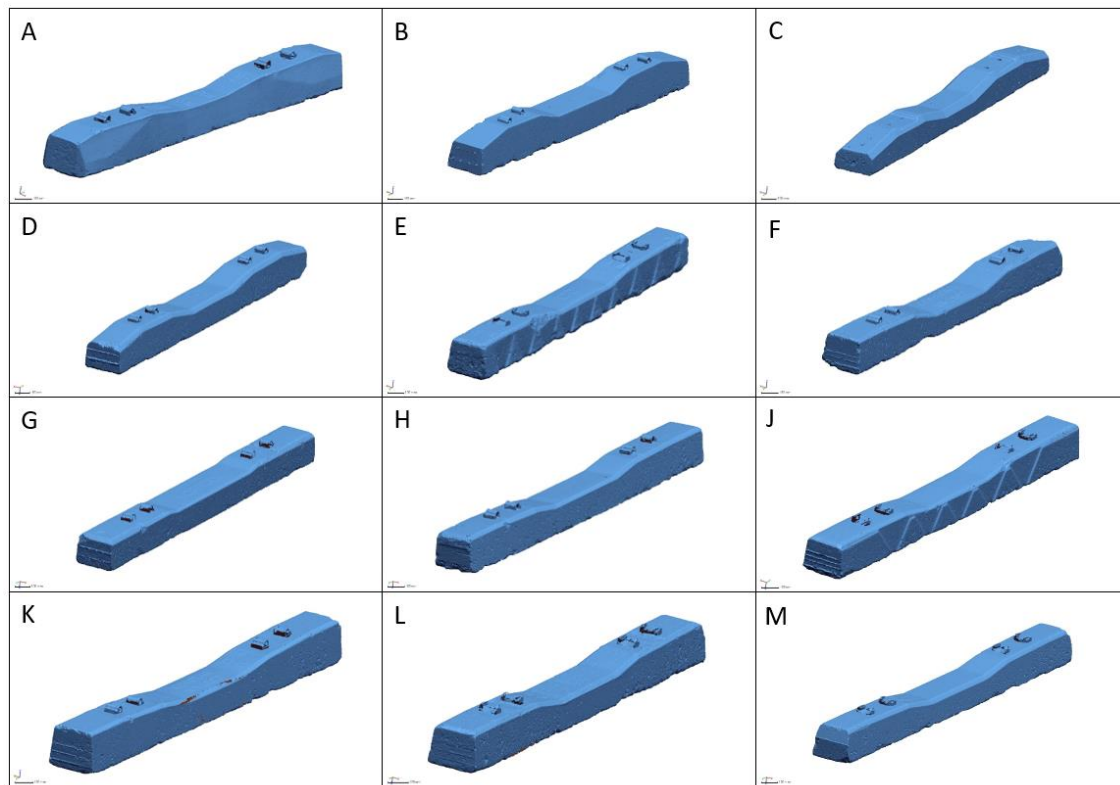


Figure 7.12: Concrete Crosstie Scans

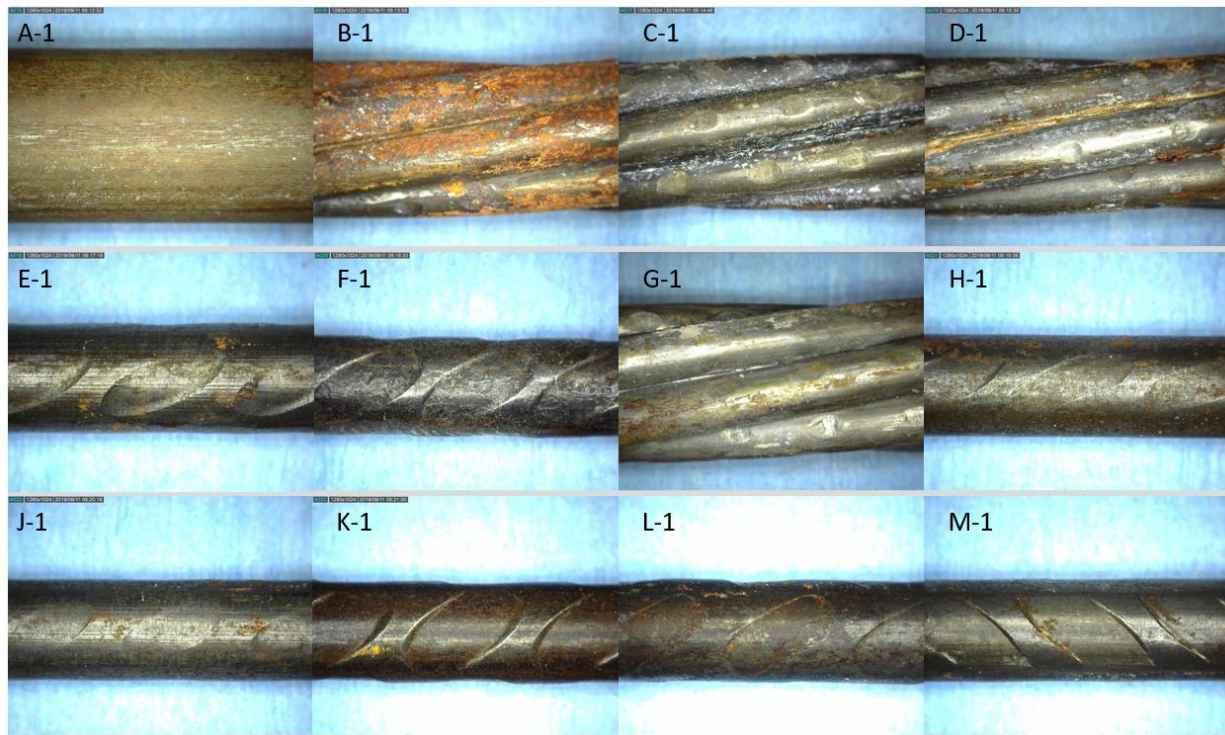
7.2.1 Crosstie Wire Specimens

Twelve unique concrete crossties types were included within the scope of the main FRA research project, each group contained six individual crossties. One crosstie from each group was cut along the rail seat cross-section, yielding 22 inch lengths of wire or strand depending on the crosstie. The wires and strands associated with each unique crosstie type are illustrated in Table 7. One of the ties, type A, was a post-tensioned design, and thus, used non-indented wire/rod that exceeded 3/8 inches in diameter. Four of the ties featured strands, comprised of a central wire with six wires twisted around the central member in a spiral pattern; each of these ties contained between 6-8 strands. The remaining seven ties utilized indented wires with nominal wire diameters falling within the 5.00mm range. Thus, the indented wires of these seven unique ties could be subjected to measurement by the indent profile system.

Table 7: Concrete Crosstie Extracted Wire Types

	Layout				
	# of Wires	Wire Type	Indentations	Dia. Wire	Pattern
A	4	Wire	Non-indented	0.415"	2-2
B	7	Strand	Non-indented	0.375"	3-4
C	6	Strand	Indented	0.375"	2-4
D	8	Strand	Indented	0.375"	4-4
E	18	Wire	Indented	5.30mm	4-4-4-6
F	26	Wire	Indented	4.86mm	10-6-10
G	8	Strand	Indented	0.385"	4-4
H	24	Wire	Indented	4.97mm	6-6-6-6
J	24	Wire	Indented	4.94mm	6-6-6-6
K	24	Wire	Indented	4.95mm	8-8-8
L	28	Wire	Indented	4.97mm	8-10-10
M	28	Wire	Indented	5.02mm	8-6-6-8

The seven wires extracted from concrete railroad ties encompassed in this section of the study are E-1, F-1, H-1, J-1, K-1, L-1, and M-1. The first letter designates the tie type that the wire originated from and the following number dictates which tie in the group that the wire was extracted from, in all cases, the first tie in a group was subjected to saw cutting and subsequent wire extraction, and thus all wires receive the same trailing designation. Note that the letter “I” is skipped in the tie type designation, this is to prevent confusion between the number “1” that immediately follows. Digital microscope images of the extracted wires are provided in Figure 7.13.

**Figure 7.13: Digital Microscope Images of Extracted Crosstie Wires**

From the digital microscope images, some notable observations for the indented wires can be made. E-1 has dish shaped ellipsoidal indentation profile, in which, a shallow sidewall angle

exists across the entirety of the perimeter. For this wire, a 10-degree sidewall angle at a depth of 100-120 microns is likely. F-1 is highly corroded, with a thoroughly pitted surface which will lead to complications with the laser scanner later. It has steep, crisp sidewall angles exceeding 20 degrees, coupled with a moderate depth; once again this indentation follows an ellipsoidal profile, but is still reasonably close to a chevron. Wire H-1 has an exceptionally shallow sidewall angle, estimated to be in the range of 5-8 degrees. This observation, in addition to the depth being on the order of 60-80microns, will ensure that this indentation has a tiny indent volume in comparison to a majority of the other specimens; indent volumes exceeding 1mm^3 are unlikely. Furthermore, the indent profile is an extremely elongated ellipse, but should cause no difficulties with the processing algorithms. J-1 has a profile that is similar to E-1, but shares significant similarities to H-1 in regards to indentation depth. However, the sidewall of J-1 is slightly steeper, but not by a considerable margin.

The deepest indent of all is likely K-1, paired with a crisp, relatively steep sidewall that is estimated to be 15-20 degrees. Average indent depths will likely be on the order of 100-130 microns. Indent L-1 has a moderate sidewall in the range of 8-13 degrees, with a shallow depth, likely falling within the bounds of 60-80microns. Its profile differs from the rest of the specimens, forming a shape that more closely resembles a pill rather than an ellipse. Indent volumes for this specimen are unlikely to exceed 0.8mm^3 . Wire type M-1, coincidentally shares significantly similar features to wire WM in the prior section. It is a true chevron type indent, in which, the depth of the indent decays asymptotically to zero at the extremities of the indent width. Furthermore, it has steep, crisp sidewalls on the order of 15-20 degrees and is likely to have a depth on the order of 100-120microns. Wire M-1 appears to have the highest manufacturing quality out of any of the wires in the group, exhibiting no imperfections, cleanly made indents, and created from a wire with no inherent cast.

7.2.2 Crosstie Wire Results

The seven chevron type indented wires extracted from concrete crossties were subjected to processing by the indent profiling system. Six of the scans were successful, however, the severe corrosive pitting on wire F-1 prevented a usable scan from being captured; laser based systems can either be tuned to capture accurate scans of diffuse or reflective surfaces, but often struggle to image surfaces that are a combination of both. Thus, six of the wires extracted from the concrete railroad ties will serve as the historical comparison to their modern counterparts highlighted in the previous section. The data captured by the indent profiling system on the six crosstie wire specimens is summarized in Table 8, in which, the mean and standard deviations are listed for parameters of particular interest. It should be noted that the parameters contained by the following table stem directly from the requirements of the two main indented wire measurement standards, as well as parameters that were found to correlate favorably with wire-concrete performance criteria. Many more geometric parameters are computed by the indent profiling system, but the information contained below represents a sampling of the most important ones.

Table 8: Crosstie Wire Indentation Data

Indent Data (Crosstie Wires)										
	ID	Nominal Dia [mm]	Orientat-ion [deg]	Total Indents	Volume [mm^3]	S.W. Area [mm^2]	Avg Depth [mm]	S.W. Angle [deg]	Avg Length [mm]	Pitch [mm]
Mean	E-1	5.216	49.1	207	1.142	3.408	0.107	9.46	4.133	6.129
	H-1	4.981	44.9	208	0.742	3.079	0.073	7.18	4.470	6.103
	J-1	4.960	55.9	207	0.800	3.032	0.088	7.26	3.969	6.101
	K-1	5.124	60.1	209	1.832	2.443	0.117	15.79	4.391	6.136
	L-1	4.936	56.3	47	0.736	3.167	0.075	9.22	3.559	6.065
	M-1	4.954	47.2	199	1.237	1.937	0.099	16.36	4.302	5.965
Standard Deviation	E-1			207	0.131	0.480	0.015	1.20	0.151	0.025
	H-1			208	0.106	0.616	0.011	1.75	0.124	0.003
	J-1			207	0.076	0.480	0.012	1.53	0.148	0.007
	K-1			209	0.141	0.568	0.011	3.55	0.160	0.026
	L-1			47	0.120	1.374	0.015	3.19	0.343	0.088
	M-1			199	0.156	0.520	0.016	5.48	0.077	0.022
S.W. Area: The average sidewall area of the left and right side of the indents.										
S.W. Angle: The average sidewall angle of the left and right side of the indents.										

A majority of the crosstie wires scanned had nominal diameters of around 5mm, with E-1 being the only exception. Five of the wires exhibited orientation angles in excess of 45° apart from wire type H-1, which missed the cut-off by a narrow margin. Many orientation angles are considerably larger than 45° as many of the indentations form highly tilted ellipses. Statistically relevant sample sizes were obtained for a majority of the wires, neglecting L-1, which suffered from severe indent deformation caused by damaged indent rollers. A full length scan was successfully captured for crosstie wire L-1, but the malformations of a majority of the indents required a shorter segment to be processed. The damage to L-1 is visualized in Figure 7.14, which depicts the damage of the wire with a digital microscope image in addition to a contour plot of the wire scan; severe damage can be seen on 2 of the 3 rows. Furthermore, the damage caused by the chipped roller teeth can be seen as increased scatter in the measurements of certain geometric parameters for wire type L-1, notably ones that are associated with indent length or sidewall characteristics such as angles and areas.

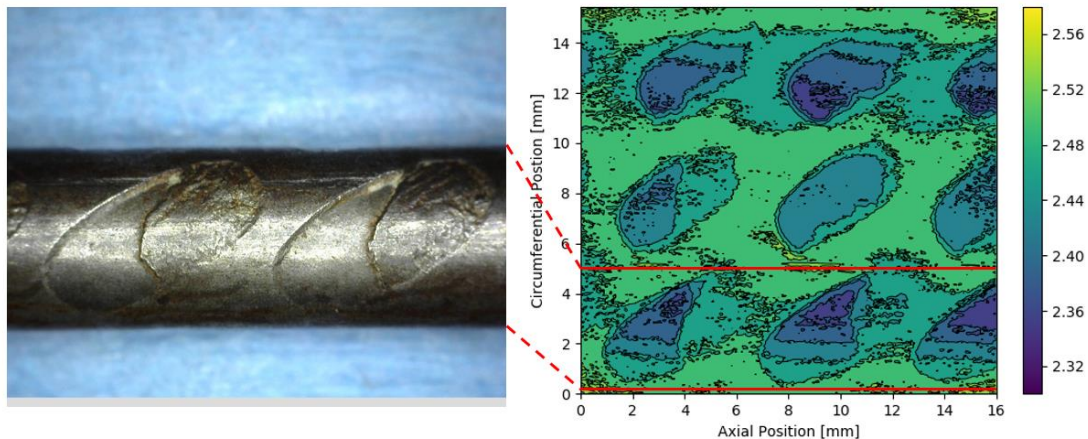


Figure 7.14: Severely Malformed Indents (Crosstie Wire L-1)

Observations of the digital microscope images earlier led to a prediction for indent volumes to not exceed 1mm^3 on average for wire types H-1, J-1, and L-1; this is clearly confirmed by the data summarized in Table 8. It was also predicted that K-1 would be the deepest indent of all, based on the microscope images, and have steep sidewall angles in comparison to other wires in the group, this is also confirmed by the data table. Overall, the sidewall angles represented by the crosstie wire group are consistent and shallow. On a separate note, many of these wires would fail to pass the requirements of ASTM A881 based on the measured indent lengths and allowable indent pitch, this can be seen in the ASTM A881 requirements for 5.00mm and 5.32mm indented wires outlined in Table 1.

The most striking difference between the historical crosstie wires and the modern wires is that the sidewall angles of the crosstie wires are considerably shallower on average in comparison to their modern counterparts. Additionally, the orientation angles of the historical wires were much more inclined and many of the indentations resembled highly stretched ellipses. However, some of the wires bore significant similarities, namely crosstie wire M-1 and cover testing wire WM from the prior section. A comparison between the height-maps of the aforementioned wires is characterized in Figure 7.15, which highlights how similar the overall shapes are.

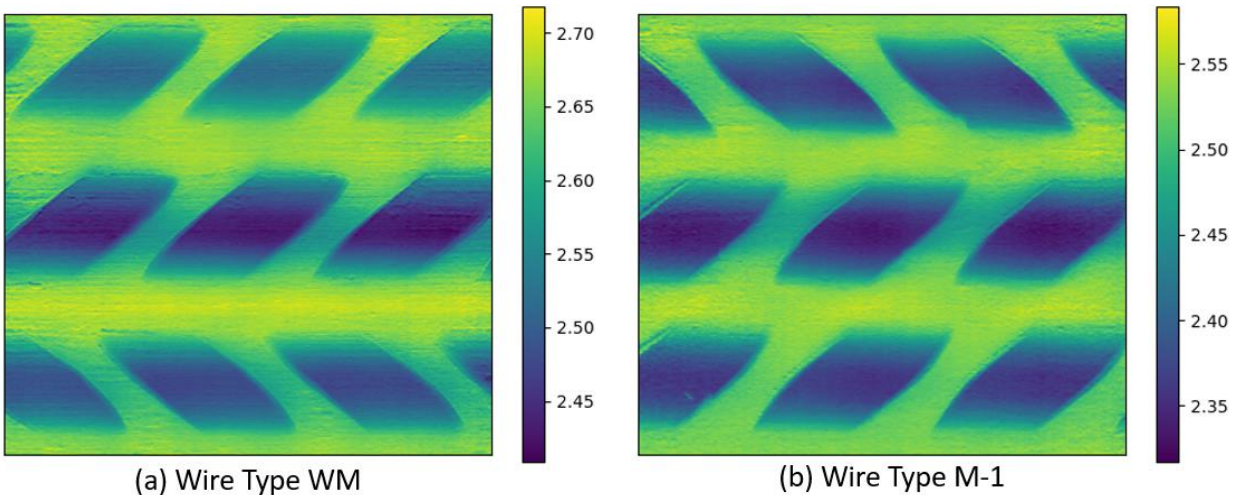


Figure 7.15: Similarities Between Wire WM and Wire M-1

7.3 Machined Indent Wires

The third group of wires, those with fabricated “machined” indents, were used for system calibration and verification of feature extraction algorithms. A set of machined indented wires of known geometry were created for a prior FRA research project. For that project, the machined wires were created for a similar purpose, to provide a system checkout for the precursor to the indent profiling system described in section 2.3. The indent geometry was formed by using custom made carbide endmills to remove material from a smooth wire with a nominal diameter of 5.32mm, analogous to wire type WA. Six separate tungsten-carbide endmills were created, each capable of generating indentations with a particular sidewall angle due to the chamfer built into the nose of the endmill. Figure 7.16, provided below, details a schematic of the endmill geometries used to form the indentations.

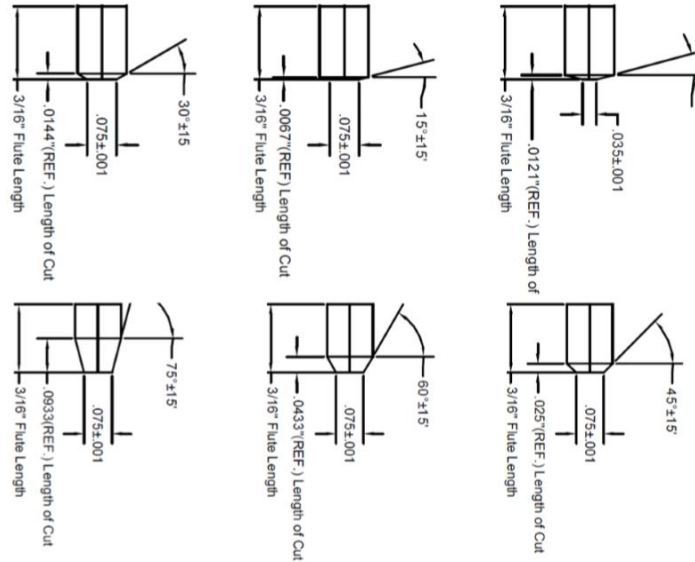


Figure 7.16: Endmill Geometry Used to Create Machined Indents

These six endmills were capable of machining indents with sidewall angles in increments of 15°, thus, indentations could be formed that varied from 15° to 90°, the most severe sidewall angle possible. Furthermore, two separate wires were fabricated for each sidewall angle, but with two separate indentation depths: shallow and deep. The tool depth was varied 0.004" ($\approx 100\mu\text{m}$) to generate the transition from shallow indentations to deep indentations; in practice, this proved challenging to achieve uniformly. Thus, 12 machined wires were fabricated with six separate sidewall angles and two unique indentation depths; a picture of the machined wires can be visualized in Figure 7.17. The indentations were machined with an indentation orientation of 45° with respect to the longitudinal axis of the wire by keeping the tool height constant and moving the milling bed appropriately. These machined wires provide indents of known geometry that prove to be helpful with system verification.



Figure 7.17: Picture of Wires With Machined Indents

7.3.1 Machined Wire Specimens

Twelve unique machined wires were subjected to scanning by the indent profiling system to assist with system checkout. The group contained six sets of indentation sidewall angles formed by the cutting tools in increments of 15° , with two separate indentation depths apiece. The indentations were formed with an orientation of 45° . Furthermore, the fabricated specimens featured machined indents on a roughly 5.5" length of wire. Each row included 18 indents, thus, an entire specimen contained 54 indents. Digital microscope images of the fabricated wires are provided in Figure 7.18.

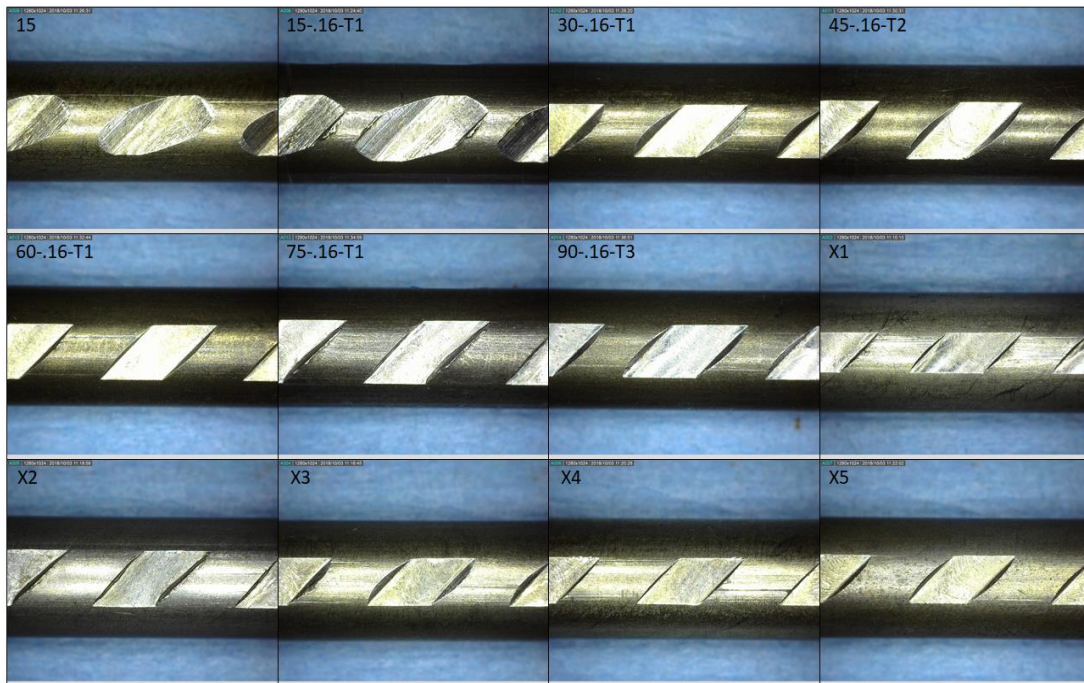


Figure 7.18: Digital Microscope Images of Machined Wires

The machined wires listed in Figure 7.18 above inherited a naming convention from the previous project, with many of the wires being labeled with the prefix of “X”; this convention likely originated when the wire labels were lost at some point. However, the indent profiling system makes wire identification trivial since it can obtain sidewall angles and indentation depths with ease. The indent profiling system results were used in addition to a shadowgraph imaging system to aid with the proper identification of the wires. The shadowgraph imaging system works by projecting light across the machined track of the indent, and enlarging the resulting shadow, much like a projector would. This shadowgraph system in particular provided a magnification increase by a factor of 20. An example of the shadowgraph imaging system can be seen below in Figure 7.19 being used to identify an indent formed by an endmill that featured a 15° chamfer angle.

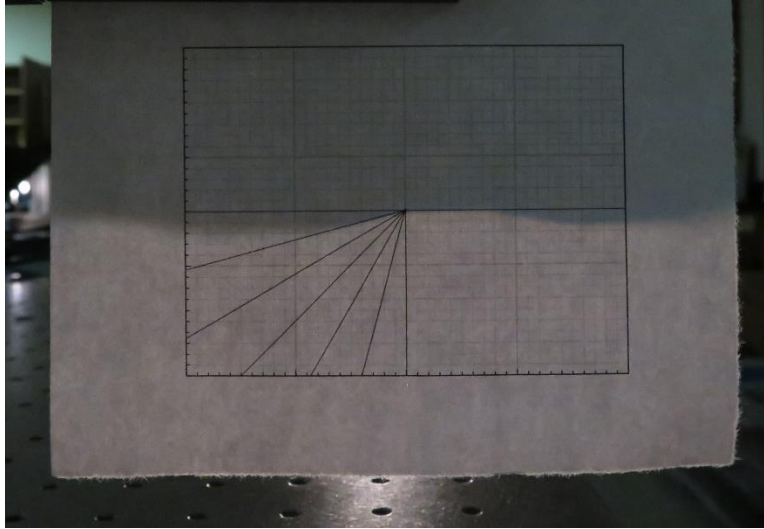


Figure 7.19: Shadowgraph Imaging of Machined Indent

The shadowgraph imaging system, in conjunction with the indent profiling system were used to properly identify the machined wires. Table 9 overviews the proper identification of the machined wires alongside the original alternate IDs to be used as a reference. The first number in the corrected ID intuitively represents the chamfer angle of the endmill used to form the indentation, whereas the letter that follows designates the intended relative depth of the wire: “S” for shallow, and “D” for deep. Note that the targeted depth difference between the shallow and deep indents with the same indent angle geometry was 0.004” ($\approx 100\mu\text{m}$). The measured centerline depth results confirm this general observation, however, the relative depths between wires of different indentation angles vary significantly. For example, the centerline depth of 15-S, is vastly different than the one measured for 30-S.

Table 9: Machined Wire Identification

ID	Alternate ID	Centerline Depth [mm]	Δdepth [μm]
15-S	15	0.304	92
15-D	15-.16-T1	0.396	
30-S	X3	0.151	99
30-D	30-.16-T1	0.250	
45-S	X5	0.148	86
45-D	45-.16-T2	0.234	
60-S	X4	0.136	106
60-D	60-.16-T1	0.242	
75-S	X2	0.287	95
75-D	75-.16-T1	0.382	
90-S	X1	0.138	76
90-D	90-.16-T3	0.213	

Some critical observations from the observed digital microscope images, along with the endmill geometry used to form the machined indentations are as follows. The indentation with the 15° sidewall angle is the deepest indentation of all. The magnitude of the centerline depth, coupled with the shallow sidewall angle ensures that 15-D has the largest volume out of any of the indents. In fact, it is so deep that the carbide endmill left a burr along the transition between the sidewall and the crest of the indent. The smallest indents, confirmed visually by the digital microscope images are 60-S and 90-S; this observation is due to the fact that both of these indent geometries have the shallowest centerline depth overall, in the range of 130-140μm. Furthermore, all indentations formed by endmills with 30° and 45° chamfers left cleanly fabricated indents, whereas the 60° endmill suffered from a chipped cutting face and left an imperfect indent geometry for the shallower indentation. Both 75° specimens were impacted by poor tool pathing, seen by the marring on the right side of the indentation, this will significantly change the measured sidewall angles later. Finally, the 90° endmill was not a straight-fluted endmill, instead it had a 45° cutting edge chamfer. Additionally, the “90°” endmill has a wider base diameter than the rest of the cutters, this can be seen in the digital microscope images since 90-16-T3 and X1 have wider tracks at the base of the indent than the rest.

7.3.2 Machined Wire Results

By scanning and processing the machined wire specimens a verification of the accuracy of the system could be obtained since the machined indents represent geometry of known dimensions. The data captured by the indent profiling system on all 12 machined wire specimens is summarized below in Table 10.

Table 10: Machined Wire Indentation Data

Indent Data (Machined Wires)								
ID	Alt. ID	Total Indents	Volume [mm ³]	S.W. Area [mm ²]	Avg Depth [mm]	S.W. Angle [deg]	Avg Length [mm]	Pitch [mm]
15-S	15	45	1.327	3.686	0.223	12.67	3.645	6.344
15-D	15-16-T1	45	2.149	5.046	0.290	13.18	4.190	6.344
30-S	X3	45	0.595	1.050	0.105	19.93	3.599	6.345
30-D	30-16-T1	45	1.249	1.582	0.184	21.84	3.730	6.343
45-S	X5	45	0.545	0.951	0.103	23.95	3.311	6.345
45-D	45-16-T2	45	1.009	1.066	0.172	30.19	3.255	6.354
60-S	X4	45	0.493	1.390	0.082	22.42	3.641	6.347
60-D	60-16-T1	45	1.082	0.872	0.178	43.14	3.205	6.343
75-S	X2	31	1.317	1.365	0.215	34.93	3.125	6.343
75-D	75-16-T1	36	2.025	1.408	0.290	49.27	3.128	6.346
90-S	X1	45	0.600	1.437	0.088	22.96	3.968	6.342
90-D	90-16-T3	45	1.091	1.030	0.156	32.43	3.817	6.343
S.W. Area: The average sidewall area of the left and right side of the indents.								
S.W. Angle: The average sidewall angle of the left and right side of the indents.								

The primary three-dimensional geometry of interest is indent volume and sidewall area, as these parameters pertain to wire-concrete criteria such as bond, transfer length, and splitting propensity. The two-dimensional characteristics used to compute these metrics correspond to average depth, average indent length, and average sidewall angle. Note that these two-dimensional parameters, particularly average depth and average sidewall angle, do not compare

directly to the chamfer of the endmill used to form the indents. This arises from the fact that the scan plane is coincident with the bore axis of the wire, and is not perpendicular to the machined track of the indent except at the centerline location.

Observations of the data contained in Table 10 match the physical observations of the digital microscope images of the wires listed in the prior subsection. As noted previously from the microscope images, 60-S and 90-S have the shallowest depth, and thus the smallest indentation volume, this is confirmed by the tabulated data. Additionally, it was observed from the images that 15-D appeared to be the largest due to the shallow sidewall angle and deepest machined depth, this is also confirmed by the tabulated data. Earlier it was noted that the 90° endmill did not appear to be a straight-fluted endmill, instead it had a 45° chamfer and a wider nose track than the other endmills as observed by shadowgraph images and images obtained from the digital microscope. This is validated by the sidewall angle data, which is exceedingly far off from the steep angle expected from a true 90° cutting tool. The average basin length data from the indent profiling system (not listed in the table above) indicates that 90-S and 90-D had wider ground tracks than the geometry formed by other endmills. Furthermore, the pitch between indents across all specimens is consistent, the average indentation pitch is 6.345mm, varying only 0.012mm (12µm) across all machined wires; this consistency is inherent to the machining process used to form the wires.

Table 11: Verification of Sidewall Angle Extraction Algorithm

Indent Data (Machined Wires)							
ID	Alt. ID	Total Indents	Volume [mm ³]	S.W. Area [mm ²]	Centerline Depth [mm]	Centerline Angle [deg]	Chamfer Angle [Deg]
15-S	15	45	1.327	3.686	0.304	10.65	14.89
30-S	X3	45	0.595	1.050	0.151	22.11	29.87
45-S	X5	45	0.545	0.951	0.148	35.88	45.64
Centerline Angle: Centerline Sidewall Angle							
Chamfer Angle: The equivalent chamfer angle that the centerline sidewall angle forms							

Verification of the reliability of the feature extraction algorithms can be provided by comparing the captured geometric features with indents of known physical shape. The indentations of these machined wires were formed by using endmills with known chamfer angles, following machine tracks that formed an indent orientation angle of 45°. Thus, the sidewall angle information extracted by the indent profiling system can be compared with the known geometry of the endmills used to form the indents. A majority of the indented wires seen in industry have sidewall angles that vary from 5-45°, and indentation depths that vary from 50-200µm, for wires with a 5.32mm nominal diameter. Therefore, the following indents were selected to verify the accuracy of the sidewall angle feature extraction algorithm: 15-S, 30-S, and 45-S. The results of these particular wires are highlighted in Table 11, in which the critical parameter used to obtain equivalent chamfer angle is listed, the centerline sidewall angle. The centerline sidewall angle is the only location on the machined indent in which the sheet-laser plane is guaranteed to be perpendicular with the machined indent track. However, the centerline angle does not measure the chamfer angle of the endmill used to form the indents, since the orientation angle of the machined track is at a 45° angle. This is illustrated in Figure 5.11, which shows the relationship between the true machined sidewall angle and the measured centerline sidewall angle.

$$\theta_{chamfer} = \tan^{-1}(\sqrt{2} \tan(\theta_{centerline})) \quad (7.1)$$

By applying the simple algebraic relation above, a direct assessment of the equivalent measured chamfer angle can be obtained. Thus, it can be seen that the equivalent chamfer angles listed in Table 11 agree quite closely with the endmill chamfer angles used to form the indentations. The angles fall within a fraction of a degree of the expected values in all circumstances. This confirms the validity of the data extraction algorithms by using indents of known, fabricated geometry.

8. Repetition Demonstration

One of the primary objectives of the indent profiling system is the collection of sufficiently large amounts of data to form statistically relevant sample sizes of extracted indent features. As such, the goal is to acquire all indent geometry associated with a complete repetition of the indent rollers used to form the indentation geometry into the steel wires. Collection of data exceeding one complete revolution of the indent rollers is unnecessary, as the resulting data would not be statistically unique since the indent rollers continue to form repetitions of previous created indents. The indent rollers, visualized in Figure 1.3, are typically 8 inches in diameter, thus, it is necessary to scan roughly 25 inches of wire to collect all unique indents formed by the indent rollers during the manufacturing process.

The indent profiling system can measure wires of 26 inch length while utilizing the tailstock of the lathe assembly, and 30 inch lengths without the tailstock, allowing the system to capture the effects of the complete indent roller repetition. Some of the wire specimens observed in Section 7 show signs of indent roller tooth damage, the component responsible for forming the geometry of the wire, leaving malformed indents. These malformed indents provide a unique visual basis for confirming the capture of a complete repetition and will be the basis of discussion of the subsections that immediately follow.

8.1 Observations of Indent Repetition

During the data collection process, multiple wires were observed that featured indent deformities caused by imperfections in the indent roller teeth. These malformed indents serve as a visual way to confirm that the indent profiling system is capturing the statistically unique indents formed by one full repetition of the indent rollers used to form the wires. These malformed indents can be thought of as the “finger print” of the associated indent roller, since these imperfect indents are easy to visually identify in subsequent repetitions of the roller. An illustration of the “finger print” is shown in Figure 8.1, in which, a corner of a indent in the center row of the scan suffers from damage caused by a chipped indent roller tooth. Deformities such as the one illustrated in the aforementioned picture represent a convenient tracking feature.

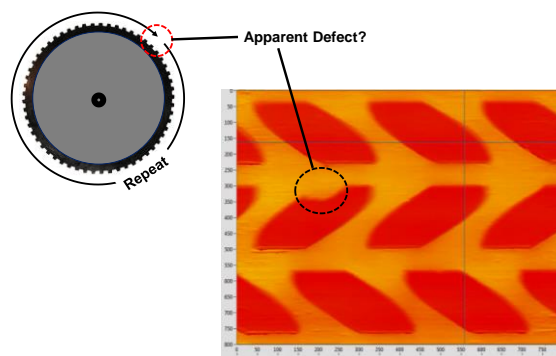


Figure 8.1: Isolation of Indent Roller Defects

This is better illustrated by referring to a more complete height-map image of an entire 26 inch scan of a specimen that was included Section 7.1. Figure 8.2 shows two detected indents that were the result of damage to roller teeth, the height-map depiction of defects in two adjacent rows are shown at the beginning of a scan.

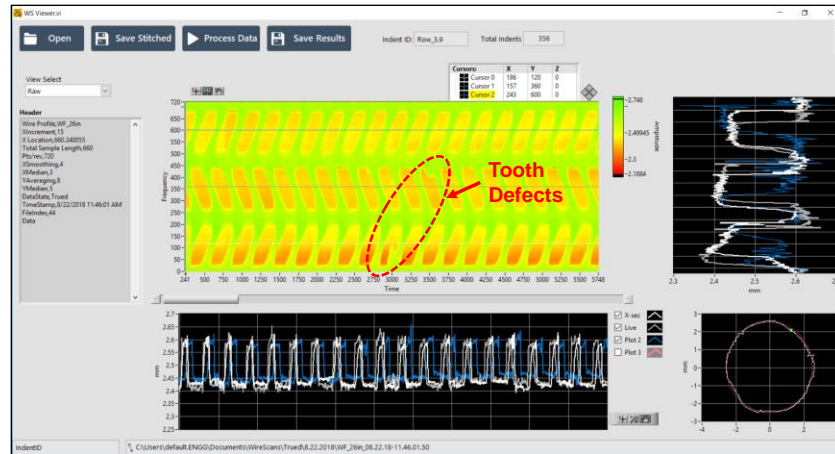
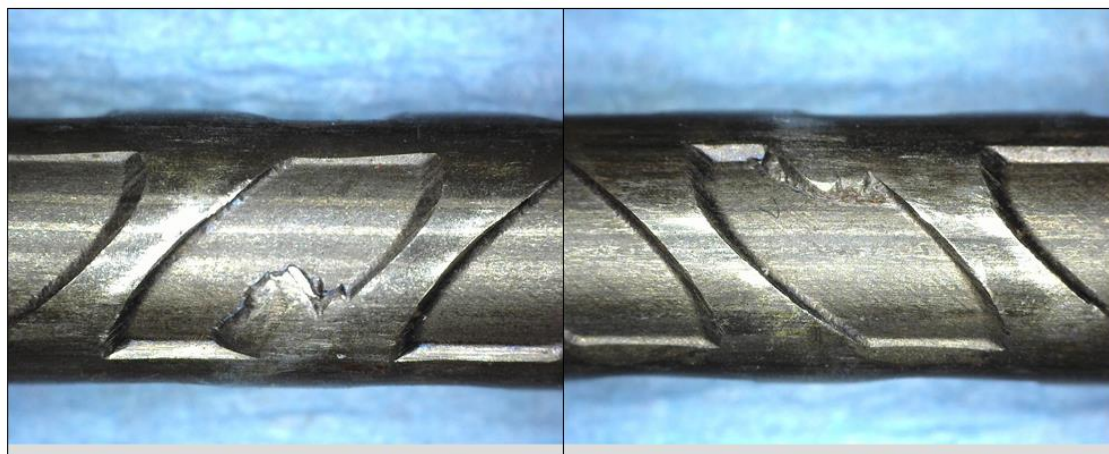


Figure 8.2: Defects Near Beginning of Scan

The wire specimen in question that displays the obvious defects is wire type WF, the same wire is listed at the beginning of the report that shows malformed indents in the three dimensional model portrayed in Figure 2.3. These defects are not a scanning error; they are physically observable malformed indents that are clearly visible to the naked eye. This observation is visible in Figure 8.3 which offers a enhance view provided by a digital microscope. Figure 8.3(a) corresponds to the defect detected in the bottom row of Figure 8.2, whereas Figure 8.3(b) corresponds to the deformity in the center indent row.



(a) Defect in Bottom Row

(b) Defect in Center Row

Figure 8.3: Digital Microscope Image of Deformed Indent (Wire WF)

Later in the completed scan, another instance of the same malformed indents is clearly visible. This is seen in Figure 8.4. The distance between these deformed indent patterns are, on average, 22.6 inches (575mm) apart from one another, corresponding to an average roller diameter of 7.2 inches. Malformed indents were found on other wire specimens as well, but are clearly visible on wires with deeper indentations. Since indent rollers are subjected to higher stresses when deeper indentations are being made, increased wear and tooth chipping is more common.

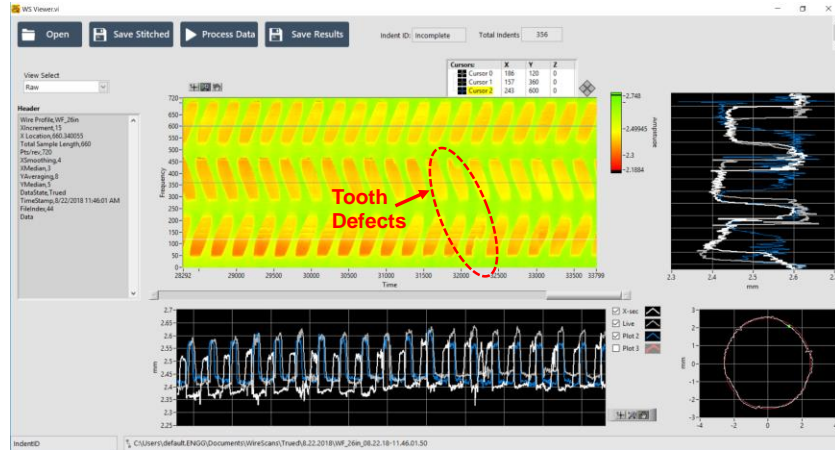


Figure 8.4: Defects Near End of Scan

8.2 Differing Indents for Individual Rows

Another interesting phenomenon that was observed by the indent profiling system is that indent rollers of varying diameters were used to create the patterns on the same indented wire. By looking at the unique indents, identified by malformed features, this observation is clear. By closer observation of Figure 8.2 and Figure 8.4 it can be noted that the positions of the deformities change positions with respect to each other as the scan progresses. This is visualized in Figure 8.5 which is a composite image of the two aforementioned figures. It can be clearly seen that the malformed indents shift in relative position from the beginning of the scan to the end of the scan after one revolution of their respective indent rollers are complete. The shift in the relative positions of the apparently identical defects suggests that something is different about the adjacent rollers.

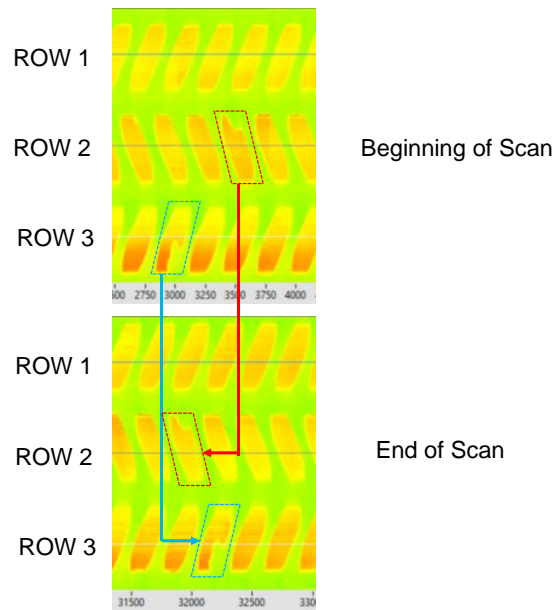


Figure 8.5: Comparison of Adjacent Indent Defects

Further inspection of the resulting processed data indicates that the pitch of each indent row is identical across the entire length of the scan. This implies that the indent rollers are made with a

varying number of teeth, and thus, have differing diameters, but preserve the indentation pitch of each row. This is confirmed by the fact that the central row has three fewer indents registered for one repetition of the indent roller. Does the differing number of teeth per indent roller, or varying roller diameter matter? Does it directly contribute significantly to accelerated wear of the smaller indent rollers since each tooth is subjected to creating more indentations than adjacent rollers? Perhaps not, but it serves as a testament the ability of the indent profiling system to identify the intricacies of the manufacturing process.

9. Correlations

Phase II of the research project involved the application of the indent profiling system to measure the indent characteristics of a multitude of indented wires. A large subset of the wires subjected to testing included wires that are frequently used in modern industry. These wires represent a diverse selection of indent depths, indentation shapes, and sidewall angles used in practice. The wires contained by this group, representing ten unique chevron type wires, were subjected to processing by the indent profiling system, the results of which were highlighted in section 7.1. The extracted geometrical features provided statistically valid sample sizes as the entire wire pattern formed by a complete revolution of the indent rollers was captured for all wire specimens.

The captured indented wire geometry could then be used in conjunction with empirical data obtained from prestressed concrete prisms created using the same ten wires. The concrete prisms were constructed for the purpose of measuring the effect of reduced concrete cover on wire-concrete performance criteria. From this combined information, the detailed indentation geometry can be correlated with wire-concrete performance criteria such as transfer length and splitting propensity to quantitatively determine which indent features contribute most significantly, or detrimentally, to desirable performance characteristics. Furthermore, it is possible to investigate which 3D geometric parameters can be reasonably approximated by 2D features extracted along the indent centerline. If the 2D parameters can be shown to correlate against already established 3D parameters that characterize wire-concrete performance criteria such as transfer length and splitting propensity, the potential for on-line production quality control in real-time may be realizable. The subject of correlations will be the source of extensive discussion in the subsections that follow.

9.1 Correlation of 2D Parameters to 3D Parameters

The indent profiling system has proven to be a valuable research tool to extract indentation geometry. The statistically relevant sample sizes that the system is capable of collecting for a myriad of wire features can be used to determine which geometric features, or combination of features, have the most significant contributions to wire-concrete performance. However, it would prove to be valuable from a quality control perspective if an indent profiling system could be placed in the production line of an indented wire manufacturing facility to give real-time feedback on wire quality. The current indent profiling system requires for a segment of wire to be cut from the end of a wire spool, and is not amenable to being placed in the production line as indented wire is being formed. Thus, it would be desirable to implement a non-contact laser based scanning system capable of collecting profile data along the indent centerlines so that the wire quality could be monitored in real-time.

The implementation of such a system would require the understanding of how the centerline 2D wire characteristics correlate against critical 3D wire parameters that were found to be sufficient in predicting performance criteria such as transfer length, bond, and splitting propensity. The extensive data collected by the indent profiling system on a multitude of indented wires can be used to ascertain such correlations.

Table 12: Potential Correlations of 2D and 3D Parameters

	2D Feature	3D Feature
Single	Centerline Depth	Average Depth
	Centerline SW Length	Sidewall Area
	Centerline SW Angle	Average SW Angle
	Centerline Profile Area	Volume
	Centerline Length	Average Length
Multivariate	Centerline Profile Area	Volume
	Indent Width	
	Centerline SW Length	Sidewall Area
	Indent Width	
	SW : Sidewall	

Certain two dimensional wire features summarized in Figure 6.13 are found to be analogous to their three dimension counterparts illustrated in Figure 6.14. The table listed above, Table 12, lists sets of two dimensional and three dimensional parameters that are highly likely to correlate well with one another. For example, since most of the 3D parameters are integrations of 2D components across the width of the indent, it is intuitive that any parameter related to the average of the 2D parameters will correlate strongly with its 3D counterpart. Centerline sidewall length (the average of the left and right side) can be shown to exhibit a very strong relationship with average sidewall area of the indent, since the centerline sidewall length is a close approximation of the average sidewall length. The list of the 2D parameters in the table above are predicted to have a direct relationship with the 3D geometry.

The cover testing wire features extracted by the indent profiling system can be found in Table 4, which summarizes the most critical geometry. However, the aforementioned table only lists a sampling of extracted features. The indent profiling system currently extracts 38 wire features that encompass centerline geometry, two dimensional profile averages, minimum and maximum values, as well as the three dimensional wire geometry, far too extensive to tabulate in the context of a paper. These parameters exist per indent, or as the average of all indents for a particular wire specimen as Table 4 implies. The data collected for a set of wires, the cover testing wires for example, can then be used with commercially available statistics processing software to determine the correlations between the parameters outlined in Table 12.

Figure 9.1 highlights the correlation between centerline depth, a fundamentally 2D parameter, and average indent depth, a 3D parameter. The plot shows values of average indent depth that were predicted by the developed correlation against the measured values of average depth. If a perfect correlation existed, all of the data points would fall along the red line, which would imply a 1:1 mapping between the predicted and measured results. However, it is often not possible to choose correlation parameters in which the predicted value is completely dependent on the independent parameters chosen for the correlation, thus scatter exists; this is also exacerbated by imperfect measurements. This scatter can be described by the R^2 -value of the correlation; this relates how far the data points deviate from the line of best fit. An R^2 -value of one implies a perfect correlation and a R^2 -value of zero implies no correlation. Unsurprisingly, a reasonable correlation exists between centerline depth and average indent depth, with a majority of the points clustering around the prediction line.

A perfect correlation is not expected to exist however for these sets of parameters as the centerline depth does not always reflect the average depth of the entire indent. Wire type WM for example has a basin that is shaped like a bowl, in which, it is deepest in the middle and asymptotically approaches a depth of zero at the extreme width of the indent. In this case, the centerline depth is clearly not indicative of the average depth of the indent. Overall, the correlation is favorable since a majority of the indents have consistent depths across the basin of the indent. The correlations that follow in this subsection were developed using the mean values of the processed cover testing wire specimens.

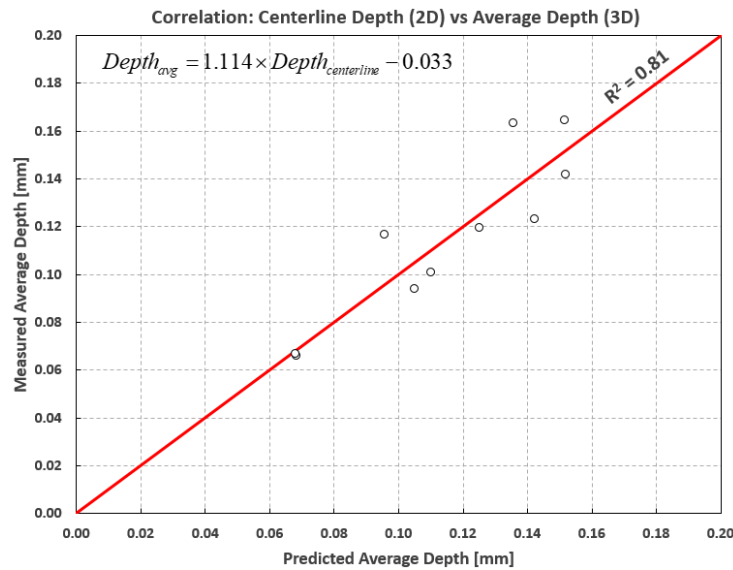


Figure 9.1: Centerline Depth (2D) vs. Average Depth (3D)

The plot listed below in Figure 9.2 clearly demonstrates a strong relationship between centerline sidewall length and the three dimensional parameter of sidewall area. By simply measuring the centerline sidewall length it is possible to get a reasonable approximation of sidewall area.

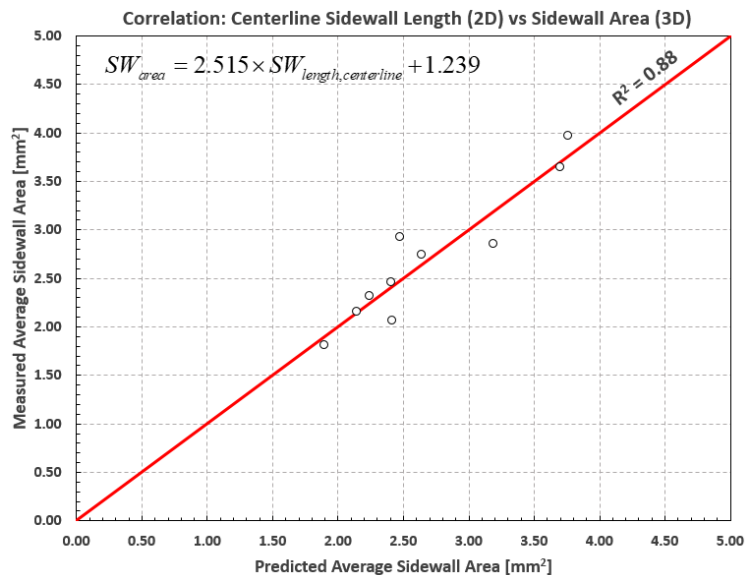


Figure 9.2: Centerline Sidewall Length (2D) vs. Sidewall Area (3D)

The correlation between centerline sidewall angle and average sidewall angle can be visualized in Figure 9.3. From this relation, it is apparent that the centerline sidewall angle is a relatively poor way to predict the average sidewall angle of the indent. This is due in part to the fact that sidewall angle can vary significantly as a function of location along the indent, additionally, it is a parameter that is notoriously challenging to measure accurately.

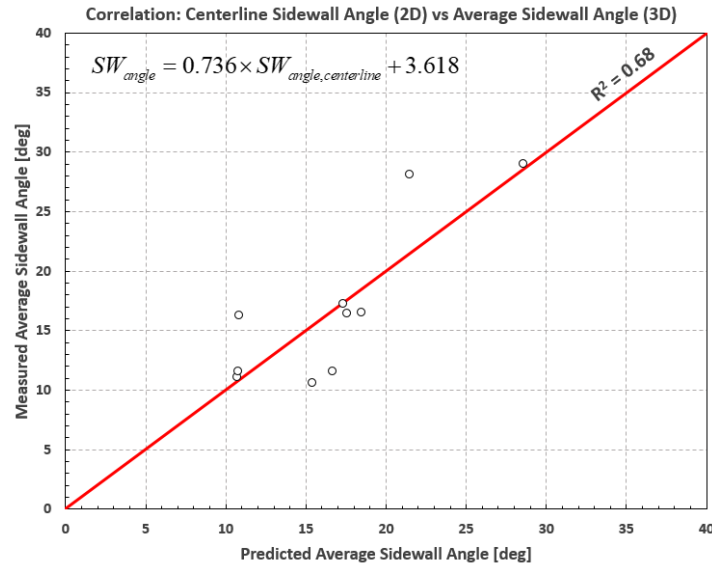


Figure 9.3: Centerline Sidewall Angle (2D) vs. Average Sidewall Angle (3D)

Likewise, centerline profile area roughly correlates with indentation volume as illustrated in Figure 9.4. Volume, fundamentally, is the integration of profile areas across the width of the indent. Volume is inherently three dimensional and requires the additional knowledge of indent width to be accurately predicted. Since indentation widths can vary from wire to wire, it should come as no surprise as to why the correlation listed below is only approximate.

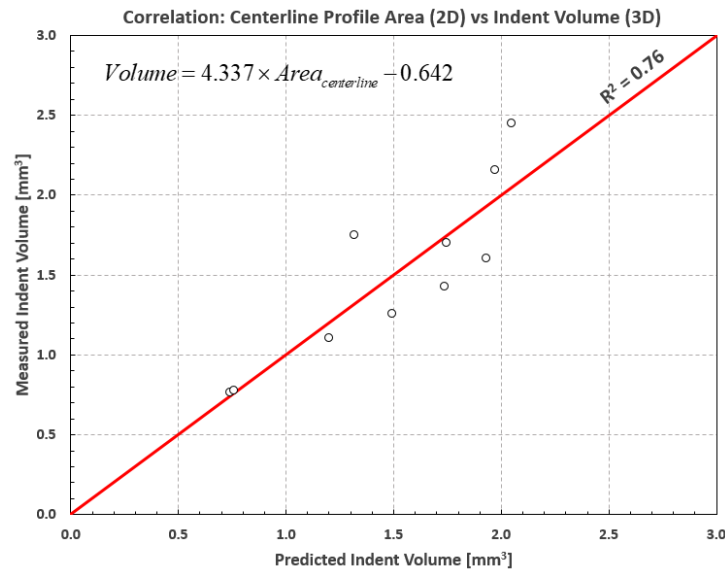


Figure 9.4: Centerline Profile Area (2D) vs. Indent Volume (3D)

Centerline indent length was shown to have no appreciable relationship with the average length of the indent, resulting in a R^2 value of 0.0002. The reason for the non-existent correlation is that indent length varies drastically depending on where it is measured along the width of the indent. This parameter is strongly influenced by the overall shape and size of the indentation geometry. Although all of the wires included in the cover testing group exhibited a chevron style indentation, the overall shapes of the indentations remained sufficiently diverse. Thus, average indent length is a function of indentation shape, and centerline length is not capable of predicting it without additional knowledge of the indentation shape.

A majority of the three dimensional indent features rely on the integration of two dimensional parameters to be obtained. Thus, features such as indent volume and indent sidewall area are not only dependent on average values of the 2D parameters, but are also reliant on the width of the indent to be accurately computed.

This can be seen in the following correlation, in which, both centerline profile area and indent width are used to determine indent volume, a fundamentally three dimensional parameter; this correlation can be visualized in Figure 9.5. The predicted volume is much more faithful to the measured values once indent width is considered in the correlation, improving the R^2 value to 0.88; the previous value was 0.76 when indent width was not included. Thus, if the nominal width of the indents is measured or previously known from the manufacturing process, it is possible to reasonably predict indent volume. While indent width is not measured along the centerline of the indent profile, it is an exceptionally easy and accurate measurement to take without the need of a complex indent measurement system.

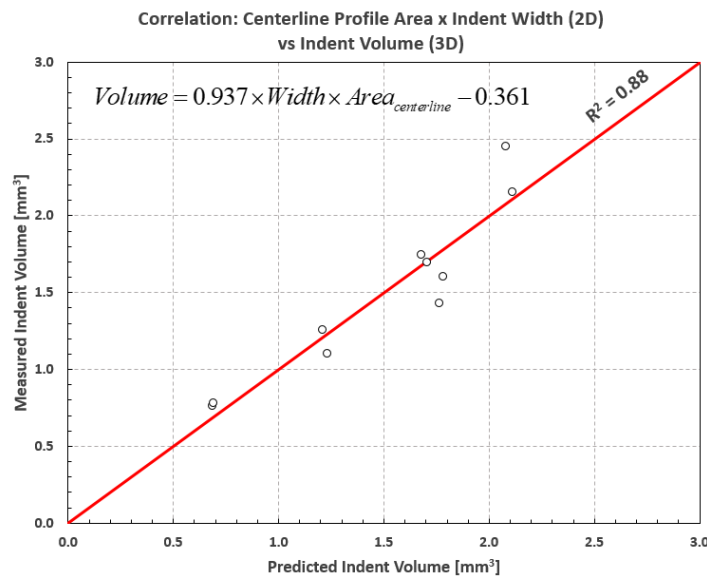


Figure 9.5: Multiple 2D Parameters Used to Evaluate Indent Volume

Indent sidewall area also receives a slight benefit to the correlation by using the centerline sidewall length in addition to the width of the indent. This improvement can be seen in Figure 9.6. However, sidewall area does not experience same amount of improvement that indent volume had when indent width was included.

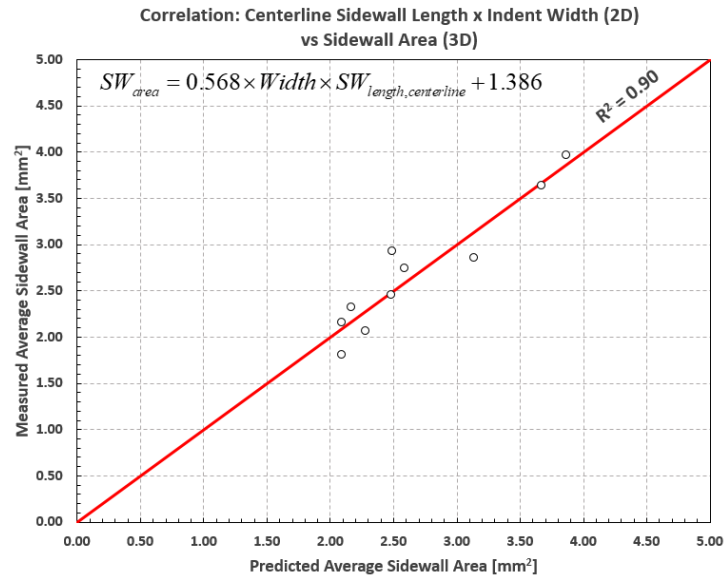


Figure 9.6: Multiple 2D Parameters Used to Evaluate Sidewall Area

The correlations in the section above demonstrate how a majority of the relationships hypothesized by Table 12 can be used to reasonably predict critical three dimensional geometry. The information evaluated along the centerline of the indents, in conjunction with knowledge of the indentation width, is generally sufficient to obtain a prediction of the 3D geometry that has been shown to correlate well with performance parameters such as transfer length and splitting propensity. Armed with this knowledge, the potential for on-line production quality control in real-time may indeed be realizable.

9.2 Empirical Concrete Prism Data

A critical component of phase II of this research project is evaluating which indented wire geometric features, or combinations of features, contribute most significantly to desirable wire-concrete performance criteria. Prior sections of this report were dedicated to the acquisition of accurate wire scans and the extraction of statistically significant quantities of detailed geometric features of a multitude of indented wires. As a result, a plethora of measured wire geometry is available to be correlated against parameters that can be used to indicate favorable wire-concrete performance.

In conjunction with the indent profiling system, sets of prestressed concrete prisms were made for the overall FRA research project. These concrete prisms were to be constructed using the same ten cover testing wires that were subjected to extensive evaluation by the indent profiling system, the results of which, are summarized in section 7. The concrete prisms were constructed with the purpose of measuring the effect of reduced concrete cover on wire-concrete performance criteria, namely, transfer length and splitting propensity. From this combined information, the detailed indentation geometry can be correlated with wire-concrete performance criteria to quantitatively determine which indent features contribute most significantly, or detrimentally, to desirable performance characteristics.

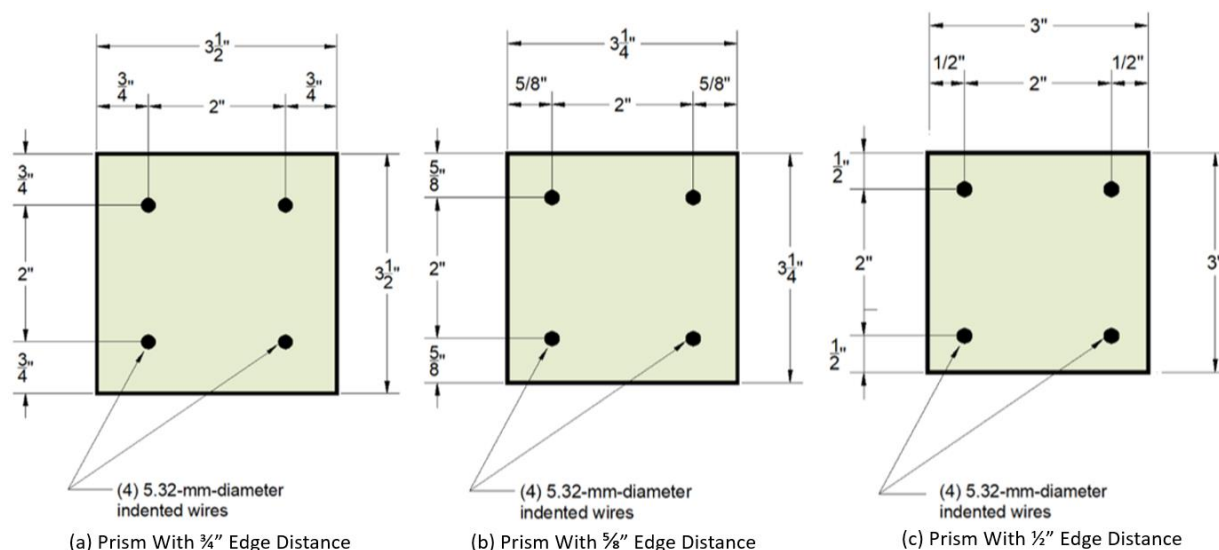


Figure 9.7: Concrete Prism Schematics

Three separate sizes of prisms were constructed to evaluate the effect of reduced concrete cover on transfer lengths and splitting propensity for ten unique chevron wires. The wire patterns of the prisms were comprised of 4 wires with equal spacing, forming a square grid with 2" spacing between wires. The overall external sizes of the prisms were then chosen to provide the desired concrete covers for the tests, the distance between the center of a wire to the nearest free surface, resulting in the following concrete covers: $\frac{3}{4}$ ", $\frac{5}{8}$ ", and $\frac{1}{2}$ ".

The prisms were cast with three separate mix designs utilizing different aggregates: Tucson, granite, and pea gravel. Furthermore, multiple concrete release strengths were tested, namely 4500psi and 6000psi for the prisms applicable to this portion of the research project. The prestress force for the fabricated prisms was targeted at 28000lbs, each wire being tensioned to 7000lbf prior to de-tensioning. The prisms were cast in metal forms to ensure high geometrical tolerances; each prism was 69 inches in length, so that a unique transfer length could be assessed on each side, provided no cracking occurred.

Overall, 161 prisms were created with ten unique chevron wires, three different concrete covers, three different aggregates, and two separate release strengths that could be used in the correlations in the subsections that follow. To evaluate the transfer length measurements of the test prisms, an automated non-contact strain measurement system was utilized, a photograph of which, can be visualized in Figure 5.7. To accomplish this, a set of reference images were taken along the length of the prism ends prior to de-tensioning, after de-tensioning another set of images were taken and a strain profile was obtained. From the strain profile, the transfer lengths on each end of a prism could be determined, provided that no cracking occurred. The transfer length is a valuable quality control parameter used in determining wire-concrete performance, it is the length over which the prestress force from the wires is completely transferred to the concrete. An illustration of what the transfer length represents is provided in Figure 9.8. From a design standpoint, it is required for the transfer length to be shorter than the distance from the edge of the tie to the railseat. Transfer length is influenced by concrete release strength, but is also heavily dependent on wire indentation geometry.

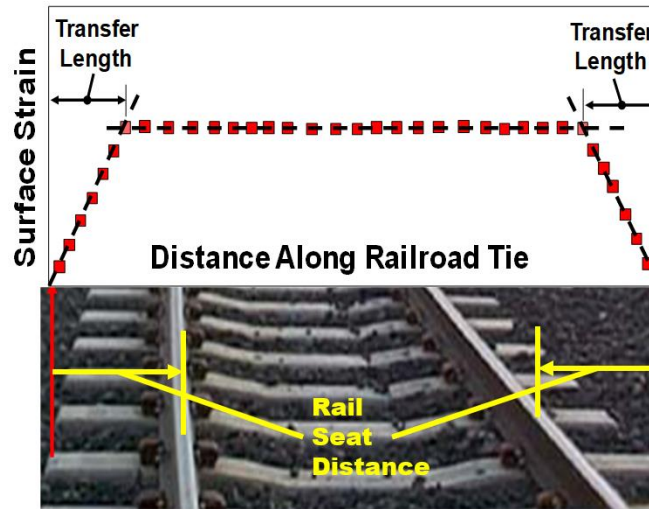


Figure 9.8: Transfer Length

In addition to the transfer length, the concrete prisms were used to assess splitting propensity. Splitting propensity is the amount of cracking that occurs after the de-tensioning process. For obvious reasons, it is desirable for this parameter to be zero, and preferable to have a significant margin of safety to guard against it. Splitting is primarily a function of prestress force, release strength, concrete cover, and can be heavily influenced by wire geometry. By reducing concrete cover to critical levels, cracking can be observed, allowing for the relationship between splitting propensity and wire geometry to be understood.

The majority of the prisms experienced cracking after the de-tensioning process. Each prism was subjected to manual assessment, in which, the cracks were drawn out for each end of the prism. This formed a “crack-map”, which tabulated the observed crack lengths and crack widths present on each prism. An example of a crack-map is illustrated in Figure 9.9.

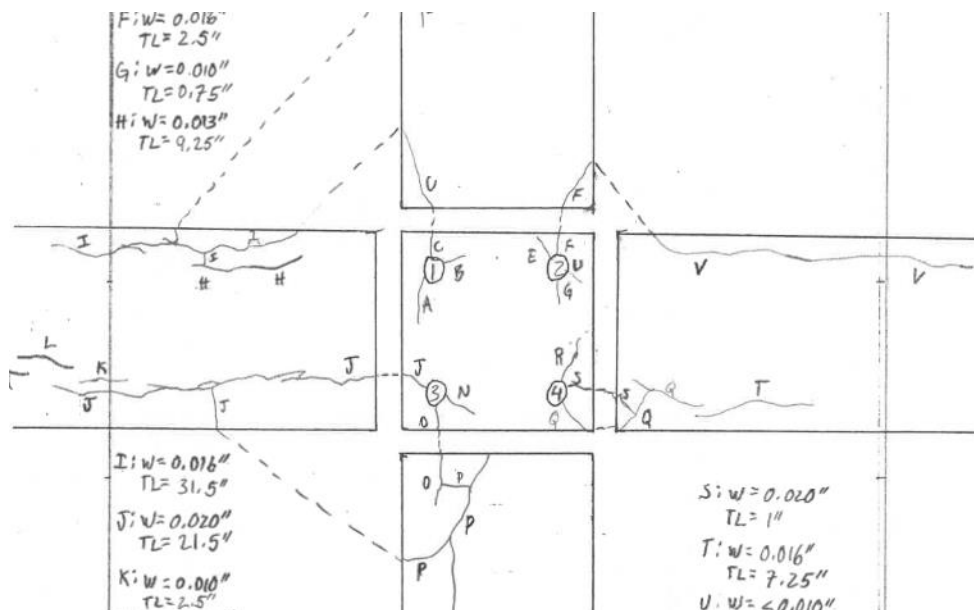


Figure 9.9: Concrete Prism Crack Map

Overall 135 prisms had visible cracks after the de-tensioning process for prisms composed of the ten different cover testing wires. Of those prisms, 58 were made with Tucson aggregates, 53 were made with granite aggregates, and 24 were constructed with pea gravel. It is important to note that fewer prisms were constructed with pea gravel than the other two aggregates, and that only one unique release strength was tested for the prisms made of pea gravel.

Furthermore, prior FRA projects involved the creation of similar concrete prisms utilizing the same cover testing wires. Those prisms were included in the correlation process in addition to the data captured by the cover testing prisms. The previous prisms were constructed with 1" concrete cover, and thus, infrequently experience splitting failures. As such, that set of prisms represented a consistent source of transfer length data since a vast majority of the prisms received valid transfer length measurements since no cracking was observed.

The transfer length and splitting propensity measurements on the test prisms resulted in an expansive amount of empirical data. This data covered ten unique chevron wires, three different concrete covers, three different aggregates, and two separate release strengths. The addition of the transfer length data obtained from prior FRA projects also provided a substantial amount of quality transfer length information. The collected performance metrics of transfer length and splitting propensity could then be correlated with the extensive amount of data collected by the indent profiling system. The resulting correlations are the primary topic of discussion in the subsections to follow.

9.3 Transfer Length Correlations

Transfer length describes an important performance characteristic in prestressed concrete members. Transfer length is the length over which the prestress force from the wires is completely transferred to the concrete, an illustration of what transfer length physically represents is provided in Figure 9.8. Prior research has shown that this parameter is influenced by concrete release strength, but is also heavily dependent on wire indentation geometry. The results obtained by the indent profiling system, coupled with empirical measurements of transfer lengths of concrete prisms constructed using the same wire specimens, have been used to correlate the relationship between certain indent geometrical features and the resulting transfer length.

Transfer length measurements from a prior FRA project were used extensively in conjunction with results from the indent profiling system. Fifteen separate sets of prisms were created with 1" concrete cover, utilizing nine different wires. Eight of these wires were identical to those highlighted in section 7.1 (WP and WQ were not available). The remaining wire, type WA, was a smooth 5.32mm wire with no indentation characteristics. Each test set included three prestressed concrete prisms, resulting in six separate transfer length measurements; these six measurements were averaged together to represent a single transfer length for the set. Additionally, three separate release strengths were tested: 3500psi, 4500psi, and 6000psi. A majority of the tests, 9 out of 15, were performed at 4500psi.

The first transfer length correlation was carried out on test sets that shared a common release strength in order to isolate the effects of wire indentation geometry on bond, and thus, transfer length. The 4500psi release strength data representing the nine unique wires was used in this case. Prior research has shown that multivariate linear regression with two select geometric parameters is sufficient to accurately predict transfer length. Indentation volume and indent sidewall area were used to develop a correlation that resulted in a R^2 -value of 0.94, indicating an exceptionally strong correlation. As indentation volumes and sidewall area increase, the transfer length sees a corresponding decrease. This makes intuitive sense as the increase in indentation volume and sidewall area allows for more interlocking with the surrounding concrete and provides additional bearing area. The correlation showing the relationship between indent volume and sidewall area on transfer length is plotted below in Figure 9.10.

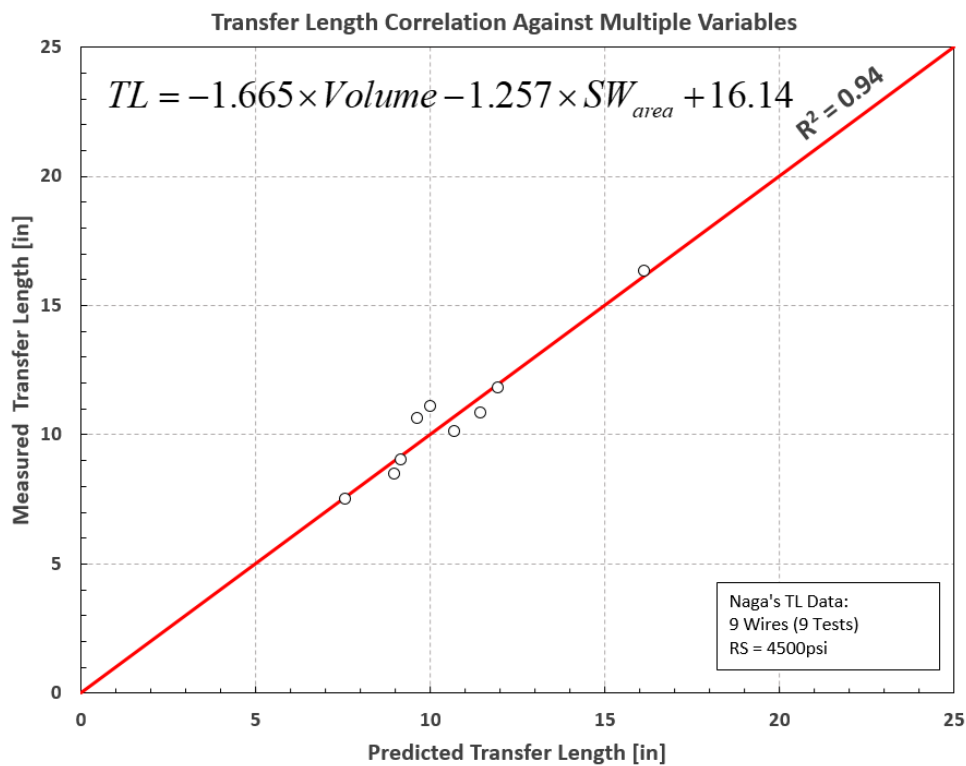


Figure 9.10: Transfer Length vs. 3D Indent Parameters (Constant Release Strength)

The second transfer length correlation that was carried out included all fifteen tests, involving three unique release strengths. Release strength has a direct influence of the transfer length, and thus, by maintaining the same geometric features, the effect of release strength on transfer length can be quantified. Furthermore, the compressive and tensile strength of concrete is directly related to the square root of release strength, therefore, the square root of release strength is included as a variable in the regression. The correlation involving the square root of release strength, indentation volume, and indent sidewall area to predict transfer length is provided in Figure 9.11. Once again, a strong correlation is observed, resulting in a R^2 -value of 0.88 with most of the points clustered next to the line of best regression. Similar to the previous correlation, increases in volume and sidewall area correspond to a decrease in transfer length. An increase in release strength has the effect of decreasing the transfer length, an observation that is matched by reality.

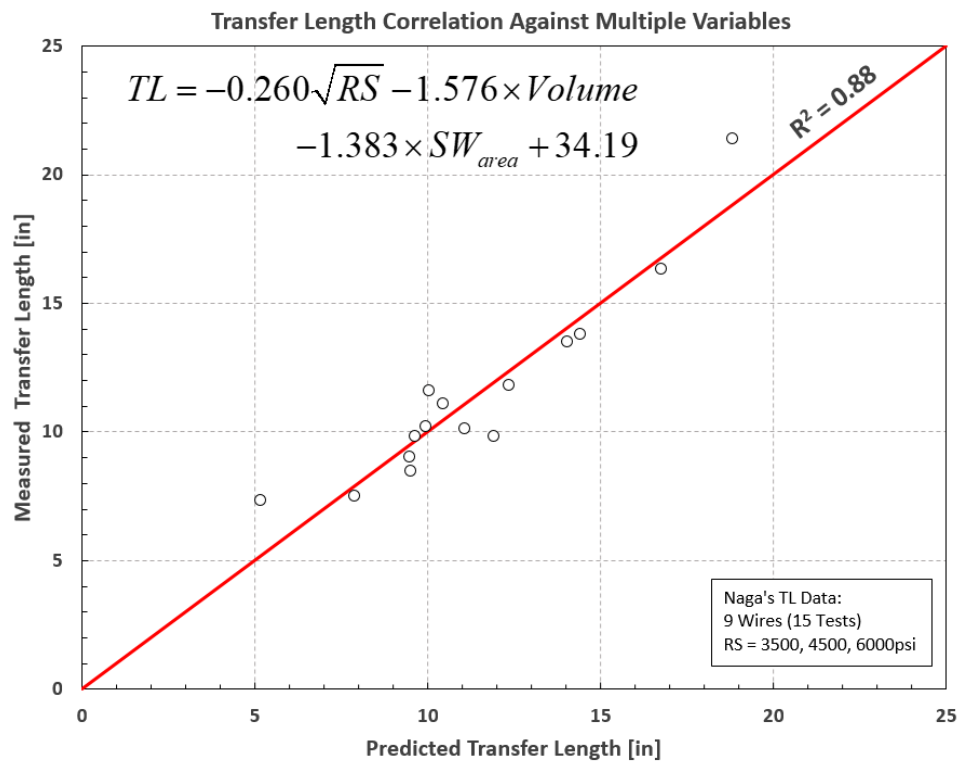


Figure 9.11: Transfer Length vs. 3D Indent Parameters (Variable Release Strength)

In section 9.1 it was shown that volume and sidewall area, fundamentally three dimensional values, could be adequately represented by indentation geometry described by the centerline data alone. Indentation volume and sidewall area prove challenging to measure by manual means. Therefore, it is a desirable alternative to develop a correlation that relates two dimensional centerline geometry data to transfer length. Such a correlation is summarized by Figure 9.12. In this third correlation, centerline profile area is substituted for indent volume, furthermore, centerline sidewall length is used to replace sidewall area. The resulting correlation provides a reasonable prediction of transfer length, exhibiting a R^2 -value of 0.90.

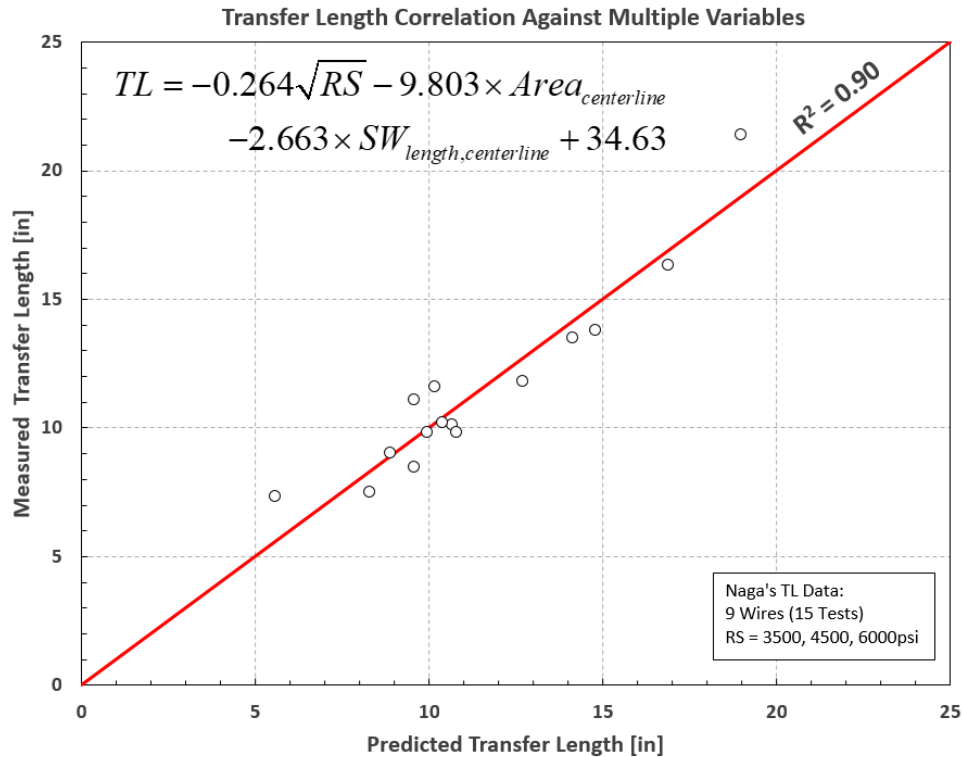


Figure 9.12: Transfer Length vs. 2D Indent Parameters (Variable Release Strength)

It has been demonstrated by this subsection that it is sufficient to describe transfer length with a three parameter regression model. One parameter, the square root of release strength, is a property of the concrete used to create the prestressed member, whereas the other two parameters quantify the effects of wire geometry on transfer length. Somewhat annoyingly, release strength is in units of psi, whereas the parameters representing indent geometry are in dimensions of millimeters. The correlations, developed from measurements of nine different wires in addition to transfer lengths from 45 unique prisms, appear to predict transfer length to an accuracy of ± 2 inches.

9.4 Crack Length Correlations (Splitting Propensity)

Splitting propensity is another important performance characteristic that is a result of the interaction between the indented wires and the concrete of the prestressed member. As the wire is de-tensioned to provide prestressing force into the concrete, the wire pulls into the member as the wire becomes slightly shorter. During this process, a certain volume of the concrete must be displaced by the indentations in the wires, resulting in potentially significant splitting forces being applied to the ends of the concrete member. This perpetuates as cracking if the radial force is sufficiently high. As a side note, smooth wires with no indentations also displace a certain amount of concrete since the wire expands due to Poisson's effect as the wire is released. Cracking is particularly prevalent at reduced concrete covers as there is less confinement provided around the wire-concrete interface. Splitting propensity (cracking) is also influenced by wire geometry as the threshold for splitting is reached. The results obtained by the indent profiling system, coupled with empirical measurements of crack lengths observed on concrete prisms constructed using the same wire specimens, have been used to correlate the relationship between certain indent geometrical features and splitting propensity.

Section 9.2 overviewed the concrete prisms that were fabricated in order to collect detailed information on splitting propensity. 161 concrete prisms were created related to this section of the project; 135 of the prisms showed visible signs of cracking. These prisms were created with three separate concrete mixes utilizing a diverse set of aggregates, two separate release strengths, three separate concrete covers, and were constructed using the ten unique chevron type cover testing wires. Of the 135 prisms that experience cracking, 58 were made with Tucson aggregates, 53 were made with granite aggregates, and 24 were constructed with pea gravel. It is important to note that fewer prisms were constructed with pea gravel than the other two aggregates, and that only one unique release strength was tested for the prisms made of pea gravel. In every case that cracking was observed the prism was evaluated with a manual crack-map and given a total "crack length", also denoted as "CL" in many of the correlation formulas outlined in this subsection. An example of a typical splitting failure is illustrated in Figure 9.13.



Figure 9.13: Cracked Prism

The first correlation between crack length and indentation geometry pertains to test specimens that were constructed with Tucson aggregates. Similar to the transfer length correlations, critical indentation features and concrete test specimen parameters were selected and then subjected to multivariate linear regression. Due to the complexity of the interactions between the wire and concrete in terms of crack length, additional geometric parameters had to be applied to get reasonable correlations. The variables chosen had to not only be strongly correlated with crack length, but also had to have very little correlation with other chosen parameters. Thus, the following wire geometric parameters were selected: average indent planform area (volume divided by average depth), sidewall area, and sidewall angle. Furthermore, concrete cover must be included since it determines the confinement of the wire-concrete interface. The resulting correlation can be seen in the following formula and Figure 9.14. It should be observed that the wire parameters that most significantly influence bond, volume and sidewall area, also have the tendency to increase the amount of observed cracking. This makes intuitive sense as a wire that has high bond, ergo a short transfer length, is also accompanied by higher splitting forces. Additionally, cover has a large effect on crack length; significantly reducing cover also reduces confinement of the prestressing wire, thus, more cracking is observed. The correlation has a R^2 -value of 0.80, and thus, is a reasonable predictor of cracking for prisms made with similar aggregates. The provided 95% confidence interval provides bands in which a majority of the crack length data will fall using the formula listed below.

$$CL = 149.1\left(\frac{Volume}{Depth_{avg}}\right) + 93.3 \times SW_{area} - 22.55 \times SW_{angle} - 1075 \times Cover - 966.7$$

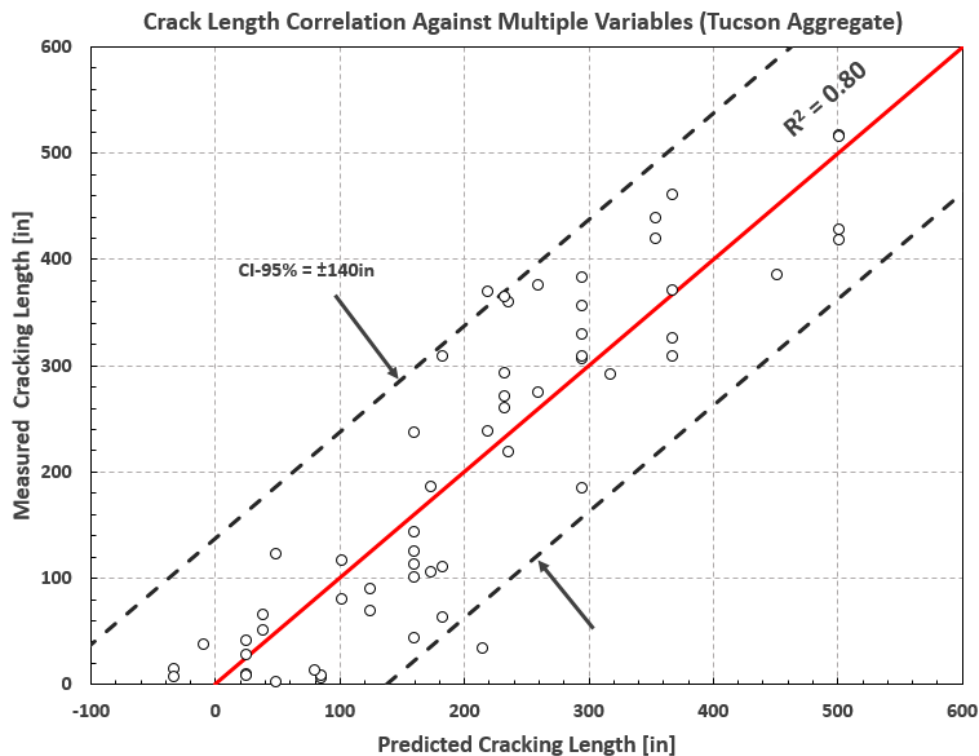


Figure 9.14: Crack Length Correlation (Tucson Aggregate)

The second correlation involves the data obtained from prisms made with granite aggregates. This aggregate was crushed, having significantly higher angularity than the other mixes, and thus, tended to resist cracking at reduced covers in comparison to the Tucson and pea gravel aggregates. The same parameters and linear regression model as the correlation for the Tucson mix was used. The derived correlation for the granite specimens can be seen in the following formula and is plotted in Figure 9.15. The same general trends in the coefficients for each parameter can be observed. However, the same 95% confidence interval has been applied to the correlated data, but the data points are not in perfect alignment with the band, or line of best regression for that matter. This implies that this aggregate is likely missing a parameter that was not included in the correlation, or one of the parameters has poor statistical significance, resulting in a lower R^2 -value of 0.71. In either case, the provided correlation is a rough predictor of cracking for prisms made with similar aggregates.

$$CL = 84.53\left(\frac{Volume}{Depth_{avg}}\right) + 85.78 \times SW_{area} - 85.78 \times SW_{angle} - 1156 \times Cover - 312.5$$

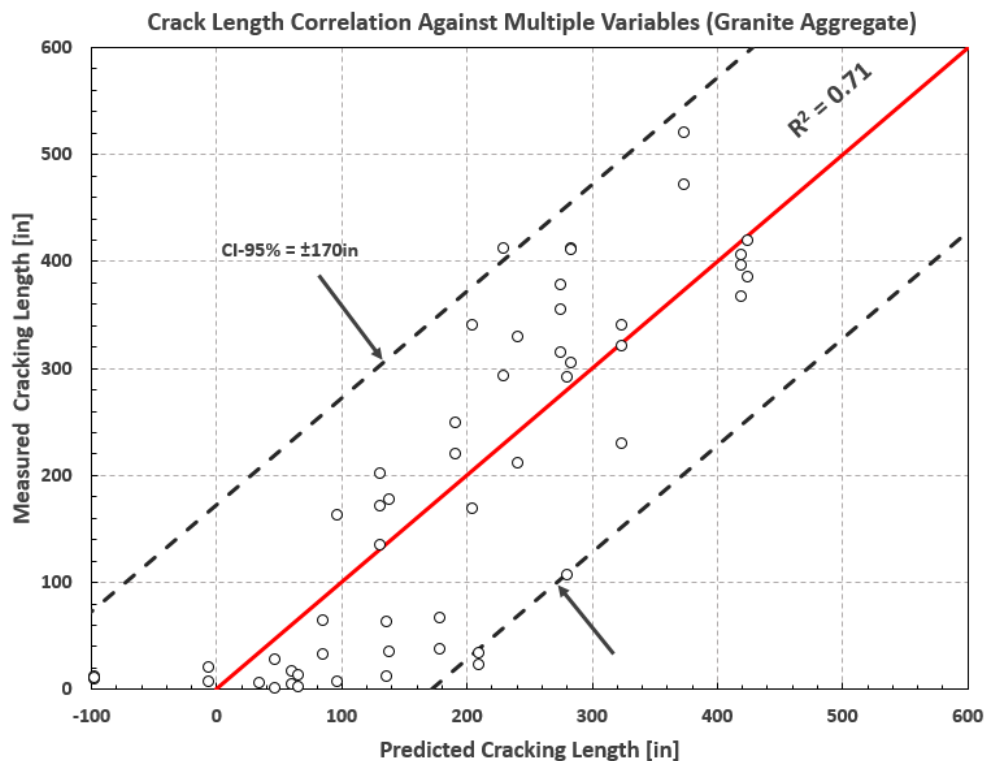


Figure 9.15: Crack Length Correlation (Granite Aggregate)

The third splitting propensity correlation pertains to data obtained for pea gravel mixes. This aggregate was comprised of rounded river rocks of small size, and thus, had poor resistance to splitting at reduced cover. As before, the same sets of parameters were selected with the same multivariate linear regression process. The correlation for pea gravel aggregates is provided in the following formula and plotted in Figure 9.16. The same general trends for the coefficients in front of the independent parameters are observed with the exception of the coefficient related to sidewall angle, which is exceptionally small. This implies that sidewall angle has little statistical significance related to pea gravel aggregates; the other parameters such as cover, average planform area, and sidewall area have a much more dominant influence on cracking. The resulting R^2 -value is 0.79, and thus, is a reasonable predictor of cracking for prisms made with similar aggregates.

$$CL = 55.95\left(\frac{Volume}{Depth_{avg}}\right) + 144.2 \times SW_{area} + 1.191 \times SW_{angle} - 1107 \times Cover - 196.4$$

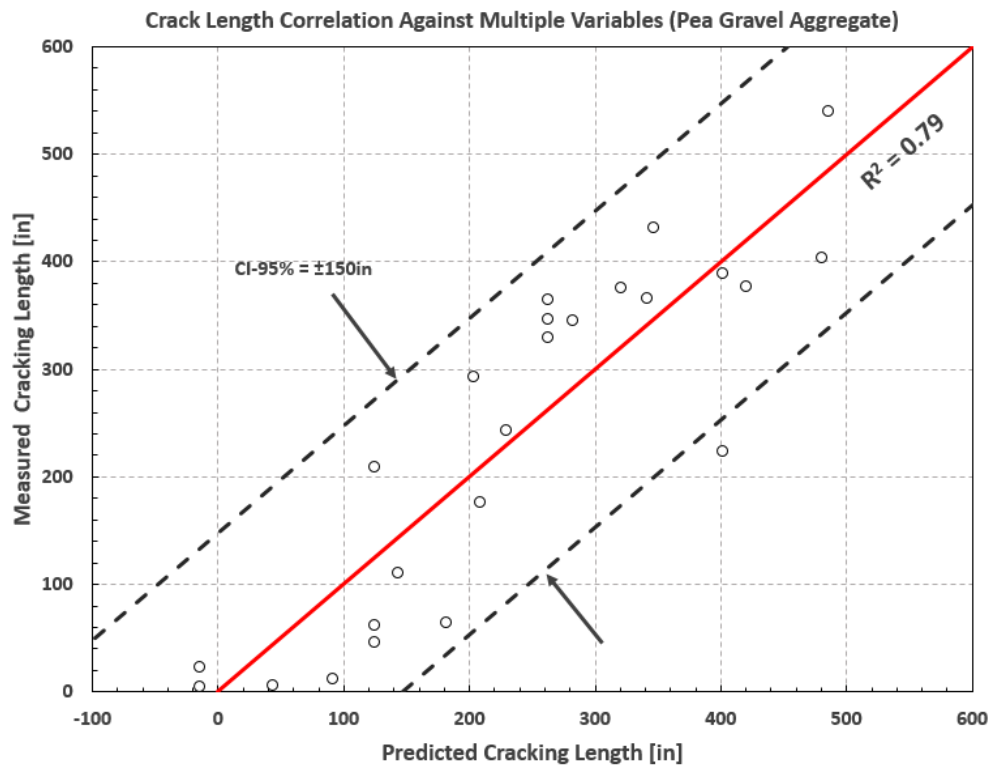


Figure 9.16: Crack Length Correlation (Pea Gravel Aggregate)

A fourth correlation can be seen below which includes all of the aforementioned prisms and aggregates that experienced cracking. Since it is a composite of all mix designs, with no parameter to differentiate between the mixes, the scatter is inherently higher; this is highlighted in Figure 9.17. While the correlation is not as refined, exhibiting a R^2 -value of 0.71, it encompasses all of the observed samples, and thus, can be used as a back-of-the-envelope way of predicting splitting propensity performance of an arbitrary mix if wire geometry and concrete cover is known.

$$CL = 106.0\left(\frac{Volume}{Depth_{avg}}\right) + 93.6 \times SW_{area} - 13.32 \times SW_{angle} - 1112 \times Cover - 967$$

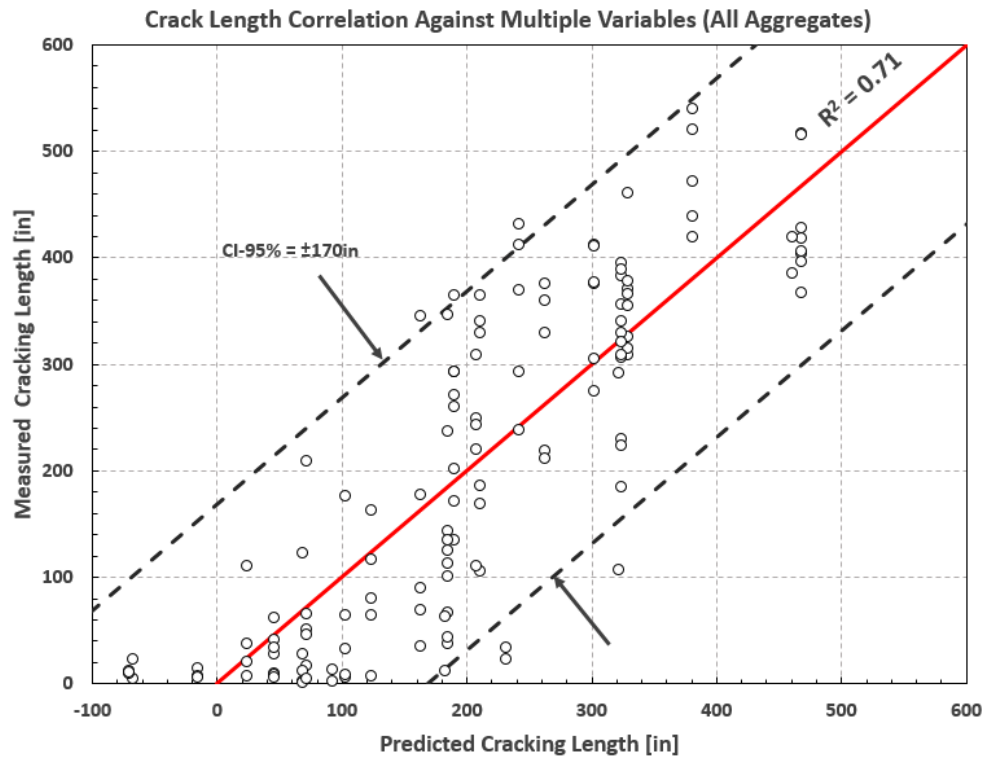


Figure 9.17: Crack Length Correlations (All Aggregates)

It has been demonstrated by this subsection that splitting propensity can be approximately described with a four parameter regression model. One parameter, the concrete cover, is a property of the prestressed member, whereas the other three parameters quantify the effects of wire geometry on splitting propensity. The following warning, similar to the transfer length correlations, must be given. The units of the splitting propensity correlations are mixed: wire geometry is measured in millimeters, or degrees in the case of sidewall angle, cover is measured in inches, and the resulting crack length is measured in inches. These correlations provide an approximate way to predict splitting behavior of members at reduced concrete cover with a wire of given geometry.

10. Go/No-Go Criteria

The indent profiling system provides the capability of assessing all of the unique indents that characterize a particular wire. Due to the large number of samples that the system can process, it is possible to identify the manufacturing variations seen across the entire length of the wire and on a row-by-row basis. These extensive measurements can then be used to determine if the sampled wire is suitable for use, passing the requirements of the aforementioned measurement standards as well as additional specifications decided upon between the consumer and the producer. The purpose of this short section is to interpret how the measured indentation geometry can be used in conjunction with current measurement standards and the newly developed correlations to determine the grounds for wire acceptance or rejection.

10.1 Evaluation by ASTM A881/ ISO 16120

The most predominant measurement standards pertaining to indented steel wires were the source of extensive discussion in section 2. These standards, ASTM A881 and ISO 16120, prescribed the acceptable ranges that certain indentation parameters must occupy, based on the nominal diameter and indentation shape of the wire being measured. Indentation centerline depth, nominal indent length, and indent pitch are amongst the required parameters to be measured. Further requirements, such as the range of acceptable values for sidewall angles, can be decided upon by mutual agreement between the consumer and the producer. The allowable ranges that these parameters must occupy are provided in Table 1 and Table 2 for both ASTM A881 and ISO 16120 respectively.

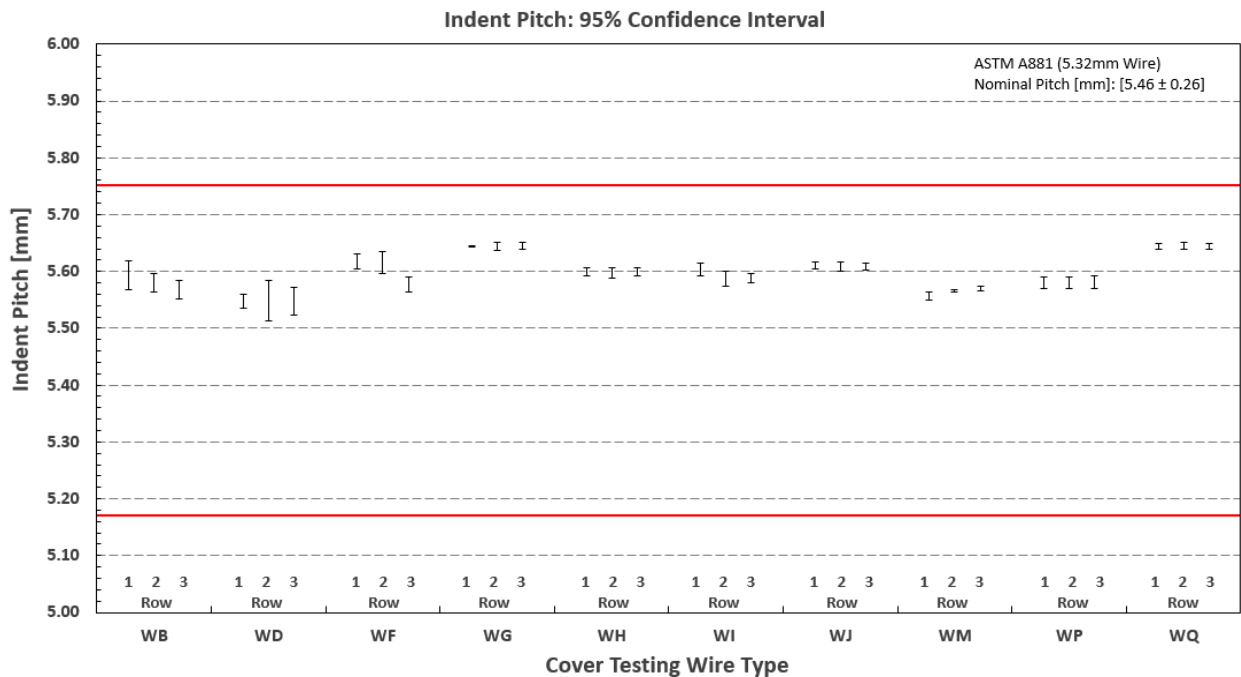


Figure 10.1: Measured Variations of Indent Pitch

Figure 10.1 provides a confidence interval plot of the measured indentation pitch of each cover testing wire that was highlighted in section 7.1. The indent profiling system extracted significant quantities of data for these wires; each indent row has over 100 unique measurements of pitch.

As such, the errors bands on the plot describe where 95% of the measured values are contained. No manufacturing process is perfect, thus, the confidence interval represents the statistical distribution of the measured values, rather than a simple mean which would not be sufficient in describing the manufacturing variations.

The red lines on the plot in Figure 10.1 indicate the allowable range dictated by ASTM A881 for indent pitch for wires with nominal diameters of 5.32mm. From the confidence intervals it is apparent that all of the wires would pass the requirements for pitch, as no confidence interval exceeds the band described by the red lines.

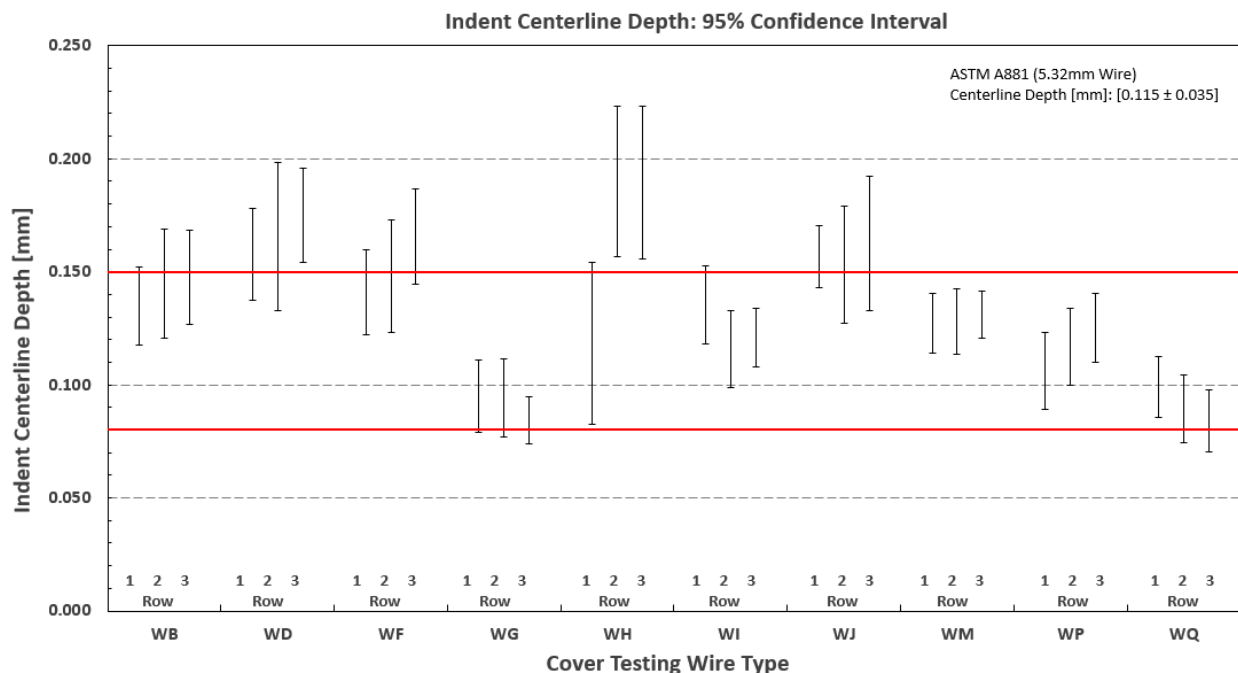


Figure 10.2: Measured Variations of Indent Centerline Depth

Another parameter required by the measurement standards is indentation depth, measured along the centerline of the indent profile. This critical parameter sees more significant manufacturing variations as the rollers are subjected to wear, damage, and differences in hydraulic loading; additionally, this parameter can vary from row to row. A confidence interval plot describes the measured indentation depth data in Figure 10.2. Once again, the red lines indicate the bounds that ASTM A881 prescribes for indent depth, falling between 80-150 μ m for 5.32mm wires. The grounds for acceptance or rejection (Go/No-Go) in this case is less obvious, as many of the confidence intervals clearly extend past the allowance band; in some situations, the intervals are completely excluded by the band.

Some of the wires, namely WM and WP, would be guaranteed to be accepted since the confidence intervals are contained completely by the band. However, the other wires have variations from the manufacturing process that prevent all of the observed indents from falling within the acceptable range for indentation depth. This implies that, depending on where the measurements are taken, some wires are not necessarily statistically impossible to meet the ASTM A881 requirement, but are statistically improbable to be accepted. Such wires include WD, WH, and WJ and can be seen in Figure 10.2. Other wires such as WB, WG, and WQ are statistically probable to be accepted, but are not guaranteed to be accepted. In either situation, the

requirements outlined by ASTM A881 are insufficient to be used to accept or deny a wire once statistically relevant sample sizes are involved. Are only the mean values to be used to determine if the wire abides by ASTM A881? Do only 80% of the indents need to fall within the allowance band? These questions are not addressed by current measurement standards, as the standards do not adequately take into account the manufacturing variations that are seen in practice.

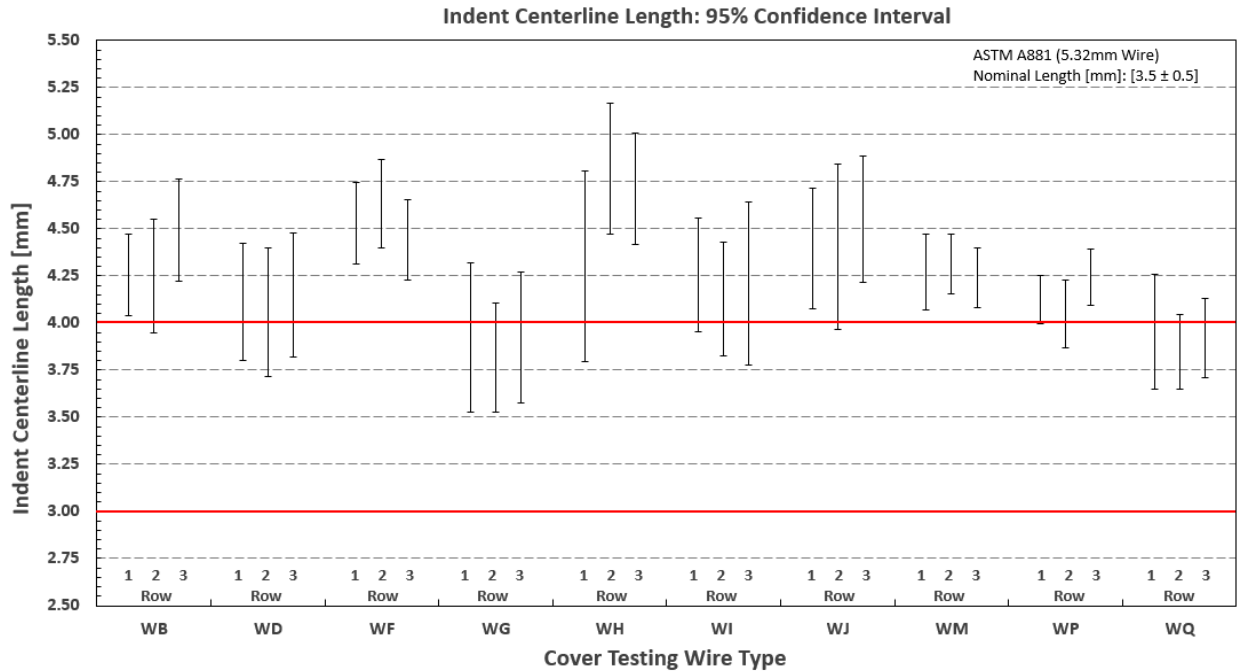


Figure 10.3: Measured Variations of Indent Length (Centerline)

Figure 10.3 reinforces the observations stated previously with a confidence interval plot of nominal indentation length. It is clear that a majority of the sampled wires have confidence intervals that fall outside of the band of allowed values. Once again, wires WG and WQ are statistically probable to pass the ASTM A881 requirement, whereas other wires would fail to meet the same criteria.

The observations of mean values alone are not sufficient to characterize the manufacturing variations seen in practice, and thus, would be a poor choice to be used as acceptance or rejection criteria. Once statistically relevant sample sizes of indent geometry measurements are involved, it is necessary to take into consideration the statistical distribution of the data that describes the variance of the manufacturing process. Thus, it is proposed that 80% of the values contained by each individual row must fall within the band of allowable values. This ensures that a majority of the indents must meet the prescribed values and that the rows must be similar in quality, but allows for variations in the manufacturing process.

10.2 Comparison to Correlations

This subsection highlights the potential use of the correlations developed in section 9 to determine the suitability of a given wire. This method represents a significant departure from the current measurement standards as it would require the wire to adhere to desired performance criteria rather than being accepted or rejected on the grounds of indentation geometry alone. It has been shown that transfer length and splitting propensity are strongly correlated with wire

geometry, and thus, certain combinations of indentation geometry directly influence performance criteria.

$$TL = -0.260\sqrt{RS} - 1.576 \times Volume - 1.383 \times SW_{area} + 34.19$$

Therefore, instead of requiring the indentation geometry to fall within a particular range, an alternative would be to specify desired values for certain performance criteria. For example, a specific transfer length may be desired at a given release strength (TL=10in, RS=4500psi). By using the transfer length correlation listed above, it is clear that certain combinations of indent volume and sidewall area can be used to achieve the desired transfer length at the particular release strength. If the transfer length and release strength are fixed values, then the geometry of a given wire dictates if the wire can, or cannot, provide the desired performance criteria.

$$CL = 106.0\left(\frac{Volume}{Depth_{avg}}\right) + 93.6 \times SW_{area} - 13.32 \times SW_{angle} - 1112 \times Cover - 967$$

This same methodology can be applied to splitting propensity (crack length) which is also significantly influenced by indent geometry. The same parameters that inherently produce better bond, and thus transfer length, are also related to increases in splitting propensity at reduced cover. Therefore, trade-offs must be made to ensure reasonable compromise between the two performance criteria. From a design standpoint, it is not realistic to have a short transfer length at a low release strength while also having adequate resistance against splitting at significantly reduced concrete cover.

If a given resistance against splitting propensity is desired, the confidence interval can be added to the crack length correlation given above. Then, for a given wire, of which the geometry is known, it is possible to calculate the amount of concrete cover required to satisfy the equation. Alternatively, if the desired splitting propensity and concrete cover is known, then it is possible to evaluate the possible combinations of wire geometry that satisfy the relation. Once again, if the desired splitting propensity and concrete cover represent fixed values, then the geometry of a given wire dictates if the wire can, or cannot, provide the desired performance criteria.

This method would allow wires to be accepted or rejected base on whether or not the indentations can provide the desired performance criteria. Current measurement standards do not state which geometric features contribute most significantly to performance criteria, and instead require the parameters to fall within prescribed bands. This does not necessarily guarantee that wires that pass ASTM A881 and ISO 16120 provide desirable performance characteristics. By evaluating the effects of wire geometry on wire-concrete performance criteria it is possible to select wires based on the desired performance characteristics, using correlations such as those listed above. This way, design is governed by performance criteria rather than arbitrary restrictions on indentation geometry.

11. Conclusions

11.1.1 insufficiencies with Current Indent Geometry Measurement Methods

In summary, the following insufficiencies with current measurement standards pertaining to indented steel wires are as follows. First, common measurement standards such as ASTM A881 and ISO 16120 do not identify which geometrical parameters contribute most significantly to the performance of the wire. Second, the measurement procedures for obtaining the required indent features for the standard do not provide repeatable, reliable results between different operators. Often the measurement process is determined by mutual agreement between the producer and the consumer and is not a standard measurement that can be compared with other manufacturing processes or products. Third, determining indent geometry for the current measurement standards is a laborious endeavor; it is time consuming and does not integrate easily into a production environment. Often, wire samples are sent out to measurement labs only when process changes have been made to check for compliance with the measurement standards. This is hardly ideal since the manufacturing process of indented steels wires varies on an hourly basis as the indent roller teeth wear down, rather than on a sparse interval as the testing schedule implies. Finally, sample sizes are not statistically relevant due to the time it takes to collect the data and the inherent uncertainties with the current measurement processes. The low sample sizes fail to capture the intricacies of the manufacturing process since no two indents are identical and significant variance can be seen across neighboring indent rows.

Early wire scanning technology took great strides to address the insufficiencies with the current measurement standards and attempted to more accurately understand the relationship between geometrical indent features and favorable performance criteria. The system could collect high resolution data and extract a variety of indent features above and beyond those dictated by current measurement standards. Some key indent features were found that corresponded with desirable wire performance. Additionally, it could extract features in a reliable, predictable manner across a wide variety of tested wires. However, the system was too slow to be a device that would be applicable to a production environment and mostly found use as a research tool. The system could not collect statistically relevant sample sizes that could accurately characterize the manufacturing process of the wires due to the considerable time it took to operate.

This report highlighted the need for a device that has the desirable capabilities of the early wire scanning system and addresses the majority of its faults. The development and implementation of such as device was described in great detail during the majority of this report. The indent profiling system that was the direct result of this research effort is significantly faster and collects statistically relevant sample sizes. The system was used to address the insufficiencies with current measurement methodologies. It was used to identify which geometrical parameters contribute most significantly to the performance of the wire by comparing captured wire geometry with empirical prestressed concrete prisms results. It could provide repeatable, reliable results for extracted indent features between different operators since the system is completely automatic and the features are extracted via computer algorithms. Furthermore, it could collect statistically relevant sample sizes, assessing all unique indents formed by the manufacturing process, in short duration. This system represents a departure from current manual methods and has proven to be a valuable research and production quality monitoring tool.

11.1.2 The Indent Profiling System

The Indent Profiling System is a non-contact laser-based device capable of measuring the indentation geometry of steel wires used in the manufacture of concrete railroad ties. It was designed to address the shortcomings of the current manual methods used to assess the quality of indented wires. The manual methods provide insufficient sample sizes due to the time-consuming nature of the measurements, furthermore, the collected information is challenging to extract in a repeatable manner using manual procedures. The indent profiling system remedies these issues by analyzing all of the unique indents formed by the indent rollers during the manufacturing process and extracting the geometric features in a repeatable, accurate manner.

During phase I of this project the key objective was to design and implement an automated indent profiling system to produce unbiased, statistically-relevant sample sizes. After motion control and data acquisition of the system was implemented, calibration techniques and data manipulation steps were developed to enhance the quality of the data being received. Then, the system was applied to measure specimens of known geometry to verify the correct and reliable operation of the system and quantify expected measurement uncertainties.

Phase II of the project involved the application of the Indent Profiling System to measure the indent characteristics of a multitude of indented wires. A sampling of these wires would be from those used in modern industry, a subset would be wires that were extracted from historical crossties that had been in track for upwards of multiple decades, and another set of wires were created with known “machined indents” for use with system checkout. In conjunction with the transfer length and splitting propensity testing of concrete prisms for this project, the Indent Profiling System results were then used to extensively investigate which geometrical parameters of indented wires contribute most significantly, or detrimentally, to prestressed member performance criteria.

The indent profiling system utilizes a blue sheet-laser to capture the indent geometry with an axial spatial resolution of 20 μ m. The laser is mounted on a lathe chassis that allows the system to scan wires up to 30 inches in length, unwrapping the three dimensional surface into a two dimensional height-map. Scan filtering is applied to reduce scan noise and enhance data visualization. Calibration procedures were developed to eliminate system misalignment and algorithms were created capable of removing the inherent bow of the indented wires. The resulting scans were within $\pm 2\mu$ m of accuracy for the trued wire surface. An assessment of the system measurement uncertainty was 8.3 μ m and could be significantly reduced with data filtering and averaging. Data processing steps were developed that could reliably identify the locations of the indent rows and could recognize individual indents. A trapezoid fit was then applied to the indent data, allowing for all relevant two and three dimensional indent features to be extracted.

One of the primary objectives of the indent profiling system was the collection of sufficiently large amounts of data to form statistically relevant sample sizes of extracted indent features. As such, the system was designed to acquire all indent geometry associated with a complete repetition of the indent rollers used to form the indentation geometry into the steel wires. Collection of data exceeding one complete revolution of the indent rollers is unnecessary, as the resulting data would not be statistically unique since the indent rollers continue to form repetitions of previous created indents. It was demonstrated in this report that the system could

be used to capture all unique indent geometry representing the complete pattern formed by the indent rollers.

The Indent Profiling System was used to measure the indent characteristics of a multitude of indented wires. The first set of wires, those commonly used in modern industry, represented a wide variety of indent depths and indentation shapes, additionally, the wires feature considerable differences in sidewall angles used in practice. These selected wires shared a common “chevron” pattern and are nominally 5.32mm in diameter. The geometrical results obtained from these modern wires were used to analyze the variations of the individual parameters on a row-by-row basis and across the entire specimen. Furthermore, concrete prestressed prisms were created using the same wires; the geometrical features could then be correlated against measured performance criteria of the test prisms, thus determining which geometrical characteristics have the most significant influence on wire-concrete performance. Wires extracted from pre-existing concrete railroad ties in service represent the second set of wires. These wires form the basis for wire geometry that tends to work well in practice, as many of the crossties that the wires were extracted from performed favorably over the course of decades. Some of the concrete ties were subjected to an estimated 4 billion gross axle tons of loading during the service life of the tie, indicating favorable wire-concrete performance. The third group of wires, those with fabricated “machined” indents, were used for system calibration and verification of feature extraction algorithms. The results from scanning the machined wires indicated that the feature extraction algorithms were functioning as intended.

During the course of this research study it was found that large variations exist from row to row on the indented wires that were subjected to processing. Often, the geometric parameters were so different from row to row that the measured statistical distributions did not overlap; this was particularly observable in metrics such as sidewall angle and sidewall area. Additionally, it was found that many of the measured parameters exceeded the bounds set by ASTM A881 and ISO 16120. The Indent Profiling System represents a departure from current manual measurement methodologies, collecting quantities of data that can adequately characterize the manufacturing process. Furthermore, the system has been used to further the understanding of how indentation geometry directly contributes to desirable performance characteristics.

11.1.3 Correlation of Indent Geometry with Performance Criteria

During the project, the Indent Profiling System proved its ability to accurately extract indentation geometry of the wires subjected to test. The calibration procedures and wire cast correction algorithms ensured that wire scans were generated with micron levels of precision. From these calibrated scans, the system could extract dozens of geometric parameters, analyzing hundreds of unique indents at a time. This allowed for manufacturing variations to be analyzed from indent to indent and on a row-by-row basis. Furthermore, the results from the Indent Profiling System were correlated with empirical performance characteristics of prisms constructed using the same wires. Strong correlations were developed that related indentation features with wire-concrete performance criteria such as transfer length and splitting propensity.

The Indent Profiling System represents a departure from current manual measurement methodologies, collecting quantities of data that can adequately characterize the manufacturing

process and has been used to further the understanding of how indentation geometry directly contributes to desirable performance characteristics.

11.1.4 Recommendation of New Measurement Standard

This report began with a review of the importance of transfer length in diagnostic testing of prestressed concrete members, and prestressed concrete railroad ties in particular. It was then noted that traditionally, transfer-length is determined from longitudinal surface strain measurements that are performed using mechanical gauges such as the Whittemore gauge, or demountable mechanical (DEMEC) strain gauges, and others devices using “contact” measuring principles. These methods involve tedious surface preparation, and are also prone to significant human errors and inaccuracies. Furthermore, these mechanical sensors can only detect lateral displacements. This report presents a new optical sensor of measuring prestress concrete surface strains. It makes use of the laser-speckle displacement that is detected by cross correlating the associated optical signals from a Charged-Coupled Device (CCD) sensor. The sensor was designed to be able to measure the surface displacement components without being affected by other surface motions that are generally present during the concrete detensioning process. The new sensor was initially tested using experiments that were conducted on a compressed concrete beam and a real prestressed concrete member during the manufacturing process. The results from this initial prototype optical strain sensor showed good consistency with contact measurements made by using both a foil strain gauge and with those obtained using the traditional mechanical Whittemore gauge.

Transfer length measurements that were conducted on pre-tensioned concrete ties at a railroad tie plant showed that the laser speckle technology provided a convenient and accurate mean to measure transfer length. The resolution of the transfer length determination was shown to depend mainly on two factors: (1) the resolution of the laser speckle sensor; (2) the estimation algorithm that is used to extract the transfer length value from the measured surface strain profile. The laser speckle sensor was demonstrated to have a resolution as high as 4 microns, or 20 microstrain if converted into strain using the nominal (8-inch Whittemore) gauge length of 203.2mm (8 in.). With respect to the transfer length estimation algorithm, the 95% Average Maximum Strain method (AMS 95%) is the classical or traditional method used in the industry. However, this traditional transfer length estimation algorithm requires human intervention and is subject to possibly significant human error. The introduction of a more accurate and reliable transfer length estimation algorithm, the Zhao-Lee (or ZL) algorithm, is discussed later in this report in some detail, including its associated measurement uncertainty.

The early prototype of the laser speckle technology showed great promise as a rapid and robust method to measure the transfer length of pre-tensioned concrete railroad ties, with short setup time and little preparation. The laser speckle sensor could be easily positioned on the concrete prisms or ties with the help of a manual traverse system, to take readings before and after detensioning. The first prototype is shown and compared to the later modular and more compact prototype dual camera system which formed the basis for the current FRA project work.

The Laser Speckle Imaging (LSI) technique, using the compact dual camera modular optical arrangement, was shown to be more accurate than the existing Whittemore strain gauge

technique because it eliminates human bias and improves repeatability of measurement. Furthermore, the technique does not require extensive operator training to achieve reliable measurements, as does the Whittemore strain gauge technique. The resolution of the LSI technique has been shown to be as low as $10\text{ }\mu\epsilon$, compared with a $25\text{ }\mu\epsilon$ accuracy for the Whittemore strain gauge technique. Much of the error associated with the use of the Whittemore strain gauge technique is due to poor repeatability, resulting in a large random error contribution. Thus, without operator training, it is difficult to get reliable transfer length measurements with the traditional Whittemore strain gauge technique. The LSI method offers a significant improvement in the reliability of estimating the transfer length.

The development of an automated version of a new non-contact device, based on Laser Speckle Imaging (LSI), was presented for measuring the transfer length of prestressed concrete railroad cross-ties. This new type of sensor had previously been shown to perform well for transfer length measurements in prestressed concrete beam applications, during manual testing with an earlier version of the device. In this report a newer dual-module design was utilized to automate the surface strain measurement process by means of a computer-controlled traversing system. It was based on the modular prototype sensor that was successfully demonstrated prior to the initiation of this project.

The automated LSI device was shown to provide accurate transfer length measurement comparable to those obtained using the traditionally Whittemore mechanical gauge, but at much higher speed, higher spatial resolution and increased repeatability. With its traversing hardware and LabVIEW interface, a 60-point sequence of surface strain measurements at 1-inch increment could be measured in about one minute on each end of a railroad concrete tie. Spatial resolutions (i.e., sampling intervals) as small as 1 mm are possible with the automated system. In addition, through the use of the unbiased Zhao-Lee algorithm based on least-squares technique for transfer length assessment, a much more reliable measurement free from human bias is achieved, along with the potential for determining the transfer length uncertainty from the statistical characteristics associated with the fitting algorithm.

The performance of the current system was previously demonstrated in field trip measurements conducted in an actual railroad concrete tie production plant, by limited sampling of the manufactured ties. This new automated LSI strain sensor, represented the next step toward the goal of fully-automated in-plant operation of transfer length measurement for real-time quality control monitoring of the railroad concrete tie production process.

A total of 220 transfer length measurements were conducted on prestressed concrete railroad ties with different concrete-mix designs and reinforcement variations at six prestressed concrete tie plants in the United States. The surface strain profiles of the railroad ties were obtained using the traditional Whittemore gage, as well as with the rapid, non-contact laser-speckle imaging (LSI) technology, that was previously developed by the authors.

The measured surface strain profiles were analyzed by both the 95% AMS method, and a new statistically-based Zhao-Lee (or ZL) method that was proposed by the authors. The ZL method was shown to be an unbiased method that provides a faster, more accurate and more reliable transfer length determination. A direct comparison between the 95% AMS method and the ZL method was achieved by applying both methods to the 220 strain profiles measured on the concrete railroad ties to determine their transfer length values. The comparison confirmed the

bias of the 95% AMS method in estimating transfer length value, as predicated by the theoretical bias equation.

The railroad tie transfer length measurements obtained from the six participating concrete tie plants ranged from a minimum of 4 inches to a maximum of 27 inches. The need for accurate and reliable measurement of transfer length is indicated by the fact that some of the values clearly exceeded the distance to the rail seat. Furthermore, other transfer lengths are clearly quite close to these rail seat distances and would be likely to exceed them over time. In either case, a potentially dangerous situation could result from tie failure under load. The newly automated LSI system is shown to provide the potential for rapid testing of manufactured ties for quality control.

There was excellent correlation between plant-phase data (crossties) and laboratory-phase data (prisms). This indicated that the laboratory prisms, cast with a similar concrete mixture, were able to accurately represent the behavior of the same reinforcement in a concrete railroad tie. The automated LSI devices performed well and enabled an unprecedented amount of data to be collected in a very short time period. As a result, 750 transfer lengths were able to be determined during the plant phase, of which 630 were from LSI data.

This study demonstrated several significant disadvantages of the traditional 95% AMS method in estimating the transfer length, including the presence of bias, the likely potential for significant human error, and the difficulty in dealing with outliers missing points in the data. The proposed ZL method displayed several advantages over the traditional 95% AMS method. It is not prone to human error and is able to achieve an unbiased transfer length estimation along with prescribed uncertainty of ± 38 mm (± 1.5 in.) in most scenarios when the sensor's gauge length is larger than 102 mm (4.00 in.). In addition, the algorithm of the ZL method was shown to be very easy to implement as a computer program. For example, an Excel macro was programmed by the authors for demonstration purposes, and is still in use.

The current investigation also exposed a fact that has been previously overlooked. Usually it was believed that a strain gauge with small gauge length could achieve more accurate estimation of the transfer length. Contrary to intuition, it was shown that, for sensors with fixed absolute resolution, sensors with smaller gauge length resulted in larger transfer length estimation error due to a decreased (relative) strain measurement resolution. In fact, the transfer length estimation error was seen to increase quickly when the gauge length of the sensor was reduced to less than 102 mm (4.00 in.).

11.1.5 Experimental Uncertainty in Transfer Length Assessment

Three different approaches were taken to quantify the measurement uncertainty associated with the Zhao-Lee transfer length assessment algorithm. The first involved a general sensitivity analysis of the system of equations used in the statistical strain profile curve fitting algorithm. The second method was an independent statistical approach, which resulted in a very simple algebraic expression for the transfer length uncertainty. The third method was a graphical interpretation of the transfer length uncertainty, and it was shown that this third approach was essentially identical with the simplified statistical approach. All three methods also gave identical estimates of the confidence interval for transfer length, based on the given uncertainty in the local strain measurement (strain sensor). It should be noted that the ZL method inherently assumes a bilinear strain profile for the pre-tensioned prismatic concrete member. However, in

some cases the real strain profile may not be bilinear. The real strain profile could be more parabolic, or could be an even more complicated curve (Yu, 2011). The ZL method was shown to have the potential to be adapted to other more complicated strain profile models, to give accurate estimation of the transfer length.

In this report the previously introduced Zhao-Lee (ZL) method for transfer length evaluation was next extended to include an arbitrary underlying prestressing force distribution. The general curve-fitting procedure was illustrated on both real prism test data, as well as on actual in-plant measured cross-tie surface strain measurements.

For prisms, it was shown that surface strain data is better represented by a bilinear underlying prestressing force distribution. For non-prismatic members, in particular for railroad cross-ties, it was shown that the exponential prestressing force distribution appears to best represent measurements of surface strain. For cross-ties, it was also shown that, consistent with the actual strain measurements, the surface strain is characterized by a series of bumps which significantly alter the strain profile from that of a prestressed prismatic member. These bumps result from the varying cross-sectional area and prestressing wire eccentricity, and preclude accurate and reliable estimation of a so-called average maximum strain.

Difficulties with the evaluation of transfer length were identified in relation to the non-prismatic cross-tie behavior. A direction for potentially removing this issue was proposed which focussed on the unbiased curve fitting parameters obtained from application of the generalized ZL method of analysis. The disadvantage is that this approach is somewhat removed from direct analysis of the strain data itself. However, it is hoped that this procedure will be valuable for accurate and reliable transfer length evaluation for use with future automated in-plant quality control measurements.

The previously generalized form of the Zhao-Lee (ZL) method for transfer length evaluation was utilized to investigate errors in processing measured surface strain on concrete railroad crossties. Crossties represent non-prismatic members, and require consideration of the varying cross-section shape and the characteristics of the underlying prestressing force distribution for assessing the transfer length. The previously developed Mean Square Error (MSE) statistical algorithm was used to determine the transfer length, assuming an underlying bilinear prestressing force distribution for simplicity.

The importance of accounting for thermal strain offset was shown through a comparison of both full-range crosstie strain measurements as well as for measurements near one end of a typical crosstie. Large differences in the resulting transfer length were shown to exist when comparing both with and without thermal strain effects, indicating that compensation for thermal strain is extremely necessary to achieve accurate measurement of transfer length in a plant environment.

Bias errors resulting from application of the traditional bilinear strain field assumption were estimated through simulation using the general non-prismatic strain profile as the “true” strain field for comparison purposes. The effects of transfer length magnitude and strain measurement range were both considered, and the bias error was shown to be negative in all cases with a maximum magnitude of about 10% of the transfer length, depending on the measurement length.

Different processing algorithms, with and without thermal strain considerations, were used to evaluate transfer length measurements conducted on hundreds of crossties under actual in-plant field testing conditions, for a wide range of different prestressing wire types. It was shown that in

spite of considerable differences in the transfer length processing methods, and significant departures from prismatic behavior, the averaged results were very consistent with the simple bilinear underlying strain profile assumption, and with the transfer length measurements on prisms obtained in a controlled laboratory testing environment.

This work represents a next step in an attempt to answer important uncertainty questions which needs to be addressed if rapid real-time transfer length is to be achieved, and if such measurements of transfer length are eventually to be used in a practical in-plant production setting as a quality control parameter.

11.1.6 The Multi-Camera Transfer Length Measurement System

Experimental results and theoretical analysis were presented showing that, by using the Zhao-Lee method, only a few discrete surface strain measurements are required to achieve accurate and reliable transfer length assessment. A simple algebraic representation of the transfer length uncertainty as a function of the strain sampling interval was developed and tested both with simulation data and with actual laboratory strain data. The result showed that the uncertainty increases as the square root of the sampling interval, and that the error is less than ± 1.5 inches for a sampling interval as high as every six inches. This discovery led to the design of a 5-camera non-contact transfer length measurement system that is capable of continuous monitoring of railroad crossties in a production plant.

The implications of the in-plant system are significant, since they indicated that for the first time it may be possible to conduct diagnostic tests on each and every railroad cross-crosstie that is produced. The advantages for a concrete crosstie manufacturing plant, from a transfer length quality control perspective, are obvious, because it will allow producer plants to ensure that transfer lengths are within an acceptable tolerance, and to identify the need to modify production (e.g., concrete mix) if transfer length specifications are out of range.

Using the ZL method and the automated LSI strain sensor, extensive plant measurements were taken in a crosstie manufacturing plant. Statistical and theoretical analysis of the in-plant crosstie transfer length measurements were obtained using an automated Laser Speckle Imaging (LSI) strain sensor system developed by the authors for rapid in-plant crosstie transfer length assessment. Through the use of selected samples of this in-plant data, the effect of strain measurement sampling interval on the resulting transfer length was investigated both theoretically and experimentally, and compared with results developed earlier for prisms. This provided a test of how well the simple uncertainty analysis developed for prismatic members would work for the more complex crosstie geometry.

Samples of crossties manufactured using prestressing wire types WA (smooth), WD (Chevron), and WF (Diamond) were selected for the sampling interval analysis. These wire types had produced crossties with relatively long (WA Smooth), intermediate (WD Chevron) and relatively short (WF Diamond) transfer lengths. For each wire type, a sample of 7 crossties was included in the analysis, representing 14 tie end transfer length measurements. For each of the three wire types analyzed, strain data was selected for crossties located during casting in the central portion of the plant casing bed.

The strain measurements were analyzed using the generalized Zhao-Lee transfer length algorithm, which accounted for the non-prismatic crosstie characteristics, and also compensated for the presence of thermal strain offset. The resulting transfer length data was pooled and

normalized so as to reveal the effect of sampling interval on the statistical scatter in the data. It was shown that, for the three different levels of transfer length tested (associated with the three prestressing wire types), the standard deviation of the measured transfer length correlated very well with a simple theory developed to estimate the uncertainty of transfer lengths for constant cross-section prismatic members. Although more analysis of the influence of non-prismatic behavior on transfer length uncertainty is needed, the results presented in this paper lend further support to the concept, developed on the basis of prism transfer length analysis, that only a few discrete surface strain measurements are required to achieve accurate and reliable in-plant transfer length assessment. This represents one more positive step toward an understanding of the system requirements needed for reliable in-plant automated transfer length assessment as an eventual in-plant quality control parameter.

Based on the results of the sampling interval study, the development of a new multi-camera method for measuring the surface strain profile on a railroad tie and assessing the associated transfer length was undertaken. The performance of the new device was then demonstrated both in a laboratory setting as well as in an actual tie manufacturing plant. Results of this testing indicated that, consistent with earlier experimental results as well as theoretical uncertainty analysis, the device performs as expected and is capable of assessing transfer length to a nominal tolerance of ± 1.5 inches with as few as 5 independent measurements of surface strain. For the current design, these independent strain measurements are obtained from simultaneous image captures of the concrete surface features from 6 adjacent cameras.

A further demonstration was given of the systems capability to not only provide transfer length measurement, but also to provide high spatial resolution measurements of the strain profile for manufactured ties. This was accomplished by manually shifting the portable system along a predetermined grid pattern and adjusting each set of 5 strain measurement by the amount of the shift. Overlapping these sets of 5 discrete strain measurements provided a high resolution picture of the tie strain profile. The procedure could also have been automated, but it was accomplished very rapidly by simply using manual positioning, since precise positioning was not critical to obtaining accurate surface strain measurements.

One of the first practical investigative applications of the new multi-camera system for measuring the surface strain profile was conducted at a turnout tie plant. The device was used to conduct a worst-case scenario on the effect of surface contaminants on bond, as evidenced by the surface strain profile and the resulting transfer length. Ties cast with smooth strand and ties cast with indented wire prestressing members were subjected to a literal soaking with lubricating oil on one end of the last tie in the respective casting bed. From the results it is evident that strands undergo slippage and the bond is severely degraded, resulting in a situation in which the strain level reaches only a small fraction of its design level. In sharp contrast, the indented wire ties, while clearly affected by the oil contamination, did achieve their design strain level in a manner similar to that observed in the uncontaminated tie ends. More importantly, the transfer length, while undergoing a significant increase, did not exceed the distance to the rail seat. Apparently, there is a significant influence of the indents so as to reduce the tendency to slip even under these extreme conditions. It is understood that these tests clearly represented worst-case situations. However, they have also proved to bring to light some major differences in the behavior of strand relative to indented wire in the presence of contaminants, suggesting that indented prestressing products may be more robust than those which are smooth.

This work represents a practical step toward the implementation of a device such as the 6-camera strain measurement system for continuous monitoring of in-plant prestressed railroad tie production, using transfer length as a quality control parameter. Furthermore, the tests presented here illustrate the usefulness of this new 6-camera system as a diagnostic tool for improving tie quality and robustness.

11.1.7 Investigation of the Thermal Offset Phenomenon

Extensive measurements of transfer length for prismatic as well as non-prismatic members, including in-plant crosstie measurements, have often revealed a significant offset in the strain profile which appears to be related to thermal expansion effects. It has been hypothesized that this thermal offset results from a difference in the temperature of the concrete member before and after the de-tensioning process; however, this has never been verified experimentally. Furthermore, existing algorithms used to assess transfer length have included a strain offset parameter for the purpose of improving the evaluation process. However, the source of this offset, and the applicability of assuming a uniform thermal offset parameter in assessing transfer length, has also never been verified experimentally.

As a further application and demonstration of the 6-camera system, a systematic investigation of the observed offset phenomena was undertaken. Measurements were conducted on thermally-instrumented prismatic members as well as non-prismatic members subjected to known temperature environments both before and after de-tensioning. The concrete members tested included a stepped member and a tapered member, the features of which are somewhat representative of the main features encountered in typical actual railroad crosstie geometry. Surface strain profiles were determined using both the traditional Whittemore gauge measurement procedure and using the new multi-camera optical non-contact surface strain measurement system developed by the authors.

As a first step in a systematic experimental investigation of the thermal offset phenomena, experimentally measured surface strain profiles were presented for concrete members that were immersed in known hot and cold environmental conditions and allowed to come to equilibrium before initiating the strain measurements. Two simplified non-prismatic prestressed concrete members were cast to represent known variations in cross-section shape and prestressing wire eccentricity, so as to demonstrate any effect of the geometry on surface strain profile variation and likewise on the thermal offset phenomena. These two non-prismatic shapes were an abrupt stepped (or block) geometry and a tapered geometry, each of which captures one of the dominant geometrical features associated with commercially produced railroad crossties.

The strain measurements revealed that the source of the offset phenomena does indeed appear to be associated with thermal expansion. The observed plateau in relative thermal shift when comparing strain measurements under hot to cold conditions is consistent with thermal expansion for the measured temperature change. In addition, there appears to be a strong indication of a non-uniform thermal expansion effect resulting from localized cooling near the ends of the concrete members. This has been further established by direct infrared camera images of surface temperature contours, and also by means of a conduction simulation model. While this non-uniformity clearly will depend on the mass of the concrete member under test, it suggests that under certain circumstances the non-uniformity in thermal offset may manifest itself in the form of a modified strain development region, essentially altering the slope of the strain development

zone near the ends of prismatic members, and likely also affecting non-prismatic members to an extent as well.

More analysis of the influence of the thermal offset behavior and its influence on transfer length, and transfer length uncertainty in particular, is needed if transfer length is to be used eventually as a production quality control parameter. However, the results presented here represent one more positive step toward an understanding of the measurement requirements needed for reliable in-plant automated transfer length assessment if it is to be used for in-plant quality control.

11.1.8 Investigation of the Effect of Non-Prismatic Shape

As a further utilization of the 6-camera strain sensor, work focused on the more dominant non-prismatic features associated with railroad crossties, in an effort to identify how well the simple 1D bending model can represent these features experimentally. In the efforts to establish and improve an unbiased algorithm for transfer length assessment, it is important that the potential errors in representing surface strain measurements be identified for accurate assessment of transfer length and for properly assessing transfer length uncertainty.

A first step in a systematic experimental investigation of the influence of cross-section and eccentricity on the resulting experimentally measured longitudinal surface strain profile has been presented here. Two simplified non-prismatic prestressed concrete members were cast to represent known variations in cross-section shape and prestressing wire eccentricity, so as to demonstrate the effect of the geometry on longitudinal surface strain profile variation. These two non-prismatic shapes were an abrupt stepped (or block) geometry and a tapered geometry, each of which captures one of the dominant geometrical features associated with commercially produced railroad crossties.

Measurements of surface strain were made using the traditional mechanical Whittemore gauge, as well as with the new multi-camera non-contact optical strain measurement system. The extent to which the one-dimensional (1D) prestressed beam bending model can represent measured surface strain is revealed in these tests, through comparison with the predicted behavior and through comparisons with the prismatic concrete member behavior. These results have important implications in relation to the experimental measurement of transfer length for non-prismatic railroad crossties.

The strain measurements were analyzed using the generalized Zhao-Lee transfer length algorithm, which accounted for the non-prismatic crosstie characteristics, and also compensated for the presence of thermal strain offset. The results suggest that the 1D bending model does a reasonable job in representing the tapered geometry, but has some difficulty in characterizing an abrupt change in cross-sectional area. This may suggest that the 1D strain model may have difficulties in represented accurately the more complex scalloped surface features associated with typical railroad crosstie geometry, and this may influence the reliability of transfer length assessment; particularly in the presence of an unknown thermal strain offset. More analysis of the influence of such non-prismatic behavior on transfer length, and transfer length uncertainty in particular, is needed if transfer length is to be used eventually as a production quality control parameter.

11.1.9 The Continuous Scanning/Traversing (CST) System

The last phase of this project involved another advance in the development of automated transfer length measurement systems for practical in-plant operation. The new device offers a significant improvement over the previously successful automated Laser-Speckle Imaging (LSI) system, provides significantly improved optical resolution of longitudinal surface strain, and is also capable of making measurements of strain in a real-time continuously scanning/traversing (CST) manner over the entire distance range of interest on the tie associated with transfer length development. The CST device features both a “jog” mode of operation, in which measurements of longitudinal surface strain are automatically captured in arbitrary spatial increments over the entire range of the computer-controlled traverse, and an “on-the-fly” mode in which measurements of longitudinal surface strain are captured without the need for stopping at each measurement location.

The capability of this new CST device was first demonstrated in the laboratory, using a new special-purpose longitudinal strain calibration setup. It was shown to be capable of a strain measurement resolution of nominally about + 20 microstrain, at traversing speeds of up to several inches per second. In addition, the new automated system was demonstrated by conducting measurements of longitudinal surface strain on prestressed concrete crossties in a manufacturing plant casting bed (Rocla Concrete Tie Plant in Sciotovalle, OH). Crosstie strain profile measurements obtained using this new CST system, in comparison to the recently introduced 6-camera manual device and in comparison to Whittemore gauge measurements, indicate unprecedented resolution of strain profile shape for in-plant measurements. In particular, it was shown to be even possible to resolve differences in the strain profile (and associated transfer length) between crossties in adjacent rows within the same casting cavity. To the best of the author’s knowledge, this type of detailed high-resolution comparison has never before been possible in a crosstie manufacturing plant.

12. References

- [1] Peterman, R. J., J. A. Ramirez, and J. Olek, "Influence of Flexure-Shear Cracking on Strand Development Length in Prestressed Concrete Members", *PCI Journal*, V. 45, No. 5, September–October 2000, pp. 76–94.
- [2] Gross, Shawn P., and Ned H. Burns, "Transfer and development length of 15.2mm (0.6 in.) diameter prestressing strand in high performance concrete: results of the Hobitzell-Buckner beam tests", Research report FHWA/TX-97/580-2, Center for transportation Research, The University of Texas at Austin, June 1995.
- [3] Kaar, P., and D. Magura., "Effect of Strand Blanketing on Performance of Pretensioned Girders", *PCI Journal*, V. 10, No. 6, December 1965, pp. 20–34.
- [4] Murphy, Robert L., "Determining the Transfer Length in Prestressed Concrete Railroad Ties Produced in the United States", Master Thesis, 2012, Kansas State University, Manhattan, Kansas, USA.
- [5] Wu C.-H., Zhao W., Beck T. and Peterman R. "Optical Sensor Developments for Measuring the Surface Strains in Prestressed Concrete Members" *Journal of Strains*, 47, Supp. 1, pp. 376-386, (2011), DOI: 10.1111/j.1475-1305.2009.00621.x.
- [6] Mark Haynes, John C.-H. Wu, B. Terry Beck, and Robert J. Peterman "Non-Contact Measurement of Wire Indent Profiles on Prestressing Reinforcement Steel" *Proceedings of the 2012 AREMA Conference*, Sept. 16-19, 2012, Chicago Illinois, USA.
- [7] Weixin Zhao, Terry Beck, Robert Peterman, John Wu, Rob Murphy and John Bloomfield, Grace Lee. "An Automated Transfer Length Measurement System for use on Concrete Railroad Ties," *The 2012 PCI Convention and National Bridge Conference*, September 29 - October 3, 2012.
- [8] Weixin Zhao ; B. Terry Beck ; Robert J. Peterman and Chih-Hang J. Wu, "A Portable Modular Optical Sensor Capable of Measuring Complex Multi-Axis Strain Fields", *Proceedings of the SPIE* 8466, Instrumentation, Metrology, and Standards for Nanomanufacturing, Optics, and Semiconductors VI, 84660Q (October 11, 2012); doi:10.1117/12.929931.
- [9] Weixin Zhao, Kyle Larsan Robert J. Peterman, B. Terry Beck, and C.-H. John Wu, "Development of a laser-speckle imaging device to determine the transfer length in pretensioned concrete members" *PCI Journal* Winter 2012, pp. 135-143.
- [10] Weixin Zhao, Robert L Murphy, Robert J Peterman, B. Terry Beck, Chih-Hang John Wu, Pelle Duong, "A Non-Contact Inspection Method to Determine the Transfer Length in Pretensioned Concrete Railroad Ties," *ASCE, Journal of Engineering Mechanics*, *Journal of Engineering Mechanics*, Volume: 139, Issue: 3, March 2013, pp. 256- 263.
- [11] Mark Haynes, John C.-H. Wu, B. Terry Beck, Naga N.B. Bodapati, and Robert J. Peterman "Prestressing Steel Reinforcement Wire Bond Index Number," *Proceedings of the 2013 Joint Rail Conference*, JRC2013-2422 April 15-18, 2013, Knoxville, Tennessee, USA. DOI: 10.1115/JRC2013-2422.
- [12] Matthew L. Arnold, Robert J. Peterman, Naga N.B. Bodapati, B. Terry Beck and John C.-H. Wu "Development of A Standard Bond Test For Indented Prestressing Wires," *Proceedings of the 2013 Joint Rail Conference*, JRC2013-2461 April 15-18, 2013, Knoxville, Tennessee, USA. doi: 10.1115/JRC2013-2461
- [13] Naga N.B. Bodapati, Weixin Zhao, Robert J. Peterman, John C.-H. Wu, B. Terry Beck, Mark Haynes and Joseph R. Holste, "Influence Of Indented Wire Geometry and Concrete

- Parameters on the Transfer Length in Prestressed Concrete Crossties,” Proceedings of the 2013 Joint Rail Conference, JRC2013-2463 April 15-18, 2013, Knoxville, Tennessee, USA. doi: 10.1115/JRC2013-2463
- [14] Weixin Zhao, B. Terry Beck, Robert J. Peterman, and John C.-H. Wu, “Development Of A 5-Camera Transfer Length Measurement System For Real-Time Monitoring Of Railroad Crosstie Production,” Proceedings of the 2013 Joint Rail Conference, JRC2013-2468 April 15-18, 2013, Knoxville, Tennessee, USA. doi: 10.1115/JRC2013-2468.
- [15] Weixin Zhao, B. Terry Beck, Robert J. Peterman, Robert Murphy, John C.-H. Wu, and Grace Lee, “A Direct Comparison Of The Traditional Method And A New Approach In Determining 220 Transfer Lengths In Prestressed Concrete Railroad Ties,” Proceedings of the 2013 Joint Rail Conference, JRC2013-2469 April 15-18, 2013, Knoxville, Tennessee, USA. doi: 10.1115/JRC2013-2469.
- [16] Mark D. Haynes, Chih-Hang J. Wu, B. Terry Beck, Robert J. Peterman (2013), “3D Non-contact Profilometry For Reinforcement Steel Quality Control,” *Proceedings of the Industrial and Systems Engineering Research Conference (ISERC)*, May 2013, San Juan, Puerto Rico.
- [17] Mark D. Haynes, Chih-Hang J. Wu, B. Terry Beck, Robert J. Peterman (2013), “Automated Real-Time Search and Analysis Algorithms for a Non-Contact 3D Profiling System,” *Proceedings of the SPIE, Volume 8791, id. 87911G 12 pp.* Munich, Germany.
- [18] Naga Bodapati, R.J. Peterman, W. Zhao, T. Beck, C.-H. Wu, J. Holste, M. Arnold, R. Benteman, R. Schweiger, “Transfer-Length Measurements On Concrete Railroad Ties Fabricated With 15 Different Prestressing Reinforcements,” 2013 PCI Convention and National Bridge Conference, September 21 – 24 at the Gaylord Texan Resort in Grapevine, Texas.
- [19] Mark Haynes, Levi DeLissa, Chih-Hang John Wu, B. Terry Beck, and Robert J. Peterman, “Design of a Non-Contact Surface Profilometry System for Automated Geometrical Dimensioning and Tolerancing,” *International Journal of Engineering Inventions* 2013 e-ISSN2278-7461, p-ISSN: 2319-6491, Vol. 3, Issue 2, Sep. 2013, PP: 15-19.
- [20] Weixin Zhao, B. Terry Beck, Robert J. Peterman, John C.-H. Wu, Grace Lee, and Naga N.B. Bodapati, “Determining Transfer Length In Pre-Tensioned Concrete Railroad Ties: Is Anew Evaluation Method Needed?” Proceedings of the 2013 ASME Rail Transportation Division Fall Technical Conference, RTDF2013-4727 October 15-17, 2013, Altoona, Pennsylvania, USA.
- [21] Joseph R. Holste, Robert J. Peterman, Naga, N.B. Bodapati, B.Terry Beck, and C.-H. John Wu, “Transfer Bond Test User to Predict Transfer Length of Concrete Railroad Ties,” Proceedings of the 2013 ASME Rail Transportation Division Fall Technical Conference, RTDF2013-4726 October 15-17, 2013, Altoona, Pennsylvania, USA.
- [22] Naga N.B. Bodapati, Weixin Zhao, Robert J. Peterman, John C.-H. Wu, B. Terry Beck, Mark Haynes and Joseph R. Holste, “Effect of Concrete Properties on Transfer Lengths in Concrete Rail-Road Ties,” Proceedings of the 2014 Joint Rail Conference, JRC2014-3859 April 2-4, 2014, Colorado Springs, Colorado, USA.
- [23] Weixin Zhao, B. Terry Beck, Robert J. Peterman, John C.-H. Wu, Naga N.B. Bodapati, and Grace Lee, “Reliable Transfer Length Assessment For Real-Time Monitoring Of Railroad Cross-Tie Production,” Proceedings of the 2014 Joint Rail Conference, JRC2014-3830 April 2-4, 2014, Colorado Springs, Colorado, USA.

- [24] Mark Haynes, John C.-H. Wu, B. Terry Beck, Naga N.B. Bodapati, and Robert J. Peterman, "Prestressing Steel Reinforcement Wire Measurement Protocol," Proceedings of the 2014 Joint Rail Conference, JRC2014-3800 April 2-4, 2014, Colorado Springs, Colorado, USA.
- [25] Joseph R. Holste, Mark Haynes, Robert J. Peterman, B. Terry Beck, John C.-H. Wu, "Tensioned Pullout Test used to Investigate Wire Splitting Propensity in Concrete Railroad Ties," Proceedings of the 2014 Joint Rail Conference, JRC2014-3799 April 2-4, 2014, Colorado Springs, Colorado, USA.
- [26] Mark Haynes, John C.-H. Wu, B. Terry Beck, Naga N.B. Bodapati, and Robert J. Peterman, "An Investigation into Non-Linear Search Modifications for Minimizing Objective Function Computations," Proceedings of the 2014 Industrial & Systems Engineering Research Conference (ISERC) Conference, ISERC2014-I393 May 31-June 3 2014, Montréal, Canada.
- [27] B. Terry Beck, Weixin Zhao, Robert J. Peterman, Chih-Hang John Wu, Joseph Holste, Naga Narendra B. Bodapati, Grace Lee, "Effect Of Surface-Strain Sampling Interval On The Reliability Of Pretensioned Concrete Railroad Tie Transfer Length Measurements," 2014 PCI Convention and National Bridge Conference, September 21 - 24 at the Gaylord National Resort in Washington, D.C.
- [28] Joseph Holste, Mark Haynes, Robert Peterman, B. Terry Beck, Chih-Hang John Wu, "Application Of Tensioned Pullout Tests To Investigate The Effect Of Prestressing Wire Indent Geometry On Bond And Splitting Characteristics," 2014 PCI Convention and National Bridge Conference, September 21 - 24 at the Gaylord National Resort in Washington, D.C.
- [29] Naga Narendra B. Bodapati, Robert J. Peterman, Weixin Zhao, B. Terry Beck, PhD, Chih-Hang John Wu, Joseph R. Holste, Matthew L. Arnold, Ryan Benteman, Robert Schweiger, "Long-Term Transfer-Length Measurements On Pretensioned Concrete Rail Road Ties," 2014 PCI Convention and National Bridge Conference, September 21 - 24 at the Gaylord National Resort in Washington, D.C.
- [30] Russell, B. W., and N. H. Burns., "Design Guidelines for Transfer, Development and Debonding of Large Diameter Seven Wire Strands in Pretensioned Concrete Girders", Report number 1210-5F., 1993, Austin, TX: Center for Transportation Research, University of Texas at Austin.
- [31] Lutch, Russell H., "Capacity optimization of a prestressed concrete railroad tie", M.S. Thesis, Civil and Environmental Engineering Department, Michigan Technological University, May 2010 (Open Access Theses & Dissertations. <http://digitalcommons.mtu.edu/etds/254>).
- [32] Yu, H., Jeong, D., "Railroad Tie Responses to Directly Applied Rail Seat Loading in Ballasted Tracks: A Computational Study", Proceedings of the ASME/ASCE/IEEE 2012 Joint Rail Conference, April 17-19, 2012, Philadelphia, Pennsylvania, USA.
- [33] Beck, B. Terry, Peterman, Robert J., Wu, Chih-Hang (John), and Bodapati, Naga Narendra B., "In-Plant Testing of a New Multi-Camera Transfer Length Measurement System for Monitoring Quality Control of Railroad Crosstie Production," Proceedings of the 2015 Joint Rail conference, March 23-26, 2015, San Jose, CA, USA.
- [34] B. Terry Beck, Aaron A. Robertson, Robert J. Peterman, Chih-Hang John Wu, "Performance of a Continuously Traversing 2-Camera Non-Contact Optical Strain Sensor for In-Plant Assessment of Prestressed Concrete Railroad Crosstie Transfer Length," Paper Number: JRC2016-5751, Proceedings of the 2016 Joint Rail Conference, Columbia, South Carolina, April 12-15, 2016.

- [35] B. Terry Beck, Aaron A. Robertson, Robert J. Peterman, Chih-Hang John Wu, Kyle A. Riding, "TRANSFER LENGTH CHARACTERIZATION OF ENTIRE CROSSTIE PLANT CASTING BED USING CONTINUOUSLY TRAVERSING DUAL-CAMERA NON-CONTACT OPTICAL STRAIN SENSORS," Paper Number JRC2017-2297, Proceedings of the 2017 Joint Rail conference, Philadelphia, Pennsylvania, April 4 - 7, 2017.
- [36] Adrijana Savic, B. Terry Beck, Aaron A. Robertson, Robert J. Peterman, Jeremiah Clark, Chih-Hang John Wu, "EFFECTS OF COVER, COMPRESSIVE STRENGTH, AND WIRE TYPE ON BOND PERFORMANCE IN PRISMATIC PRESTRESSED CONCRETE MEMBERS," JRC2018-6153, Proceedings of the 2018 ASME Joint Rail Conference (JRC 2018), April 18-20, 2018, Pittsburgh, PA, USA.
- [37] Haynes, Mark Davis. (2015). *QUALITY BY DESIGN: Improving Pre-Stressed Reinforcement for Concrete Railroad Ties via Geometrical Dimensioning and Tolerancing* (Doctoral Dissertation). Retrieved from K-REx.
- [38]

Appendix A.

Wire Report Summary

This Appendix contains the reports for the wires that were scanned and processed by the indent profiling system. Each report contains a general overview of the data and highlights some of the most important data from the analysis, along with a ASTM A881 and ISO 16120 report for each indented wire. A 2D representation of a single scan segment is also provided for each report to assist with data visualization. The reports appear in the following order indicated in the figure below.

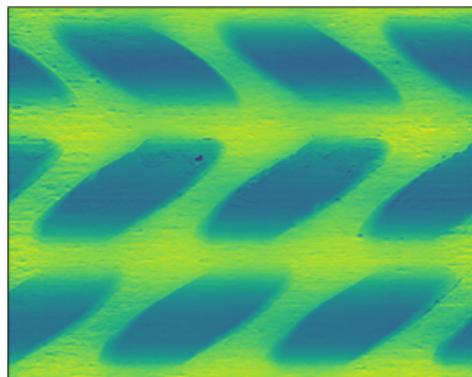
Cover Testing	Crosstie Wires	Machined Wires
WB	E-1	15
WD	F-1	15-.16-T1
WF	H-1	30-.16-T1
WG	J-1	45-.16-T2
WH	K-1	60-.16-T1
WI	L-1	75-.16-T1
WJ	M-1	90-.16-T3
WM		X1
WP		X2
WQ		X3
		X4
		X5

TEST REPORT: INDENT PROFILER

WIRE ID:WB

PAGE 1/4

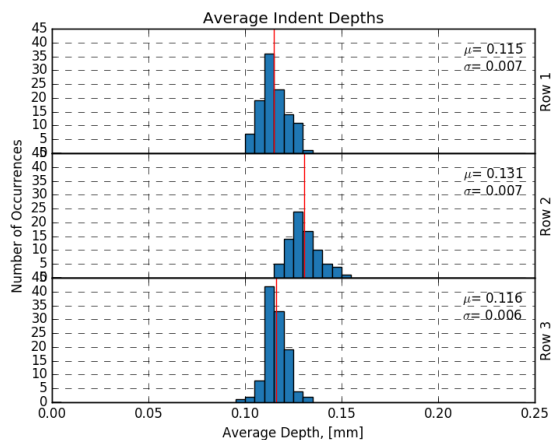
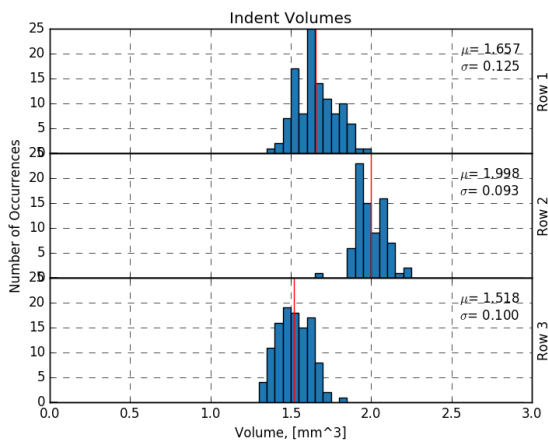
Scan Information				
Wire ID	WB_630mm_Trued_10.26.18			
Length [mm]	630			
Scan Date	10.26.18			
Proc Date	09.17.19			
Stat Date	09.17.19			
ID	Indents	Nominal Dia [mm]	Orientat-ion [deg]	Distance [mm]
Total	302	5.153	47.7	2.193
Row 1	111		47.1	1.996
Row 2	80		48.3	2.291
Row 3	111		-47.6	2.291



Indent Data								
ID	Indents	Volume [mm^3]	S.W. Area [mm^2]	Avg Depth [mm]	S.W. Angle [deg]	Avg Length [mm]	Width [mm]	Pitch [mm]
Total	302	1.696	2.922	0.119	16.45	4.060	4.009	5.580
Row 1	111	1.657	2.997	0.115	15.54	3.995	4.129	5.593
Row 2	80	1.998	3.263	0.131	18.28	3.934	4.494	5.581
Row 3	111	1.518	2.600	0.116	16.03	4.215	3.540	5.568

S.W. Area: The average sidewall area of the left and right side of the indents.

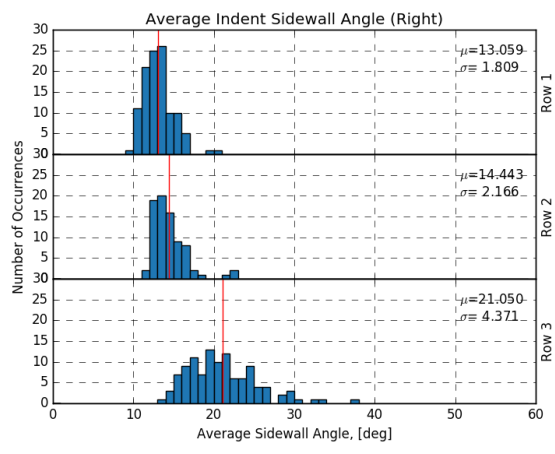
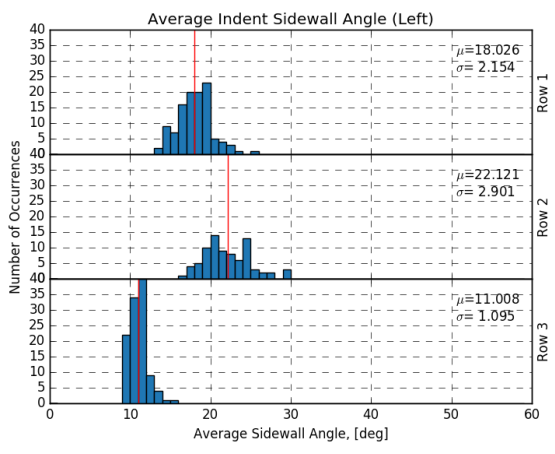
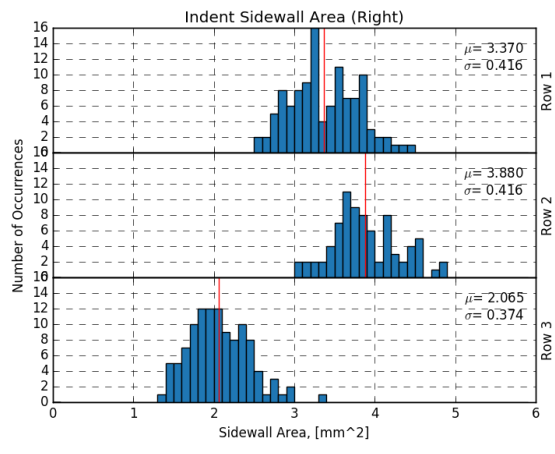
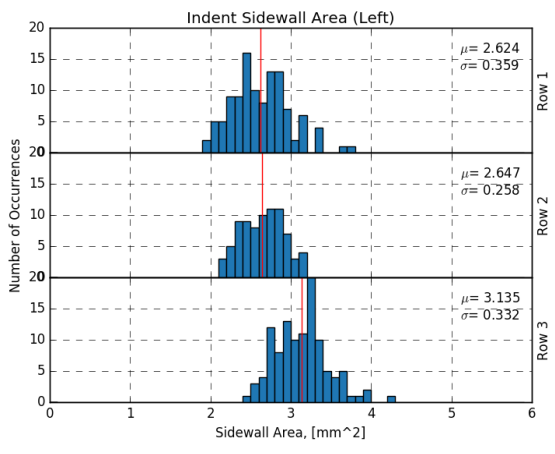
S.W. Angle: The average sidewall angle of the left and right side of the indents.



TEST REPORT: INDENT PROFILER

WIRE ID:WB

PAGE 2/4



TEST REPORT: ASTM A881

WIRE ID:WB

PAGE 3/4

SAMPLE ID		WB_630mm_Trued_10.26.18
SAMPLE LENGTH [MM]		630
NOMINAL DIAMETER [MM]		5.153
TEST ITEM	STANDARD VALUE	ACTUAL VALUE
INDENT DEPTH [MM]	0.115±0.035	0.119
SIDEWALL ANGLE [DEG]	In Contract	16.4
INDENT LENGTH [MM]	3.5±0.5	4.341
INDENT PITCH [MM]	5.46±0.29	5.58
ORIENTATION ANGLE [DEG]	≥45°	47.7
OUT OF ROUND [MM]	≤0.08	TBD

TEST REPORT: ISO 16120

WIRE ID:WB

SAMPLE ID		WB_630mm_TrueD_10.26.18
SAMPLE LENGTH		630
NOMINAL DIAMETER		5.153
TEST ITEM	STANDARD VALUE	ACTUAL VALUE
INDENT LENGTH [MM]	3.5±0.5	4.341
INDENT DEPTH [MM]	0.15±0.05	0.119
INDENT SPACING [MM]	5.50±0.50	5.58
INDENT DISTANCE [MM]	$\Sigma e \leq 3.343$	2.00, 2.29, 2.29
AVG DIAMETER [MM]	—	TBD
OVALITY	$\leq 0.01 \times D$	TBD

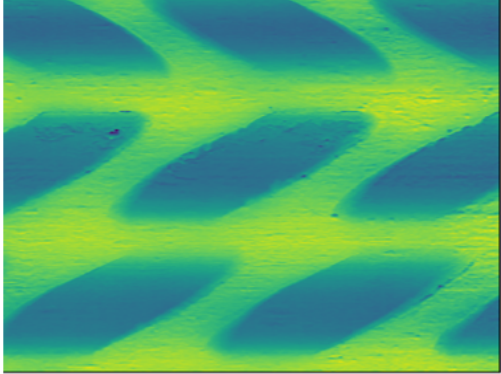
PAGE 4 / 4

TEST REPORT: INDENT PROFILER

WIRE ID:WD

PAGE 1/4

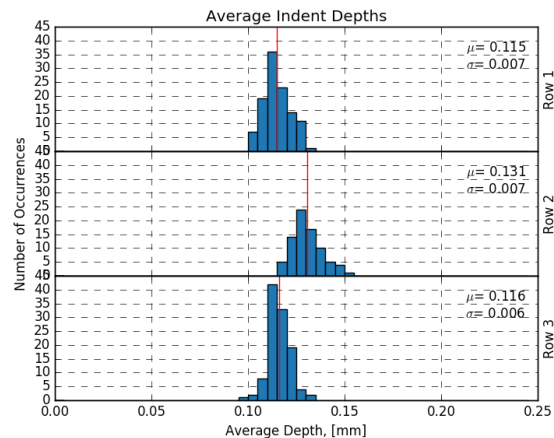
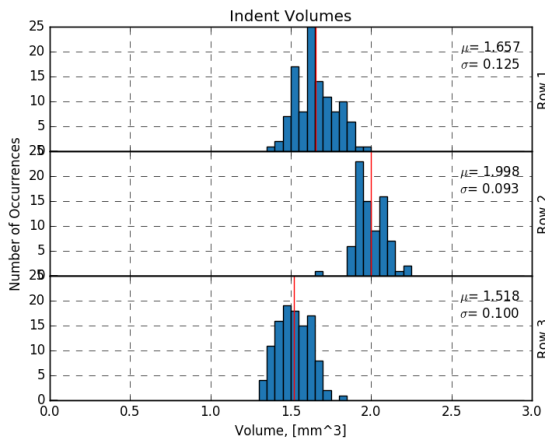
Scan Information					
Wire ID	WD_630mm_Trueid_10.26.18				
Length [mm]	630				
Scan Date	10.26.18				
Proc Date	9.17.19				
Stat Date	9.17.19				
ID	Indents	Nominal Dia [mm]	Orientat-ion [deg]	Distance [mm]	
Total	337	5.257	58.4	2.510	
Row 1	113		59.1	2.547	
Row 2	112		-56.0	2.491	
Row 3	112		57.8	2.491	



Indent Data								
ID	Indents	Volume [mm^3]	S.W. Area [mm^2]	Avg Depth [mm]	S.W. Angle [deg]	Avg Length [mm]	Width [mm]	Pitch [mm]
Total	337	1.600	2.744	0.141	17.22	3.512	3.854	5.548
Row 1	113	1.556	2.728	0.135	17.22	3.666	3.792	5.548
Row 2	112	1.558	2.577	0.140	17.55	3.392	3.867	5.548
Row 3	112	1.687	2.926	0.149	16.89	3.476	3.904	5.548

S.W. Area: The average sidewall area of the left and right side of the indents.

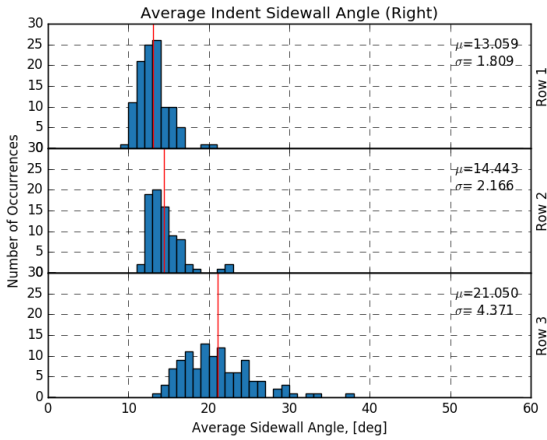
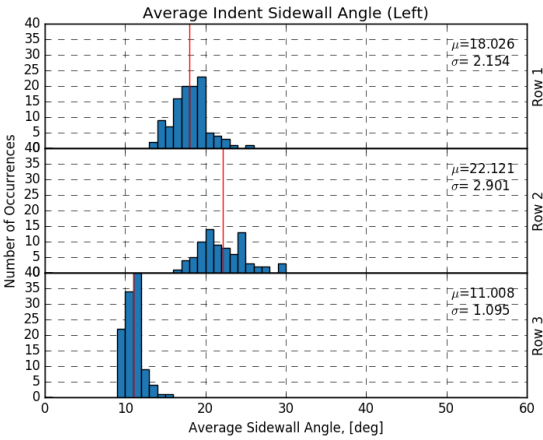
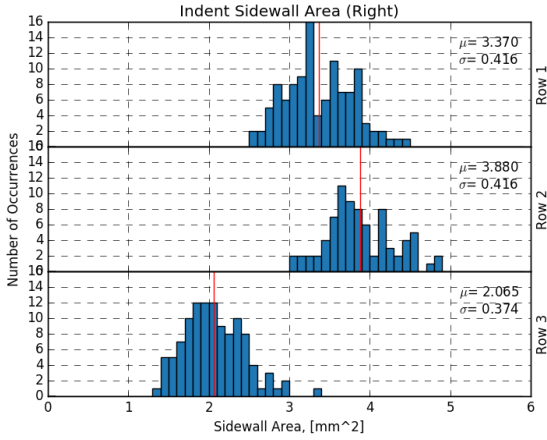
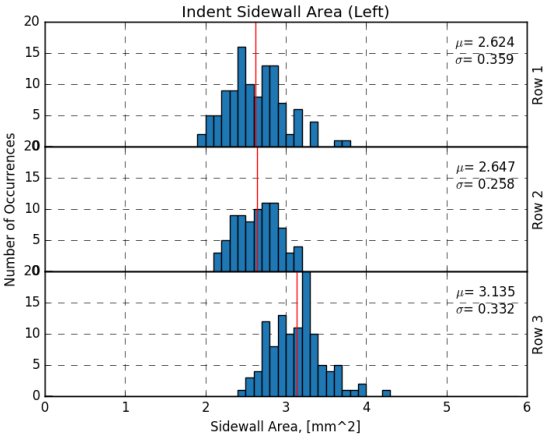
S.W. Angle: The average sidewall angle of the left and right side of the indents.



TEST REPORT: INDENT PROFILER

WIRE ID:WD

PAGE 2/4



TEST REPORT: ASTM A881

WIRE ID:WD

PAGE 3/4

SAMPLE ID		WD_630mm_Trued_10.26.18
SAMPLE LENGTH [MM]		630
NOMINAL DIAMETER [MM]		5.257
TEST ITEM	STANDARD VALUE	ACTUAL VALUE
INDENT DEPTH [MM]	0.115±0.035	0.141
SIDEWALL ANGLE [DEG]	In Contract	17.2
INDENT LENGTH [MM]	3.5±0.5	4.106
INDENT PITCH [MM]	5.46±0.29	5.55
ORIENTATION ANGLE [DEG]	≥45°	58.4
OUT OF ROUND [MM]	≤0.08	TBD

TEST REPORT: ISO 16120

WIRE ID:WD

PAGE 4/4

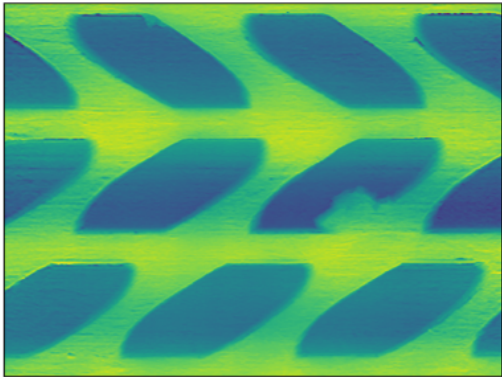
SAMPLE ID		WD_630mm_True_10.26.18
SAMPLE LENGTH		630
NOMINAL DIAMETER		5.257
TEST ITEM	STANDARD VALUE	ACTUAL VALUE
INDENT LENGTH [MM]	3.5±0.5	4.106
INDENT DEPTH [MM]	0.15±0.05	0.141
INDENT SPACING [MM]	5.50±0.50	5.55
INDENT DISTANCE [MM]	$\Sigma e \leq 3.343$	2.55, 2.49, 2.49
AVG DIAMETER [MM]	-	TBD
OVALITY	$\leq 0.01 \times D$	TBD

TEST REPORT: INDENT PROFILER

WIRE ID:WF

PAGE 1/4

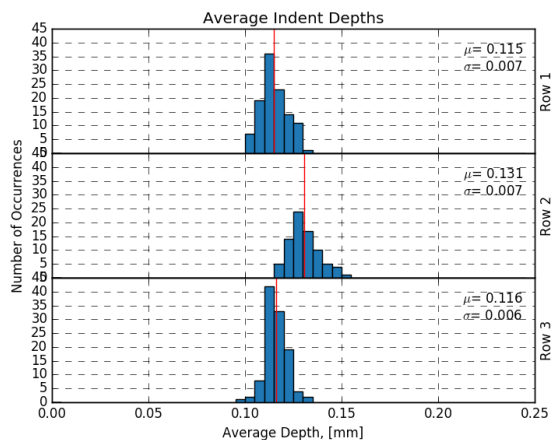
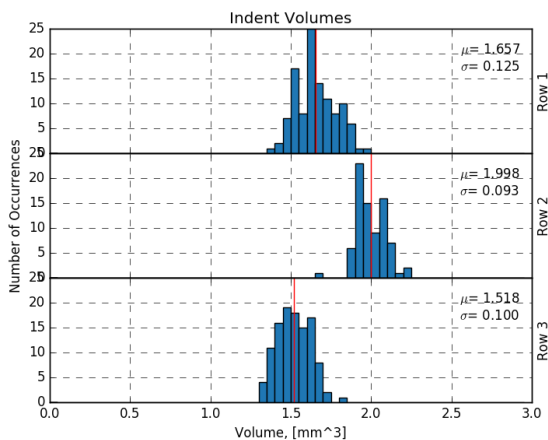
Scan Information					
Wire ID		WF_630mm_Trueid_10.26.18			
Length [mm]		630			
Scan Date		10.26.18			
Proc Date		9.17.19			
Stat Date		9.17.19			
ID	Indents	Nominal Dia [mm]	Orientat-ion [deg]	Distance [mm]	
Total	333	5.195	48.4	2.143	
Row 1	111		50.0	2.129	
Row 2	111		47.3	2.150	
Row 3	111		-47.9	2.150	



Indent Data								
ID	Indents	Volume [mm^3]	S.W. Area [mm^2]	Avg Depth [mm]	S.W. Angle [deg]	Avg Length [mm]	Width [mm]	Pitch [mm]
Total	333	2.446	2.452	0.163	28.07	4.014	4.197	5.604
Row 1	111	2.362	2.269	0.155	27.23	4.034	4.198	5.617
Row 2	111	2.457	2.589	0.161	27.48	4.069	4.239	5.616
Row 3	111	2.518	2.498	0.174	29.52	3.939	4.155	5.577

S.W. Area: The average sidewall area of the left and right side of the indents.

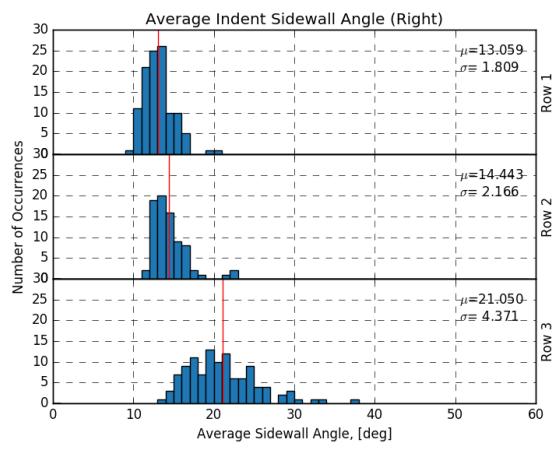
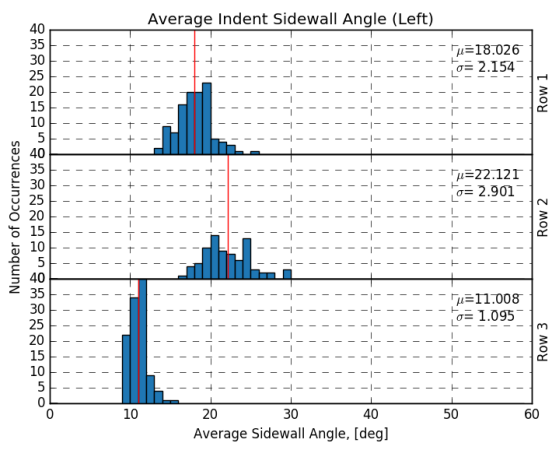
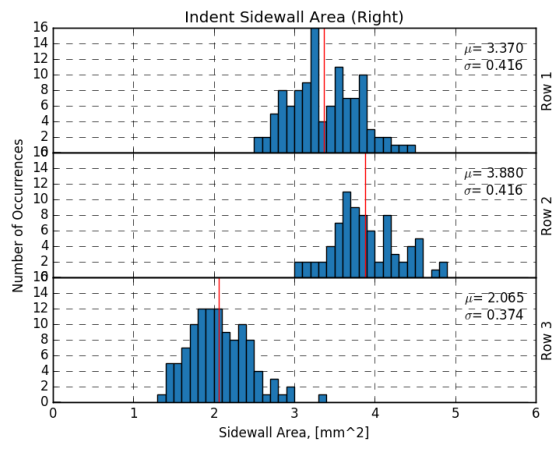
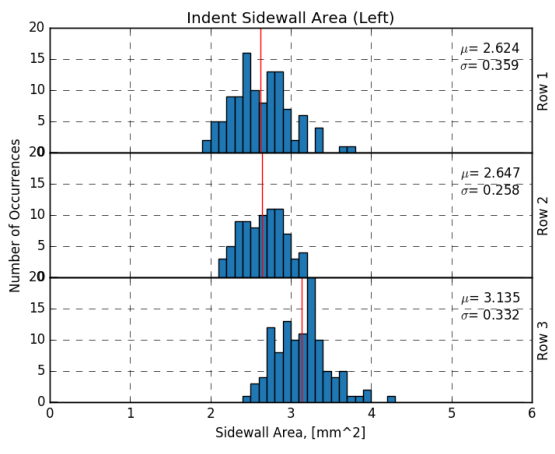
S.W. Angle: The average sidewall angle of the left and right side of the indents.



TEST REPORT: INDENT PROFILER

WIRE ID:WF

PAGE 2/4



TEST REPORT: ASTM A881

WIRE ID:WF

PAGE 3/4

SAMPLE ID		WB_630mm_Trued_10.26.18
SAMPLE LENGTH [MM]		630
NOMINAL DIAMETER [MM]		5.195
TEST ITEM	STANDARD VALUE	ACTUAL VALUE
INDENT DEPTH [MM]	0.115±0.035	0.163
SIDEWALL ANGLE [DEG]	In Contract	28.1
INDENT LENGTH [MM]	3.5±0.5	4.534
INDENT PITCH [MM]	5.46±0.29	5.60
ORIENTATION ANGLE [DEG]	≥45°	48.4
OUT OF ROUND [MM]	≤0.08	TBD

TEST REPORT: ISO 16120

WIRE ID:WF

PAGE 4/4

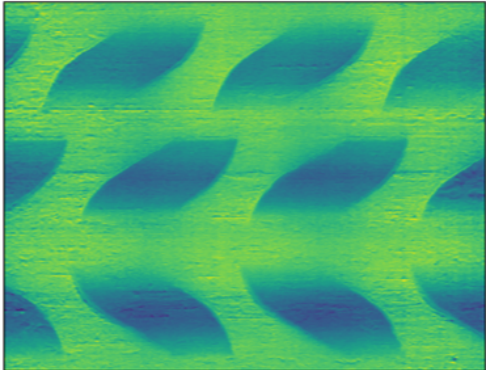
SAMPLE ID		WB_630mm_True_d_10.26.18
SAMPLE LENGTH		630
NOMINAL DIAMETER		5.195
TEST ITEM	STANDARD VALUE	ACTUAL VALUE
INDENT LENGTH [MM]	3.5±0.5	4.534
INDENT DEPTH [MM]	0.15±0.05	0.163
INDENT SPACING [MM]	5.50±0.50	5.60
INDENT DISTANCE [MM]	$\Sigma e \leq 3.343$	2.13, 2.15, 2.15
AVG DIAMETER [MM]	-	TBD
OVALITY	$\leq 0.01 \times D$	TBD

TEST REPORT: INDENT PROFILER

WIRE ID:WG

PAGE 1/4

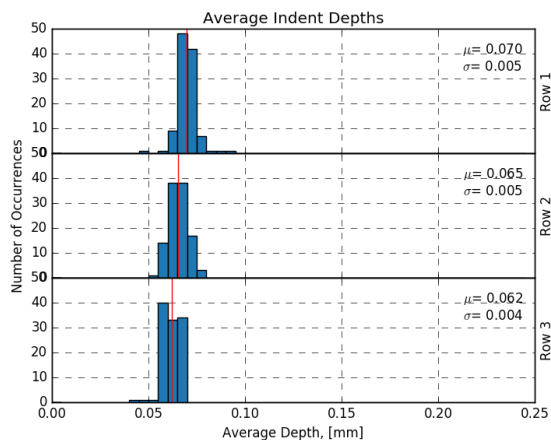
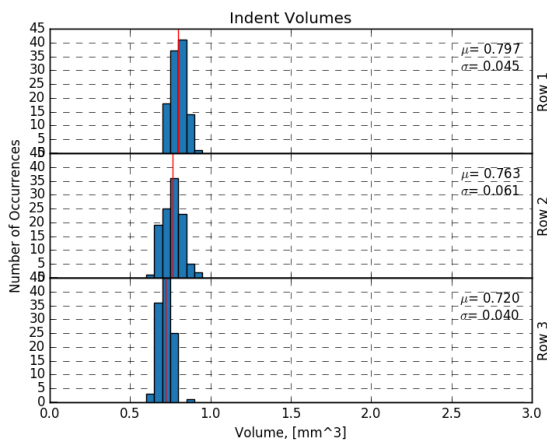
Scan Information					
Wire ID	WG_630mm_True_11.05.18				
Length [mm]	630				
Scan Date	11.05.18				
Proc Date	09.17.19				
Stat Date	09.17.19				
ID	Indents	Nominal Dia [mm]	Orientation [deg]	Distance [mm]	
Total	332	5.324	56.1	3.047	
Row 1	111		-57.9	3.031	
Row 2	111		56.0	3.054	
Row 3	110		54.3	3.054	



Indent Data								
ID	Indents	Volume [mm^3]	S.W. Area [mm^2]	Avg Depth [mm]	S.W. Angle [deg]	Avg Length [mm]	Width [mm]	Pitch [mm]
Total	332	0.760	2.317	0.066	10.56	3.885	3.502	5.644
Row 1	111	0.797	2.405	0.070	9.95	3.855	3.512	5.644
Row 2	111	0.763	2.308	0.065	10.66	3.895	3.527	5.644
Row 3	110	0.720	2.236	0.062	11.07	3.906	3.467	5.645

S.W. Area: The average sidewall area of the left and right side of the indents.

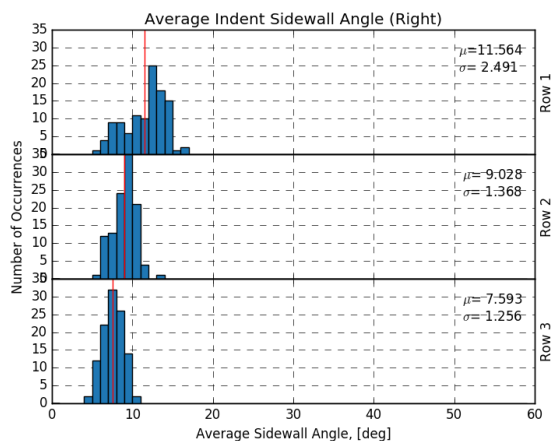
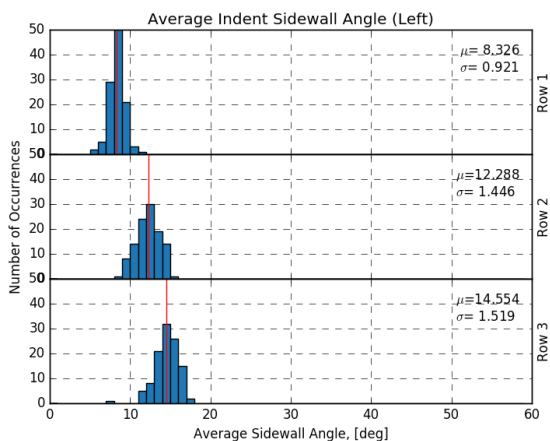
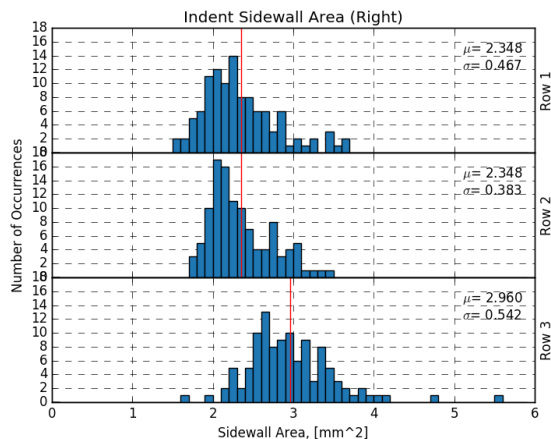
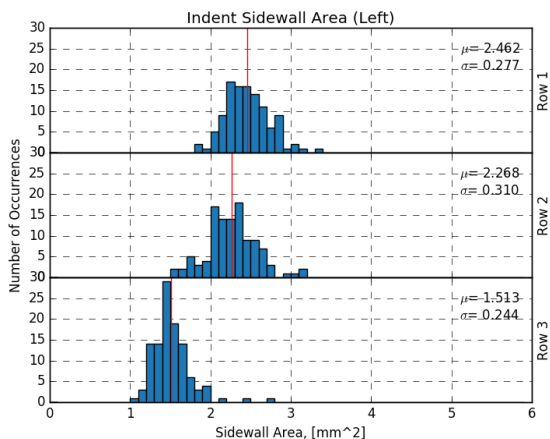
S.W. Angle: The average sidewall angle of the left and right side of the indents.



TEST REPORT: INDENT PROFILER

WIRE ID:WG

PAGE 2/4



TEST REPORT: ASTM A881

WIRE ID:WG

PAGE 3/4

SAMPLE ID		WG_630mm_Trued_11.05.18
SAMPLE LENGTH [MM]		630
NOMINAL DIAMETER [MM]		5.324
TEST ITEM	STANDARD VALUE	ACTUAL VALUE
INDENT DEPTH [MM]	0.115±0.035	0.066
SIDEWALL ANGLE [DEG]	In Contract	10.6
INDENT LENGTH [MM]	3.5±0.5	3.888
INDENT PITCH [MM]	5.46±0.29	5.64
ORIENTATION ANGLE [DEG]	≥45°	56.1
OUT OF ROUND [MM]	≤0.08	TBD

TEST REPORT: ISO 16120

WIRE ID:WG

PAGE 4/4

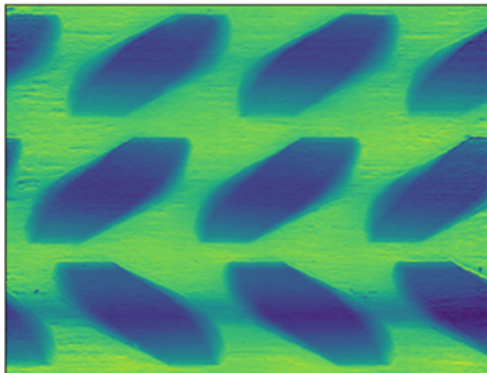
SAMPLE ID		WG_630mm_True_d_11.05.18
SAMPLE LENGTH		630
NOMINAL DIAMETER		5.324
TEST ITEM	STANDARD VALUE	ACTUAL VALUE
INDENT LENGTH [MM]	3.5±0.5	3.888
INDENT DEPTH [MM]	0.15±0.05	0.066
INDENT SPACING [MM]	5.50±0.50	5.64
INDENT DISTANCE [MM]	$\Sigma e \leq 3.343$	3.03, 3.05, 3.05
AVG DIAMETER [MM]	-	TBD
OVALITY	$\leq 0.01 \times D$	TBD

TEST REPORT: INDENT PROFILER

WIRE ID:WH

PAGE 1/4

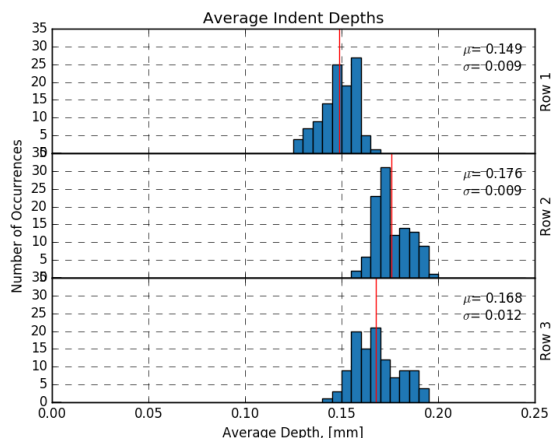
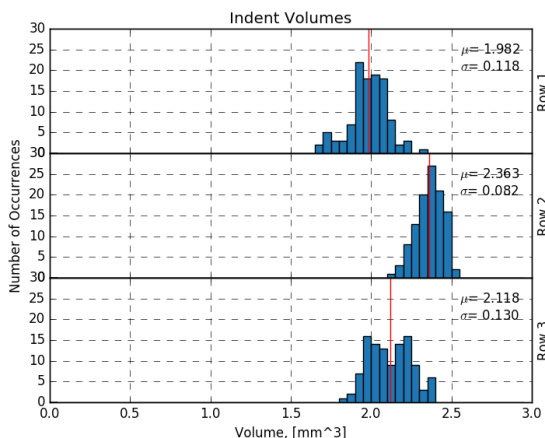
Scan Information					
Wire ID		WH_630mm_Trued_10.26.18			
Length [mm]		630			
Scan Date		10.26.18			
Proc Date		09.17.19			
Stat Date		09.17.19			
ID	Indents	Nominal Dia [mm]	Orientat-ion [deg]	Distance [mm]	
Total	332	5.107	51.0	1.873	
Row 1	111		-50.6	1.765	
Row 2	111		50.9	1.927	
Row 3	110		51.4	1.927	



Indent Data								
ID	Indents	Volume [mm^3]	S.W. Area [mm^2]	Avg Depth [mm]	S.W. Angle [deg]	Avg Length [mm]	Width [mm]	Pitch [mm]
Total	332	2.154	3.961	0.164	17.17	3.676	4.383	5.599
Row 1	111	1.982	3.852	0.149	14.33	3.639	4.523	5.599
Row 2	111	2.363	4.062	0.176	19.42	3.676	4.426	5.598
Row 3	110	2.118	3.970	0.168	17.75	3.713	4.198	5.599

S.W. Area: The average sidewall area of the left and right side of the indents.

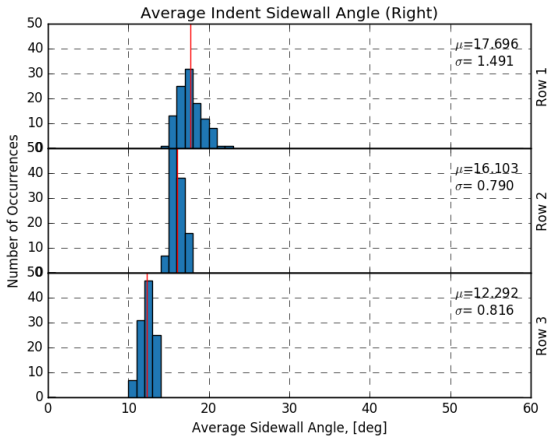
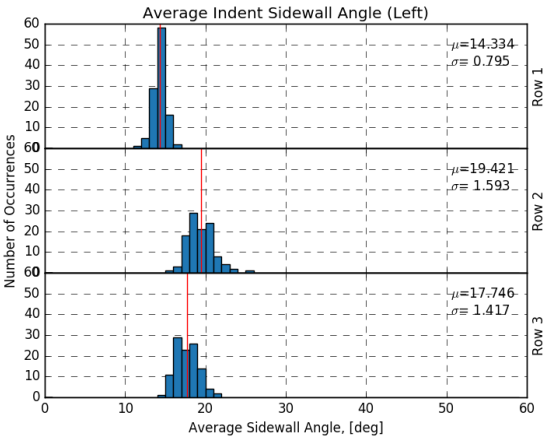
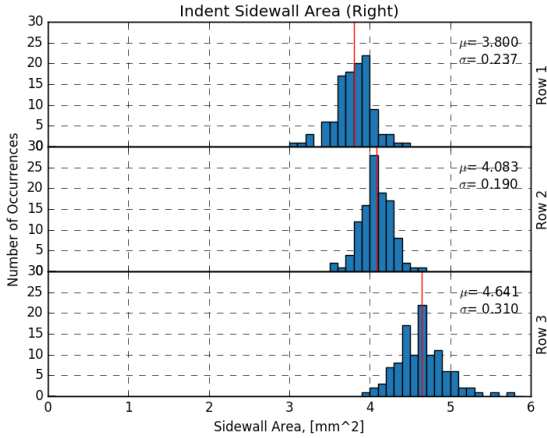
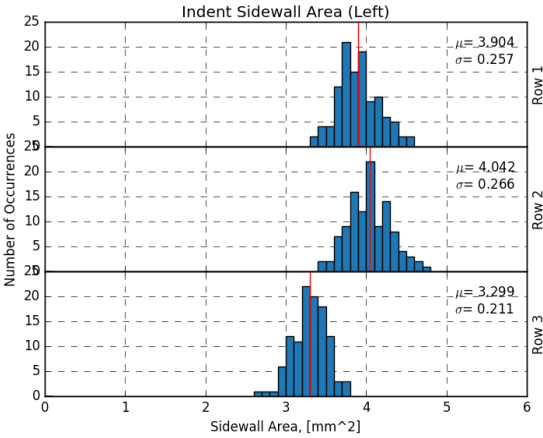
S.W. Angle: The average sidewall angle of the left and right side of the indents.



TEST REPORT: INDENT PROFILER

WIRE ID:WH

PAGE 2/4



TEST REPORT: ASTM A881

WIRE ID:WH

PAGE 3/4

SAMPLE ID		WH_630mm_Trued_10.26.18
SAMPLE LENGTH [MM]		630
NOMINAL DIAMETER [MM]		5.107
TEST ITEM	STANDARD VALUE	ACTUAL VALUE
INDENT DEPTH [MM]	0.115±0.035	0.164
SIDEWALL ANGLE [DEG]	In Contract	17.2
INDENT LENGTH [MM]	3.5±0.5	4.610
INDENT PITCH [MM]	5.46±0.29	5.60
ORIENTATION ANGLE [DEG]	≥45°	51.0
OUT OF ROUND [MM]	≤0.08	TBD

TEST REPORT: ISO 16120

WIRE ID:WH

PAGE 4/4

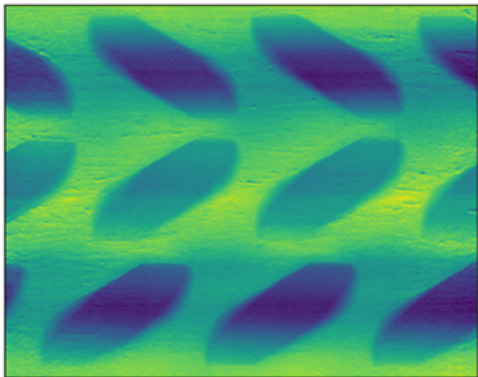
SAMPLE ID		WH_630mm_Trued_10.26.18
SAMPLE LENGTH		630
NOMINAL DIAMETER		5.107
TEST ITEM	STANDARD VALUE	ACTUAL VALUE
INDENT LENGTH [MM]	3.5±0.5	4.610
INDENT DEPTH [MM]	0.15±0.05	0.164
INDENT SPACING [MM]	5.50±0.50	5.60
INDENT DISTANCE [MM]	$\Sigma e \leq 3.343$	1.77, 1.93, 1.93
AVG DIAMETER [MM]	-	TBD
OVALITY	$\leq 0.01 \times D$	TBD

TEST REPORT: INDENT PROFILER

WIRE ID:WI

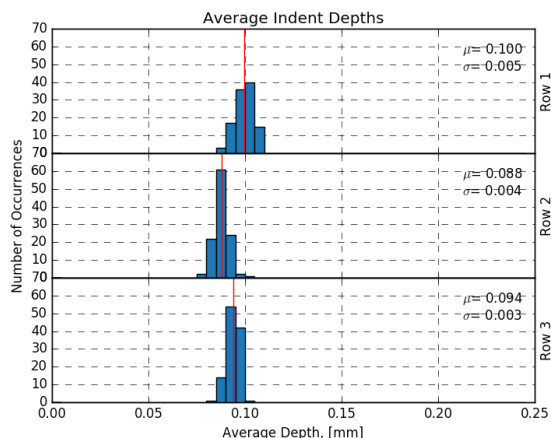
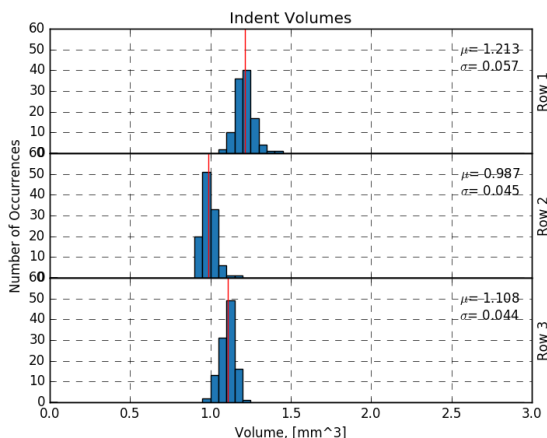
PAGE 1/4

Scan Information					
Wire ID		WI_630mm_TrueD_10.26.18			
Length [mm]		630			
Scan Date		10.26.18			
Proc Date		09.17.19			
Stat Date		09.17.19			
ID	Indents	Nominal Dia [mm]	Orientat-ion [deg]	Distance [mm]	
Total	335	5.208	50.1	2.445	
Row 1	111		51.0	2.350	
Row 2	112		50.1	2.493	
Row 3	112		-49.3	2.493	



Indent Data								
ID	Indents	Volume [mm^3]	S.W. Area [mm^2]	Avg Depth [mm]	S.W. Angle [deg]	Avg Length [mm]	Width [mm]	Pitch [mm]
Total	335	1.102	2.850	0.094	11.02	3.436	3.999	5.593
Row 1	111	1.213	3.101	0.100	11.16	3.410	4.258	5.604
Row 2	112	0.987	2.642	0.088	10.90	3.458	3.768	5.587
Row 3	112	1.108	2.808	0.094	11.01	3.441	3.972	5.588

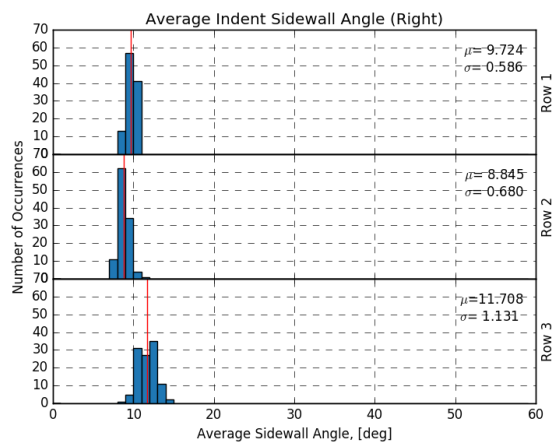
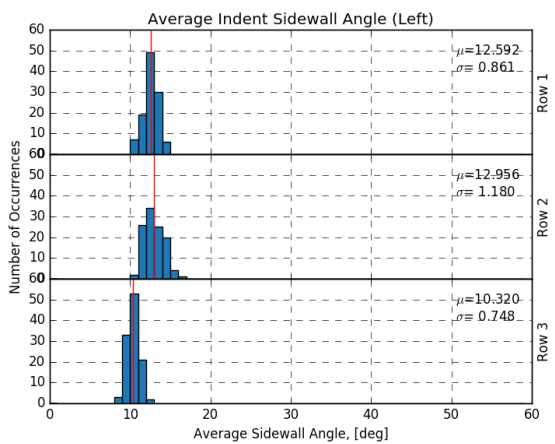
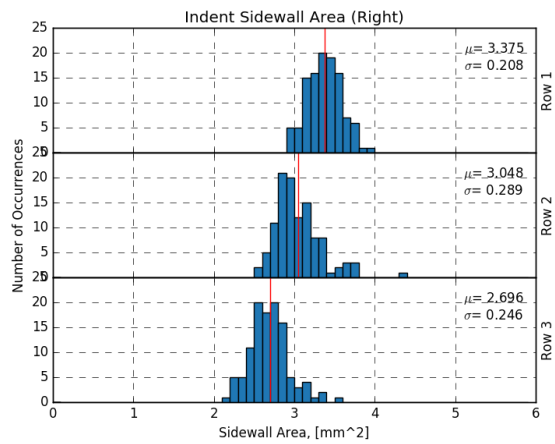
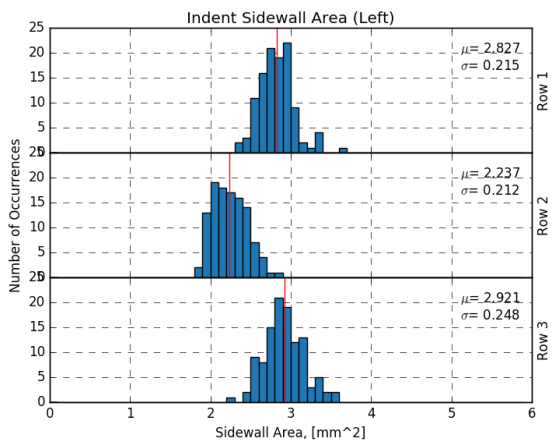
S.W. Area: The average sidewall area of the left and right side of the indents.
S.W. Angle: The average sidewall angle of the left and right side of the indents.



TEST REPORT: INDENT PROFILER

WIRE ID:WI

PAGE 2/4



TEST REPORT: ASTM A881

WIRE ID:WI

PAGE 3/4

SAMPLE ID		WI_630mm_Trued_10.26.18
SAMPLE LENGTH [MM]		630
NOMINAL DIAMETER [MM]		5.208
TEST ITEM	STANDARD VALUE	ACTUAL VALUE
INDENT DEPTH [MM]	0.115±0.035	0.094
SIDEWALL ANGLE [DEG]	In Contract	11.0
INDENT LENGTH [MM]	3.5±0.5	4.197
INDENT PITCH [MM]	5.46±0.29	5.59
ORIENTATION ANGLE [DEG]	≥45°	50.1
OUT OF ROUND [MM]	≤0.08	TBD

TEST REPORT: ISO 16120

WIRE ID:WI

PAGE 4/4

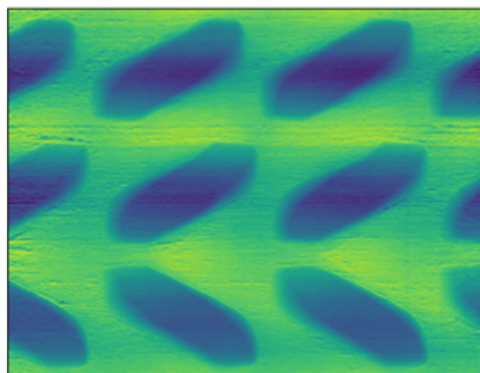
SAMPLE ID		WI_630mm_True_d_10.26.18
SAMPLE LENGTH		630
NOMINAL DIAMETER		5.208
TEST ITEM	STANDARD VALUE	ACTUAL VALUE
INDENT LENGTH [MM]	3.5±0.5	4.197
INDENT DEPTH [MM]	0.15±0.05	0.094
INDENT SPACING [MM]	5.50±0.50	5.59
INDENT DISTANCE [MM]	$\Sigma e \leq 3.343$	2.35, 2.49, 2.49
AVG DIAMETER [MM]	-	TBD
OVALITY	$\leq 0.01 \times D$	TBD

TEST REPORT: INDENT PROFILER

WIRE ID:WJ

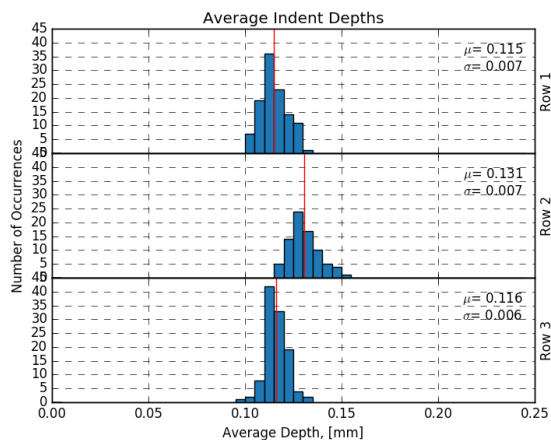
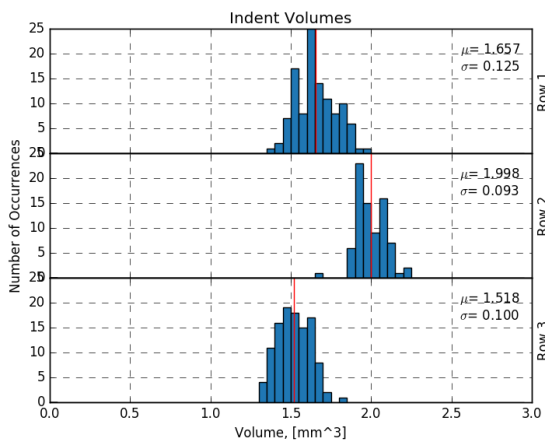
PAGE 1/4

Scan Information				
Wire ID	WJ_630mm_TrueD_10.26.18			
Length [mm]	630			
Scan Date	10.26.18			
Proc Date	09.17.19			
Stat Date	09.17.19			
ID	Indents	Nominal Dia [mm]	Orientat- ion [deg]	Distance [mm]
Total	333	5.211	50.8	2.295
Row 1	111		-50.9	2.280
Row 2	111		51.0	2.302
Row 3	111		50.5	2.302



Indent Data								
ID	Indents	Volume [mm^3]	S.W. Area [mm^2]	Avg Depth [mm]	S.W. Angle [deg]	Avg Length [mm]	Width [mm]	Pitch [mm]
Total	333	1.428	3.638	0.123	11.52	3.411	4.134	5.609
Row 1	111	1.449	3.639	0.123	12.45	3.357	4.229	5.610
Row 2	111	1.337	3.425	0.116	10.69	3.478	3.990	5.608
Row 3	111	1.497	3.849	0.130	11.41	3.397	4.184	5.609

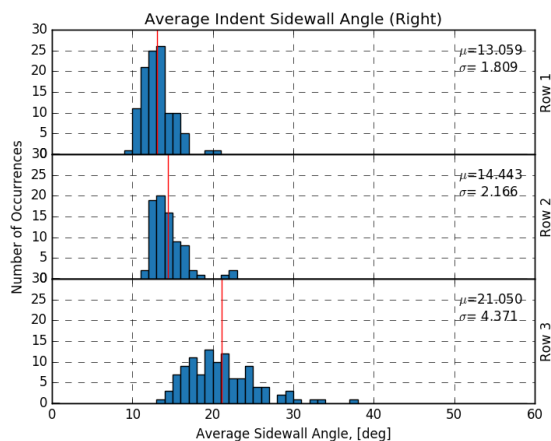
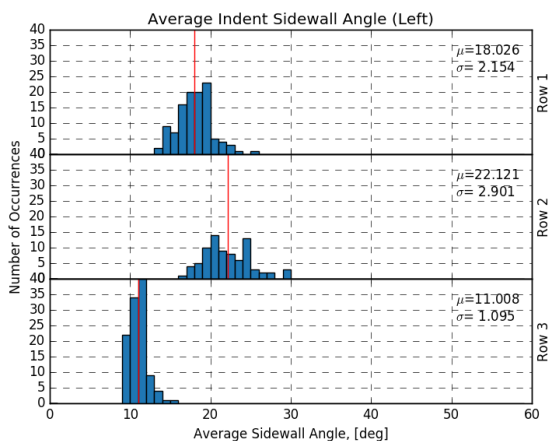
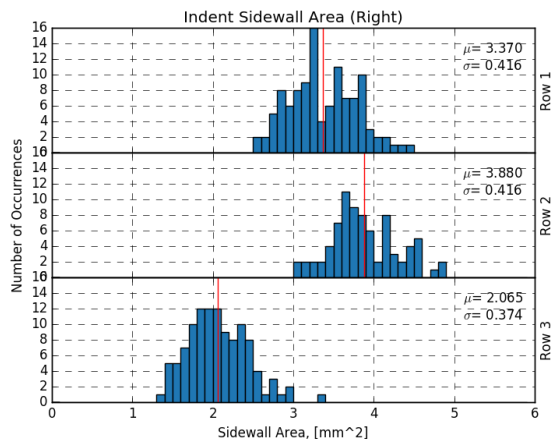
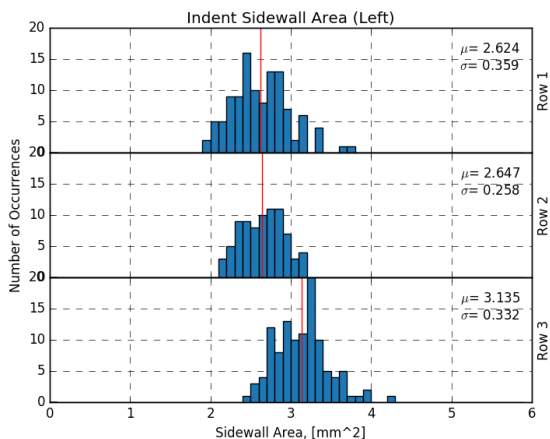
S.W. Area: The average sidewall area of the left and right side of the indents.
S.W. Angle: The average sidewall angle of the left and right side of the indents.



TEST REPORT: INDENT PROFILER

WIRE ID:WJ

PAGE 2/4



TEST REPORT: ASTM A881

WIRE ID:WJ

PAGE 3/4

SAMPLE ID		WJ_630mm_Trued_10.26.18
SAMPLE LENGTH [MM]		630
NOMINAL DIAMETER [MM]		5.211
TEST ITEM	STANDARD VALUE	ACTUAL VALUE
INDENT DEPTH [MM]	0.115±0.035	0.123
SIDEWALL ANGLE [DEG]	In Contract	11.5
INDENT LENGTH [MM]	3.5±0.5	4.453
INDENT PITCH [MM]	5.46±0.29	5.61
ORIENTATION ANGLE [DEG]	≥45°	50.8
OUT OF ROUND [MM]	≤0.08	TBD

TEST REPORT: ISO 16120

WIRE ID:WJ

PAGE 4/4

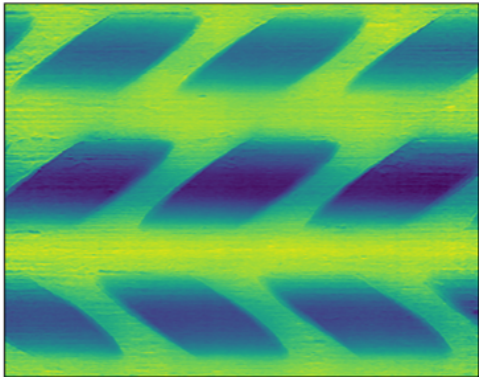
SAMPLE ID		WJ_630mm_True_d_10.26.18
SAMPLE LENGTH		630
NOMINAL DIAMETER		5.211
TEST ITEM	STANDARD VALUE	ACTUAL VALUE
INDENT LENGTH [MM]	3.5±0.5	4.453
INDENT DEPTH [MM]	0.15±0.05	0.123
INDENT SPACING [MM]	5.50±0.50	5.61
INDENT DISTANCE [MM]	$\Sigma e \leq 3.343$	2.28, 2.30, 2.30
AVG DIAMETER [MM]	-	TBD
OVALITY	$\leq 0.01 \times D$	TBD

TEST REPORT: INDENT PROFILER

WIRE ID:WM

PAGE 1/4

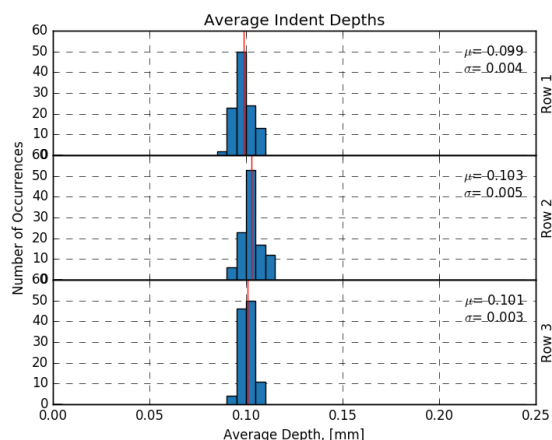
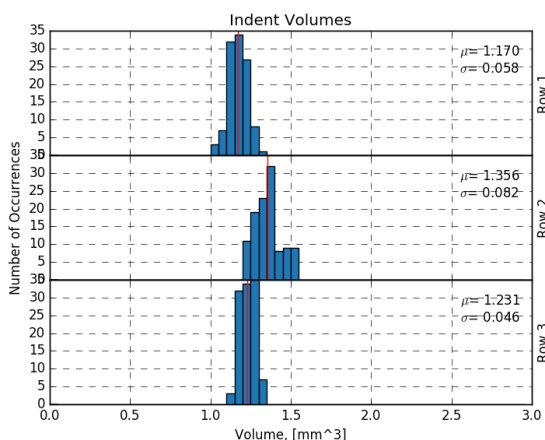
Scan Information					
Wire ID		WM_630mm_TrueD_10.26.18			
Length [mm]		630			
Scan Date		10.26.18			
Proc Date		09.17.19			
Stat Date		09.17.19			
ID	Indents	Nominal Dia [mm]	Orientat-ion [deg]	Distance [mm]	
Total	334	5.175	47.3	2.811	
Row 1	112		-47.6	2.811	
Row 2	111		46.4	2.811	
Row 3	111		48.0	2.811	



Indent Data								
ID	Indents	Volume [mm^3]	S.W. Area [mm^2]	Avg Depth [mm]	S.W. Angle [deg]	Avg Length [mm]	Width [mm]	Pitch [mm]
Total	334	1.252	2.062	0.101	16.41	4.085	3.411	5.564
Row 1	112	1.170	2.129	0.099	13.62	4.096	3.300	5.556
Row 2	111	1.356	2.185	0.103	17.19	4.099	3.631	5.566
Row 3	111	1.231	1.872	0.101	18.44	4.060	3.302	5.571

S.W. Area: The average sidewall area of the left and right side of the indents.

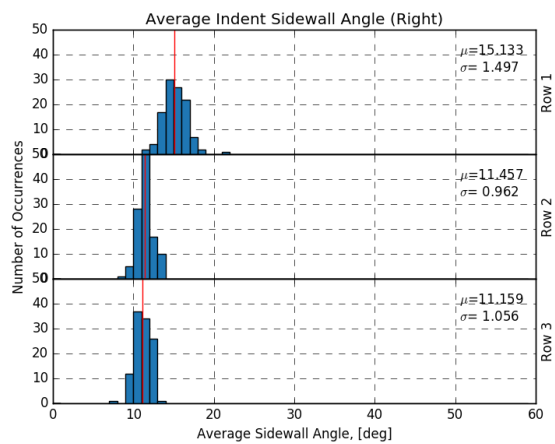
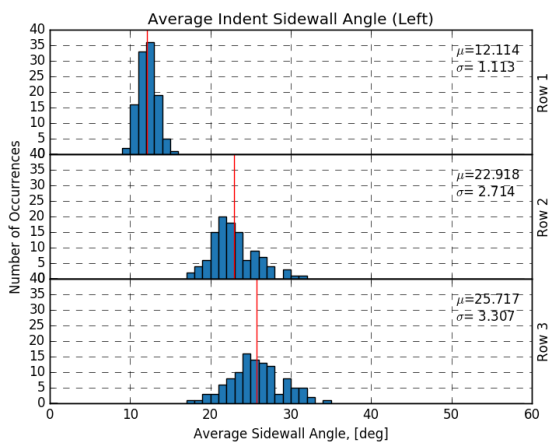
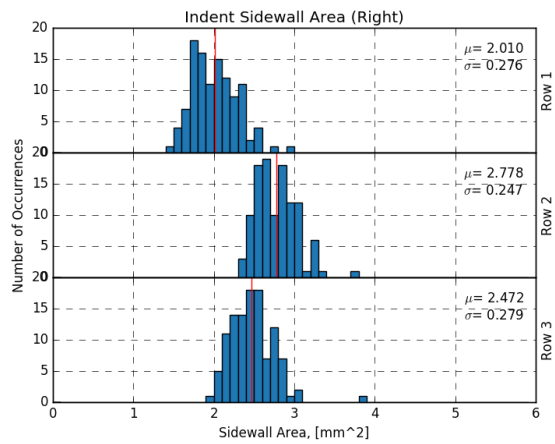
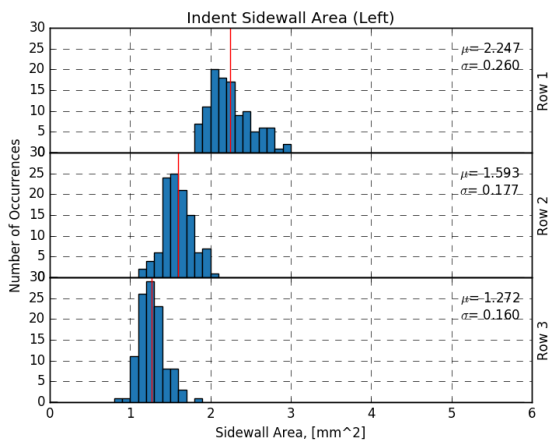
S.W. Angle: The average sidewall angle of the left and right side of the indents.



TEST REPORT: INDENT PROFILER

WIRE ID:WM

PAGE 2/4



TEST REPORT: ASTM A881

WIRE ID:WM

PAGE 3/4

SAMPLE ID		WM_630mm_Trued_10.26.18
SAMPLE LENGTH [MM]		630
NOMINAL DIAMETER [MM]		5.175
TEST ITEM	STANDARD VALUE	ACTUAL VALUE
INDENT DEPTH [MM]	0.115±0.035	0.101
SIDEWALL ANGLE [DEG]	In Contract	16.4
INDENT LENGTH [MM]	3.5±0.5	4.275
INDENT PITCH [MM]	5.46±0.29	5.56
ORIENTATION ANGLE [DEG]	≥45°	47.3
OUT OF ROUND [MM]	≤0.08	TBD

TEST REPORT: ISO 16120

WIRE ID:WM

PAGE 4/4

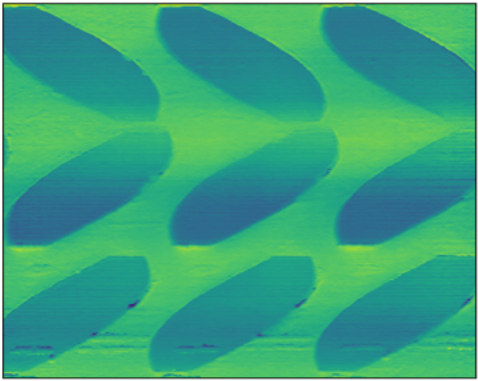
SAMPLE ID		WM_630mm_Trued_10.26.18
SAMPLE LENGTH		630
NOMINAL DIAMETER		5.175
TEST ITEM	STANDARD VALUE	ACTUAL VALUE
INDENT LENGTH [MM]	3.5±0.5	4.275
INDENT DEPTH [MM]	0.15±0.05	0.101
INDENT SPACING [MM]	5.50±0.50	5.56
INDENT DISTANCE [MM]	$\Sigma e \leq 3.343$	2.81, 2.81, 2.81
AVG DIAMETER [MM]	-	TBD
OVALITY	$\leq 0.01 \times D$	TBD

TEST REPORT: INDENT PROFILER

WIRE ID:WP

PAGE 1/4

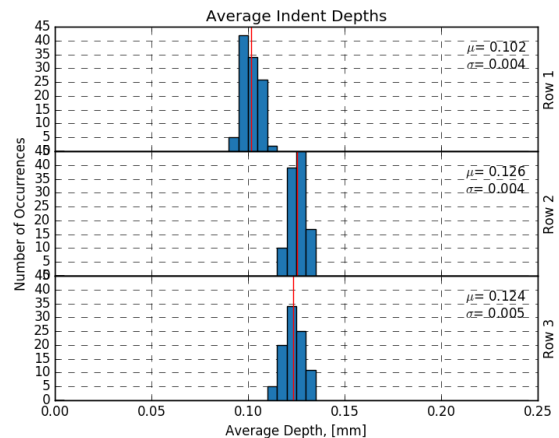
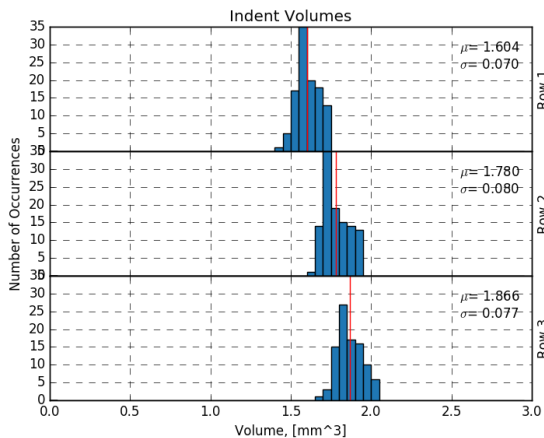
Scan Information					
Wire ID		WP_630mm_Trued_10.26.18			
Length [mm]		630			
Scan Date		10.26.18			
Proc Date		09.17.19			
Stat Date		09.17.19			
ID	Indents	Nominal Dia [mm]	Orientat-ion [deg]	Distance [mm]	
Total	315	5.283	50.3	1.689	
Row 1	109		52.5	1.599	
Row 2	111		50.6	1.734	
Row 3	95		-47.9	1.734	



Indent Data								
ID	Indents	Volume [mm^3]	S.W. Area [mm^2]	Avg Depth [mm]	S.W. Angle [deg]	Avg Length [mm]	Width [mm]	Pitch [mm]
Total	315	1.745	1.803	0.117	29.00	3.444	4.817	5.581
Row 1	109	1.604	1.711	0.102	26.49	3.323	5.087	5.581
Row 2	111	1.780	1.797	0.126	27.22	3.497	4.576	5.581
Row 3	95	1.866	1.915	0.124	33.97	3.521	4.790	5.581

S.W. Area: The average sidewall area of the left and right side of the indents.

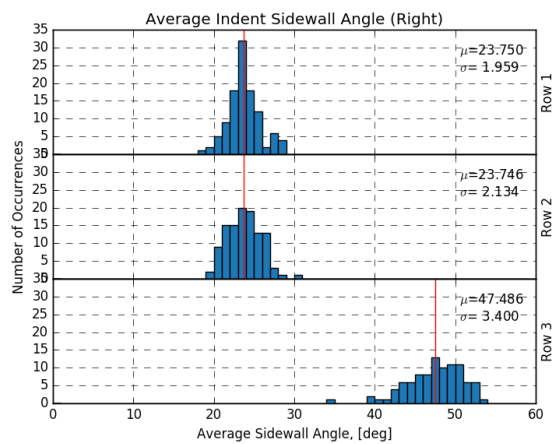
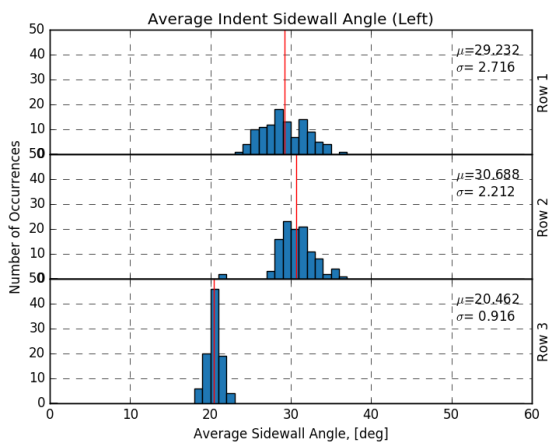
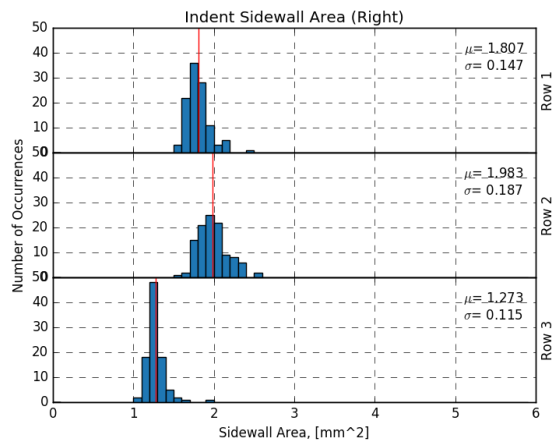
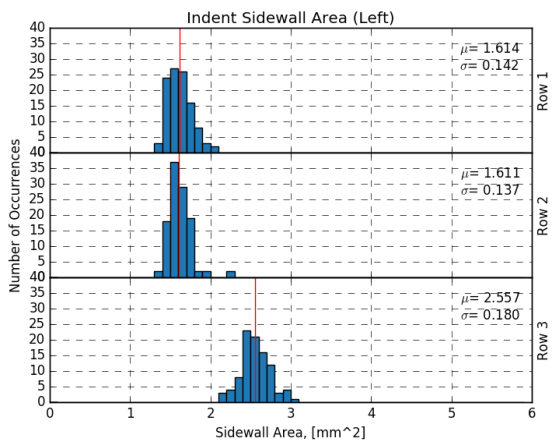
S.W. Angle: The average sidewall angle of the left and right side of the indents.



TEST REPORT: INDENT PROFILER

WIRE ID:WP

PAGE 2/4



TEST REPORT: ASTM A881

WIRE ID:WP

PAGE 3/4

SAMPLE ID		WP_630mm_Trued_10.26.18
SAMPLE LENGTH [MM]		630
NOMINAL DIAMETER [MM]		5.283
TEST ITEM	STANDARD VALUE	ACTUAL VALUE
INDENT DEPTH [MM]	0.115±0.035	0.117
SIDEWALL ANGLE [DEG]	In Contract	29.0
INDENT LENGTH [MM]	3.5±0.5	4.134
INDENT PITCH [MM]	5.46±0.29	5.58
ORIENTATION ANGLE [DEG]	≥45°	50.3
OUT OF ROUND [MM]	≤0.08	TBD

TEST REPORT: ISO 16120

WIRE ID:WP

PAGE 4/4

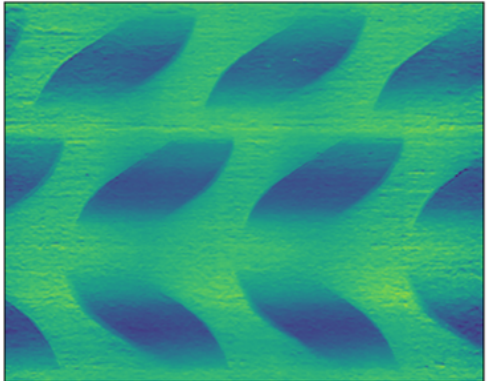
SAMPLE ID		WP_630mm_Trued_10.26.18
SAMPLE LENGTH		630
NOMINAL DIAMETER		5.283
TEST ITEM	STANDARD VALUE	ACTUAL VALUE
INDENT LENGTH [MM]	3.5±0.5	4.134
INDENT DEPTH [MM]	0.15±0.05	0.117
INDENT SPACING [MM]	5.50±0.50	5.58
INDENT DISTANCE [MM]	$\Sigma e \leq 3.343$	1.60, 1.77, 1.77
AVG DIAMETER [MM]	-	TBD
OVALITY	$\leq 0.01 \times D$	TBD

TEST REPORT: INDENT PROFILER

WIRE ID:WQ

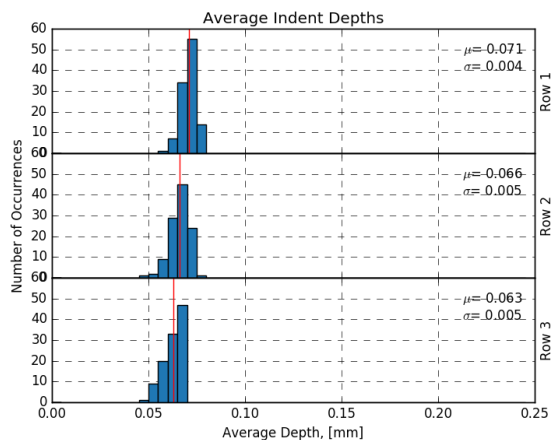
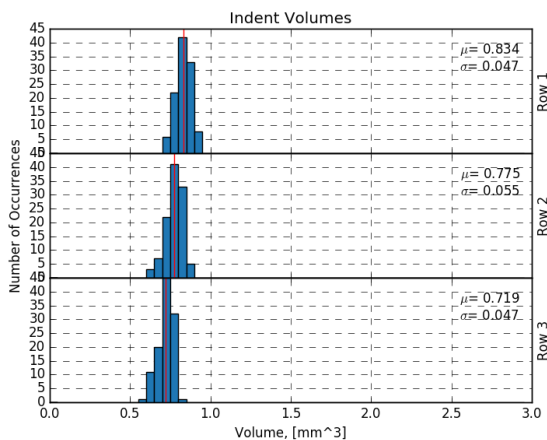
PAGE 1/4

Scan Information				
Wire ID	WQ_630mm_Trueid_10.26.18			
Length [mm]	630			
Scan Date	10.26.18			
Proc Date	09.17.19			
Stat Date	09.17.19			
ID	Indents	Nominal Dia [mm]	Orientat-ion [deg]	Distance [mm]
Total	332	5.288	55.8	3.052
Row 1	111		-55.9	3.000
Row 2	111		58.6	3.078
Row 3	110		52.7	3.078



Indent Data								
ID	Indents	Volume [mm^3]	S.W. Area [mm^2]	Avg Depth [mm]	S.W. Angle [deg]	Avg Length [mm]	Width [mm]	Pitch [mm]
Total	332	0.776	2.149	0.067	11.58	3.878	3.482	5.645
Row 1	111	0.834	2.196	0.071	11.48	3.844	3.541	5.643
Row 2	111	0.775	2.180	0.066	11.36	3.907	3.518	5.645
Row 3	110	0.719	2.070	0.063	11.90	3.883	3.385	5.645

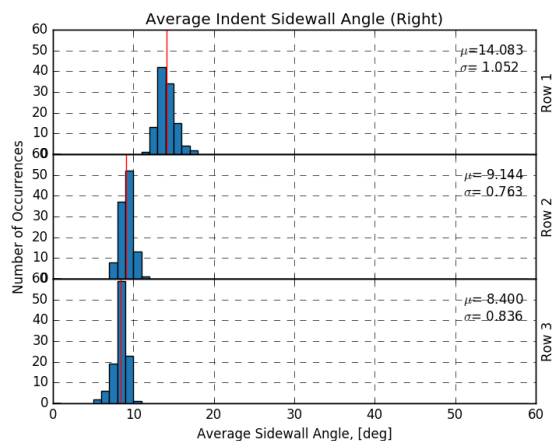
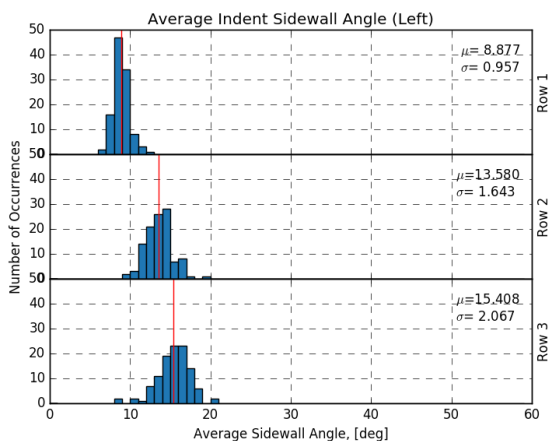
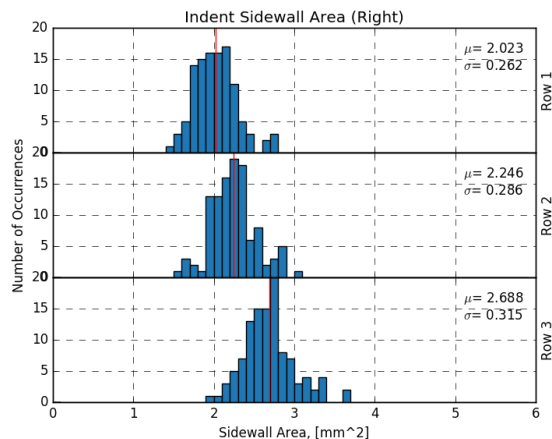
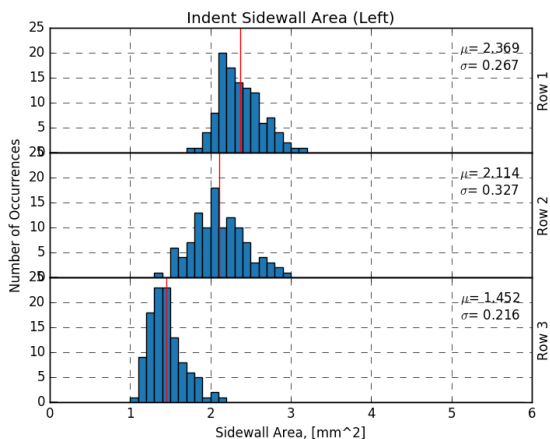
S.W. Area: The average sidewall area of the left and right side of the indents.
S.W. Angle: The average sidewall angle of the left and right side of the indents.



TEST REPORT: INDENT PROFILER

WIRE ID:WQ

PAGE 2/4



TEST REPORT: ASTM A881

WIRE ID:WQ

PAGE 3/4

SAMPLE ID		WQ_630mm_Trued_10.26.18
SAMPLE LENGTH [MM]		630
NOMINAL DIAMETER [MM]		5.288
TEST ITEM	STANDARD VALUE	ACTUAL VALUE
INDENT DEPTH [MM]	0.115±0.035	0.067
SIDEWALL ANGLE [DEG]	In Contract	11.6
INDENT LENGTH [MM]	3.5±0.5	3.907
INDENT PITCH [MM]	5.46±0.29	5.65
ORIENTATION ANGLE [DEG]	≥45°	55.8
OUT OF ROUND [MM]	≤0.08	TBD

TEST REPORT: ISO 16120

WIRE ID:WQ

PAGE 4/4

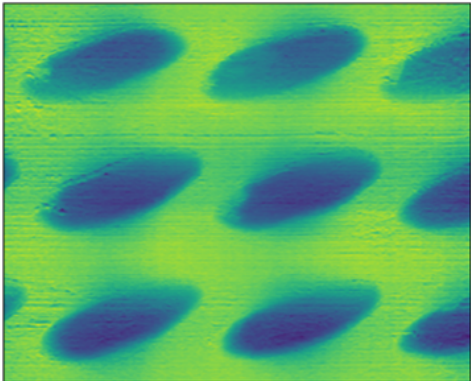
SAMPLE ID		WQ_630mm_True_d_10.26.18
SAMPLE LENGTH		630
NOMINAL DIAMETER		5.288
TEST ITEM	STANDARD VALUE	ACTUAL VALUE
INDENT LENGTH [MM]	3.5±0.5	3.907
INDENT DEPTH [MM]	0.15±0.05	0.067
INDENT SPACING [MM]	5.50±0.50	5.65
INDENT DISTANCE [MM]	$\Sigma e \leq 3.343$	3.00, 3.08, 3.08
AVG DIAMETER [MM]	-	TBD
OVALITY	$\leq 0.01 \times D$	TBD

TEST REPORT: INDENT PROFILER

WIRE ID:E-1

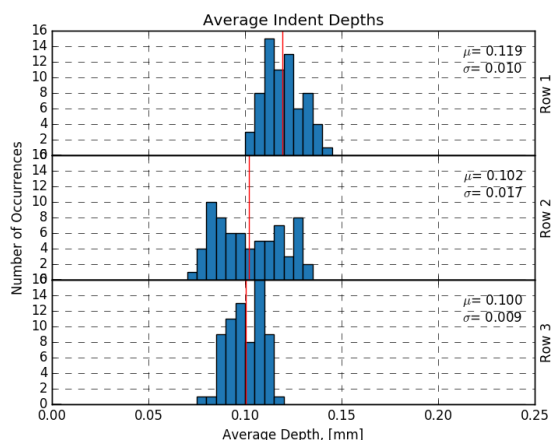
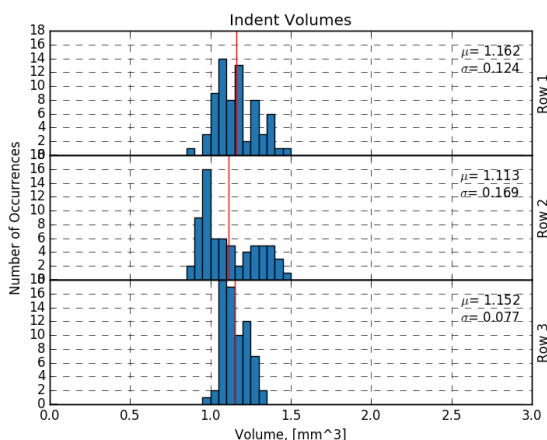
PAGE 1/4

Scan Information					
Wire ID		E1_435mm_Trued_12.18.18			
Length [mm]		435			
Scan Date		12.18.18			
Proc Date		09.17.19			
Stat Date		09.17.19			
ID	Indents	Nominal Dia [mm]	Orientat-ion [deg]	Distance [mm]	
Total	207	5.216	49.1	3.646	
Row 1	69		49.7	3.764	
Row 2	69		51.6	3.587	
Row 3	69		46.2	3.587	



Indent Data								
ID	Indents	Volume [mm^3]	S.W. Area [mm^2]	Avg Depth [mm]	S.W. Angle [deg]	Avg Length [mm]	Width [mm]	Pitch [mm]
Total	207	1.142	3.408	0.107	9.46	4.133	3.240	6.129
Row 1	69	1.162	3.219	0.119	9.99	4.126	3.007	6.109
Row 2	69	1.113	3.375	0.102	9.02	4.079	3.349	6.162
Row 3	69	1.152	3.629	0.100	9.37	4.195	3.363	6.117

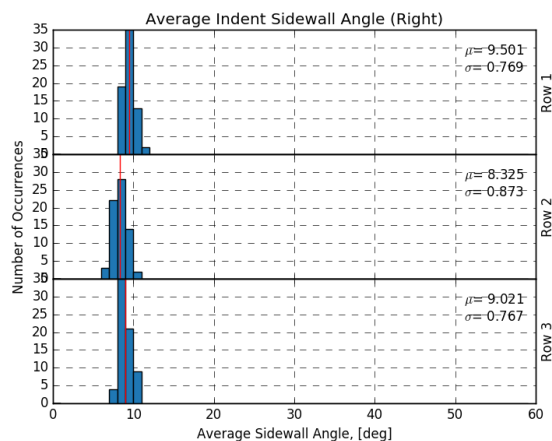
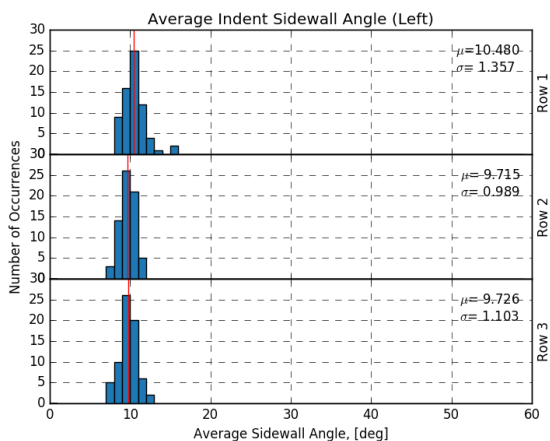
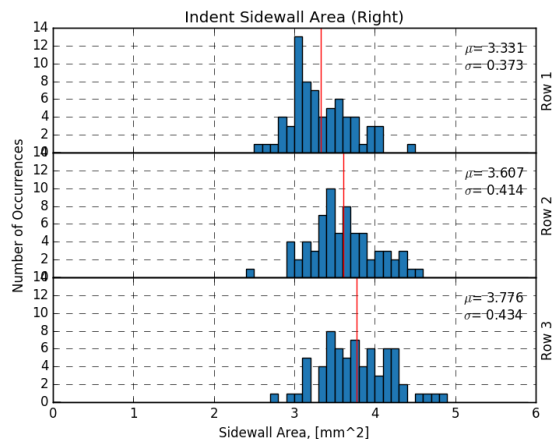
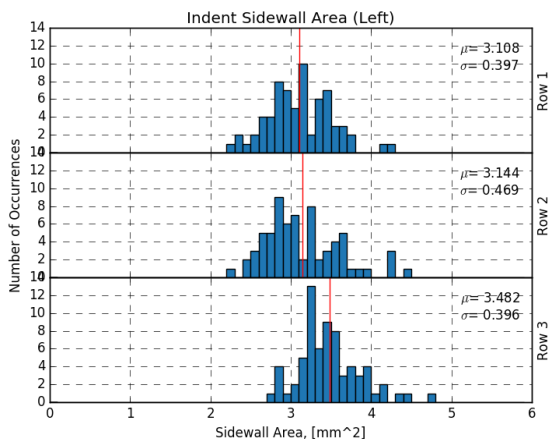
S.W. Area: The average sidewall area of the left and right side of the indents.
S.W. Angle: The average sidewall angle of the left and right side of the indents.



TEST REPORT: INDENT PROFILER

WIRE ID:E-1

PAGE 2/4



TEST REPORT: ASTM A881

WIRE ID:E-1

PAGE 3/4

SAMPLE ID		E1_435mm_Trued_12.18.18
SAMPLE LENGTH [MM]		435
NOMINAL DIAMETER [MM]		5.216
TEST ITEM	STANDARD VALUE	ACTUAL VALUE
INDENT DEPTH [MM]	0.115±0.035	0.107
SIDEWALL ANGLE [DEG]	In Contract	9.5
INDENT LENGTH [MM]	3.5±0.5	4.570
INDENT PITCH [MM]	5.46±0.29	6.13
ORIENTATION ANGLE [DEG]	≥45°	49.1
OUT OF ROUND [MM]	≤0.08	TBD

TEST REPORT: ISO 16120

WIRE ID:E-1

PAGE 4/4

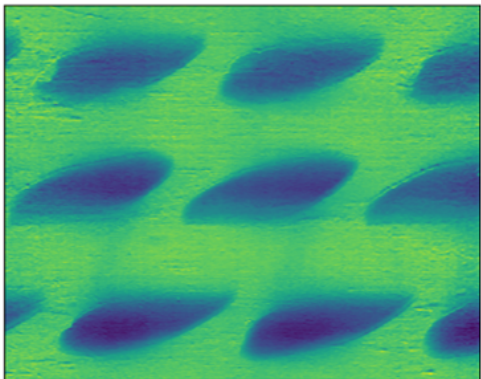
SAMPLE ID		E1_435mm_Trued_12.18.18
SAMPLE LENGTH		435
NOMINAL DIAMETER		5.216
TEST ITEM	STANDARD VALUE	ACTUAL VALUE
INDENT LENGTH [MM]	3.5±0.5	4.570
INDENT DEPTH [MM]	0.15±0.05	0.107
INDENT SPACING [MM]	5.50±0.50	6.13
INDENT DISTANCE [MM]	$\Sigma e \leq 3.343$	3.76, 3.59, 3.59
AVG DIAMETER [MM]	-	TBD
OVALITY	$\leq 0.01 \times D$	TBD

TEST REPORT: INDENT PROFILER

WIRE ID:H-1

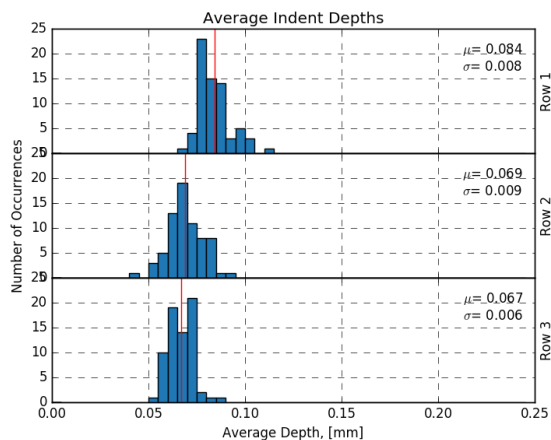
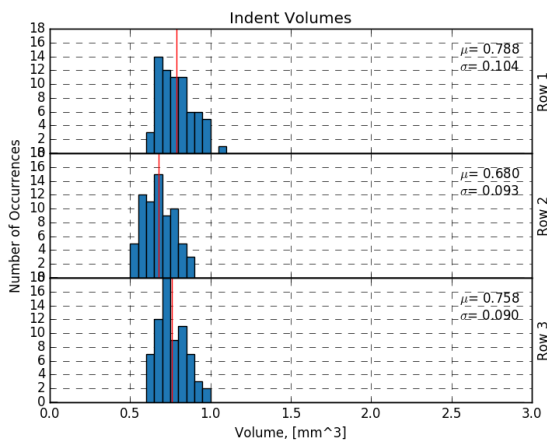
PAGE 1/4

Scan Information				
Wire ID	H1_435mm_Trued_12.18.18			
Length [mm]	435			
Scan Date	12.18.18			
Proc Date	09.17.19			
Stat Date	09.17.19			
ID	Indents	Nominal Dia [mm]	Orientat-ion [deg]	Distance [mm]
Total	208	4.981	44.9	3.819
Row 1	69		46.1	3.941
Row 2	70		42.1	3.757
Row 3	69		46.5	3.757



Indent Data								
ID	Indents	Volume [mm^3]	S.W. Area [mm^2]	Avg Depth [mm]	S.W. Angle [deg]	Avg Length [mm]	Width [mm]	Pitch [mm]
Total	208	0.742	3.079	0.073	7.18	4.470	2.797	6.103
Row 1	69	0.788	2.847	0.084	8.17	4.411	2.651	6.100
Row 2	70	0.680	3.160	0.069	6.79	4.485	2.725	6.105
Row 3	69	0.758	3.228	0.067	6.60	4.514	3.017	6.104

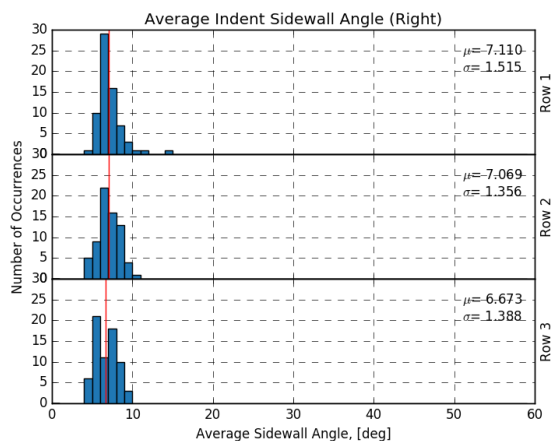
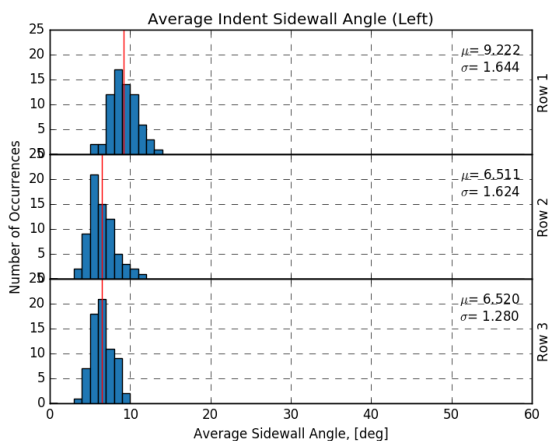
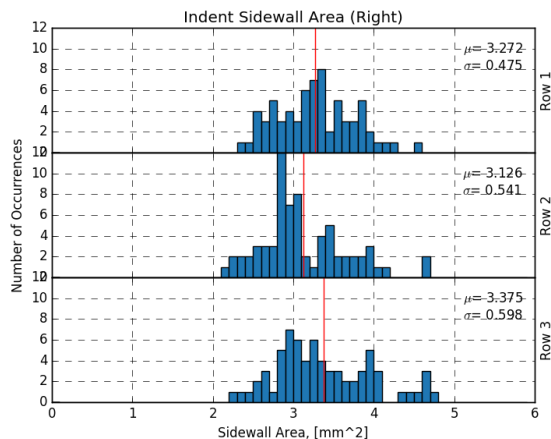
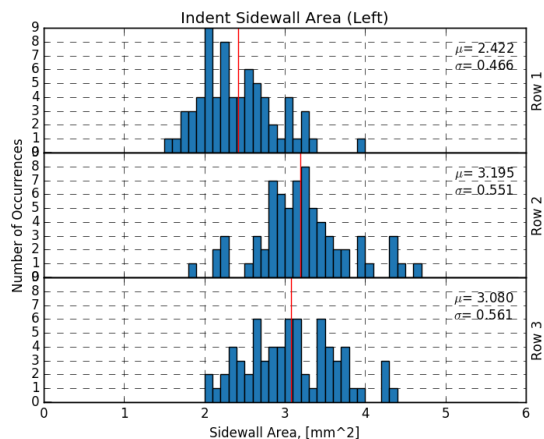
S.W. Area: The average sidewall area of the left and right side of the indents.
S.W. Angle: The average sidewall angle of the left and right side of the indents.



TEST REPORT: INDENT PROFILER

WIRE ID:H-1

PAGE 2/4



TEST REPORT: ASTM A881

WIRE ID:H-1

PAGE 3/4

SAMPLE ID		H1_435mm_Trued_12.18.18
SAMPLE LENGTH [MM]		435
NOMINAL DIAMETER [MM]		4.981
TEST ITEM	STANDARD VALUE	ACTUAL VALUE
INDENT DEPTH [MM]	0.115±0.035	0.073
SIDEWALL ANGLE [DEG]	In Contract	7.2
INDENT LENGTH [MM]	3.5±0.5	4.647
INDENT PITCH [MM]	5.46±0.29	6.10
ORIENTATION ANGLE [DEG]	≥45°	44.9
OUT OF ROUND [MM]	≤0.08	TBD

TEST REPORT: ISO 16120

WIRE ID:H-1

PAGE 4/4

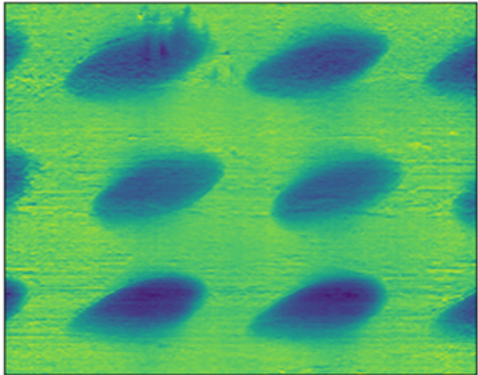
SAMPLE ID		H1_435mm_Trued_12.18.18
SAMPLE LENGTH		435
NOMINAL DIAMETER		4.981
TEST ITEM	STANDARD VALUE	ACTUAL VALUE
INDENT LENGTH [MM]	3.5±0.5	4.647
INDENT DEPTH [MM]	0.15±0.05	0.073
INDENT SPACING [MM]	5.50±0.50	6.10
INDENT DISTANCE [MM]	$\Sigma e \leq 3.343$	3.94, 3.76, 3.76
AVG DIAMETER [MM]	-	TBD
OVALITY	$\leq 0.01 \times D$	TBD

TEST REPORT: INDENT PROFILER

WIRE ID: J-1

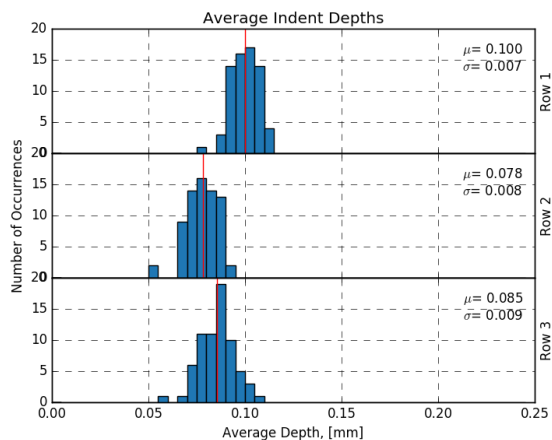
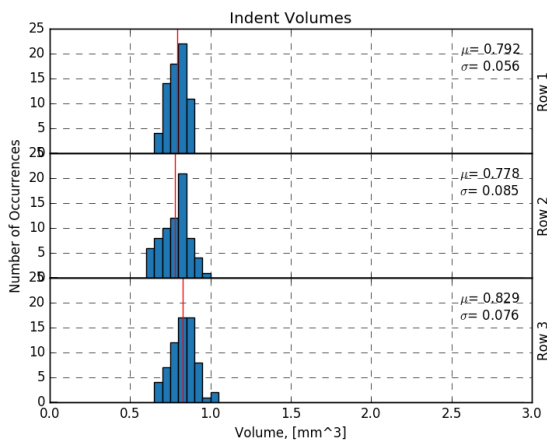
PAGE 1/4

Scan Information				
Wire ID	J1_435mm_True_12.18.18			
Length [mm]	435			
Scan Date	12.18.18			
Proc Date	09.17.19			
Stat Date	09.17.19			
ID	Indents	Nominal Dia [mm]	Orientation [deg]	Distance [mm]
Total	207	4.960	55.9	3.519
Row 1	69		52.1	3.657
Row 2	70		58.9	3.450
Row 3	68		56.6	3.450



Indent Data								
ID	Indents	Volume [mm ³]	S.W. Area [mm ²]	Avg Depth [mm]	S.W. Angle [deg]	Avg Length [mm]	Width [mm]	Pitch [mm]
Total	207	0.800	3.032	0.088	7.26	3.969	2.984	6.101
Row 1	69	0.792	2.961	0.100	7.55	3.889	2.662	6.103
Row 2	70	0.778	3.181	0.078	6.54	3.968	3.225	6.102
Row 3	68	0.829	2.950	0.085	7.71	4.052	3.063	6.098

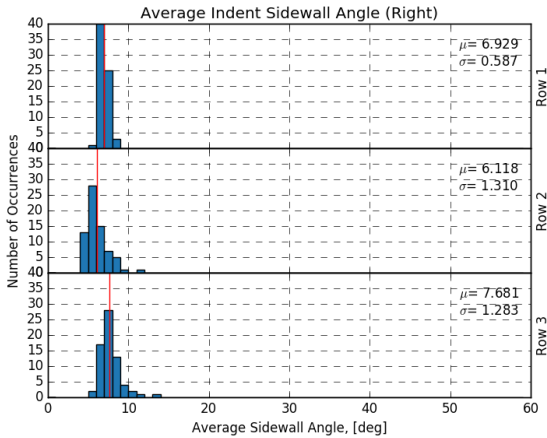
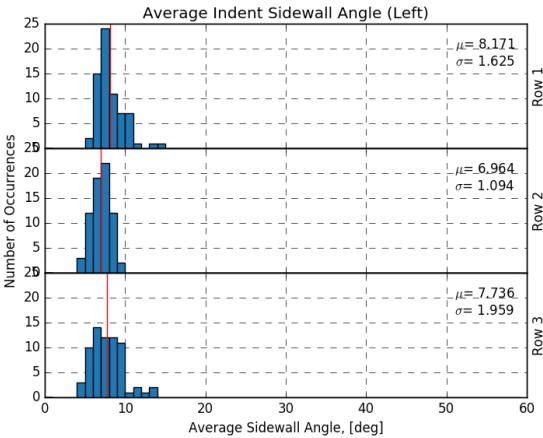
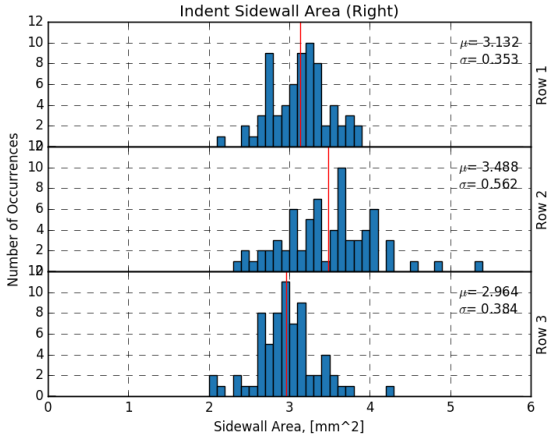
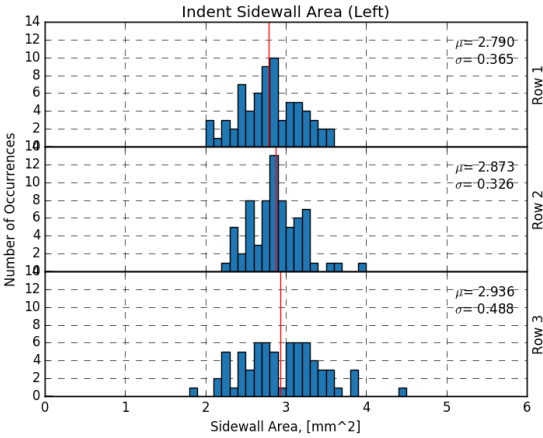
S.W. Area: The average sidewall area of the left and right side of the indents.
S.W. Angle: The average sidewall angle of the left and right side of the indents.



TEST REPORT: INDENT PROFILER

WIRE ID: J-1

PAGE 2/4



TEST REPORT: ASTM A881

WIRE ID: J-1

PAGE 3/4

SAMPLE ID		J1_435mm_Trued_12.18.18
SAMPLE LENGTH [MM]		435
NOMINAL DIAMETER [MM]		4.960
TEST ITEM	STANDARD VALUE	ACTUAL VALUE
INDENT DEPTH [MM]	0.115±0.035	0.088
SIDEWALL ANGLE [DEG]	In Contract	7.3
INDENT LENGTH [MM]	3.5±0.5	4.180
INDENT PITCH [MM]	5.46±0.29	6.10
ORIENTATION ANGLE [DEG]	≥45°	55.9
OUT OF ROUND [MM]	≤0.08	TBD

TEST REPORT: ISO 16120

WIRE ID: J-1

PAGE 4/4

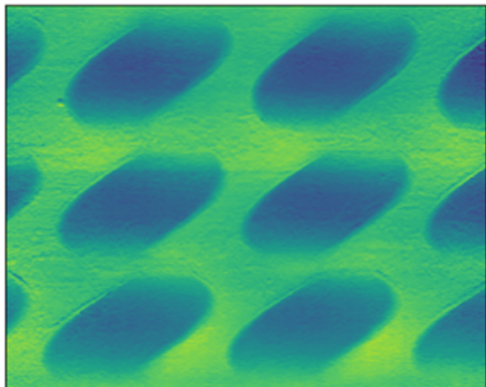
SAMPLE ID		J1_435mm_TrueD_12.18.18
SAMPLE LENGTH		435
NOMINAL DIAMETER		4.960
TEST ITEM	STANDARD VALUE	ACTUAL VALUE
INDENT LENGTH [MM]	3.5±0.5	4.180
INDENT DEPTH [MM]	0.15±0.05	0.088
INDENT SPACING [MM]	5.50±0.50	6.10
INDENT DISTANCE [MM]	$\Sigma e \leq 3.343$	3.66, 3.45, 3.45
AVG DIAMETER [MM]	-	TBD
OVALITY	$\leq 0.01 \times D$	TBD

TEST REPORT: INDENT PROFILER

WIRE ID:K-1

PAGE 1/4

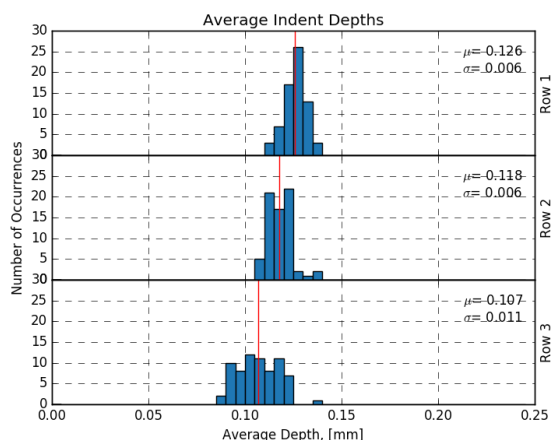
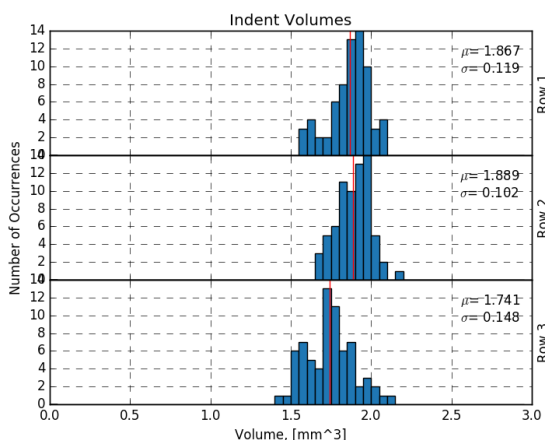
Scan Information					
Wire ID	K1_435mm_Trued_12.18.18				
Length [mm]	435				
Scan Date	12.18.18				
Proc Date	09.17.19				
Stat Date	09.17.19				
ID	Indents	Nominal Dia [mm]	Orientat-ion [deg]	Distance [mm]	
Total	209	5.124	60.1	2.789	
Row 1	69		61.7	2.878	
Row 2	70		57.3	2.744	
Row 3	70		61.3	2.744	



Indent Data								
ID	Indents	Volume [mm^3]	S.W. Area [mm^2]	Avg Depth [mm]	S.W. Angle [deg]	Avg Length [mm]	Width [mm]	Pitch [mm]
Total	209	1.832	2.443	0.117	15.79	4.391	4.001	6.136
Row 1	69	1.867	2.420	0.126	15.78	4.362	3.806	6.119
Row 2	70	1.889	2.330	0.118	16.96	4.290	4.120	6.119
Row 3	70	1.741	2.577	0.107	14.63	4.522	4.074	6.169

S.W. Area: The average sidewall area of the left and right side of the indents.

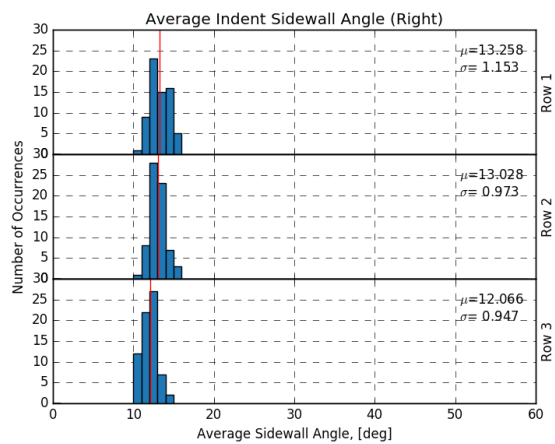
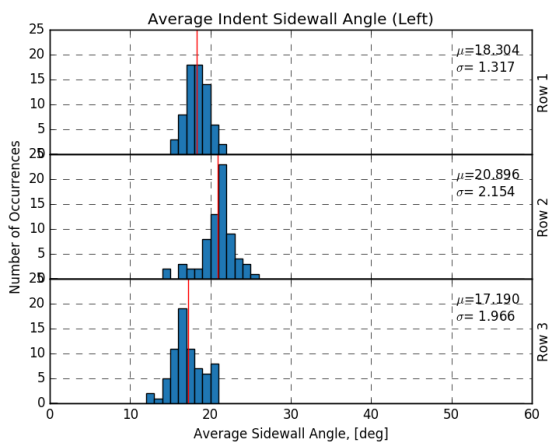
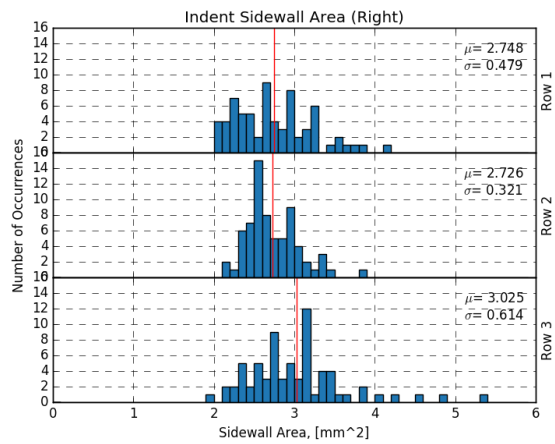
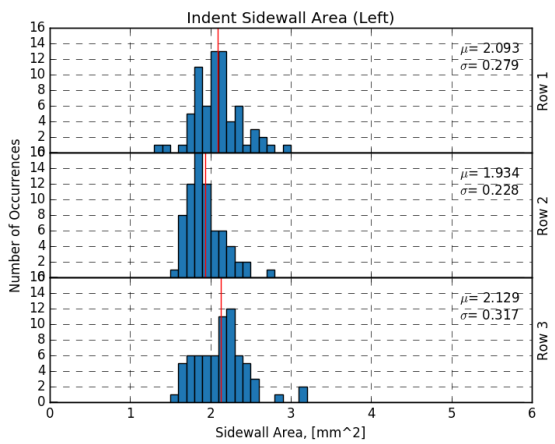
S.W. Angle: The average sidewall angle of the left and right side of the indents.



TEST REPORT: INDENT PROFILER

WIRE ID:K-1

PAGE 2/4



TEST REPORT: ASTM A881

WIRE ID:K-1

PAGE 3/4

SAMPLE ID		K1_435mm_Trued_12.18.18
SAMPLE LENGTH [MM]		435
NOMINAL DIAMETER [MM]		5.124
TEST ITEM	STANDARD VALUE	ACTUAL VALUE
INDENT DEPTH [MM]	0.115±0.035	0.117
SIDEWALL ANGLE [DEG]	In Contract	15.8
INDENT LENGTH [MM]	3.5±0.5	4.857
INDENT PITCH [MM]	5.46±0.29	6.14
ORIENTATION ANGLE [DEG]	≥45°	60.1
OUT OF ROUND [MM]	≤0.08	TBD

TEST REPORT: ISO 16120

WIRE ID:K-1

PAGE 4/4

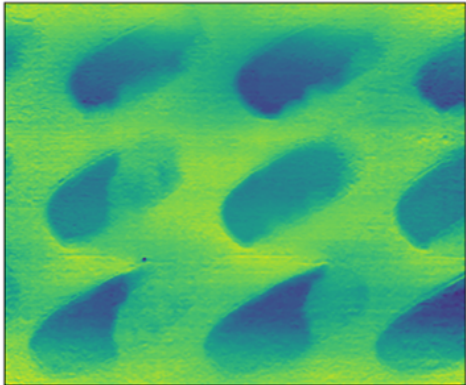
SAMPLE ID		K1_435mm_Trued_12.18.18
SAMPLE LENGTH		435
NOMINAL DIAMETER		5.124
TEST ITEM	STANDARD VALUE	ACTUAL VALUE
INDENT LENGTH [MM]	3.5±0.5	4.857
INDENT DEPTH [MM]	0.15±0.05	0.117
INDENT SPACING [MM]	5.50±0.50	6.14
INDENT DISTANCE [MM]	$\Sigma e \leq 3.343$	2.88, 2.74, 2.74
AVG DIAMETER [MM]	-	TBD
OVALITY	$\leq 0.01 \times D$	TBD

TEST REPORT: INDENT PROFILER

WIRE ID:L-1

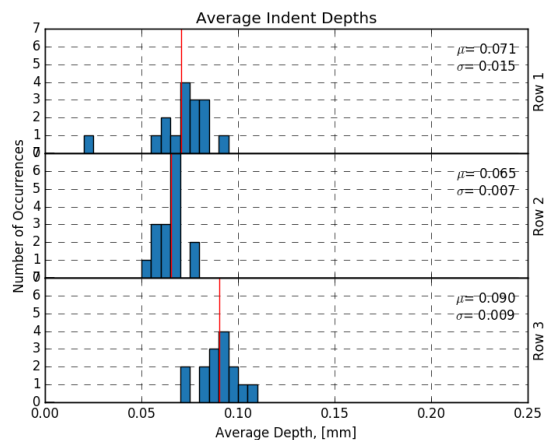
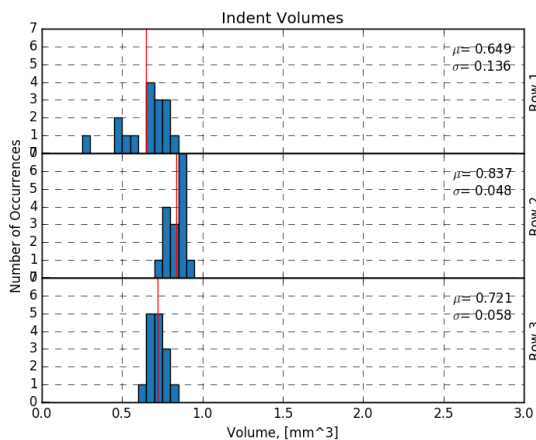
PAGE 1/4

Scan Information				
Wire ID	L1_435mm_Trueed_12.18.18			
Length [mm]	435			
Scan Date	12.18.18			
Proc Date	09.17.19			
Stat Date	09.17.19			
ID	Indents	Nominal Dia [mm]	Orientat-ion [deg]	Distance [mm]
Total	47	4.936	56.3	2.727
Row 1	16		64.5	2.422
Row 2	16		52.1	2.879
Row 3	15		52.4	2.879



Indent Data								
ID	Indents	Volume [mm^3]	S.W. Area [mm^2]	Avg Depth [mm]	S.W. Angle [deg]	Avg Length [mm]	Width [mm]	Pitch [mm]
Total	47	0.736	3.167	0.075	9.22	3.559	3.845	6.065
Row 1	16	0.649	2.285	0.071	10.70	3.300	4.037	6.082
Row 2	16	0.837	3.931	0.065	7.99	3.713	4.341	6.052
Row 3	15	0.721	3.294	0.090	8.96	3.672	3.110	6.061

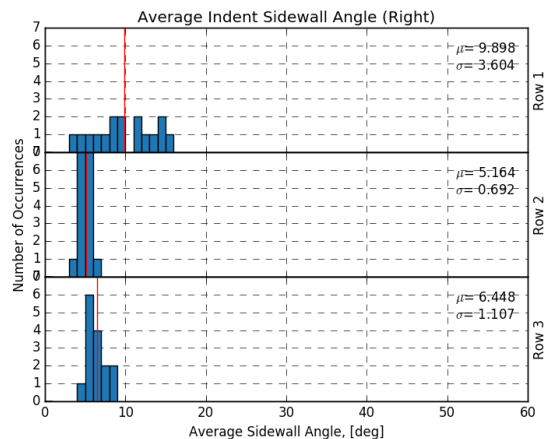
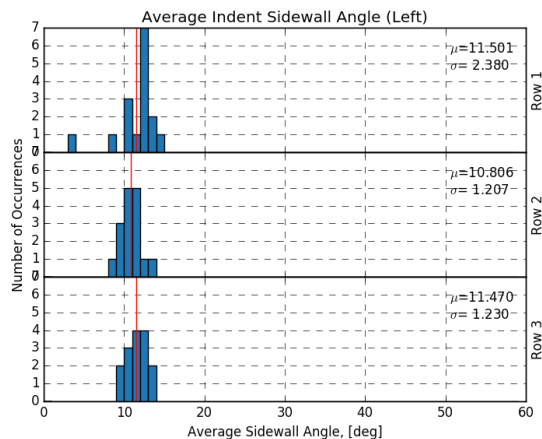
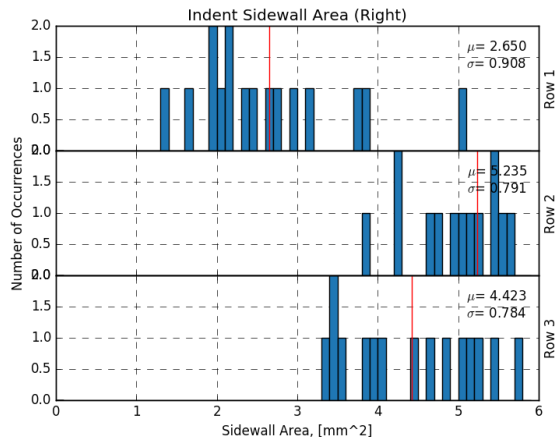
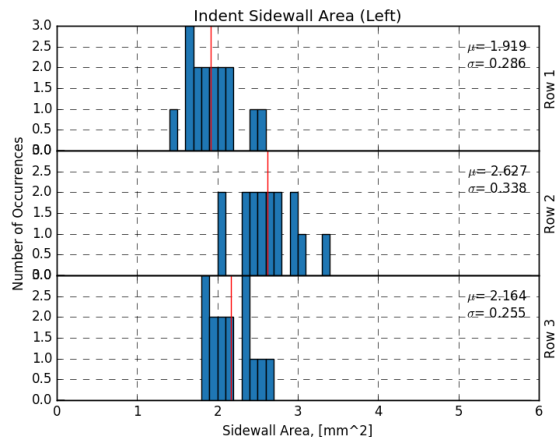
S.W. Area: The average sidewall area of the left and right side of the indents.
S.W. Angle: The average sidewall angle of the left and right side of the indents.



TEST REPORT: INDENT PROFILER

WIRE ID:L-1

PAGE 2/4



TEST REPORT: ASTM A881

WIRE ID:L-1

PAGE 3/4

SAMPLE ID		L1_435mm_Trued_12.18.18
SAMPLE LENGTH [MM]		435
NOMINAL DIAMETER [MM]		4.936
TEST ITEM	STANDARD VALUE	ACTUAL VALUE
INDENT DEPTH [MM]	0.115±0.035	0.075
SIDEWALL ANGLE [DEG]	In Contract	9.2
INDENT LENGTH [MM]	3.5±0.5	3.880
INDENT PITCH [MM]	5.46±0.29	6.07
ORIENTATION ANGLE [DEG]	≥45°	56.3
OUT OF ROUND [MM]	≤0.08	TBD

TEST REPORT: ISO 16120

WIRE ID:L-1

PAGE 4/4

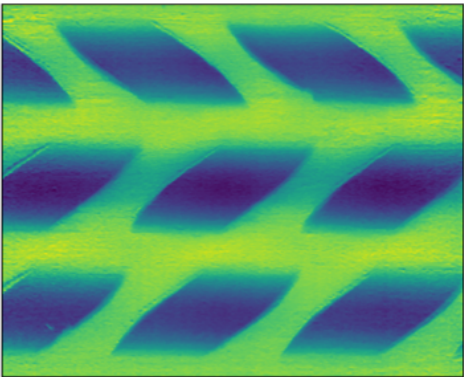
SAMPLE ID		L1_435mm_Trued_12.18.18
SAMPLE LENGTH		435
NOMINAL DIAMETER		4.936
TEST ITEM	STANDARD VALUE	ACTUAL VALUE
INDENT LENGTH [MM]	3.5±0.5	3.880
INDENT DEPTH [MM]	0.15±0.05	0.075
INDENT SPACING [MM]	5.50±0.50	6.07
INDENT DISTANCE [MM]	$\Sigma e \leq 3.343$	2.42, 2.88, 2.88
AVG DIAMETER [MM]	-	TBD
OVALITY	$\leq 0.01 \times D$	TBD

TEST REPORT: INDENT PROFILER

WIRE ID:M-1

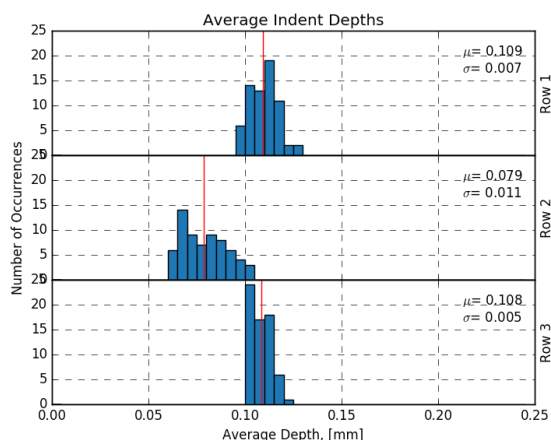
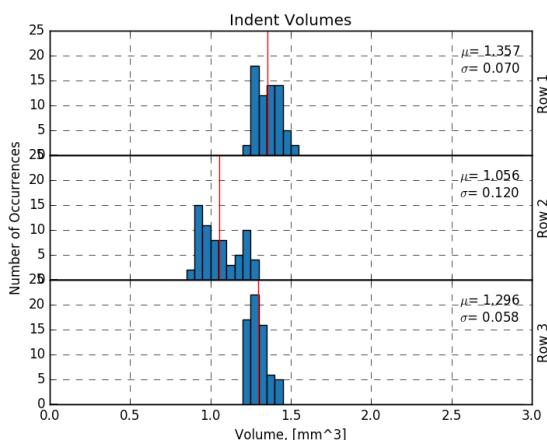
PAGE 1/4

Scan Information				
Wire ID	M1_435mm_TrueD_12.18.18			
Length [mm]	435			
Scan Date	12.18.18			
Proc Date	09.17.19			
Stat Date	09.17.19			
ID	Indents	Nominal Dia [mm]	Orientation [deg]	Distance [mm]
Total	199	4.954	47.2	3.062
Row 1	67		46.5	3.000
Row 2	66		51.6	3.092
Row 3	66		-43.4	3.092



Indent Data								
ID	Indents	Volume [mm ³]	S.W. Area [mm ²]	Avg Depth [mm]	S.W. Angle [deg]	Avg Length [mm]	Width [mm]	Pitch [mm]
Total	199	1.237	1.937	0.099	16.36	4.302	3.288	5.965
Row 1	67	1.357	1.808	0.109	17.34	4.282	3.211	5.949
Row 2	66	1.056	2.386	0.079	11.55	4.333	3.630	5.996
Row 3	66	1.296	1.617	0.108	20.18	4.292	3.023	5.952

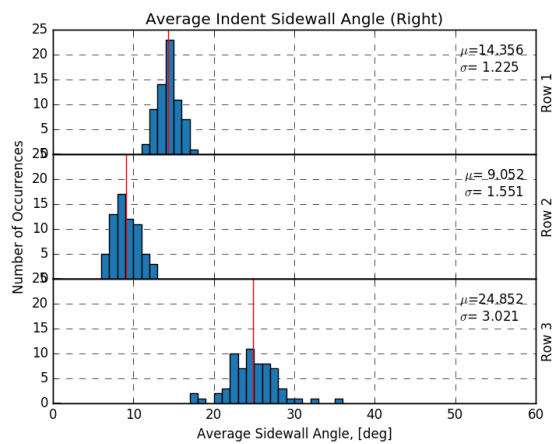
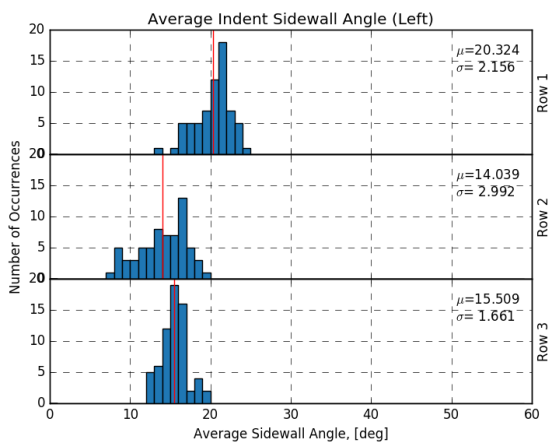
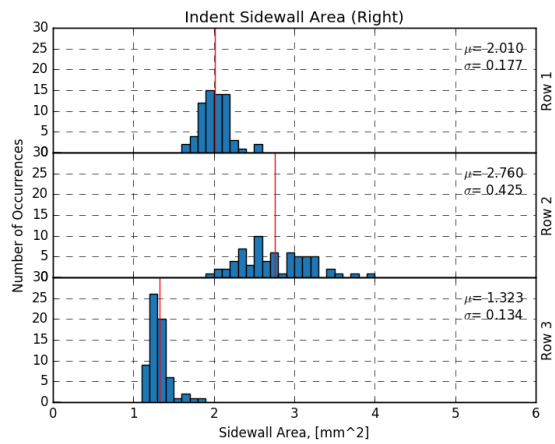
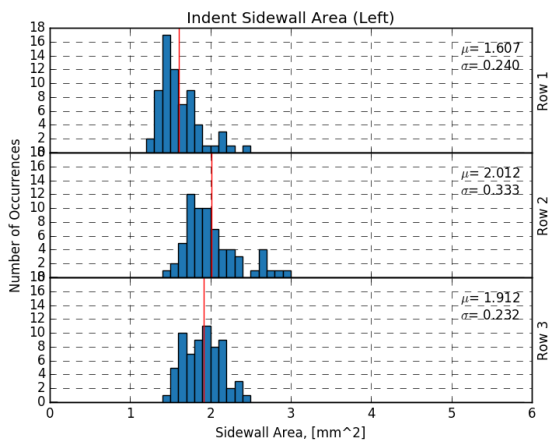
S.W. Area: The average sidewall area of the left and right side of the indents.
S.W. Angle: The average sidewall angle of the left and right side of the indents.



TEST REPORT: INDENT PROFILER

WIRE ID:M-1

PAGE 2/4



TEST REPORT: ASTM A881

WIRE ID:M-1

PAGE 3/4

SAMPLE ID		M1_435mm_Trued_12.18.18
SAMPLE LENGTH [MM]		435
NOMINAL DIAMETER [MM]		4.954
TEST ITEM	STANDARD VALUE	ACTUAL VALUE
INDENT DEPTH [MM]	0.115±0.035	0.099
SIDEWALL ANGLE [DEG]	In Contract	16.4
INDENT LENGTH [MM]	3.5±0.5	4.491
INDENT PITCH [MM]	5.46±0.29	5.97
ORIENTATION ANGLE [DEG]	≥45°	47.2
OUT OF ROUND [MM]	≤0.08	TBD

TEST REPORT: ISO 16120

WIRE ID:M-1

PAGE 4/4

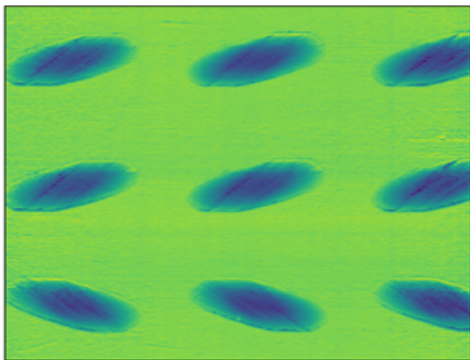
SAMPLE ID		M1_435mm_Trued_12.18.18
SAMPLE LENGTH		435
NOMINAL DIAMETER		4.954
TEST ITEM	STANDARD VALUE	ACTUAL VALUE
INDENT LENGTH [MM]	3.5±0.5	4.491
INDENT DEPTH [MM]	0.15±0.05	0.099
INDENT SPACING [MM]	5.50±0.50	5.97
INDENT DISTANCE [MM]	$\Sigma e \leq 3.343$	3.00, 3.09, 3.09
AVG DIAMETER [MM]	-	TBD
OVALITY	$\leq 0.01 \times D$	TBD

TEST REPORT: INDENT PROFILER

WIRE ID:15-S

PAGE 1/4

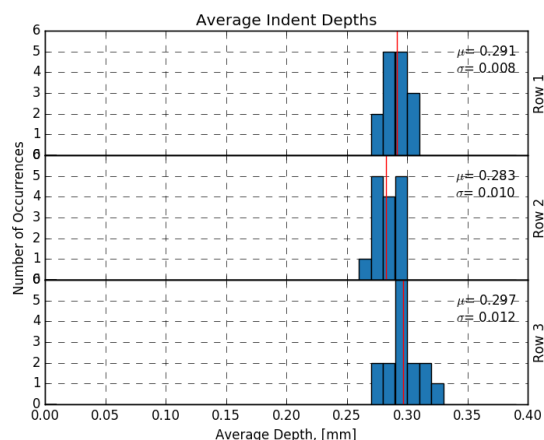
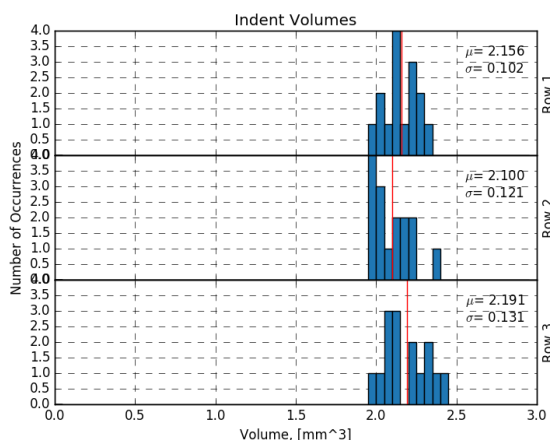
Scan Information				
Wire ID	15-16-T1_105mm_TrueD_11.15.18			
Length [mm]	105			
Scan Date	11.15.18			
Proc Date	09.17.19			
Stat Date	09.17.19			
ID	Indents	Nominal Dia [mm]	Orientat-ion [deg]	Distance [mm]
Total	45	5.176	46.8	4.550
Row 1	15		42.7	4.576
Row 2	15		44.9	4.537
Row 3	15		-52.7	4.537



Indent Data								
ID	Indents	Volume [mm^3]	S.W. Area [mm^2]	Avg Depth [mm]	S.W. Angle [deg]	Avg Length [mm]	Width [mm]	Pitch [mm]
Total	45	2.149	5.046	0.290	13.18	4.190	2.604	6.344
Row 1	15	2.156	5.293	0.291	13.32	4.210	2.572	6.329
Row 2	15	2.100	5.159	0.283	12.63	4.207	2.595	6.336
Row 3	15	2.191	4.684	0.297	13.59	4.154	2.647	6.367

S.W. Area: The average sidewall area of the left and right side of the indents.

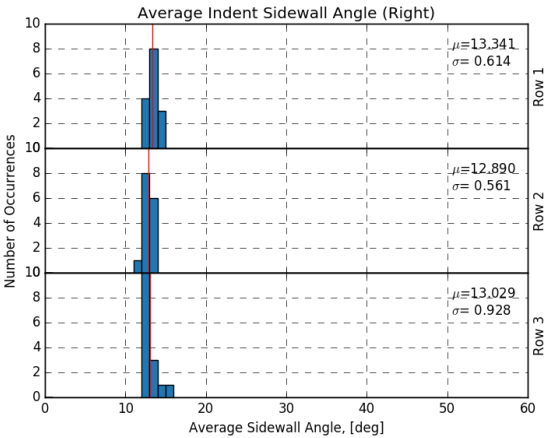
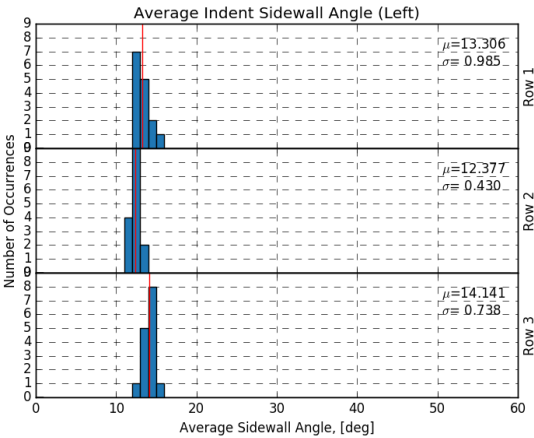
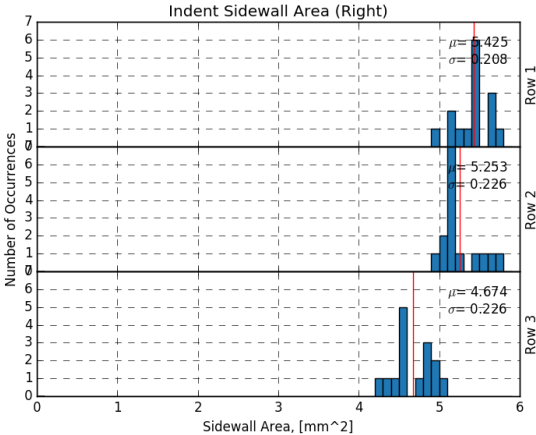
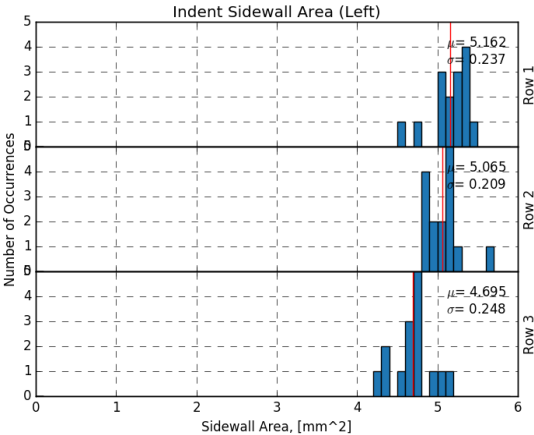
S.W. Angle: The average sidewall angle of the left and right side of the indents.



TEST REPORT: INDENT PROFILER

WIRE ID:15-S

PAGE 2/4



TEST REPORT: ASTM A881

WIRE ID:15-S

PAGE 3/4

SAMPLE ID		15-.16-T1_105mm_True
SAMPLE LENGTH [MM]		105
NOMINAL DIAMETER [MM]		5.176
TEST ITEM	STANDARD VALUE	ACTUAL VALUE
INDENT DEPTH [MM]	0.115±0.035	0.290
SIDEWALL ANGLE [DEG]	In Contract	13.2
INDENT LENGTH [MM]	3.5±0.5	4.503
INDENT PITCH [MM]	5.46±0.29	6.34
ORIENTATION ANGLE [DEG]	≥45°	46.8
OUT OF ROUND [MM]	≤0.08	TBD

TEST REPORT: ISO 16120

WIRE ID:15-S

PAGE 4/4

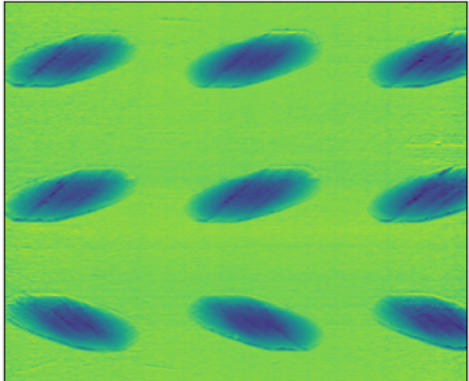
SAMPLE ID		15-.16-T1_105mm_True
SAMPLE LENGTH		105
NOMINAL DIAMETER		5.176
TEST ITEM	STANDARD VALUE	ACTUAL VALUE
INDENT LENGTH [MM]	3.5 ± 0.5	4.503
INDENT DEPTH [MM]	0.15 ± 0.05	0.290
INDENT SPACING [MM]	5.50 ± 0.50	6.34
INDENT DISTANCE [MM]	$\Sigma e \leq 3.343$	4.58, 4.54, 4.54
AVG DIAMETER [MM]	-	TBD
OVALITY	$\leq 0.01 \times D$	TBD

TEST REPORT: INDENT PROFILER

WIRE ID:15-D

PAGE 1/4

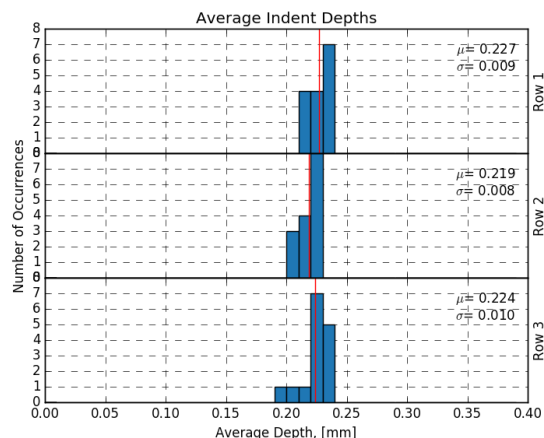
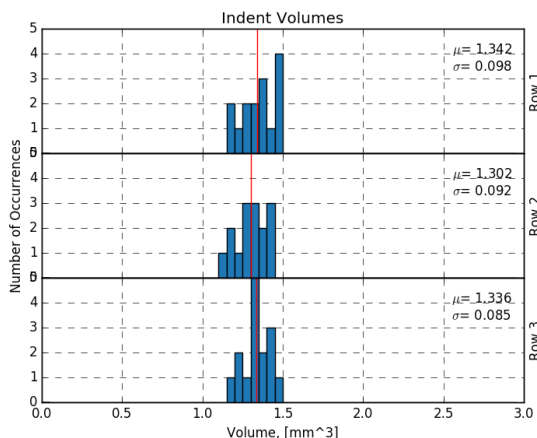
Scan Information				
Wire ID	15_105mm_Trued_11.16.18			
Length [mm]	105			
Scan Date	11.16.18			
Proc Date	09.17.19			
Stat Date	09.17.19			
ID	Indents	Nominal Dia [mm]	Orientat-ion [deg]	Distance [mm]
Total	45	5.257	47.4	4.947
Row 1	15		-44.3	4.942
Row 2	15		50.2	4.949
Row 3	15		47.8	4.949



Indent Data								
ID	Indents	Volume [mm^3]	S.W. Area [mm^2]	Avg Depth [mm]	S.W. Angle [deg]	Avg Length [mm]	Width [mm]	Pitch [mm]
Total	45	1.327	3.686	0.223	12.67	3.645	2.352	6.344
Row 1	15	1.342	3.918	0.227	13.35	3.627	2.363	6.368
Row 2	15	1.302	3.432	0.219	12.56	3.625	2.339	6.336
Row 3	15	1.336	3.708	0.224	12.09	3.684	2.353	6.329

S.W. Area: The average sidewall area of the left and right side of the indents.

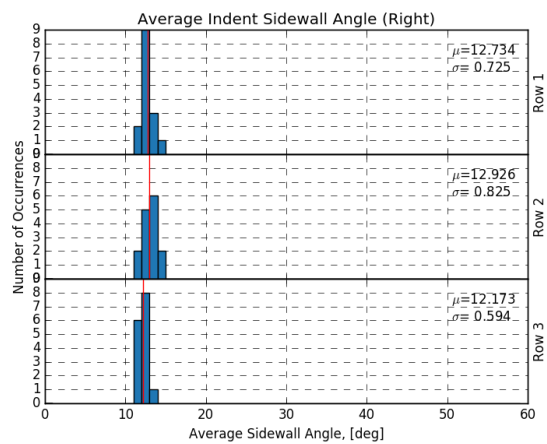
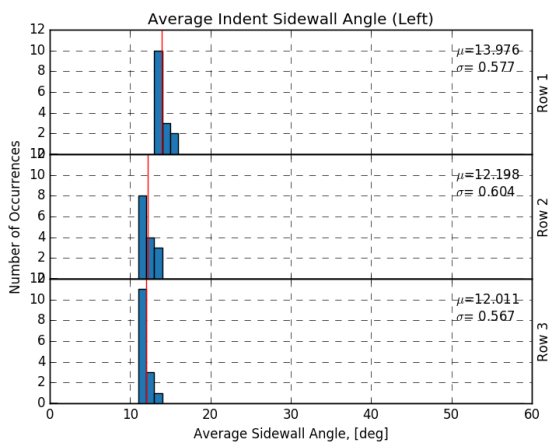
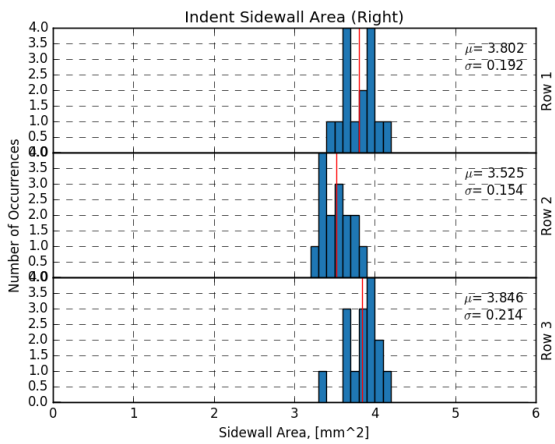
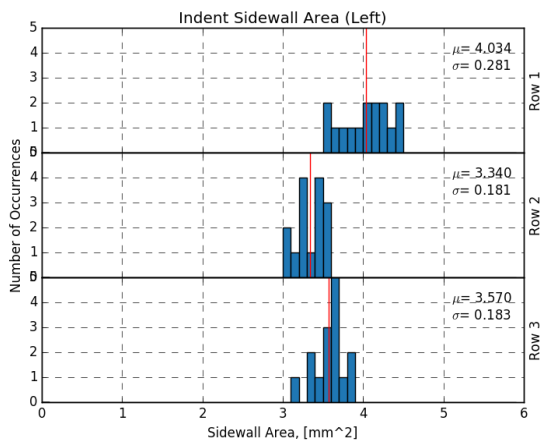
S.W. Angle: The average sidewall angle of the left and right side of the indents.



TEST REPORT: INDENT PROFILER

WIRE ID:15-D

PAGE 2/4



TEST REPORT: ASTM A881

WIRE ID:15-D

PAGE 3/4

SAMPLE ID		15_105mm_Trued_11.16.18
SAMPLE LENGTH [MM]		105
NOMINAL DIAMETER [MM]		5.257
TEST ITEM	STANDARD VALUE	ACTUAL VALUE
INDENT DEPTH [MM]	0.115±0.035	0.223
SIDEWALL ANGLE [DEG]	In Contract	12.7
INDENT LENGTH [MM]	3.5±0.5	5.059
INDENT PITCH [MM]	5.46±0.29	6.34
ORIENTATION ANGLE [DEG]	≥45°	47.4
OUT OF ROUND [MM]	≤0.08	TBD

TEST REPORT: ISO 16120

WIRE ID:15-D

PAGE 4/4

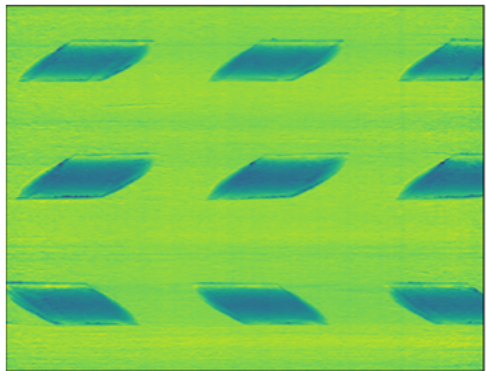
SAMPLE ID		15_105mm_Trued_11.16.18
SAMPLE LENGTH		105
NOMINAL DIAMETER		5.257
TEST ITEM	STANDARD VALUE	ACTUAL VALUE
INDENT LENGTH [MM]	3.5±0.5	5.059
INDENT DEPTH [MM]	0.15±0.05	0.223
INDENT SPACING [MM]	5.50±0.50	6.34
INDENT DISTANCE [MM]	$\Sigma e \leq 3.343$	4.94, 4.95, 4.95
AVG DIAMETER [MM]	-	TBD
OVALITY	$\leq 0.01 \times D$	TBD

TEST REPORT: INDENT PROFILER

WIRE ID:30-S

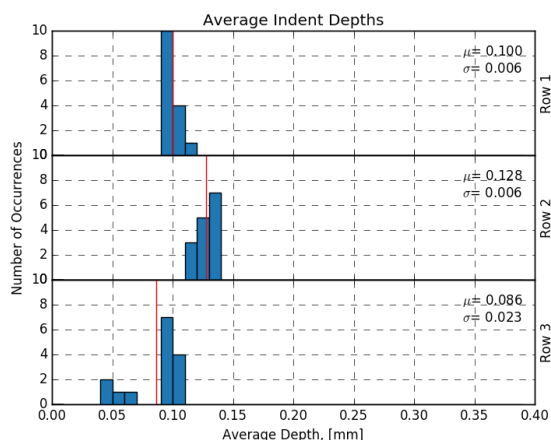
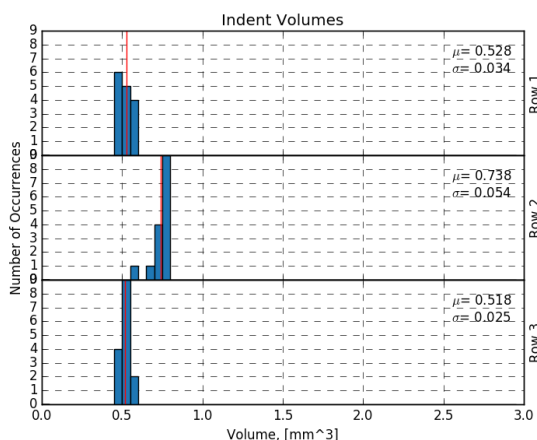
PAGE 1/4

Scan Information				
Wire ID	X3_105mm_Trued_11.16.18			
Length [mm]	105			
Scan Date	11.16.18			
Proc Date	09.17.19			
Stat Date	09.17.19			
ID	Indents	Nominal Dia [mm]	Orientat-ion [deg]	Distance [mm]
Total	45	5.303	47.6	5.455
Row 1	15		-45.1	5.557
Row 2	15		45.8	5.404
Row 3	15		51.9	5.404



Indent Data								
ID	Indents	Volume [mm^3]	S.W. Area [mm^2]	Avg Depth [mm]	S.W. Angle [deg]	Avg Length [mm]	Width [mm]	Pitch [mm]
Total	45	0.595	1.050	0.105	19.93	3.599	1.945	6.345
Row 1	15	0.528	0.928	0.100	19.42	3.553	1.760	6.370
Row 2	15	0.738	1.069	0.128	22.50	3.567	1.889	6.330
Row 3	15	0.518	1.153	0.086	17.88	3.678	2.187	6.333

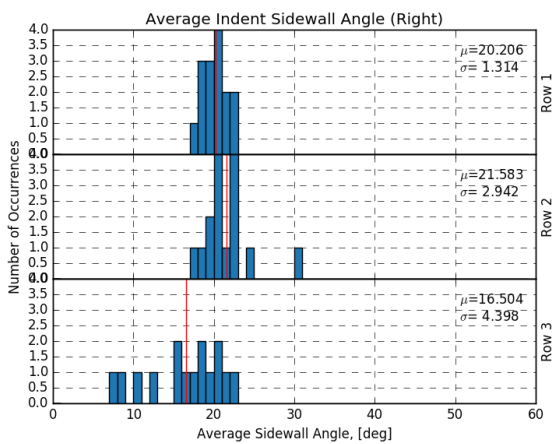
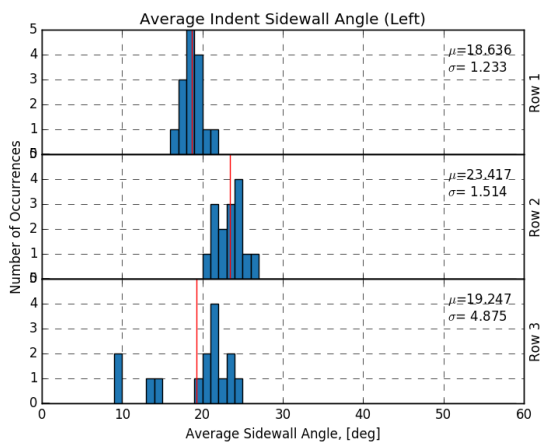
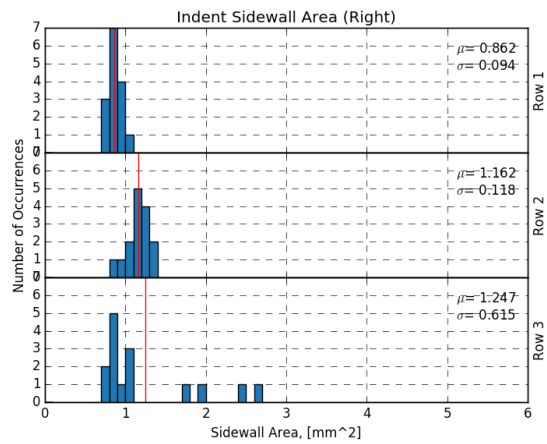
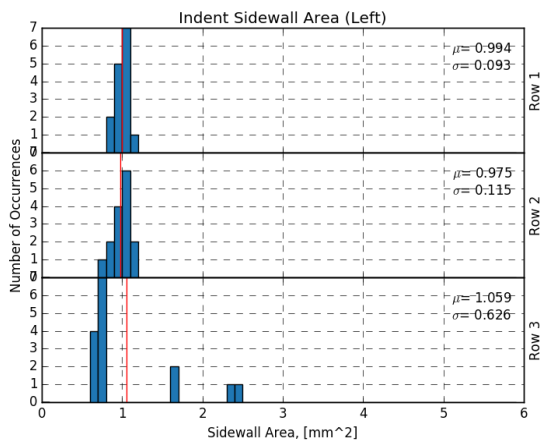
S.W. Area: The average sidewall area of the left and right side of the indents.
S.W. Angle: The average sidewall angle of the left and right side of the indents.



TEST REPORT: INDENT PROFILER

WIRE ID:30-S

PAGE 2/4



TEST REPORT: ASTM A881

WIRE ID:30-S

PAGE 3/4

SAMPLE ID		X3_105mm_Trued_11.16.18
SAMPLE LENGTH [MM]		105
NOMINAL DIAMETER [MM]		5.303
TEST ITEM	STANDARD VALUE	ACTUAL VALUE
INDENT DEPTH [MM]	0.115±0.035	0.105
SIDEWALL ANGLE [DEG]	In Contract	19.9
INDENT LENGTH [MM]	3.5±0.5	3.609
INDENT PITCH [MM]	5.46±0.29	6.35
ORIENTATION ANGLE [DEG]	≥45°	47.6
OUT OF ROUND [MM]	≤0.08	TBD

TEST REPORT: ISO 16120

WIRE ID:30-S

PAGE 4/4

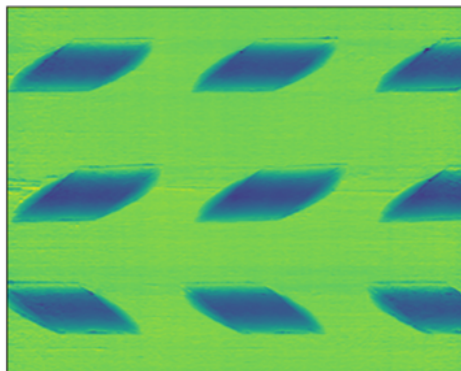
SAMPLE ID		X3_105mm_Trued_11.16.18
SAMPLE LENGTH		105
NOMINAL DIAMETER		5.303
TEST ITEM	STANDARD VALUE	ACTUAL VALUE
INDENT LENGTH [MM]	3.5±0.5	3.609
INDENT DEPTH [MM]	0.15±0.05	0.105
INDENT SPACING [MM]	5.50±0.50	6.35
INDENT DISTANCE [MM]	$\Sigma e \leq 3.343$	5.56, 5.40, 5.40
AVG DIAMETER [MM]	-	TBD
OVALITY	$\leq 0.01 \times D$	TBD

TEST REPORT: INDENT PROFILER

WIRE ID: 30-D

PAGE 1/4

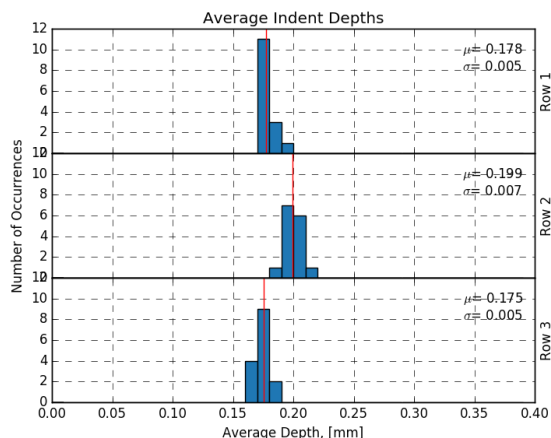
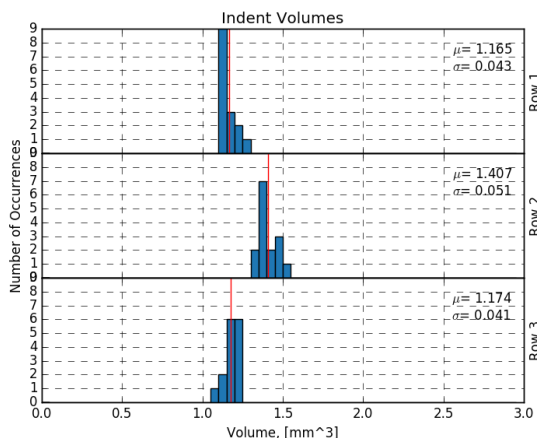
Scan Information				
Wire ID	30-16-T1_105mm_TrueD_11.15.18			
Length [mm]	105			
Scan Date	11.15.18			
Proc Date	09.17.19			
Stat Date	09.17.19			
ID	Indents	Nominal Dia [mm]	Orientation [deg]	Distance [mm]
Total	45	5.254	47.4	5.120
Row 1	15		-49.2	5.135
Row 2	15		44.3	5.112
Row 3	15		48.7	5.112



Indent Data								
ID	Indents	Volume [mm^3]	S.W. Area [mm^2]	Avg Depth [mm]	S.W. Angle [deg]	Avg Length [mm]	Width [mm]	Pitch [mm]
Total	45	1.249	1.582	0.184	21.84	3.730	2.145	6.343
Row 1	15	1.165	1.475	0.178	21.91	3.705	2.091	6.364
Row 2	15	1.407	1.817	0.199	21.82	3.788	2.219	6.329
Row 3	15	1.174	1.453	0.175	21.79	3.696	2.126	6.336

S.W. Area: The average sidewall area of the left and right side of the indents.

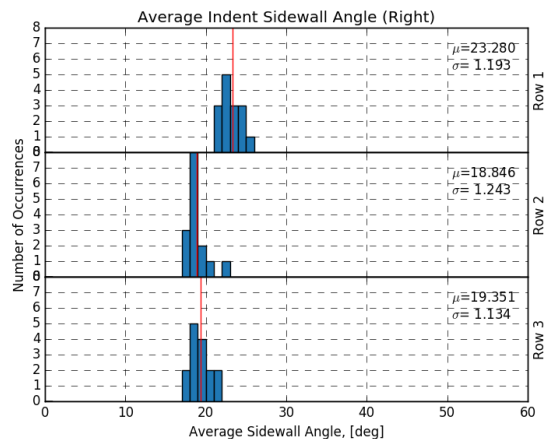
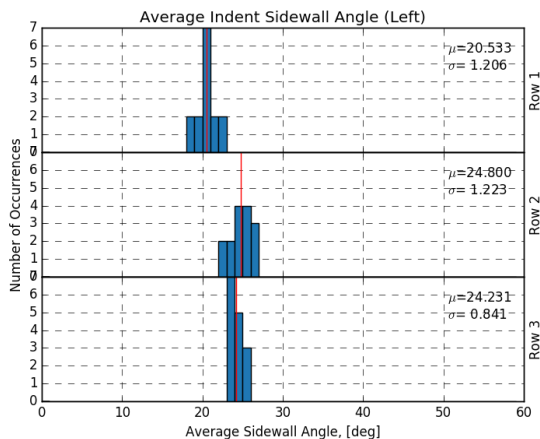
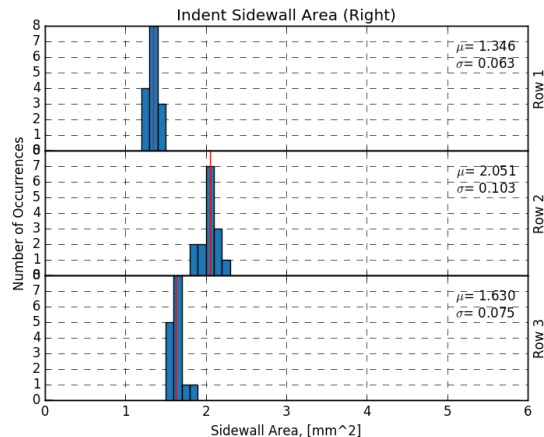
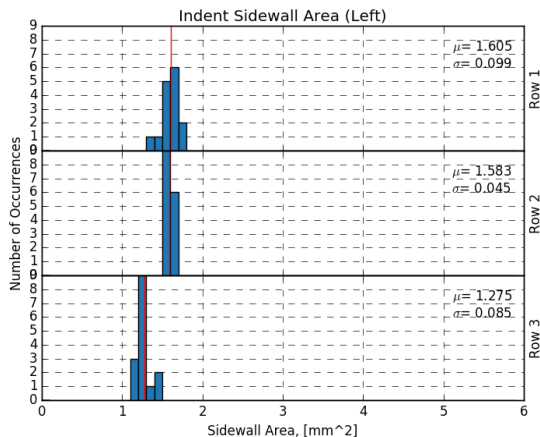
S.W. Angle: The average sidewall angle of the left and right side of the indents.



TEST REPORT: INDENT PROFILER

WIRE ID:30-D

PAGE 2/4



TEST REPORT: ASTM A881

WIRE ID:30-D

PAGE 3/4

SAMPLE ID		30-.16- T1_105mm_Trued_11.15.18
SAMPLE LENGTH [MM]		105
NOMINAL DIAMETER [MM]		5.254
TEST ITEM	STANDARD VALUE	ACTUAL VALUE
INDENT DEPTH [MM]	0.115±0.035	0.184
SIDEWALL ANGLE [DEG]	In Contract	21.8
INDENT LENGTH [MM]	3.5±0.5	4.062
INDENT PITCH [MM]	5.46±0.29	6.34
ORIENTATION ANGLE [DEG]	≥45°	47.4
OUT OF ROUND [MM]	≤0.08	TBD

TEST REPORT: ISO 16120

WIRE ID:30-D

PAGE 4/4

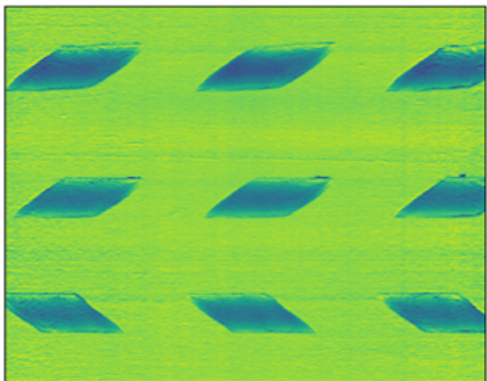
SAMPLE ID		30-.16- T1_105mm_Trued_11.15.18
SAMPLE LENGTH		105
NOMINAL DIAMETER		5.254
TEST ITEM	STANDARD VALUE	ACTUAL VALUE
INDENT LENGTH [MM]	3.5±0.5	4.062
INDENT DEPTH [MM]	0.15±0.05	0.184
INDENT SPACING [MM]	5.50±0.50	6.34
INDENT DISTANCE [MM]	$\Sigma e \leq 3.343$	5.14, 5.11, 5.11
AVG DIAMETER [MM]	-	TBD
OVALITY	$\leq 0.01 \times D$	TBD

TEST REPORT: INDENT PROFILER

WIRE ID: 45-S

PAGE 1/4

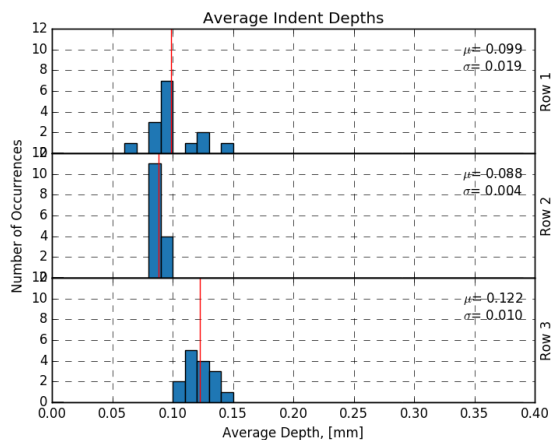
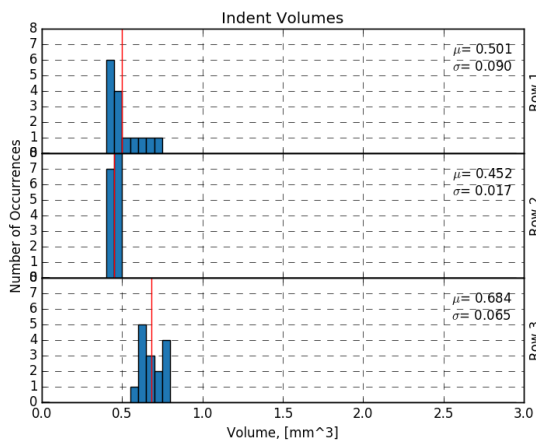
Scan Information					
Wire ID	X5_105mm_Trued_11.16.18				
Length [mm]	105				
Scan Date	11.16.18				
Proc Date	09.17.19				
Stat Date	09.17.19				
ID	Indents	Nominal Dia [mm]	Orientat-ion [deg]	Distance [mm]	
Total	45	5.312	48.1	5.446	
Row 1	15		-44.2	5.490	
Row 2	15		59.8	5.424	
Row 3	15		40.3	5.424	



Indent Data								
ID	Indents	Volume [mm^3]	S.W. Area [mm^2]	Avg Depth [mm]	S.W. Angle [deg]	Avg Length [mm]	Width [mm]	Pitch [mm]
Total	45	0.545	0.951	0.103	23.95	3.311	1.882	6.345
Row 1	15	0.501	0.996	0.099	22.76	3.313	1.855	6.354
Row 2	15	0.452	0.777	0.088	21.65	3.351	1.813	6.343
Row 3	15	0.684	1.081	0.122	27.44	3.268	1.979	6.337

S.W. Area: The average sidewall area of the left and right side of the indents.

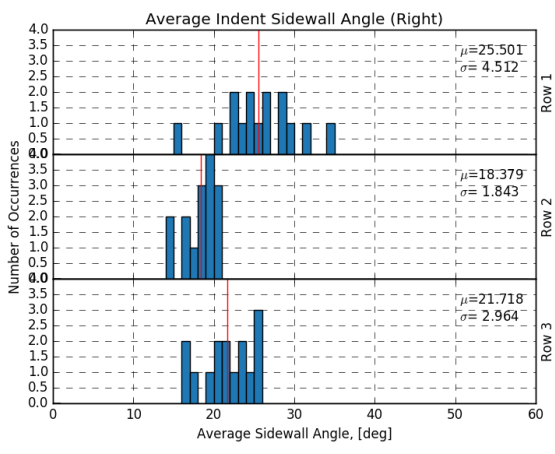
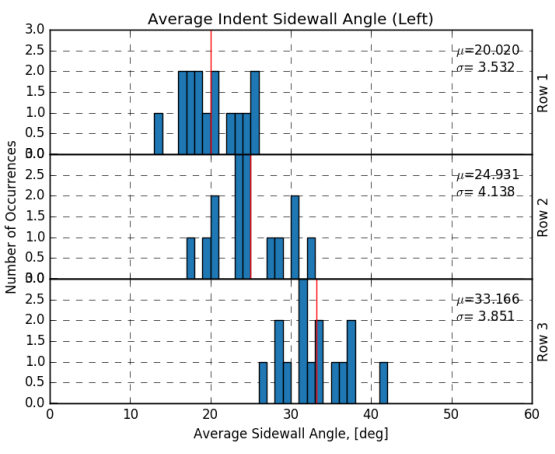
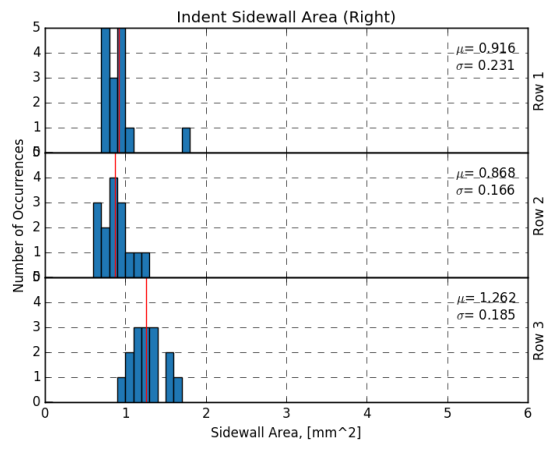
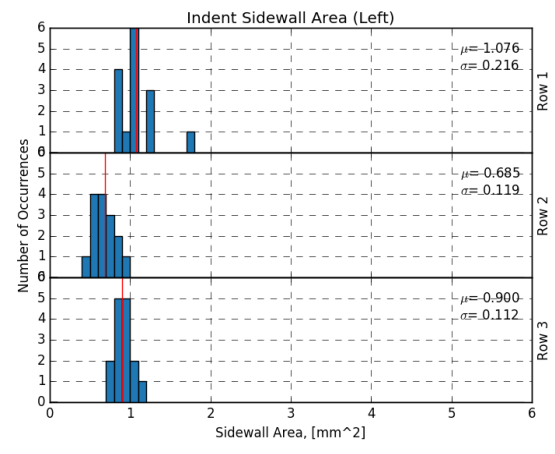
S.W. Angle: The average sidewall angle of the left and right side of the indents.



TEST REPORT: INDENT PROFILER

WIRE ID:45-S

PAGE 2/4



TEST REPORT: ASTM A881

WIRE ID:45-S

PAGE 3/4

SAMPLE ID		X5_105mm_Trued_11.16.18
SAMPLE LENGTH [MM]		105
NOMINAL DIAMETER [MM]		5.312
TEST ITEM	STANDARD VALUE	ACTUAL VALUE
INDENT DEPTH [MM]	0.115±0.035	0.103
SIDEWALL ANGLE [DEG]	In Contract	24.0
INDENT LENGTH [MM]	3.5±0.5	3.172
INDENT PITCH [MM]	5.46±0.29	6.35
ORIENTATION ANGLE [DEG]	≥45°	48.1
OUT OF ROUND [MM]	≤0.08	TBD

TEST REPORT: ISO 16120

WIRE ID:45-S

PAGE 4/4

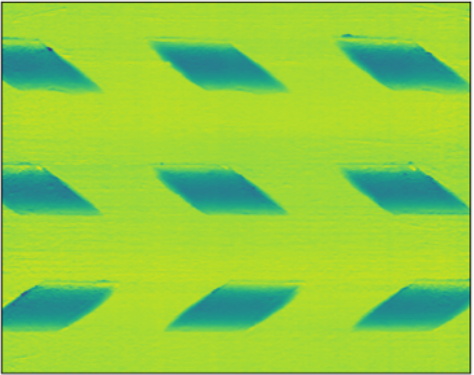
SAMPLE ID		X5_105mm_Trued_11.16.18
SAMPLE LENGTH		105
NOMINAL DIAMETER		5.312
TEST ITEM	STANDARD VALUE	ACTUAL VALUE
INDENT LENGTH [MM]	3.5±0.5	3.172
INDENT DEPTH [MM]	0.15±0.05	0.103
INDENT SPACING [MM]	5.50±0.50	6.35
INDENT DISTANCE [MM]	$\Sigma e \leq 3.343$	5.49, 5.42, 5.42
AVG DIAMETER [MM]	-	TBD
OVALITY	$\leq 0.01 \times D$	TBD

TEST REPORT: INDENT PROFILER

WIRE ID: 45-D

PAGE 1/4

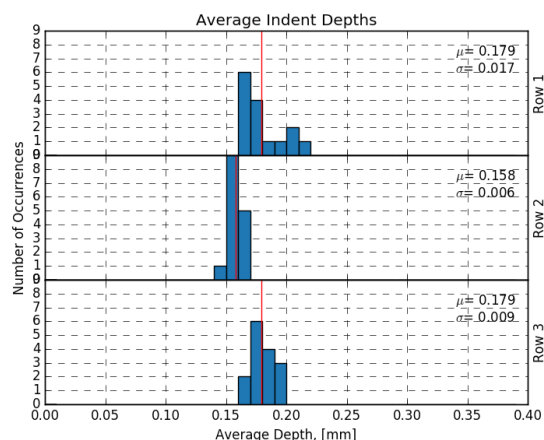
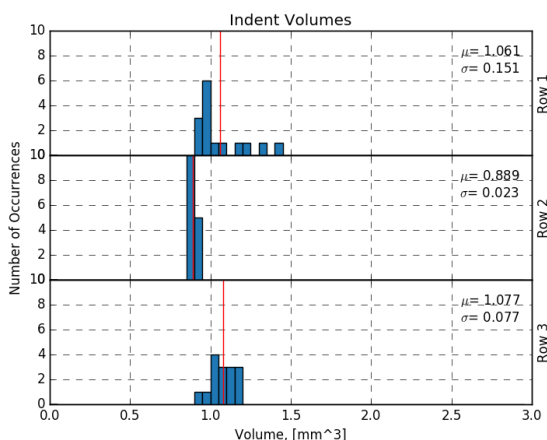
Scan Information					
Wire ID		45-16-T2_105mm_TrueD_11.15.18			
Length [mm]		105			
Scan Date		11.15.18			
Proc Date		9.17.19			
Stat Date		9.17.19			
ID	Indents	Nominal Dia [mm]	Orientat-ion [deg]	Distance [mm]	
Total	45	5.255	47.0	5.192	
Row 1	15		46.6	5.240	
Row 2	15		-47.4	5.168	
Row 3	15		-47.1	5.168	



Indent Data								
ID	Indents	Volume [mm^3]	S.W. Area [mm^2]	Avg Depth [mm]	S.W. Angle [deg]	Avg Length [mm]	Width [mm]	Pitch [mm]
Total	45	1.009	1.066	0.172	30.19	3.255	2.070	6.354
Row 1	15	1.061	1.046	0.179	31.12	3.307	2.023	6.336
Row 2	15	0.889	0.993	0.158	28.67	3.222	2.035	6.362
Row 3	15	1.077	1.159	0.179	30.76	3.237	2.152	6.364

S.W. Area: The average sidewall area of the left and right side of the indents.

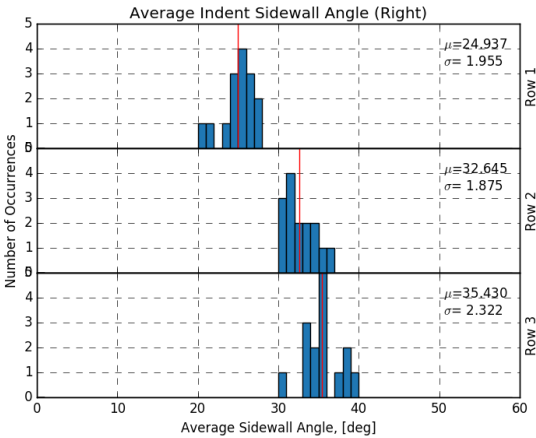
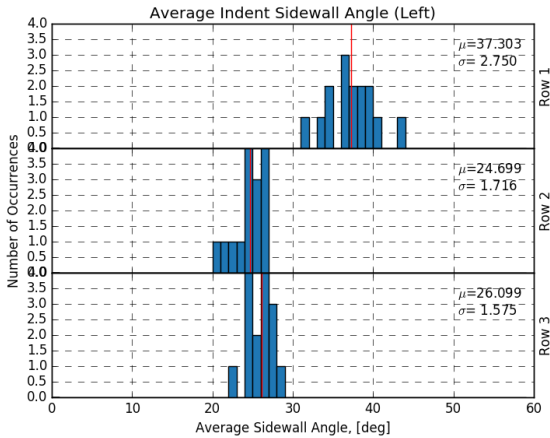
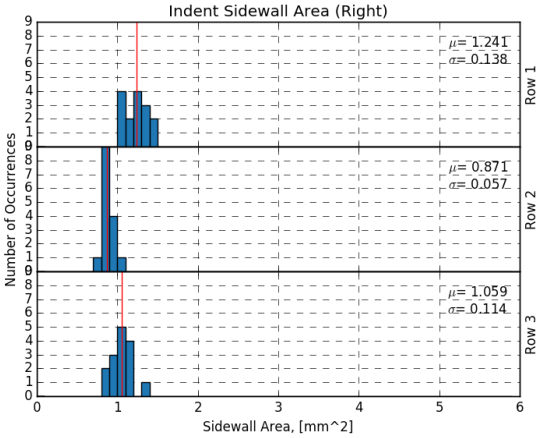
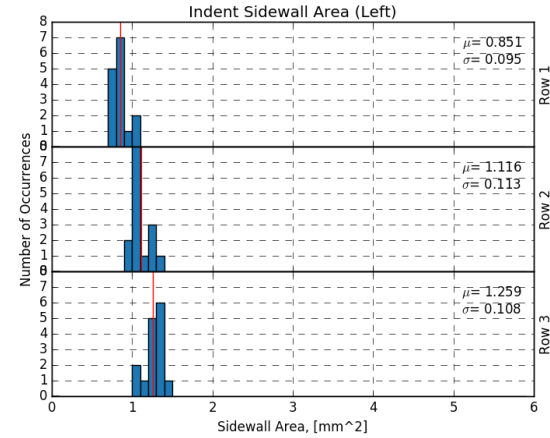
S.W. Angle: The average sidewall angle of the left and right side of the indents.



TEST REPORT: INDENT PROFILER

WIRE ID:45-D

PAGE 2/4



TEST REPORT: ASTM A881

WIRE ID:45-D

PAGE 3/4

SAMPLE ID		45-.16- T2_105mm_Trued_11.15.18
SAMPLE LENGTH [MM]		105
NOMINAL DIAMETER [MM]		5.255
TEST ITEM	STANDARD VALUE	ACTUAL VALUE
INDENT DEPTH [MM]	0.115±0.035	0.172
SIDEWALL ANGLE [DEG]	In Contract	30.2
INDENT LENGTH [MM]	3.5±0.5	3.370
INDENT PITCH [MM]	5.46±0.29	6.35
ORIENTATION ANGLE [DEG]	≥45°	47.0
OUT OF ROUND [MM]	≤0.08	TBD

TEST REPORT: ISO 16120

WIRE ID:45-D

PAGE 4/4

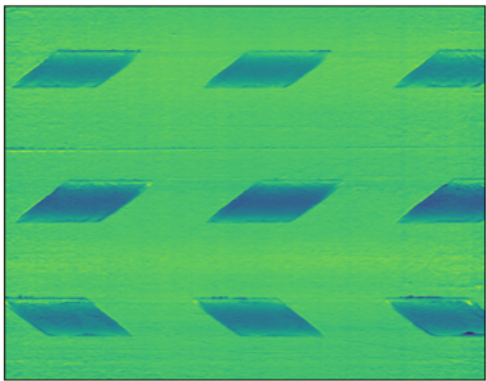
SAMPLE ID		45-.16- T2_105mm_TrueD_11.15.18
SAMPLE LENGTH		105
NOMINAL DIAMETER		5.255
TEST ITEM	STANDARD VALUE	ACTUAL VALUE
INDENT LENGTH [MM]	3.5±0.5	3.370
INDENT DEPTH [MM]	0.15±0.05	0.172
INDENT SPACING [MM]	5.50±0.50	6.35
INDENT DISTANCE [MM]	$\Sigma e \leq 3.343$	5.24, 5.17, 5.17
AVG DIAMETER [MM]	-	TBD
OVALITY	$\leq 0.01 \times D$	TBD

TEST REPORT: INDENT PROFILER

WIRE ID: 60-S

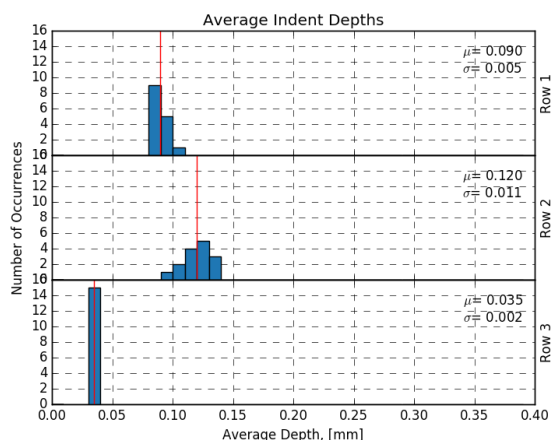
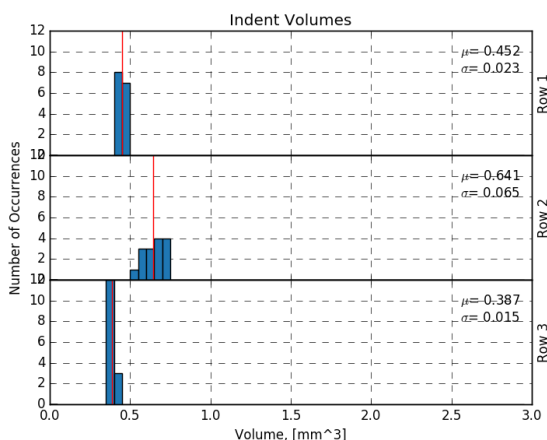
PAGE 1/4

Scan Information					
Wire ID	X4_105mm_Trued_11.16.18				
Length [mm]	105				
Scan Date	11.16.18				
Proc Date	09.17.19				
Stat Date	09.17.19				
ID	Indents	Nominal Dia [mm]	Orientat-ion [deg]	Distance [mm]	
Total	45	5.300	48.3	4.839	
Row 1	15		-44.1	5.532	
Row 2	15		50.9	4.493	
Row 3	15		49.9	4.493	



Indent Data								
ID	Indents	Volume [mm^3]	S.W. Area [mm^2]	Avg Depth [mm]	S.W. Angle [deg]	Avg Length [mm]	Width [mm]	Pitch [mm]
Total	45	0.493	1.390	0.082	22.42	3.641	2.525	6.347
Row 1	15	0.452	0.859	0.090	24.16	3.326	1.808	6.369
Row 2	15	0.641	0.732	0.120	34.55	3.300	1.883	6.338
Row 3	15	0.387	2.579	0.035	8.54	4.296	3.885	6.334

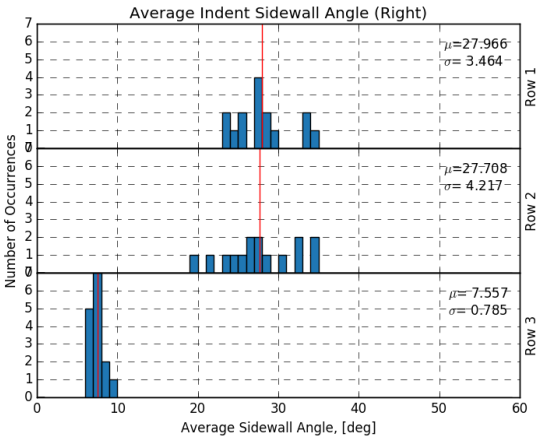
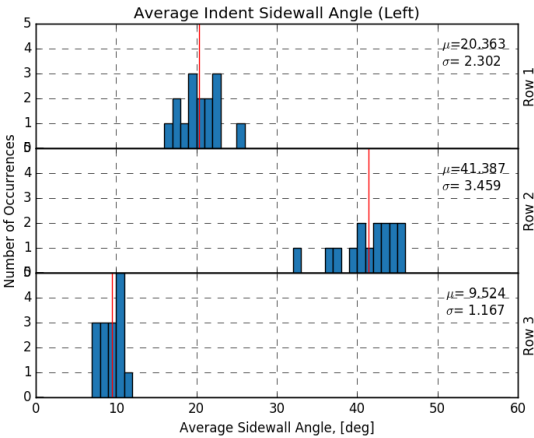
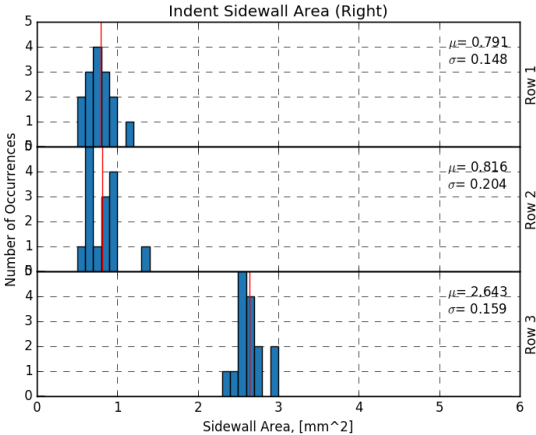
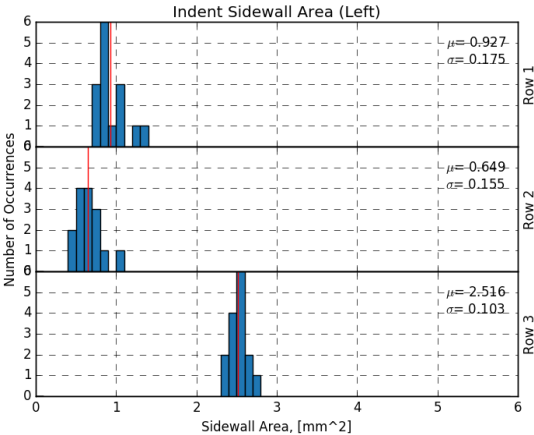
S.W. Area: The average sidewall area of the left and right side of the indents.
S.W. Angle: The average sidewall angle of the left and right side of the indents.



TEST REPORT: INDENT PROFILER

WIRE ID: 60-S

PAGE 2/4



TEST REPORT: ASTM A881

WIRE ID:60-S

PAGE 3/4

SAMPLE ID		X4_105mm_Trued_11.16.18
SAMPLE LENGTH [MM]		105
NOMINAL DIAMETER [MM]		5.300
TEST ITEM	STANDARD VALUE	ACTUAL VALUE
INDENT DEPTH [MM]	0.115±0.035	0.082
SIDEWALL ANGLE [DEG]	In Contract	22.4
INDENT LENGTH [MM]	3.5±0.5	3.204
INDENT PITCH [MM]	5.46±0.29	6.35
ORIENTATION ANGLE [DEG]	≥45°	48.3
OUT OF ROUND [MM]	≤0.08	TBD

TEST REPORT: ISO 16120

WIRE ID:60-S

PAGE 4/4

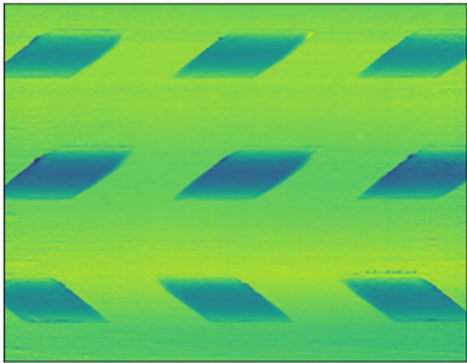
SAMPLE ID		X4_105mm_Trued_11.16.18
SAMPLE LENGTH		105
NOMINAL DIAMETER		5.300
TEST ITEM	STANDARD VALUE	ACTUAL VALUE
INDENT LENGTH [MM]	3.5±0.5	3.204
INDENT DEPTH [MM]	0.15±0.05	0.082
INDENT SPACING [MM]	5.50±0.50	6.35
INDENT DISTANCE [MM]	$\Sigma e \leq 3.343$	5.53, 4.49, 4.49
AVG DIAMETER [MM]	-	TBD
OVALITY	$\leq 0.01 \times D$	TBD

TEST REPORT: INDENT PROFILER

WIRE ID: 60-D

PAGE 1/4

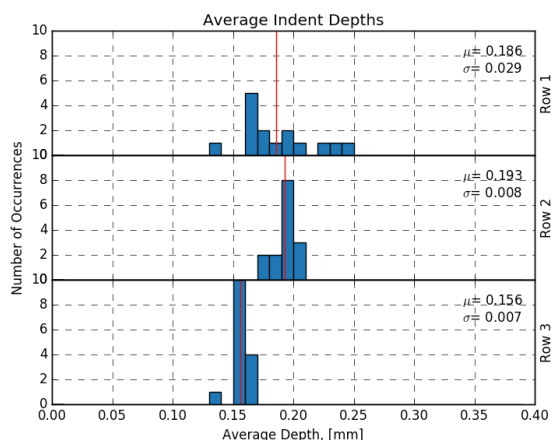
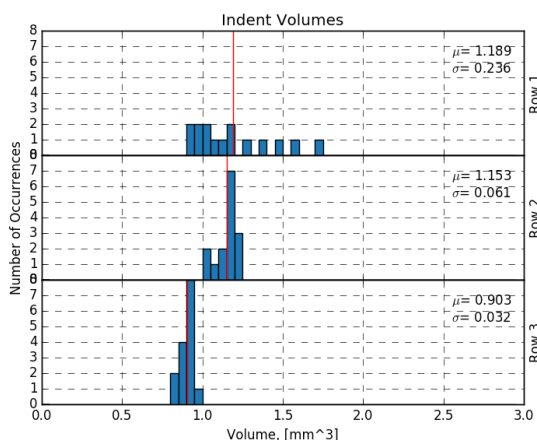
Scan Information				
Wire ID	60-16-T1_105mm_TrueD_11.15.18			
Length [mm]	105			
Scan Date	11.15.18			
Proc Date	09.17.19			
Stat Date	09.17.19			
ID	Indents	Nominal Dia [mm]	Orientat-ion [deg]	Distance [mm]
Total	45	5.236	47.9	5.182
Row 1	15		-50.1	5.103
Row 2	15		47.0	5.222
Row 3	15		46.5	5.222



Indent Data								
ID	Indents	Volume [mm^3]	S.W. Area [mm^2]	Avg Depth [mm]	S.W. Angle [deg]	Avg Length [mm]	Width [mm]	Pitch [mm]
Total	45	1.082	0.872	0.178	43.14	3.205	2.107	6.343
Row 1	15	1.189	0.956	0.186	42.15	3.216	2.239	6.365
Row 2	15	1.153	0.842	0.193	46.84	3.192	2.087	6.330
Row 3	15	0.903	0.818	0.156	40.41	3.208	1.995	6.334

S.W. Area: The average sidewall area of the left and right side of the indents.

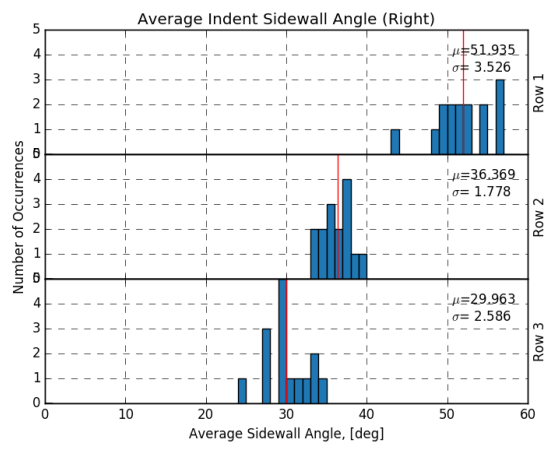
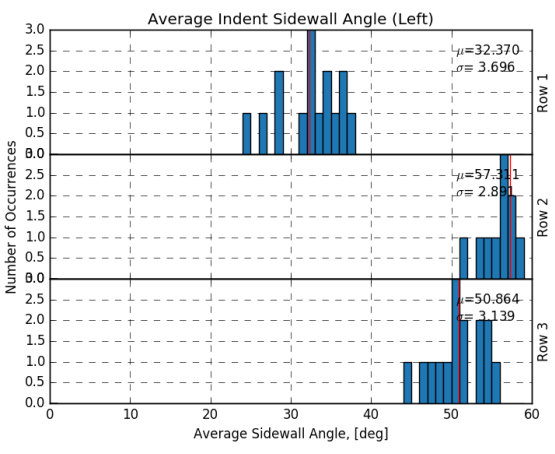
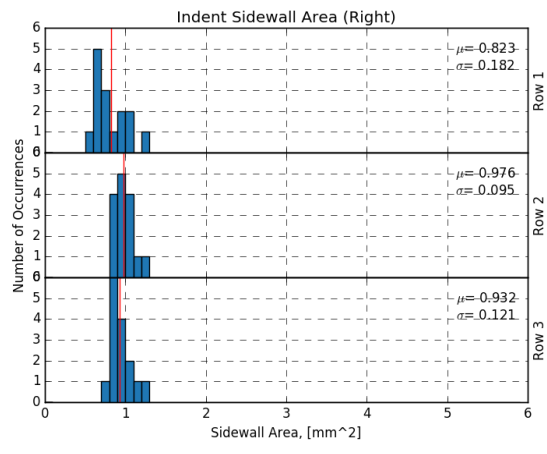
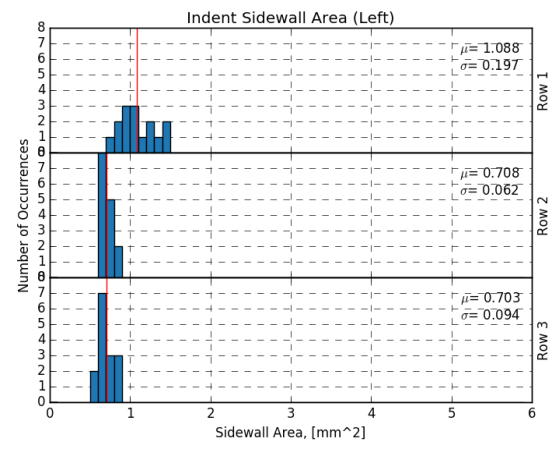
S.W. Angle: The average sidewall angle of the left and right side of the indents.



TEST REPORT: INDENT PROFILER

WIRE ID: 60-D

PAGE 2/4



TEST REPORT: ASTM A881

WIRE ID: 60-D

PAGE 3/4

SAMPLE ID		60-.16- T1_105mm_Trued_11.15.18
SAMPLE LENGTH [MM]		105
NOMINAL DIAMETER [MM]		5.236
TEST ITEM	STANDARD VALUE	ACTUAL VALUE
INDENT DEPTH [MM]	0.115±0.035	0.178
SIDEWALL ANGLE [DEG]	In Contract	43.1
INDENT LENGTH [MM]	3.5±0.5	3.225
INDENT PITCH [MM]	5.46±0.29	6.34
ORIENTATION ANGLE [DEG]	≥45°	47.9
OUT OF ROUND [MM]	≤0.08	TBD

TEST REPORT: ISO 16120

WIRE ID:60-D

PAGE 4/4

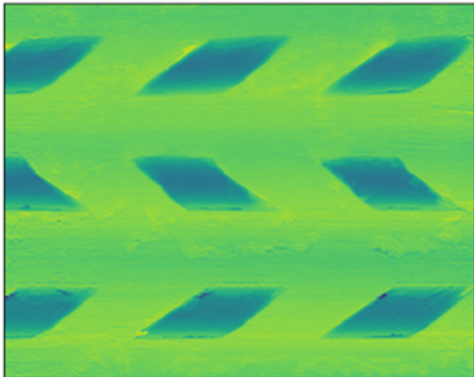
SAMPLE ID		60-.16- T1_105mm_Trued_11.15.18
SAMPLE LENGTH		105
NOMINAL DIAMETER		5.236
TEST ITEM	STANDARD VALUE	ACTUAL VALUE
INDENT LENGTH [MM]	3.5±0.5	3.225
INDENT DEPTH [MM]	0.15±0.05	0.178
INDENT SPACING [MM]	5.50±0.50	6.34
INDENT DISTANCE [MM]	$\Sigma e \leq 3.343$	5.10, 5.22, 5.22
AVG DIAMETER [MM]	-	TBD
OVALITY	$\leq 0.01 \times D$	TBD

TEST REPORT: INDENT PROFILER

WIRE ID: 75-S

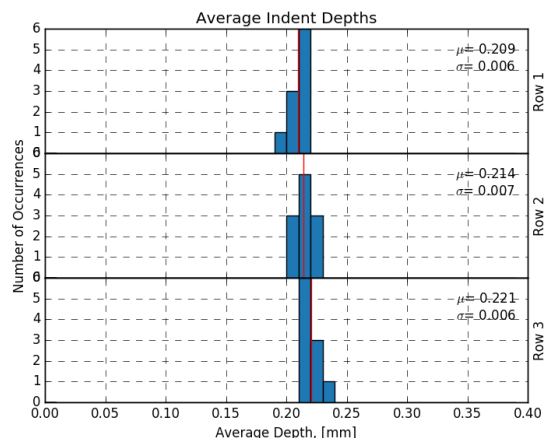
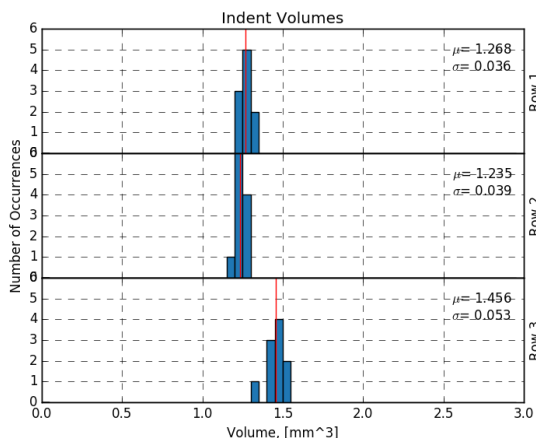
PAGE 1/4

Scan Information				
Wire ID	X2_105mm_TrueD_11.16.18			
Length [mm]	105			
Scan Date	11.16.18			
Proc Date	09.17.19			
Stat Date	09.17.19			
ID	Indents	Nominal Dia [mm]	Orientat-ion [deg]	Distance [mm]
Total	31	5.263	44.5	4.978
Row 1	10		41.9	5.048
Row 2	11		-50.7	4.942
Row 3	10		40.8	4.942



Indent Data								
ID	Indents	Volume [mm^3]	S.W. Area [mm^2]	Avg Depth [mm]	S.W. Angle [deg]	Avg Length [mm]	Width [mm]	Pitch [mm]
Total	31	1.317	1.365	0.215	34.93	3.125	2.296	6.343
Row 1	10	1.268	1.330	0.209	36.35	3.164	2.220	6.331
Row 2	11	1.235	1.190	0.214	35.17	3.054	2.242	6.365
Row 3	10	1.456	1.593	0.221	33.23	3.164	2.430	6.330

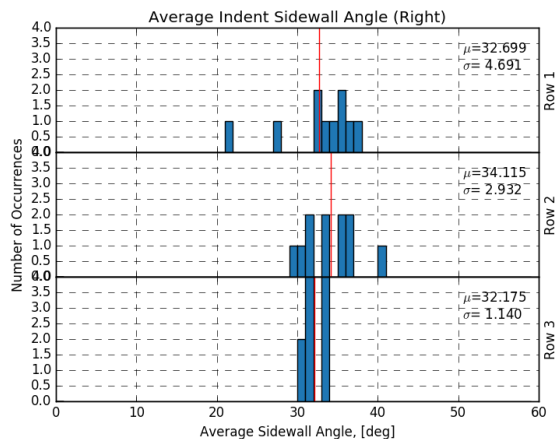
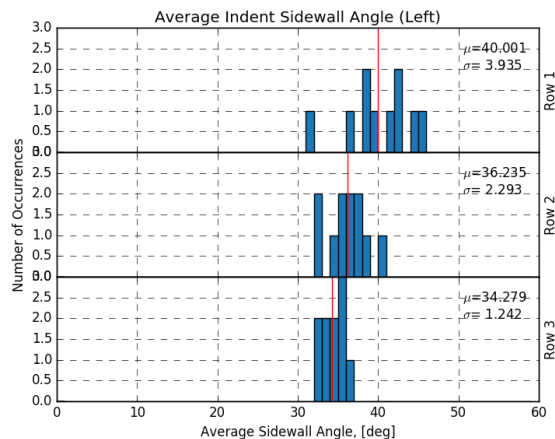
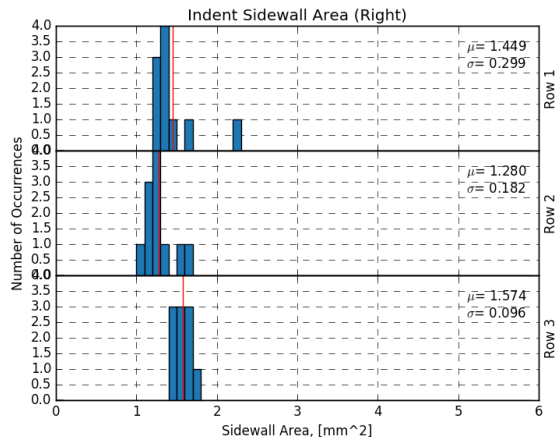
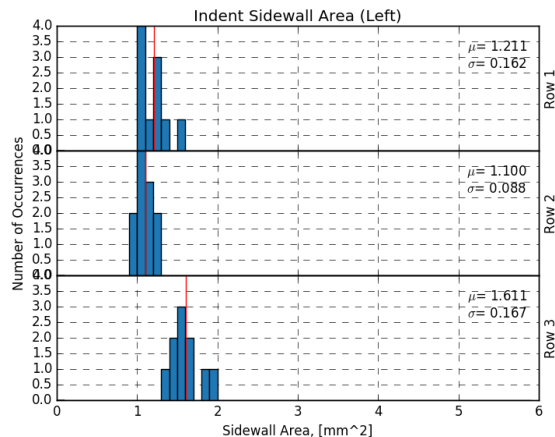
S.W. Area: The average sidewall area of the left and right side of the indents.
S.W. Angle: The average sidewall angle of the left and right side of the indents.



TEST REPORT: INDENT PROFILER

WIRE ID:75-S

PAGE 2/4



TEST REPORT: ASTM A881

WIRE ID:75-S

PAGE 3/4

SAMPLE ID		X2_105mm_Trued_11.16.18
SAMPLE LENGTH [MM]		105
NOMINAL DIAMETER [MM]		5.263
TEST ITEM	STANDARD VALUE	ACTUAL VALUE
INDENT DEPTH [MM]	0.115±0.035	0.215
SIDEWALL ANGLE [DEG]	In Contract	34.9
INDENT LENGTH [MM]	3.5±0.5	3.111
INDENT PITCH [MM]	5.46±0.29	6.34
ORIENTATION ANGLE [DEG]	≥45°	44.5
OUT OF ROUND [MM]	≤0.08	TBD

TEST REPORT: ISO 16120

WIRE ID:75-S

PAGE 4/4

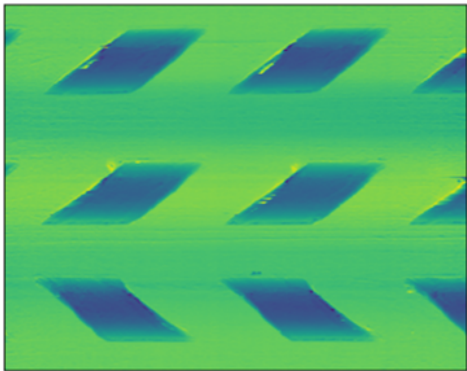
SAMPLE ID		X2_105mm_Trued_11.16.18
SAMPLE LENGTH		105
NOMINAL DIAMETER		5.263
TEST ITEM	STANDARD VALUE	ACTUAL VALUE
INDENT LENGTH [MM]	3.5±0.5	3.111
INDENT DEPTH [MM]	0.15±0.05	0.215
INDENT SPACING [MM]	5.50±0.50	6.34
INDENT DISTANCE [MM]	$\Sigma e \leq 3.343$	5.05, 4.94, 4.94
AVG DIAMETER [MM]	-	TBD
OVALITY	$\leq 0.01 \times D$	TBD

TEST REPORT: INDENT PROFILER

WIRE ID: 75-D

PAGE 1/4

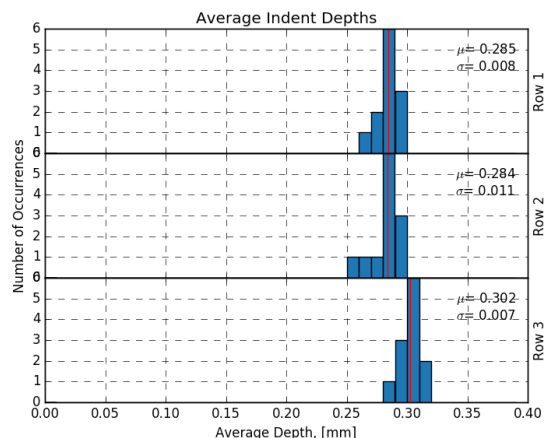
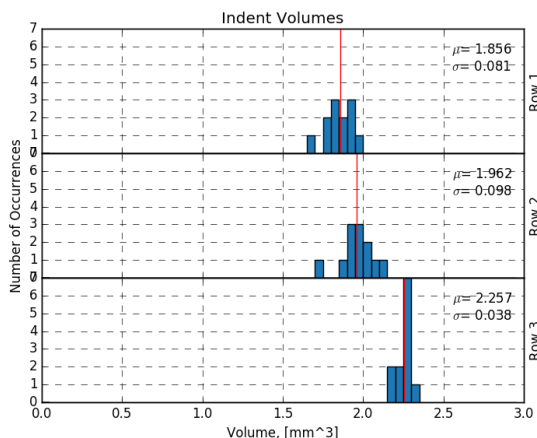
Scan Information					
Wire ID	75-16-T1_105mm_TrueD_11.15.18				
Length [mm]	105				
Scan Date	11.15.18				
Proc Date	09.17.19				
Stat Date	09.17.19				
ID	Indents	Nominal Dia [mm]	Orientat-ion [deg]	Distance [mm]	
Total	36	5.182	46.9	4.673	
Row 1	12		-48.1	4.714	
Row 2	12		48.3	4.653	
Row 3	12		44.4	4.653	



Indent Data								
ID	Indents	Volume [mm^3]	S.W. Area [mm^2]	Avg Depth [mm]	S.W. Angle [deg]	Avg Length [mm]	Width [mm]	Pitch [mm]
Total	36	2.025	1.408	0.290	49.27	3.128	2.536	6.346
Row 1	12	1.856	1.331	0.285	49.50	3.029	2.492	6.370
Row 2	12	1.962	1.354	0.284	48.31	3.125	2.506	6.337
Row 3	12	2.257	1.540	0.302	50.02	3.232	2.611	6.333

S.W. Area: The average sidewall area of the left and right side of the indents.

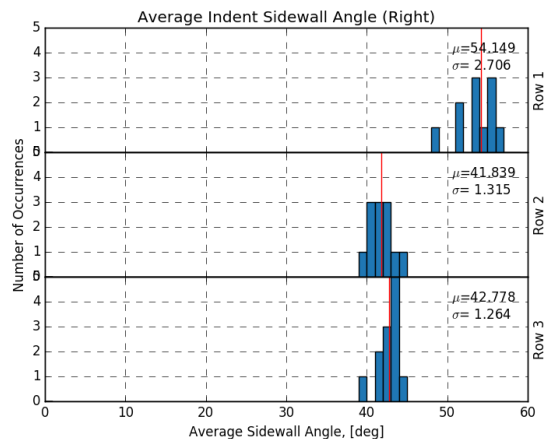
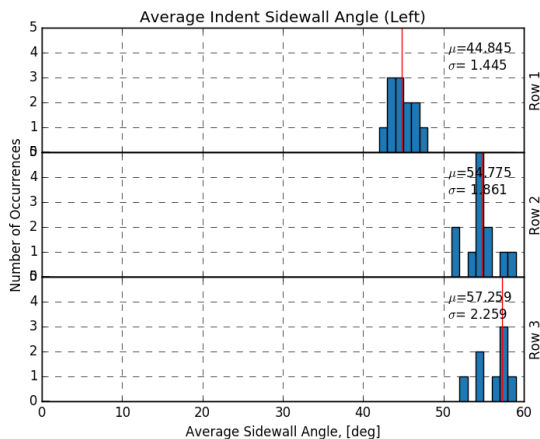
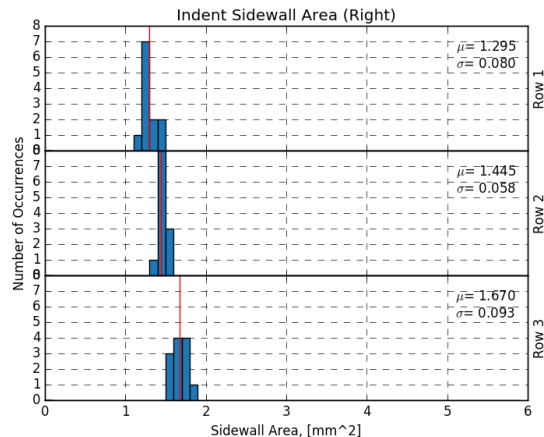
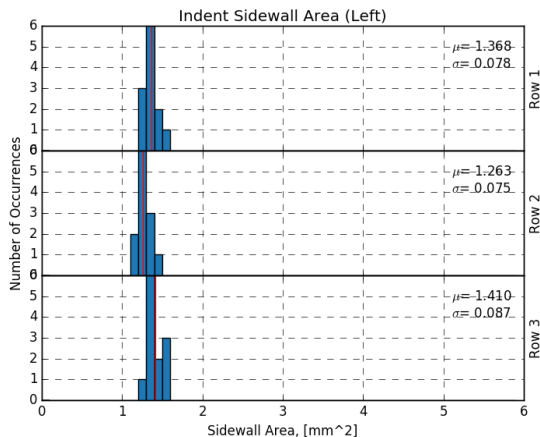
S.W. Angle: The average sidewall angle of the left and right side of the indents.



TEST REPORT: INDENT PROFILER

WIRE ID:75-D

PAGE 2/4



TEST REPORT: ASTM A881

WIRE ID:75-D

PAGE 3/4

SAMPLE ID		75-.16- T1_105mm_Trued_11.15.18
SAMPLE LENGTH [MM]		105
NOMINAL DIAMETER [MM]		5.182
TEST ITEM	STANDARD VALUE	ACTUAL VALUE
INDENT DEPTH [MM]	0.115±0.035	0.290
SIDEWALL ANGLE [DEG]	In Contract	49.3
INDENT LENGTH [MM]	3.5±0.5	3.134
INDENT PITCH [MM]	5.46±0.29	6.346
ORIENTATION ANGLE [DEG]	≥45°	46.9
OUT OF ROUND [MM]	≤0.08	TBD

TEST REPORT: ISO 16120

WIRE ID:75-D

PAGE 4/4


SAMPLE ID		75-.16- T1_105mm_TrueD_11.15.18
SAMPLE LENGTH		105
NOMINAL DIAMETER		5.182
TEST ITEM	STANDARD VALUE	ACTUAL VALUE
INDENT LENGTH [MM]	3.5±0.5	3.134
INDENT DEPTH [MM]	0.15±0.05	0.290
INDENT SPACING [MM]	5.50±0.50	6.35
INDENT DISTANCE [MM]	$\Sigma e \leq 3.343$	4.71, 4.65, 4.65
AVG DIAMETER [MM]	-	TBD
OVALITY	$\leq 0.01 \times D$	TBD

TEST REPORT: INDENT PROFILER

WIRE ID: 90-S

PAGE 1/4

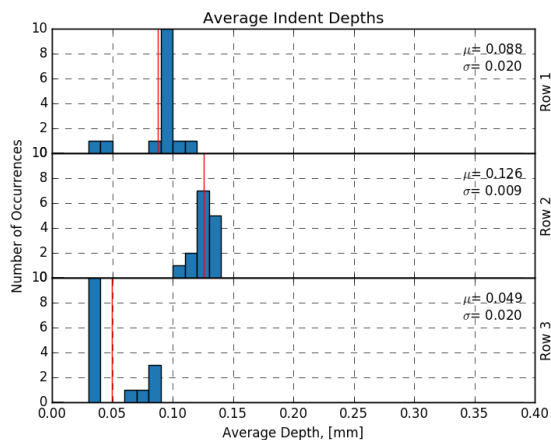
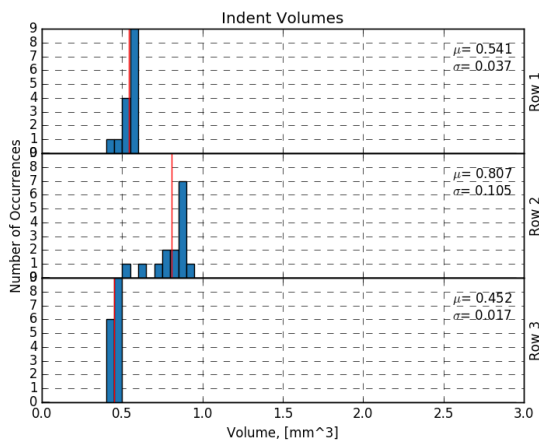
Scan Information				
Wire ID	X1_105mm_Trued_11.16.18			
Length [mm]	105			
Scan Date	11.16.18			
Proc Date	09.17.19			
Stat Date	09.17.19			
ID	Indents	Nominal Dia [mm]	Orientation [deg]	Distance [mm]
Total	45	5.296	44.9	4.890
Row 1	15		50.9	5.292
Row 2	15		43.3	4.689
Row 3	15		-40.6	4.689



Indent Data								
ID	Indents	Volume [mm ³]	S.W. Area [mm ²]	Avg Depth [mm]	S.W. Angle [deg]	Avg Length [mm]	Width [mm]	Pitch [mm]
Total	45	0.600	1.437	0.088	22.96	3.968	2.402	6.342
Row 1	15	0.541	1.052	0.088	24.05	3.863	2.087	6.326
Row 2	15	0.807	0.920	0.126	31.50	3.744	1.934	6.333
Row 3	15	0.452	2.340	0.049	13.35	4.298	3.184	6.366

S.W. Area: The average sidewall area of the left and right side of the indents.

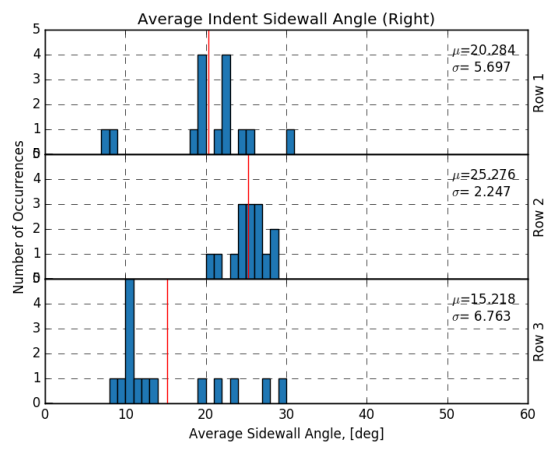
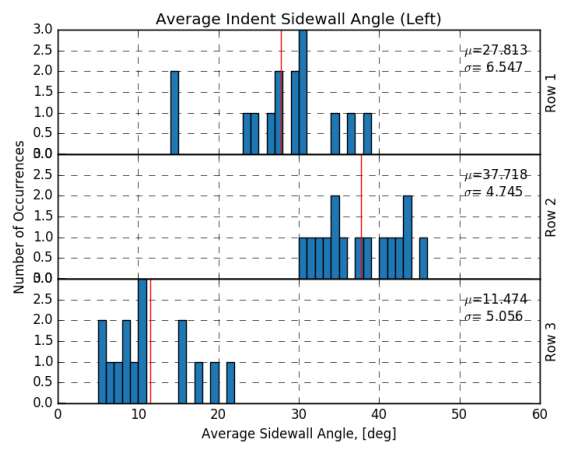
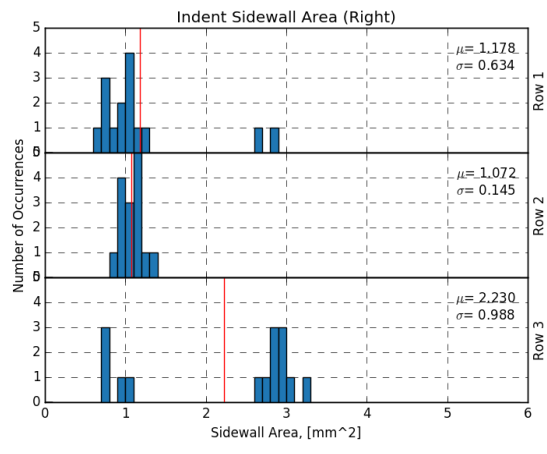
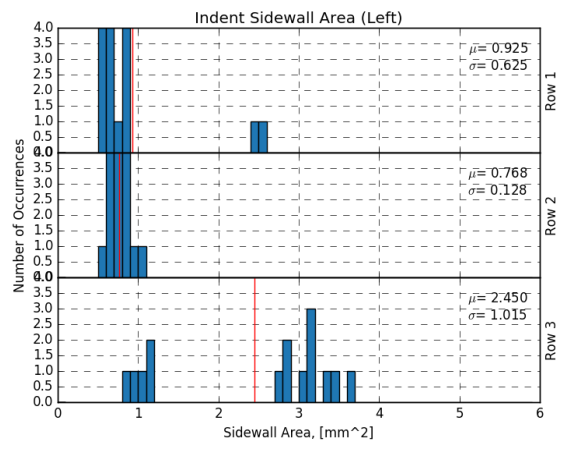
S.W. Angle: The average sidewall angle of the left and right side of the indents.



TEST REPORT: INDENT PROFILER

WIRE ID:90-S

PAGE 2/4



TEST REPORT: ASTM A881

WIRE ID:90-S

PAGE 3/4

SAMPLE ID		X1_105mm_Trued_11.16.18
SAMPLE LENGTH [MM]		105
NOMINAL DIAMETER [MM]		5.296
TEST ITEM	STANDARD VALUE	ACTUAL VALUE
INDENT DEPTH [MM]	0.115±0.035	0.088
SIDEWALL ANGLE [DEG]	In Contract	23.0
INDENT LENGTH [MM]	3.5±0.5	3.731
INDENT PITCH [MM]	5.46±0.29	6.34
ORIENTATION ANGLE [DEG]	≥45°	44.9
OUT OF ROUND [MM]	≤0.08	TBD

TEST REPORT: ISO 16120

WIRE ID:90-S

PAGE 4/4

SAMPLE ID		X1_105mm_Trued_11.16.18
SAMPLE LENGTH		105
NOMINAL DIAMETER		5.296
TEST ITEM	STANDARD VALUE	ACTUAL VALUE
INDENT LENGTH [MM]	3.5±0.5	3.731
INDENT DEPTH [MM]	0.15±0.05	0.088
INDENT SPACING [MM]	5.50±0.50	6.34
INDENT DISTANCE [MM]	$\Sigma e \leq 3.343$	5.29, 4.69, 4.69
AVG DIAMETER [MM]	-	TBD
OVALITY	$\leq 0.01 \times D$	TBD

TEST REPORT: INDENT PROFILER

WIRE ID: 90-D

PAGE 1/4

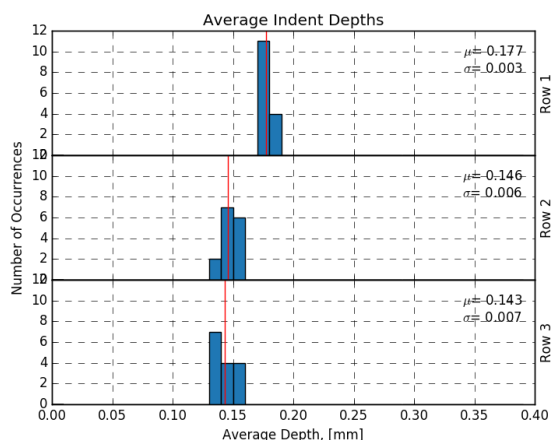
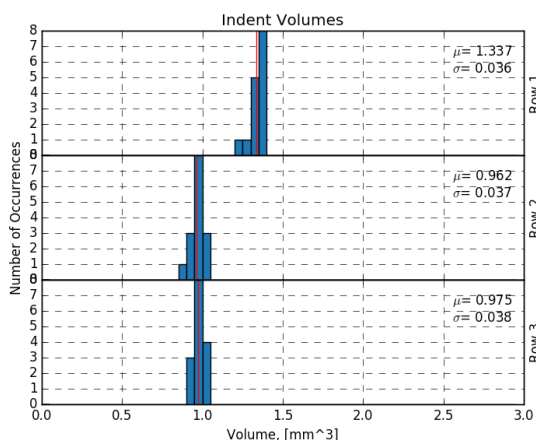
Scan Information				
Wire ID	90-.16-T3_105mm_Trued_11.15.18			
Length [mm]	105			
Scan Date	11.15.18			
Proc Date	09.17.19			
Stat Date	09.17.19			
ID	Indents	Nominal Dia [mm]	Orientat-ion [deg]	Distance [mm]
Total	45	5.264	47.9	5.250
Row 1	15		46.0	5.215
Row 2	15		-52.6	5.268
Row 3	15		45.1	5.268

Not Available

Indent Data								
ID	Indents	Volume [mm^3]	S.W. Area [mm^2]	Avg Depth [mm]	S.W. Angle [deg]	Avg Length [mm]	Width [mm]	Pitch [mm]
Total	45	1.091	1.030	0.156	32.43	3.817	2.069	6.343
Row 1	15	1.337	1.167	0.177	32.70	3.862	2.189	6.333
Row 2	15	0.962	0.886	0.146	32.63	3.823	1.945	6.365
Row 3	15	0.975	1.037	0.143	31.97	3.767	2.072	6.331

S.W. Area: The average sidewall area of the left and right side of the indents.

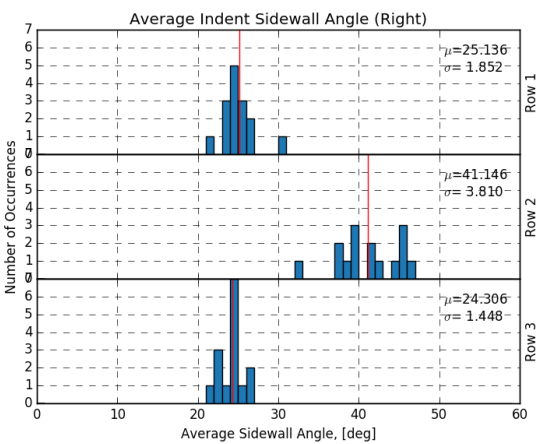
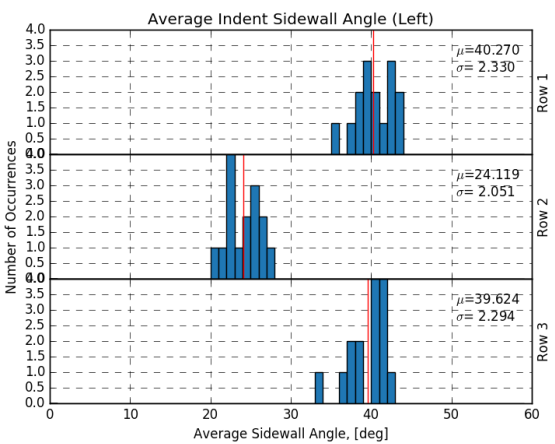
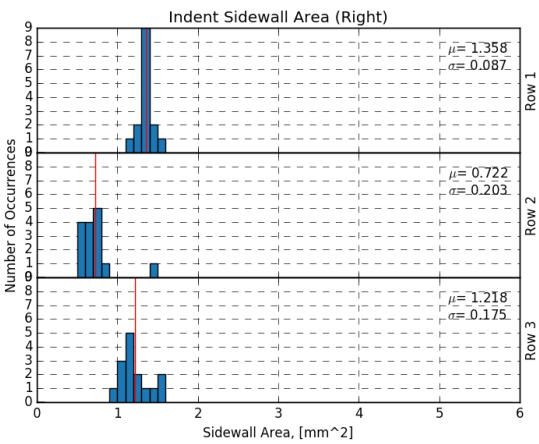
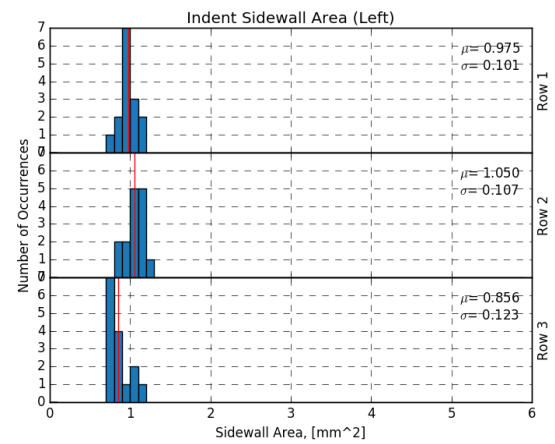
S.W. Angle: The average sidewall angle of the left and right side of the indents.



TEST REPORT: INDENT PROFILER

WIRE ID: 90-D

PAGE 2/4



TEST REPORT: ASTM A881

WIRE ID: 90-D

PAGE 3/4

SAMPLE ID		90-.16- T3_105mm_TrueD_11.15.18
SAMPLE LENGTH [MM]		105
NOMINAL DIAMETER [MM]		5.264
TEST ITEM	STANDARD VALUE	ACTUAL VALUE
INDENT DEPTH [MM]	0.115±0.035	0.156
SIDEWALL ANGLE [DEG]	In Contract	32.4
INDENT LENGTH [MM]	3.5±0.5	3.921
INDENT PITCH [MM]	5.46±0.29	6.34
ORIENTATION ANGLE [DEG]	≥45°	47.9
OUT OF ROUND [MM]	≤0.08	TBD

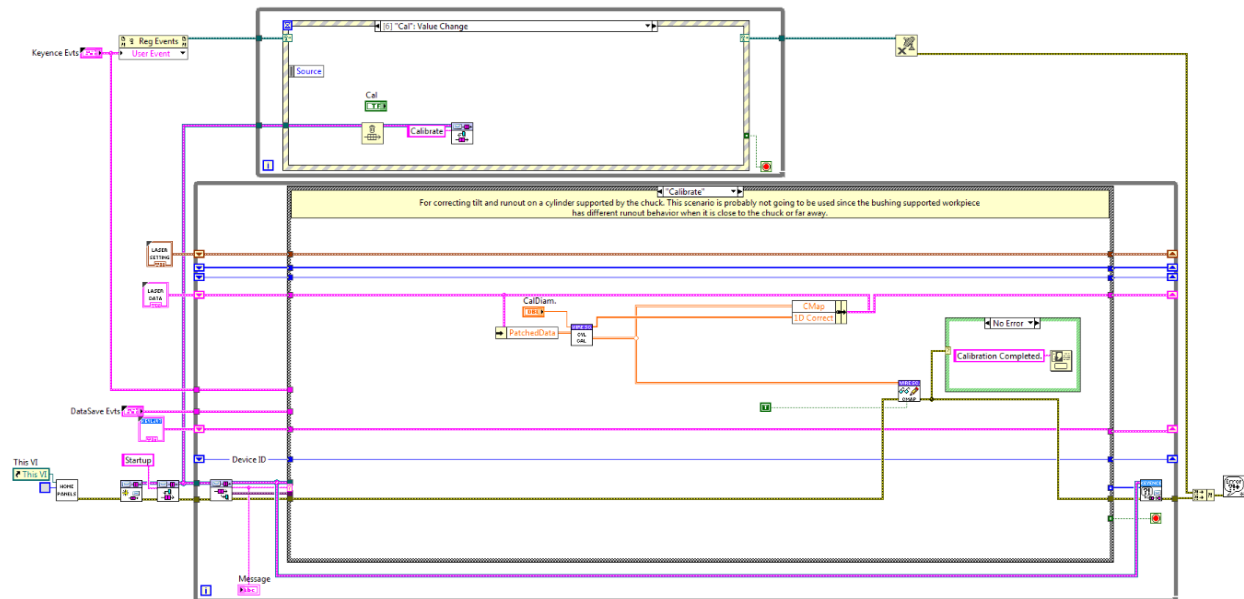
TEST REPORT: ISO 16120

WIRE ID:90-D

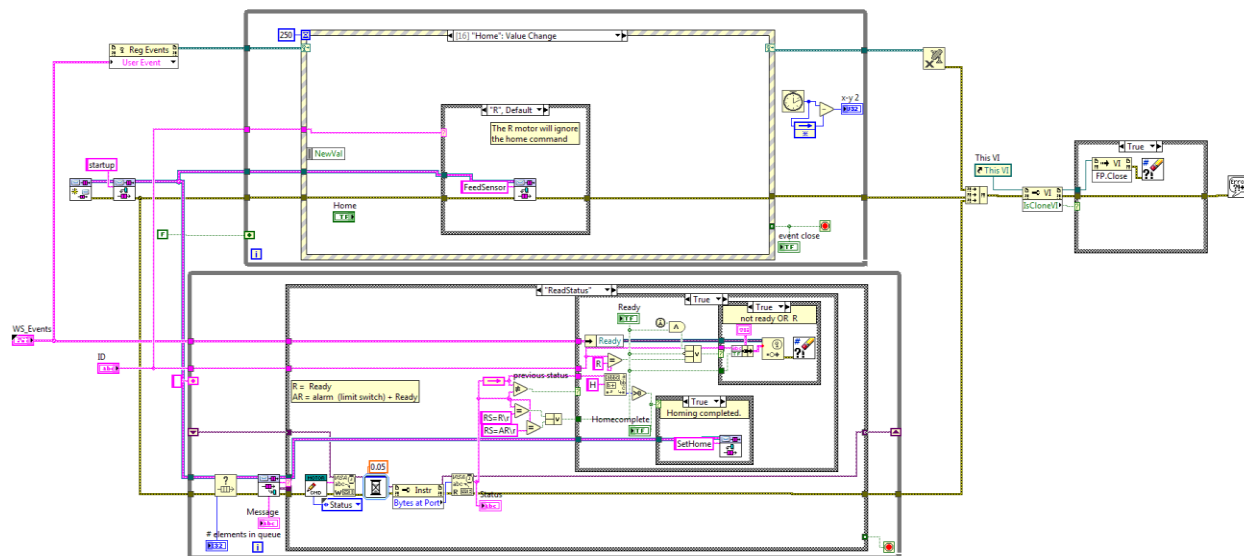
PAGE 4/4

SAMPLE ID		90-.16-T3_105mm_True_11.15.18
SAMPLE LENGTH		105
NOMINAL DIAMETER		5.264
TEST ITEM	STANDARD VALUE	ACTUAL VALUE
INDE NT LENGTH [MM]	3.5±0.5	3.921
INDE NT DEPT H [MM]	0.15±0.05	0.156
INDE NT SPACING [MM]	5.50±0.50	3.34
INDE NT DISTANCE [MM]	$\Sigma e \leq 3.343$	5.22, 5.27, 5.27
AVG DIAMETER [MM]	-	TBD
OVALITY	$\leq 0.01 \times D$	TBD

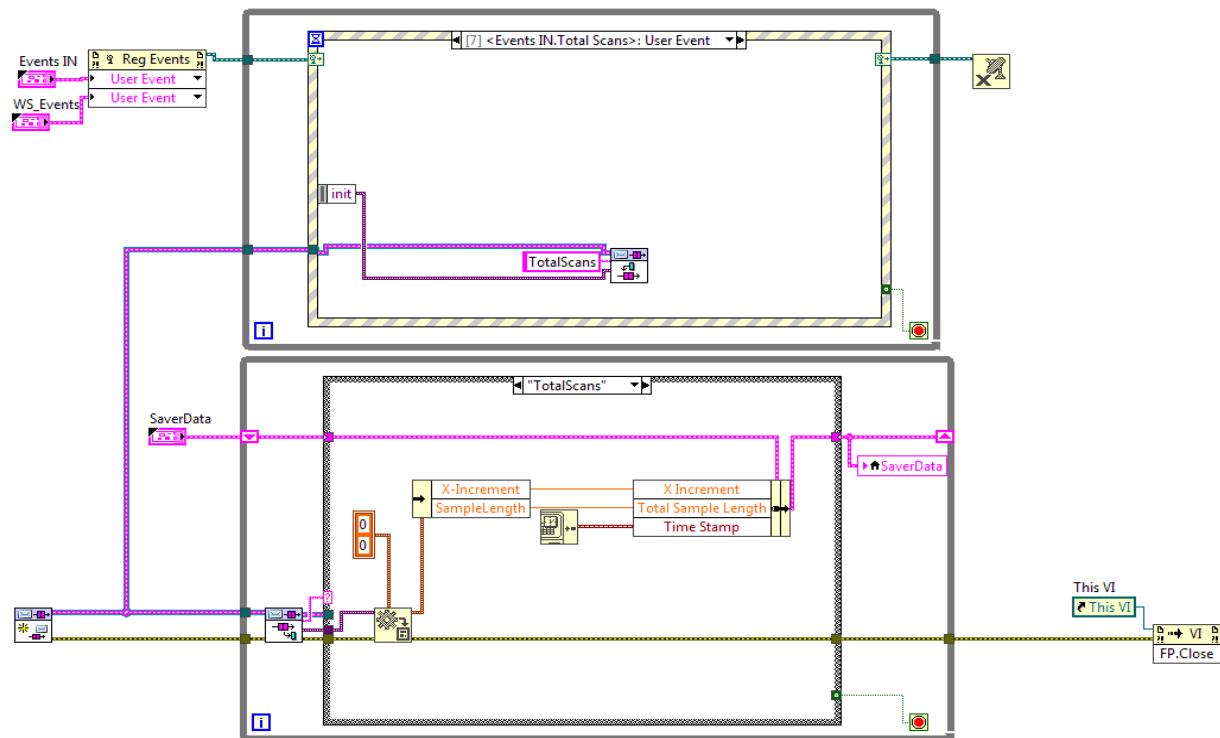
Keyence_Interface: Utilized by WS_Main and handles the communication with the Keyence laser line scanner.



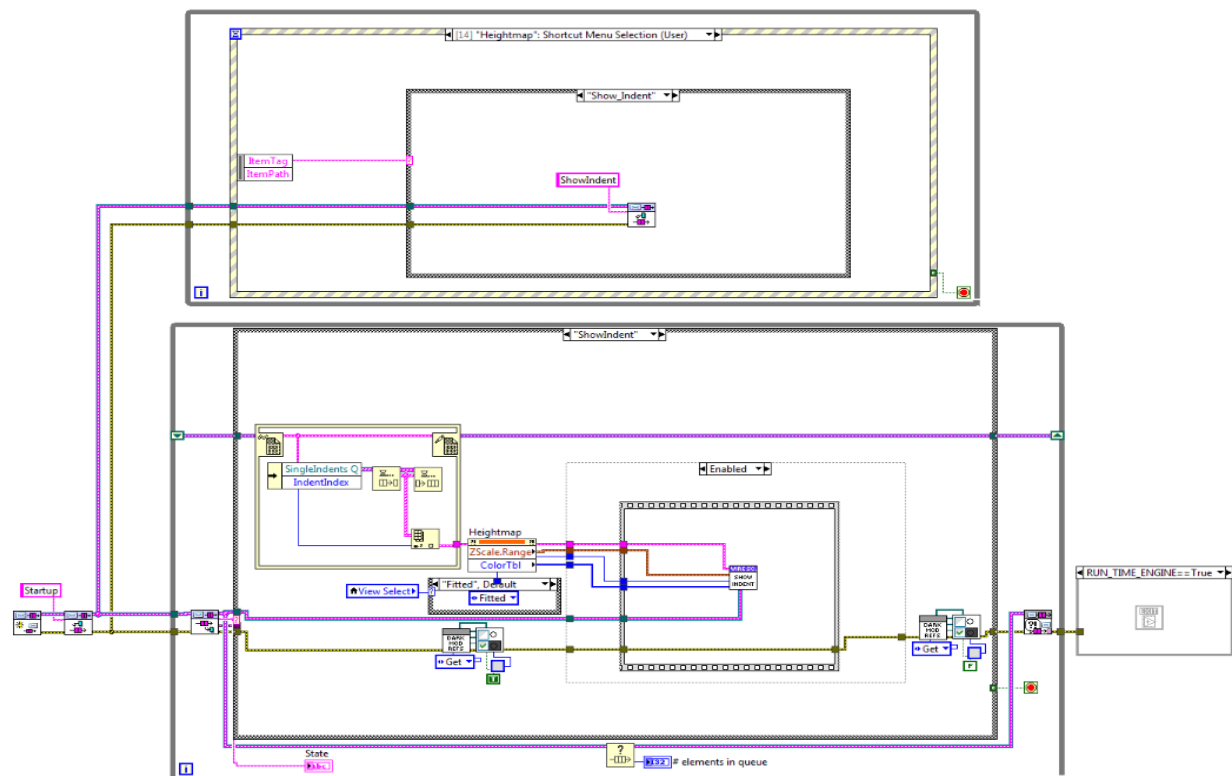
Motor_Control: Launched by WS_Main and handles the stepper motor control for rotation and axial movement.



Save_Data: Used by WS_Main to handle the saving of the scan files to permanent storage.



WS_Viewer: The application that opens the scan files and processes them.



Abbreviations and Acronyms

CL	Crack Length
FFT	Fast Fourier Transform
TL	Transfer Length
VI	Virtual Interface